Investigating astrocytic tau spread in models of tauopathy

Reid, Matt

Awarding institution:
King's College London

Investigating astrocytic tau spread in models of tauopathy

Matthew J. Reid

Kings College London
Institute of Psychiatry, Psychology and Neuroscience,
Basic & Clinical Neuroscience,
Maurice Wohl Neuroscience Institute,
Denmark Hill Campus
London, SE5 9RT

October 2022

Acknowledgements

There are many people I want to thank for getting me here. Foremost are my supervisors Wendy and Bea, without which this work wouldn't have been possible. Thank you for helping steer me through the rollercoaster of a PhD project, not to mention the impacts of a global pandemic. Your guidance and support have been essential to making this happen.

Lab work is always made easier by the people around you; a big thank you to my current and former lab members Emily, Katie, Saskia, Paula, Chen, Louisa, Cindy, Diana and Huzefa (and not forgetting DPR Dan), for creating a positive and friendly environment on the first floor of the Wohl. Shared lab meetings have also provided me with invaluable advice from Diane Hanger and Maria Jimenez-Sanchez.

My previous RA supervisor Deepak Srivastava was instrumental in pushing and supporting me into applying for a PhD. Thank you to him and other members of his lab, Leo and Lucia, for continued advice throughout the project.

Finally, I couldn’t have done this without the support of family and friends. I owe my parents a great deal for supporting and encouraging me to get this far. Thanks to past and present housemates for listening to the rants, and recent housemates Seyi, Danny, Dan, Ruth and Rob for enduring me while I navigated the intense final months of write up.

Declarations

I hereby declare that all work presented in this thesis is my own, with the exception of the following:

- Peripheral tau spread experiments in mice and quantified data in section 3.3.2 were previously conducted by Matthew Wade.
- A portion of the images in section 3.3.3 were collected by Diana Flores Dominiquez and her MSc student Julia Jamka.
- The raw data analysed for astrocyte numbers and reactivity in section 3.3.4 were collected by MSc/MSci students Julia Jamka and Rahatil Chowdhury, the latter under my in-lab supervision.

Covid-19 Impact Statement

The Covid-19 global pandemic caused significant disruption during the data collection period of this project. Research labs at King's were shut for significant lengths or time and were only reopened to largely reduced capacity. This, combined with the knock-on effects in regard to supplier delays and sample collections from collaborative Brain Bank at King's, meant that many experiments were curtailed or abandoned. Some samples sets were therefore limited, and some of the planned astrocyte reactivity as well as co-culture experiments in the final results chapter could not be completed.

Table of Abbreviations

Acronym	Meaning
ACM	Astrocyte conditioned media
AD	Alzheimer's disease
AGD	Argyrophilic grain disease
ALP	autophagy lysosomal pathway
ALS	amyotrophic lateral sclerosis
ANOVA	Analysis of variance
APOE	Apolipoprotein E
APP	Amyloid-precursor protein
ARTAG	Age-related tau astrogliopathy
Aβ	Amyloid-beta
BBB	Blood-brain barrier
bvFTD	Behavioural variant frontotemporal dementia
CBD	Corticobasal degeneration
CBS	Corticobasal syndrome
CNS	Central Nervous System
CNS	Central nervous system
CT	Cycle threshold
CTE	Chronic traumatic encephalopathy
CTR/CTRL	Control
DIV	Days in vitro
DMEM	Dulbecco's Modified Eagle Medium
DPBS	Dulbecco's PBS
EC	Entorhinal cortex
EM	Electron microscopy
ENS	Enteric nervous system
EOAD	Early onset Alzheimer's disease
FBD	Familial British disease
FBS	Fetal bovine serum
FDD	Familial Danish Disease
FRET	Fluorescence resonance energy transfer

FTD	Frontotemporal dementia
FTLD	Frontotemporal lobar dementia
FTLD-TAU	Frontotemporal lobar dementia tau
GFAP	Glial fibrillary associated protein
GGT	Globular glial tauopathy
GPT	GGT-PSP-Tau (fold)
GWAS	Genome-wide association study
HBSS	Hank's balanced salt solution
HSPG	Heparan sulphate proteoglycans
HSS	High-speed supernatant
ICC	Immunocytochemistry
IHC	Immunohistochemistry
iPSC	Induced pluripotent stem cell
KO	Knockout
LDL	Low density lipoprotein
LDLR	Low-density lipoprotein receptor
LLPS	Liquid-liquid phase separation
LNT	Limbic-predominant neuronal inclusion body 4R tauopathy'
LSS	Low speed supernatant
LTD	Long term depression
MTBD	Microtubule binding domain
NE	Neural expansion (medium)
NFT	Neurofibrillary tangle
NGS	Normal goat serum
NI	Neural Induction (medium)
NPC	Neural progenitor cell
PART	Primary age-related tauopathy
PBS	phosphate buffered saline
PCR	Polymerase chain reaction
PD	Parkinson's disease
PET	Positron emission tomography

PHF	Paired helical filament
PID	Pick's disease
PM	Post-mortem
PMD	Post-mortem delay
PNS	Peripheral nervous system
PRD	Proline rich domain
PSP	Progressive supranuclear palsy
PTM	Post-translational modification
PXXP	Pro-X-Pro
RT-qPCR	Reverse transcription quantitative PCR
SD	Standard deviation
SEM	Standard error of the mean
SF	Straight filament
SI	Sarkosyl insoluble
SIP	Sarkosyl insoluble pellet
TBS	Tris-Buffered Saline
TFEB	Transcription factor EB
TPM	Transcripts per million
UPS	Ubiquitin proteasome system
UV	Ultraviolet
WB	Western blot
WT	Wild-type

Abstract

Tauopathies are a family of neurodegenerative disorders in which highly phosphorylated and aggregated tau proteins are deposited as neurofibrillary pathology. Primary tauopathies, in which tau forms the dominant pathology, include progressive supranuclear palsy (PSP) and Pick's disease (PiD). Alzheimer's disease (AD), the most common cause of dementia, is considered a secondary tauopathy since β-amyloid peptides are deposited in plaques alongside tau deposits in the form of neurofibrillary tangles. Tauopathies are a heterogeneous group of disorders with variations in the brain regions affected, the isoform and structure of the deposited tau, and the type of neural cells that tau is deposited, all of which combine to influencing clinical outcomes.

Preliminary data from this laboratory, that is extended in this thesis, showed that there is some regional specificity in the deposition of tau isolated from postmortem tauopathy brain, following its peripheral administration to mice expressing wild-type human tau in the absence of mouse tau (htau mice). This suggested that there may be regional vulnerability to different species of tau. In addition, a close association of astrocytes with large tau deposits was noted. This suggested that astrocytes respond to tau and may contribute to tau spread. Indeed, recent work has shown that astrocytes can internalise different forms of recombinant and brain-derived tau.

To investigate this further, a human induced pluripotent stem cell (iPSC)-astrocyte model was established and characterised in comparison to induced neural precursor cell-astrocytes (iNPC-astrocytes). iPSC-astrocytes, more so than iNPC-astrocytes, showed the progressive appearance of mature astrocyte gene expression and morphological changes. iPSC-astrocytes were therefore selected for further investigation. Treating iPSC-astrocyte with tau aggregates isolated from postmortem AD brain showed that astrocytes efficiently internalise human tau, clearing these aggregates slowly over time. Moreover, internalised tau aggregates appeared to localise with high levels of GFAP and S100B, two astrocytic molecules that have previously been associated with progression of tauopathy pathology. There were variations in the rate of tau uptake and clearance that are likely related to molecular properties of the human tau, with some further indications of varied seeding ability of endogenous astrocytic tau. Astrocytes showed varied changed in gene expression in response to tau uptake including in genes implicated in astrocyte reactivity, protein

degradation and clearance. However, when astrocyte conditioned medium from astrocytes exposed to tau aggregates was collected and applied to iPSC-neurons, there were no overt changes in neuron health.

Together, these data demonstrate that astrocytes respond to the presence of tau aggregates in their local environment. This data adds to a growing body of evidence that astrocytes may contribute to tau spread by internalising tau aggregates from extracellular spaces or tau that is contained within apoptotic cells. It is not clear whether this is a protective response or if the astrocytes may release seed-competent tau species into media to facilitate its spread. Several signalling pathways were identified for further investigation to determine the precise mechanisms involved in this function of astrocytes, and it will be of interest to determine how the scale of these changes relates to molecular characteristics of different tau species.

Table of Contents

List of Figures

List of Tables

1 Introduction

1.1 Introduction to tauopathies

Tauopathies comprise a group of neurodegenerative diseases characterised by the progressive accumulation of hyperphosphorylated tau aggregates in the brain. Although they share a common tau pathology, tauopathies can be distinguished based on unique patterns of tau deposition, including variations in the isoforms and conformational structures of the aggregated tau species that spread across connected brain regions, resulting in distinct clinical manifestations. Moreover, cellular involvement with tau pathology, including that of astrocytes, can help to distinguish and confirm diagnosis post-mortem (Kovacs, 2015). This will be elaborated in subsequent sections and is summarised in Table 1.1.

1.1.1 Primary Tauopathies

Primary tauopathies are named because tau aggregates are the predominant pathological hallmark. They are often collectively referred to as a subset of frontotemporal lobar dementia (FTLD) syndromes - frontotemporal lobar dementia tau (FTLD-tau) - due to their overlap with FTLD pathology and clinical manifestations (Kovacs, 2015). However, FTLD-tau are united by the involvement of abnormal forms of tau, and within this grouping are distinct FTLD-tau phenotypes which are recognised based on characteristics of the tau aggregates, cell type involvement, and the compartmentalisation of tau in astrocytes (Kovacs, 2015, 2020). These can further be distinguished by the predominant tau isoforms that aggregate. Tau is alternatively spliced (Section 1.2.1 and Figure 1.4a) giving rise to tau isoforms containing either 3 or 4 microtubule-binding repeats referred to as 3R or 4R tau. Tauopathies can be classified by which of these tau isoforms predominate in pathological tau deposits. (See Table 1.1 for an overview of the clinical manifestations of tauopathies along with their genetic causes and affected brain regions.) The differences in the conformational folds of tau fibrils are discussed in section 1.3.3. Of particular interest to this thesis are the primary tauopathies corticobasal degeneration (CBD), progressive supranuclear palsy (PSP) and Pick's disease (PiD), along with the secondary tauopathy Alzheimer's disease (AD).

1.1.1.1 Corticobasal degeneration

CBD is a rare, progressive neurodegenerative disorder that is characterised by neuronal and glial tau pathology in both white and grey matter in corticostriatal areas, and neuronal loss in focal cortical regions and in the substantia nigra (Dickson et al., 2002). It can present with highly varying clinical features but is commonly characterised by corticobasal syndrome, which was first described by Rebeiz et al. (1968). This group of features includes asymmetric progressive rigidity and apraxia, sometimes with limb dystonia and myoclonus (muscle jerking). While CBD is commonly referred to as a movement disorder, it often presents with cognitive deficits that are now considered part of its clinical manifestation. This includes behavioural variant frontotemporal dementia (bvFTD) that comprises personality changes, perseveration, disinhibition, executive dysfunction, obsessive compulsive behaviours and impaired insight (Neary et al., 1998).

CBD clinically overlaps with PSP, and also varies in its presentation, so post-mortem neuropathological analysis is essential for accurate diagnosis. This is often validated by tau-positive neuropil threads in grey and white matter of the cortex, basal ganglia, diencephalon and rostral brainstem (Dickson et al., 2002). CBD is characterised by the presence of 4 repeat (4R) tau-rich astrocytic plaques in distal end processes in most (Forrest et al., 2019) but not all (Ling et al., 2020) cases. By SDS-PAGE, tau aggregates isolated from CBD brain contain a unique 37 kDa truncated tau fragment (Arai et al., 2001). A distinct tau filament fold for CBD was described in 2020 (Zhang et al., 2020) that is made of 4R tau filaments and is separate from other tauopathy folds, including that of PSP (Shi et al., 2021). Astrocytic pathology also plays a key role in distinguishing CBD from PSP (Komori et al., 1998).

1.1.1.2 Progressive supranuclear palsy

PSP is another rare 4R tauopathy that is often mistakenly diagnosed as CBD. Clinically, it can also present with corticobasal syndrome (CBS) symptoms, but this is most often associated with rare subvariants (Oide et al., 2002; Tsuboi et al., 2005). PSP is typically characterised by Richardson syndrome early after onset, which can also occur in CBD cases but generally at later stages of disease (Williams et al., 2005, 2008). Richardson syndrome is a group of clinical features that includes postural instability with falls, as well as vertical supranuclear palsy, dysphagia, dysarthria and cognitive disturbances related to frontal

cortex (Steele et al., 1964). Myoclonus and apraxia, symptoms common in CBD (Armstrong et al., 2013), are absent from PSP.

Atrophy and neuronal loss are common in PSP in the globus pallidus, subthalammic nucleus and substantia nigra, and also the striatum and thalamus. Areas of the brainstem are often affected that cover various nuclei, and cholinergic neurons in this region also appear to be particularly vulnerable (Warren et al., 2005). The cerebellar dentate gyrus is also often affected (Steele et al., 1964). The cerebral cortex and limbic lobe are often spared, at least until late-stage disease (Kouri et al., 2011).

Neurofibrillary tangles of 4R tau are found in the basal ganglia, diencephalon, brainstem and spinal cord (Dickson et al., 2007), and are at highest levels in the frontal, parietal and motor cortices (Kovacs et al., 2020). See Figure 1.2a for a detailed overview of tau pathology in PSP. Tufted astrocytes are the main pathological hallmark of PSP (Nishimura et al., 1992). These are observed in most PSP cases, including subvariants (Shiga et al., 2015; Kovacs et al., 2020). This astroglial tau pathology predominates in cortical areas and the striatum, with noted difference in subtypes in the thalamus, subthalamus and susbtantia nigra regions (Kovacs et al., 2020). Oligodendrocytes are also affected in PSP and this tau pathology is observed in subcortical nuclei (Kovacs et al., 2020).

Neuronal loss correlates with tau accumulation where there are areas of neuronal tau pathology such as subcortical and brainstem regions – but areas of high astroglial tau pathology such as the cortex do not necessarily translate to neuronal loss (Kovacs et al., 2020).

While PSP and CBD are mainly sporadic, although autosomal dominant PSP has been studied in at least 19 families of which some carry *MAPT* mutations(Fujioka et al., 2014). Genetic risk for both PSP and CBD is also associated with single nucleotide polymorphisms in the H1 haplotype of the *MAPT* locus (Höglinger et al., 2011; Kouri et al., 2015).

1.1.1.3 Pick's disease

PiD is a rare neurodegenerative disease and was named after a physician that recorded extensive atrophy to the frontotemporal lobe of a patient with progressive language and behavioural disturbances (Pick, 1892). The modern description now includes the dominance

of round neuronal tau inclusions (Pick bodies) that contain predominantly 3R tau (Dickson, 2001). Clinically, those affected show behavioural changes and impairment of executive functions – known as bivariant (bv) FTD (Rascovsky et al., 2011). Also, language issues such as aphasia are common (Gorno-Tempini et al., 2011), together with some movement impairment (Irwin et al., 2016a).

The proposed spread of tau pathology in PiD begins from the frontotemporal neocortex and limbic areas, gradually affecting subcortical regions including the brainstem, the motor cortex and eventually the visual cortex in some cases (Irwin et al., 2016a) (Figure 1.2b). The cellular pathology observed in affected areas includes a total loss of large pyramidal neurons, and the Pick bodies are present in middle and lower cortical layers. Pick bodies dominate the limbic and paralimbic cortices and ventral temporal lobe, where cell loss is also greatest (Dickson, 2001). Ramified astrocytic tau inclusions are often found in PiD cases, although these are not often described as a diagnostic criterion, as with PSP and CBD. Astrocytes with this tau pathology are often seen in the midfrontal- and orbitofrontal cortex (Irwin et al., 2016a).

A unique PiD tau filament fold of 3R tau has recently been defined (Falcon et al., 2018). There has, however, been noted instances of 4R tau aggregates in PiD (Zhukareva et al., 2002), particularly in Pick bodies, and 4R tau astrocytic inclusions have also been observed (Irwin et al., 2016a). In a specific familial case, 4R tau in Pick bodies were observed but in the absence of 4R tau glial inclusions (Hogg et al., 2003). In most sporadic cases, however, astrocyte tau inclusions are 3R tau positive (Irwin et al., 2016a).

1.1.2 Alzheimer's disease

AD is the most common cause of dementia. Dementia due to AD has been proposed to contribute to between 60 and 90% of all dementia cases (Prince et al., 2016). Global dementia cases are predicted to reach 113 million worldwide by 2050, more than double the prevalence today (Nichols et al., 2022).

Due to the presence of extracellular amyloid-beta (Aβ) plaques that accumulate alongside tau deposits, Alzheimer's disease (AD) is referred to as a secondary tauopathy.

1.1.2.1 Genetics of AD

1.1.2.1.1 Early onset (familial) AD

Early onset AD (EOAD) affects those younger than 65 years of age and is caused by rare genetic mutations and only accounts for approximately 2% of total AD cases (Ott et al., 1995; Guerreiro et al., 2012). The discovery of the genes conferring this risk has led to a greater understanding of mechanisms driving AD. The genetic mutations that cause EOAD occur in the *APP* and *PSEN1/2* genes, encoding proteins related to Aβ production and deposition (Thambisetty et al., 2013).

The *APP* gene is located on chromosome 21q21 and encodes the type 1 transmembrane amyloid precursor protein (APP). APP is proteolytically cleaved by α- and γ-secretases, leading to non-amyloidogenic fragments, or by β- and γ-secretases leading to the production of varying lengths of Aβ peptides which can be deposited as extracellular amyloid fibrils (Thinakaran and Koo, 2008). Over 30 dominant mutations in the *APP* gene are known to cause EOAD, accounting for about 14% of these cases, while two recessive mutations in *APP* have also been reported to cause EOAD (reviewed in (Guerreiro et al., 2012)).

Most mutations in *APP* are within the binding domains of secretases, for example the Swedish mutation (KM670/67NL) alters β-secretase cleavage efficiency (Mullan et al., 1992). Some mutations can also duplicate *APP* and the surrounding sequence (Guerreiro et al., 2012). Moreover, individuals with Down syndrome who have trisomy of chromosome 21 have an 80% risk of developing AD by the age of 65, showing that there is a gene dosage effect (McCarron et al., 2017).

EOAD is also caused by mutations in *PSEN1* and *PSEN2, which* encode proteins that are key components of the γ-secretase complex (Bergmans and de Strooper, 2010). More than 170 mutations in *PSEN1* have been shown to cause EOAD, whereas AD-causing mutations in *PSEN2* are much rarer (Raux et al., 2005). While these mutations act in a dominant fashion, the result is normally a loss of function that may not increase overall Aβ production, but instead alter the ratio of toxic and highly amyloidogenic Aβ42 peptides relative to Aβ40 species (Bergmans and de Strooper, 2010).

1.1.2.1.2 Late onset (sporadic) AD.

Many genetic risk factors for sporadic AD have been identified, particularly from genome-wide association studies (GWAS) (Escott-Price and Hardy, 2022). In general, confirmed risk genes fall into one of three categories: lipid signalling, immune response, and endosomal trafficking, the latter including those implicated in synaptic function and apoptosis (Khani et al., 2022). Common single nucleotide variation in apolipoprotein E (*APOE)* are amongst the most recognised and significant risk factors for AD. ApoE exists as three isoforms, E2, E3 and E4, with E3 being the most common in the population. ApoE4 dose dependently increases and E2 decreases the risk of developing AD (Slooter et al., 1998). Other genetic risk factors, such as *TREM2*, which influences microglial function and is associated with innate immunity functions, have more recently been identified (Bellenguez et al., 2017). Variants of the endosomal trafficking gene *SORL1* are verified to increase sporadic AD risk, with some variants on par with *APOE ε4* penetrance (Small et al., 2017). Overall, however, it seems that genetic contribution is, thus far, only a modest contributor to overall risk of developing AD (Knopman et al., 2021).

It is worth noting that although tau deposits invariably develop in AD, mutations in the *MAPT* gene are not often sufficient to induce AD pathology, unlike in some other tauopathies (Table 1.1).

1.1.2.2 Neuropathology of AD

Neuropathological evaluation is required to accurately diagnose clinically suspected AD, because symptoms can overlap with other types of dementias (see Table 1.1). While macroscopic alterations to the brain are clear, including cortical atrophy in limbic lobe structures (Perl, 2010), this is not specific to AD. Therefore, microscopic analysis of Aβ and tau pathology is required for an accurate diagnosis. This microscopic pathology emerges long before clinical symptoms manifest (Aisen et al., 2017), highlighting the need for a combination of tools for accurate diagnosis at a disease stage when interventions are likely to be most effective.

The generation of Aβ plaques is synonymous with AD, having been originally described in 1907 by Alois Alzheimer (Stelzmann et al., 1995). The abnormal processing of APP creates small Aβ40 and Aβ42 peptides that fold into beta-pleated sheets which readily form fibrils, with Aβ42 being the most fibrillogenic (O'Brien and Wong, 2011). These fibrils are deposited as extracellular plaques, which are most commonly described as being either diffuse or

having a dense core (neuritic), and which are readily distinguished using congophilic dyes, or more accurately by anti-Aβ peptide antibodies (Figure 1.1a-b).

Aβ plaques appear in a stereotypical regional pattern as disease progresses, and attempts were made by Heiko and Eva Braak to stage this process (Braak and Braak, 1997). This was then refined by more sensitive staining for Aβ plaques and divided in to five phases (Thal et al., 2002). Phase 1 involves the neocortex, moving into the allocortex in phase 2, the striatum and other subcortical nuclei in phase 3, and some Aβ deposits in the brainstem in phase 4 and further into the cerebellum in phase 5. Aβ deposition in the temporal lobe is common in phases 1-4.

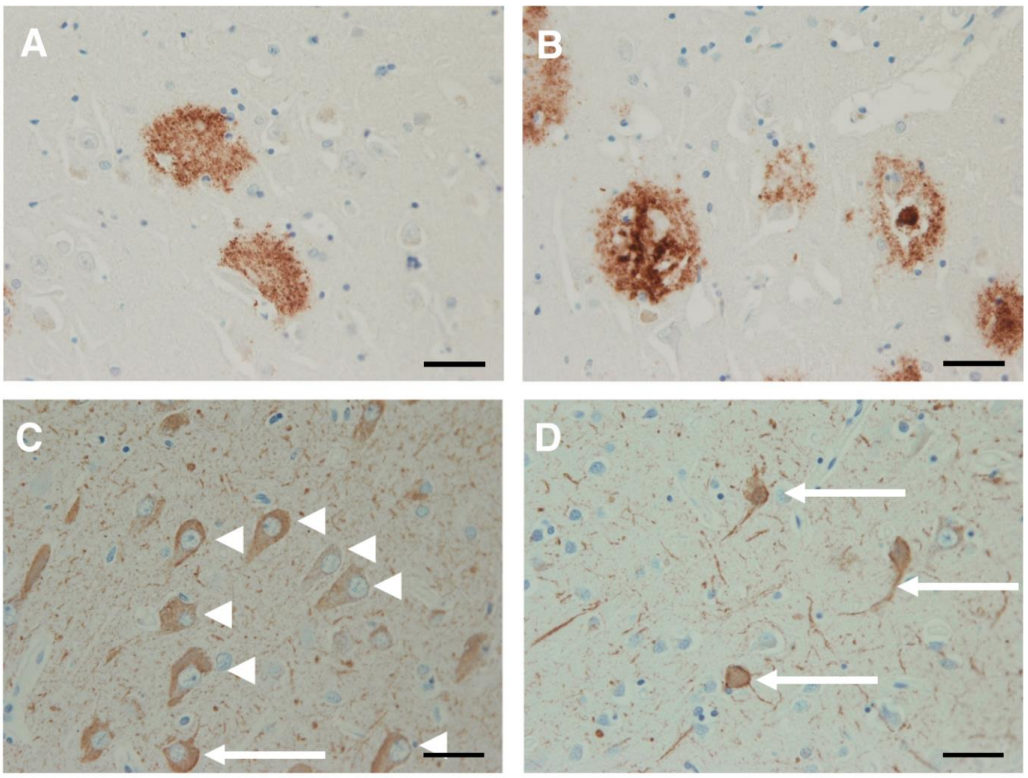

Figure 1.1 Hallmark plaque and tau neurofibrillary tangle pathology in AD.

Immunohistochemistry of human AD brain sections labelled with antibodies against Aβ and showing (A) diffuse and (B) dense core/neuritic Aβ plaques. (C-D) show neurofibrillary pathology with intracellular pre-tangles of misfolded tau (arrow heads), which can mature to dense neurofibrillary tangles containing bundles of cross-linked tau filaments in the soma, axon and dendrites (arrows). Black scale bar = 40 μm. Figure adapted from Fig. 2 and Fig. 4 of Deture and Dickson (2019).

A definitive AD diagnosis also requires the detection of neurofibrillary tau. Neurofibrillary tangles (NFTs) are intracellular bundles of highly phosphorylated and aggregated tau fibrils organised as paired helical filaments (PHFs) or straight filaments (SF) (Crowther, 1991a), which share the same protofilament seed competent core (Fitzpatrick et al., 2017). These can be observed in neuronal soma as well as axon and dendrites, known as neuropil threads. A pre-tangle stage can be observed in which misfolded tau that has not yet aggregated accumulates (Deture and Dickson, 2019) (Figure 1.1c-d). The morphology of neurofibrillary tangles can vary, and this is generally related to the cell type affected (Perl, 2010). Once a neuron dies under the burden of the aggregated tau, they give rise to "ghost tangles" in which the tau pathology remains in the absence of a discernible cell (Deture and Dickson, 2019). The remaining insoluble tau filaments can interact with extracellular proteins including Aβ and neighbouring glial cells.

Like Aβ, tau follows a spatial and temporal pattern of tau deposition. This is known as Braak staging (Braak and Braak, 1991), with refinements (Braak et al., 2011) (Figure 1.2c). Essentially, in early stage 1 neurofibrillary tangle deposition is first observed in the entorhinal cortex, particularly affecting pyramidal cells, spreading to the anterodorsal nucleus of the thalamus in stage 2. There is minimal involvement of the hippocampus or isocortex at this stage but the CA1 region of the hippocampus, pyramidal neurons of the subiculum and basal forebrain harbour pathology in Stage 3. In Stage 4, more NFT deposition is seen in CA1 but also CA4, and further the amygdala and some of the putamen and accumbens nucleus are affected. In these stages 3 and 4, previous affected areas show more dense pathology. In Stage 5, most of the hippocampus is affected, as well as broad areas of the isocortex. Finally, at Stage 6 all previously affected areas show dense tau burden, with some pathology also observed in the primary motor and sensory cortices, and greater areas of the thalamus, hypothalamus and substantia nigra. It is worth noting that the updated analysis by Heiko Braak and colleagues suggests that tau pathology in sporadic AD cases may begin earlier, possibly in the lower brainstem (Braak et al., 2011).

Interestingly, a more recent study in large cohorts suggest this may be more complex, with four dominant spread patterns discovered in AD cases that depend on factors such as age and *APOE* genotype (Vogel et al., 2021). Further investigation is required to determine the other cellular and molecular factors that determine tau spread patterning in AD.

Interestingly, the deposition of neurofibrillary tangles correlates strongly with clinical progression of the disease, but neuronal loss continues to increase after the number of neurofibrillary tangles has plateaued (Gómez-Isla et al., 1997). This is in contrast to Aβ burden, which does not appear to correlate well with clinical outcome (Giannakopoulos et al., 2003)(Hanseeuw et al., 2019). In fact, synapse loss, which precedes neuronal loss (Scheff et al., 2006), is the best correlate of cognitive decline (Forner et al., 2017).

Neuropathological studies have also observed a correlation between AD pathology and the presence of activated microglia and astrocytes. Both cluster in the vicinity of Aβ plaques (Itagaki et al., 1989), with *activated* microglia and astrocytes are observed in these regions [(Heneka et al., 2015) (Fig. 2b, d)]. Not only this, but the presence of reactive astrocytes positively correlates with neurofibrillary tangle burden and disease progression (Serrano-Pozo et al., 2011b). Microglia activation may happen early in disease, whereas astrocyte reactivity may occur during later stages, indicating a dynamic and evolving contribution to disease progression that may correlate with Aβ and tau burden (Vehmas et al., 2003)

1.1.2.3 Amyloid cascade hypothesis

Neuronal and synaptic loss, and therefore clinical symptoms, are best correlated with the accumulation of modified forms of tau protein (Serrano-Pozo et al., 2011a), including phosphorylated tau oligomers (Perez-Nievas et al., 2013). The mechanisms connecting the accumulation of Aβ plaques and tau tangles are not well understood. As AD-causing mutations affect Aβ production and Aβ deposition can precede the appearance of tau tangles, it was proposed that Aβ was upstream of tau changes in AD by (Hardy and Higgins, 1992) in the 'amyloid cascade hypothesis'. Essentially, it was hypothesized that increased Aβ production led to changes in glial activation and tau modifications that cause neuronal cell death. While the hypothesis has undergone many revisions over the years, including by its authors (Selkoe and Hardy, 2016), it is considered by some to have hindered research into other areas and even to be responsible for failed clinical trials. Recent efforts are now focussed on investigation of newly discovered risk genes and environmental triggers (Frisoni et al., 2022). Whether initiated independently or as part of a cascade, the two pathological systems associated with these proteins still interact at different levels in the brain. For example, there is evidence of converging pathogenic mechanisms at the synapse that involve both Aβ and tau (Spires-Jones and Hyman, 2014). Overall, it seems clear that the

downstream repercussions of both Aβ and tau accumulation cannot act in isolation. The complexity of interactions between these pathogenic mechanisms still needs refining.

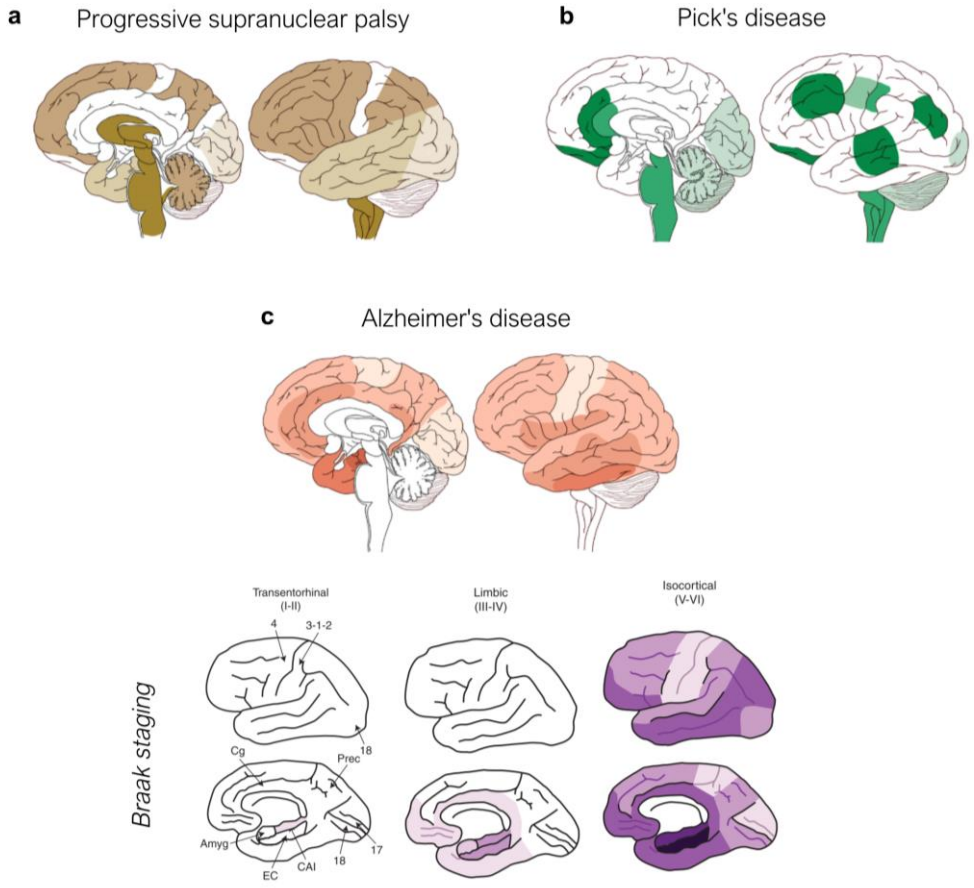

Figure 1.2 Tau pathology spread in tauopathy brains.

Figures illustrate the spatial-temporal distribution of aggregated tau in the three main tauopathies studied in this thesis. lighter colour = later involvement, shown in medial and lateral views. (**a**) Tau progression in PSP has seven stages. Stage 0/I, pallido-luyso-nigral axis shows tau burden. Stage II/III, tau invades basal ganglia, dentate nucleus and pedunculopontine nucleus. Stage IV/V, tau reaches frontoparietal and temporal lobes. Stage VI/VII, occipital cortices, substantia nigra, subthalamic nucleus and globus pallidus are involved. (**b**) Tau progression in PiD has four stages. Stage I, tau is deposited in the angular gyrus, limbic and frontotemporal regions. Stage II/III involves white matter tracts, subcortical structures (thalamus, striatum), serotonergic/noradrenergic brainstem nuclei, primary motor cortex and pre-cerebellar nuclei. Stage IV, tau enters visual cortex and cerebellar. (**c**) Tau progression in AD has six stages. Stage I/II, tau is deposited in transentorhinal area. Stage III/IV, severe involvement of entorhinal, hippocampus and limbic areas. Stage V/VI, tau pathology emerges in primary and secondary neocortex. Below in purple is Braak staging, darker colour = higher density of tau pathology. Amyg = Amygdala; EC = Entorhinal cortex; CA1 = Cornus ammonis 1 hippocampal subfield; Cg = Cingulate cortex; Prec = Precuneus; 4 = Primary motor cortex; 3-1-2 = Primary sensory cortex; 17 = Primary visual cortex; 18 =Associative visual cortex. Figures adapted from Serrano-Pozo et al. (2011a); Zhang et al. (2022)

Table 1.1 Summary of key characteristics of primary tauopathies

The main clinical manifestations, genetic causes, tau aggregate isoform composition and affected brain regions in major tauopathies.
PiD, Pick's disease; PSP, progressive supranuclear palsy; CBD, corticobasal degeneration; AGD, argyrophilic grain disease; GGT, globular glial tauopathy; ARTAG, age-related tau astrogliopathy; AD, Alzheimer's disease; PART, primary age-related tauopathy; CTE, ftld; 3R, 3-repeat tau; 4R, 4-repeat tau.

Disease	PiD	PSP	CBD	AGD	GGT	ARTAG	AD	PART	CTE
Common clinical symptoms	Aphasia, several behavioural changes including and personality changes, cognitive changes at later stages of disease.	Balance and motor deficits, dysphagia and aphagia.	Motor problems (often one-sided), aphagia, dysphagia.	Amnestic mild cognitive impairment often accompanied by neuropsychiatric symptoms.	Behavioural changes, mood swings, short-term memory loss.	Often no cognitive impairment or dementia related symptoms. Focal pathology may correlate with specific deficits, especially in the presence of co-pathology.	Dementia; progressive episodic memory deficits; navigational and multi-tasking difficulties; diverse behavioural and personality changes.	Associated with cognitive impairment and mild AD-like symptoms.	Behavioural changes, mood swings, short-term memory loss.
MAPT cause/risk	Mostly sporadic; MAPT mutations (exon 9, 10, 11, 12, 13 and intron 9, 10).	Mostly sporadic, H1/H1c MAPT haplotype increases risk; MAPT mutations (exon 1, 10, and intron 10);	Mostly sporadic; H1 MAPT haplotype increases risk; MAPT mutations (exon 10, 13 & intron 10);	H1 MAPT haplotype may increase risk; MAPT mutations (exon 10)	H1 MAPT haplotype; MAPT mutations (exons 1, 10, 11, intron 10).	*Depending on sub-type and classification*	Mostly sporadic; APP, PSEN1, PSEN2; No MAPT mutations	*Depending on sub-type and classification*	*Unknown* (external causes)
Tau inclusion isoforms	3R	4R	4R	4R	4R	4R	3R & 4R	3R & 4R	3R & 4R

Affected brain regions	Frontal and temporal cortices.	Precentral cortex, subcortex (globus pallidus, substantia nigra, pontine nuclei, subthalamic nuclei).	Frontal and temporal cortices.	Medial temporal lobe.	Frontal, precentral and/or temporal cortices.	Grey and/or white matter, perivascular, subpial, subependymal.	Entorhinal cortex and hippocampus, spreading to most regions except the cerebellum.	Entorhinal cortex, hippocampus.	Begins focally at depths of cerebral sulci, spreads widely to frontal temporal lobes.
References	(Forrest et al., 2018, 2019); (Dickson, 2001; Dickson et al., 2011; Josephs et al., 2011; Ferrer et al., 2014).	(Forrest et al., 2018, 2019); (Cairns et al., 2007; Kovacs and Budka, 2010).	(Forrest et al., 2018, 2019); (Dickson et al., 2011; Ling et al., 2016).	(Forrest et al., 2018, 2019); (Botez et al., 1999; Saito et al., 2004).	(Forrest et al., 2018, 2019); (Ahmed et al., 2013).	(Forrest et al., 2018, 2019); (Kovacs et al., 2016; Kovacs, 2018).	(Guerreiro et al., 2012); (Braak and Braak, 1991; Braak et al., 2011).	(Forrest et al., 2018, 2019); (Crary et al., 2014; Jellinger et al., 2015).	(Forrest et al., 2018, 2019); (Stein et al., 2014; McKee et al., 2015, 2016).

1.2 Tau

Tau is a microtubule associated protein, present in high amounts in the axons of neurons (Aronov et al., 2001), but that is also present in dendrites, both pre- and post-synaptic compartments (Ittner et al., 2010; Frandemiche et al., 2014) and within the nucleus (Loomis et al., 1990). Glial cells, including astrocytes, also express tau in humans, albeit at lower levels than neurons (Zhang et al., 2014; Darmanis et al., 2015; Seiberlich et al., 2015; McKenzie et al., 2018).

1.2.1 The *MAPT* gene and tau spicing

Tau is encoded by the *MAPT* gene on chromosome 17q21. It comprises 16 exons, with exons 0 and 14 not being translated. Exons 4A, 6 and 8 are expressed only in the peripheral nervous system (Wang and Mandelkow, 2016). In the brain, the remaining exons (2, 3 and 10) undergo alternative splicing to generate six isoforms defined by the number of amino-terminal domains (N), encoded by exons 2 and 3, and by the number of carboxyl-terminal repeat domains (R), encoded by exon 10. This generates tau isoforms that are known as 0N, 1N or 2N if they have 0, 1 or 2 N inserts respectively, and 3R or 4R depending on whether exon 10 is included (Figure 1.4a).

Tau splicing is regulated by developmental stage and tissue type, which determines isoform expression that is highly variable (Andreadis, 2005). The 2N isoforms are relatively underrepresented in the human CNS, comprising just 9% of tau isoforms compared to 37% and 54% of 0N and 1N isoforms respectively (Goedert and Jakes, 1990), but are prevalent in skeletal muscle (Wei and Andreadis, 1998). Generally, 3R and 4R isoforms are equally present in the human cortex (Goedert and Jakes, 1990), but their ratio varies according to brain and cell type (Goedert et al., 1989b), and this variation may play a role in region and cell type vulnerability to tau spread. Interestingly, the ratio of tau isoforms varies between species. For example, 3R tau is underrepresented in mice to the extent that it is only transiently expressed early in mouse development (Kosik et al., 1989; Llorens-Martin et al., 2012).

1.2.2 Functions of tau

Tau was originally identified as being crucial for microtubule stabilisation (Weingarten et al., 1975). It is therefore key for reorganisation of the cytoskeleton and without such can lead to neuronal death (Feinstein and Wilson, 2005). Tau is now noted to play a role in other important physiological functions (Figure 1.3) such as axonal transport by competing with motor proteins kinesin and dynein for microtubule binding, altering protein transport speed along microtubules (Dixit et al., 2008). It can also reduce the number of motors that interact with cargoes, inhibiting their transport in axons (Stamer et al., 2002), as well as by acting as cargo itself (Konzack et al., 2007), Utton et al. 2005). However, axonal transport in mice is unaffected by tau deletion or overexpression, suggesting there may be compensatory mechanisms in place *in vivo* (Yuan et al., 2008).

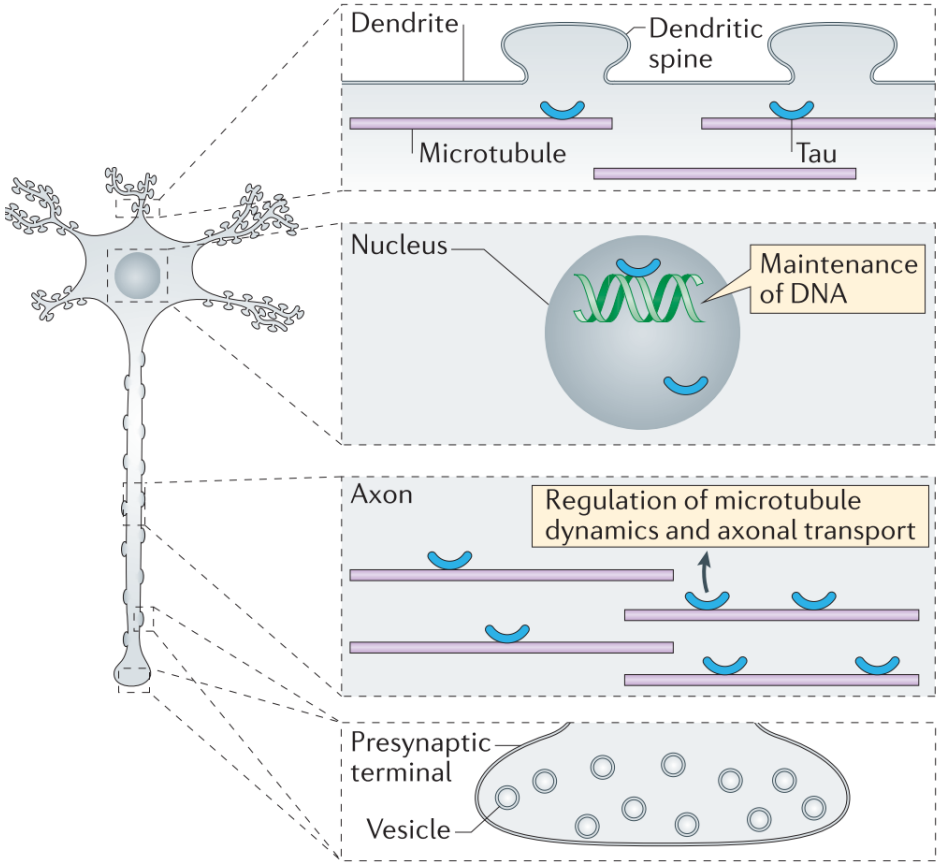

Figure 1.3 Functions of tau in neurons of the CNS.
In physiological environments, tau is mainly located in axons and plays an important role in stabilising microtubules and regulating axon transport, protecting DNA and RNA in the nucleus, and potentially having a physiological role in synaptic compartments. Figure adapted from Fig.3 of Wang and Mandelkow (2016).

Tau is also implicated in the formation of axons, where tau knockdown had been shown to inhibit neurite outgrowth *in vitro* (Yuan et al., 2008), and overexpression can induce long cellular processes even in non-neuronal cells (Knops et al., 1991). Tau is present in dendrites in physiological conditions, and synaptic activity has been shown to allow the trafficking of endogenous tau to excitatory post-synaptic compartments (Frandemiche et al., 2014). It is now postulated that tau may have a physiological role at the synapse (Robbins et al., 2021).

Tau is also found in the nucleus, and there is evidence it may be important for both DNA and RNA protection (Sultan et al., 2011; Violet et al., 2014). Other tau functions, such as regulating neuronal activity (DeVos et al., 2013), have been inferred by disease mouse models or tau knockdown models, but whether these translate into physiological functions remains unclear (Wang and Mandelkow, 2016). Tau knockout mouse models show no overt phenotype except altered microtubule organisation, which may be as a result of compensation by MAP1A (Harada et al., 1994).

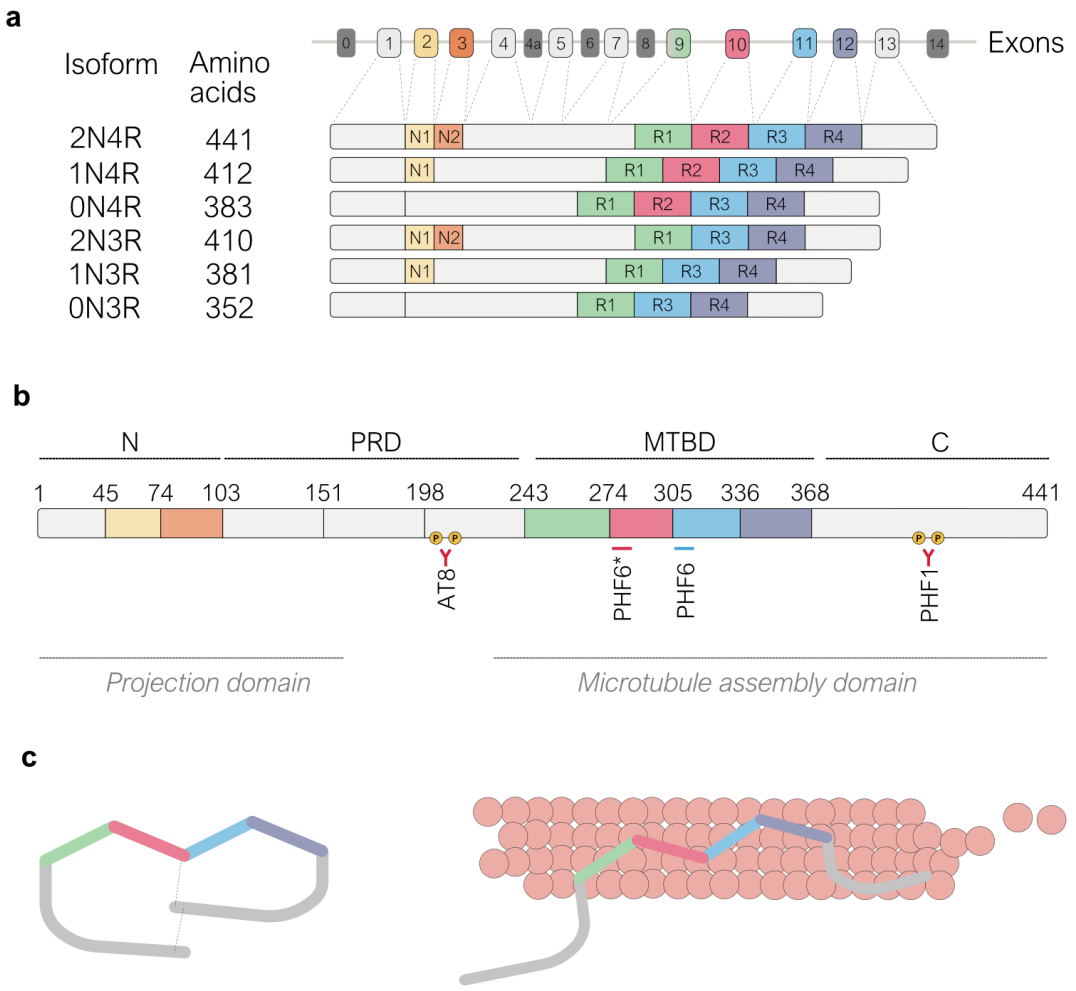

Figure 1.4 Tau isoforms, protein domains and folding dynamics.

(**a**) The human MAPT gene encodes 6 tau isoforms that are translated from 16 exons. Those indicated in dark grey are not translated as either part of the 5' untranslated region (exon 0), or only in the peripheral nervous system (exons 4a; 6; 8). Exons 2, 3 and 10 are alternatively spliced in the CNS to determine the 6 tau isoforms. The translated tau protein can be divided into an N terminal region (N), proline rich domain (PRD, microtubule binding domain (MTBD) and C-terminus (C). (**b**) Functionally, the *microtubule assembly domain* contains the MTBD and C domains and this binds to and stabilises microtubules. This region contains PHF6 and PHF6* that are implicated in aggregation. The projection domain projects away from the microtubules. The proline rich area in between contains many Thr-Pro and Ser-Pro motifs that are targets of many kinases, and hence this region becomes hyperphosphorylated in AD and other tauopathies. Many well characterised phosphorylation dependent antibodies associated with tau aggregation, such as AT8, target this region. Many mutations in tau are around the repeat domains (R1-4) (exons 9-12). (**c**) Tau monomers in solution do not have a stable conformation but can form transient paperclip like structures (left) which may protect from aggregation. Tau binds microtubules with the microtubule assembly domain section (right), while the projection domain extends away.

1.2.3 Tau protein structure

The tau protein is a polyelectrolyte – containing both negatively charged and positively charged domains, as well as being hydrophilic and thus very water soluble (Wang and Mandelkow, 2016; Zeng et al., 2021). This allows it to bind multiple targets and have various functions as described in the previous section. It has four distinct domains (Figure 1.4b), a proline rich domain (PRD) and a microtubule binding domain (MTBD) flanked by N and C terminal domains.

The N-terminal residues (1-150) of tau are key for its subcellular localisation (Paholikova et al., 2015), and for interactions with plasma membranes (Pooler et al., 2013). The PRD has seven Pro-X-Pro (PXXP) motifs which easily bind to Src homology-3 (SH3)-containing proteins, including protein kinases such as Fyn (Usardi et al., 2011). In this domain tau also binds protein encoded by the AD risk factor gene *BIN1* at its SH3 domain at proline-216 (Glennon et al., 2020), as well as a diverse array of proteins that likely have roles in tau signalling functions (Guo et al., 2017).

As the name suggests, the MTBD of tau is key for its role in stabilising microtubules (Weingarten et al., 1975), mediated by sequences in the domains themselves (Sillen et al., 2007) as well as the sequences that separate these domains (Mukrasch et al., 2007b), which likely accounts for varying tau isoform affinities for microtubules. Moreover, the MTBD of tau can also interact with actin in parallel with microtubules (Elie et al., 2015), allowing for a bridge and possible coordination between cytoskeletal components.

The C-terminal domain may be key for maintaining a physiological conformation of tau, whereas mutations in this area exert conformational effects, and therefore alter access of kinases and phosphatases to phosphorylation sites (Connell et al., 2001).

Tau isoforms, and therefore monomer length, depend on alternative splicing of N-terminal repeats and MTBDs. Early experiments have suggested that tau monomers do not have a well-defined three-dimensional shape (Zeng et al., 2021). However, motifs within tau can increase propensity to take on secondary structures (Mukrasch et al., 2007a), that may be transient or residual. The PHF6 and PHF6* motifs (highlighted on Figure 1.4b), for example, readily adopt β-sheet strands, with implications for tau aggregation (von Bergen et al., 2000) (Section 1.3.3). Even so, tau can still form electrostatic interactions between domains, with

fluorescence resonance energy transfer (FRET) techniques revealing these between the C-terminal domain and both MTBD and N domains, allowing tau, at least transiently, to adopt a compact paperclip like structure in solution (Jeganathan et al., 2006) (Figure 1.4c).

The tau protein can also be divided into two major domains based on its microtubule function: The microtubule assembly domain at the C-terminal end, and the N-terminal projection domain (Figure 1.4b). The assembly domain is neutral and therefore able to bind microtubules (Lee et al., 1989). The projection domain is acidic, projects away from the microtubules and is important for microtubule spacing in dendrites and axons (Chen et al., 1992). In between is a proline rich region which is targeted by many proline-directed kinases such as GSK (Glycogen synthase kinase) 3β and CDK5, both of which are implicated in the development of tau pathology (Pei et al., 1997; Cruz et al., 2003), and able to phosphorylate multiple sites in tau (Guo et al., 2017).

1.3 Tau in disease

1.3.1 *MAPT* mutations and polymorphisms

The first mutation identified in *MAPT* by Hutton et al. (1998) demonstrated that mutations in tau cause forms of dementia. Since then, sixty-five *MAPT* mutations have been discovered, including those that affect the splicing of exon 10, potentially disrupting the balance of 3R and 4R isoforms and thus increasing the propensity of tau to aggregate (Goedert et al., 2021).

Risk of tauopathies is also conferred by *MAPT* haplotypes, in which a 900 kb inversion (H1) or noninversion (H2) (Stefansson et al., 2005) of part of the MAPT sequence can influence disease risk. H1 inheritance has been identified as a risk factor for PSP, Parkinson's disease (PD), CBD and amyotrophic lateral sclerosis (ALS) (Baker et al., 1999; Di Maria et al., 2000; Zappia et al., 2003; Ma et al., 2018). It does not change risk for PiD (Morris et al., 2002), highlighting differences in disease mechanisms between tauopathies. The H2 haplotype is associated with higher expression of exon 3-containing tau isoforms (coding for N-terminal insert) in grey matter (Caffrey et al., 2008), suggesting that inclusion of the second N-terminal insert may confer the protection against disease observed in H2 haplotype carriers. Indeed, tau isoforms that contain the translated exon 3 have shown reduced aggregation kinetics *in* vitro (Zhong et al., 2012).

As mentioned previously, mutations in *MAPT* that cause familial forms of FTLD-Tau, either alter tau splicing or increase its propensity for aggregation. Many disease-causing mutations are clustered around exons 9-12 that encode the microtubule bring repeats R1-4, including intronic mutations around exon 10, and a small number in exon 13 (Goedert et al., 2021). These mutations affect the splicing of tau, altering 3R:4R ratios. These may also impact tau aggregation, since 4R tau is kinetically favourable for aggregation *in vitro* (Zhong et al., 2012).

While many mutations in and around exon 10 impact splicing, some can also affect tau at the protein level, such as P301L, P301S and P301T mutations that have been key for generating mouse models of tauopathies (Ramsden et al., 2005). There have been some suggestions for how these mutations might increase tau aggregation. Wild-type tau is proposed to aggregate less efficiently because the PHF6 motif is shielded by adjacent regions (Mirbaha et al., 2018), and indeed the P301L mutation was shown to disrupt this shielding (Chen et al., 2019), inducing a seed competent form of tau monomer that may explain the aggregation propensity of this type of tau. Tau with mutations in this region also have reduced affinity for microtubules (Barghorn et al., 2000), increasing tau monomer availability for aggregation. These mechanisms may explain how some primary tauopathies can develop, but they do not account for the mechanisms underlying tau aggregation in sporadic tauopathies, especially in AD for which no *MAPT* mutations are associated.

1.3.2 Post-translation modifications of tau

The specific mechanism by which tau monomers form ordered tau filaments in tauopathies is not completely understood. However, multiple drivers of tau aggregation have been identified that alone or in combination may contribute to these pathogenic conformations.

This may be explained, at least in part, by the fact that tau undergoes multiple posttranslational modifications (PTMs) including phosphorylation, acetylation, glycosylation, glycation, deamidation, isomerisation, nitration, methylation, ubiquitination, sumoylation and truncation (Wang and Mandelkow, 2016; Goedert et al., 2021). Some of these, such as N-glycosylation, may suppress tau dephosphorylation, and may help to maintain and stabilise PHF structure (Wang et al., 1996). Acetylation has been shown to reduce degradation of phosphorylated tau in a tauopathy mouse model (Min et al., 2010), and acetylation at K280 impacts the functions of tau in microtubule assembly and enhances aggregation *in vitro* (Haj-

Yahya and Lashuel, 2018). These various posttranslational modifications, alone or in combination, may drive tau aggregation during disease.

The most well characterised modification of tau is phosphorylation. Tau has over 85 potential sites for phosphorylation in its longest 2N4R isoform (Hanger et al., 2009). Tau phosphorylation is not only a feature of disease, but is crucial for its function, with phosphorylation sites in the MTBDs (Drewes et al., 1995) and PRD (Biernat and Mandelkow, 1999) altering binding to microtubules as well as neuronal membranes (Pooler et al., 2012). In line with this, tau is phosphorylated throughout development, with evidence of tau phosphorylation in human fetal brain tissue that may even result in the formation of non-toxic aggregates, likely owing to the fact the phosphorylation pattern was observed to differ from that found in AD brain (Hefti et al., 2019). After birth, tau phosphorylation is reduced (Yu et al., 2009), and phosphorylation changes have also been linked to other physiological processes in mammals such as hibernation (Su et al., 2008).

Hyperphosphorylation of tau is invariably observed in AD, is seen to precede aggregation, and has therefore long been considered a causative mechanism (Kim et al., 1988). Up to 50 tau sites are known to be phosphorylated in AD (Hanger et al., 2007; Giacomini et al. 2018). 17 Thr-Pro or Ser-Pro motifs are hyperphosphorylated in tauopathies, and many disease-associated antibodies including AT8 target these motifs (Figure 1.4b) (Gandhi et al., 2015). Because phosphorylation is important for the normal physiological function of tau, such as binding to microtubules, changes can have downstream consequences for both aggregation and normal cellular function (discussed in Section 1.3.6).

In PSP and CBD, differences in tau phosphorylation compared to AD have been noted, where prepared tau fibrils from postmortem brain less readily react with phosphorylated tau antibodies and may indicate a comparatively reduced level of phosphorylation (Wray et al., 2008). Recently, tau phosphorylated at serine 208 was seen to strongly associate with neurofibrillary tangles in AD but not as clearly with tau aggregates in tufted astrocytes of PSP or astrocytic plaques in CBD (Xia et al., 2020). While phosphorylation profiles may vary, PSP tau is still labelled by common AD phospho-tau antibodies, and these label aggregates across different tauopathy brain (Xia et al., 2021).

There are also differences in post-translational modifications of pathogenic tau among cases within the same tauopathy. An analysis of an AD cohort found greatly variable

phosphorylation of soluble, oligomeric and seed competent tau, and found that phosphorylation of tau at specific sites correlated with higher tau seeding activity *in vitro* as well as worse clinical outcomes (Dujardin 2020). A study of a larger cohort (Wesseling et al., 2020) found that phosphorylation at specific sites correlated with soluble tau low molecular weight species, whereas oligomeric high molecular weight tau showed 20 distinguishing phospho-sites as well as acetylation and ubiquitination sites in the MTBDs, the latter two of which were unique to seed competent tau. They also showed that C-terminal cleavage is common in aggregated tau. Further, they notice that the proline rich region of insoluble tau aggregates accumulated more phosphorylation as a function of tau fibril size, whereas at the microtubule binding domain tau is acetylated and ubiquitinated and these features positively correlated with fibril size. The result is an increased negative charge in the proline rich region and decreased positive charge in MTBD, which would increase the ability of tau to misfold and aggregate. Interestingly, another study comparing PTMs in CBD and AD tau saw that there were both overlap and distinct PTM profiles (Arakhamia et al., 2020).

In addition, liquid-liquid phase separation (LLPS), a process by which membrane-less organelles form, is now thought to be important in protein aggregation in some neurodegenerative diseases and is especially linked to *C9orf72*-linked amyotrophic lateral sclerosis (ALS) and frontotemporal dementia (FTD) (Solomon et al., 2021). For full length tau, even without a low-complexity domain which is a key mediator of interactions for LLPS, phase separation has been observed via electrostatic interactions and hydrophobic interactions (Boyko et al., 2019; Lin et al., 2020). Although the body of evidence suggests this mechanism is certainly not necessary for tau aggregation, it may influence or work in parallel to enhance overall tau fibril formation (Goedert et al., 2021).

1.3.3 Tauopathy filament structures

In Alzheimer's disease, it has long been observed that tau inclusions are formed of paired helical filaments (PHF) as well as straight filaments (SF) (Terry, 1963; Yagishita et al., 1981), that were suspected to contain an ordered core (Crowther, 1991b). For other tauopathies for which *MAPT* mutations are implicated, initial evidence suggested the molecular structure of tau fibrils differs from AD (Crowther and Goedert, 2000). Advances in electron microscopy (EM), through the advent of Cryo-EM, have allowed for the structure of tau filaments from post-mortem tissue to be resolved at incredibly high resolution. This work has since been able to confirm that PHF and SF are indeed structural variants as once proposed

(Crowther, 1991b), both sharing identical protofilament cores comprising residues 306 - 378 (Fitzpatrick et al., 2017). Further, this group has now been able to distinguish distinct folds in different tauopathies that match remarkably well with confirmed diagnosis (Shi et al., 2021).

Other tauopathies present distinct tau fibril folds (Figure 1.4). Some, such as AD and primary age-related tauopathy (PART) share a common tau fold that contain R3 and R4 MTBDs, and thus are composed of both 3R and 4R tau. Pick's disease fold contains R1 MTBD, and not R3, hence its association with 3R tau. Other tauopathies are composed of just 4R tau filaments with the R3 MTBD. Some, such as globular glial tauopathy (GGT), show evidence of more than one fold that may distinguish previously unknown subtypes (Shi et al., 2021). These researchers also found a PSP case that displayed a different tau fold (named GGT-PSP-Tau (GPT) fold – see Figure 1.5) from both typical and atypical PSP, potentially representing a new subtype they termed 'limbic-predominant neuronal inclusion body 4R tauopathy' (LNT), because of its distinct 4R tau pathology in those regions. It remains to be seen if other LNT cases exist, but this demonstrates the ability of structural techniques to distinguish between pathologies, and this work provides strong evidence that tau filament structures are a strong determinant of disease type.

This high resolution of protein structure has now afforded insight into how the tau protein is able to fold into various core structures to form different filament structures. There are two hexapeptide motifs (PHF6 and PHF6*) at the beginning of the R2 and R3 regions of tau that have a propensity to form β-sheets and were once proposed as key for the assembly of tau into ordered filaments (Von Bergen et al., 2000). Indeed, at least one of these appears in the folded cores of all tau filaments identified to date (Shi et al., 2021). 4R tau contains two of these motifs, and 3R tau just one, and this may go some way to explain the propensity of 4R tau to aggregate (Zhong et al., 2012).

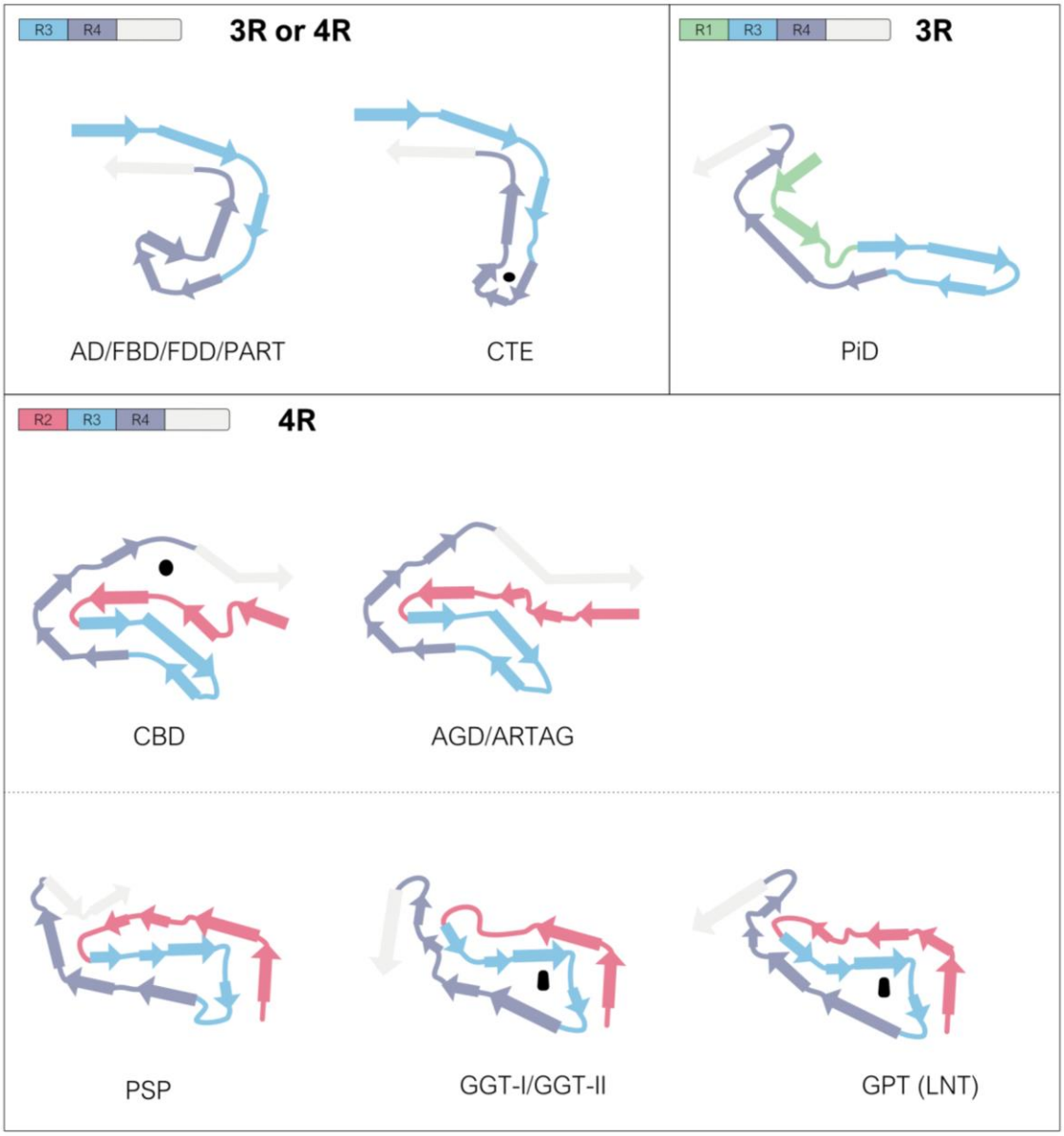

Figure 1.5 Tau protein filament classification.

Structural representation of core tau folds in tauopathies, grouped by the tau isoform (3R or 4R) included in the filament. Thick arrows represent the β-sheet strands, coloured to indicate the microtubule binding repeat (R1-4) from which they are derived. The part of the tau protein involved in each fold is indicated (top left of each section), with the light grey section representing the C-terminal domain. Black dots represent unknown (non-tau) internal densities found in some folds. Structural representations and classifications were adapted from Shi et al. (2021).The fold for the newly discovered PSP variant (LNT) was dubbed the 'GPT' fold by Shi and colleagues for its similarity to both PSP and GGT folds.

AD, Alzheimer's disease; FBD, Familial British Disease; FDD, Familial Danish Disease; PART, primary age-related tauopathy; CTE, chronic traumatic encephalopathy; PiD, Pick's disease; CBD, corticobasal degeneration; AGD, argyrophilic grain disease; ARTAG, age-related tau astrogliopathy; PSP, progressive supranuclear palsy; GGT, globular glial tauopathy; LNT limbic-predominant neuronal inclusion body 4R tauopathy.

1.3.4 Tau release and spread

It has long been observed that tau aggregates deposit in a predictable spatiotemporal pattern throughout tauopathy brain (Braak et al., 2011) that correlate well with clinical manifestations (Brier et al., 2016). The mechanisms of tau spread are still being elucidated, but there is clear evidence of a prion like mechanism of tau spread, where tau aggregates are released from a donor neuron and these can act as seeds to propagate tau monomers that can be internalised by or otherwise influence recipient cells (Jucker and Walker, 2018). Several mechanisms have been proposed to regulate these two phases of tau spread– release and uptake.

1.3.4.1 Tau release

While pathogenic tau fibrils may be transferred between neurons via tunnelling nanotubes that can link neurons (Tardivel et al., 2016), there is also a body of evidence demonstrating the existence of extracellular tau. Early studies have shown that endogenous tau can be released from neurons in healthy physiological conditions, using a rat cell culture model (Pooler et al., 2013) that built on previous evidence of tau molecules released into extracellular spaces *in vitro* (Karch et al., 2013) and *in vivo* (Yamada et al., 2011). C-terminally truncated tau fragments have also been measured in the media of human and rodent cultured neurons (Kanmert et al., 2015), as well as AD patient derived neurons (Bright et al., 2015).

Extracellular tau can also be associated with extracellular vesicles such as exosomes (Pooler et al., 2013; Kanmert et al., 2015) and these can be longer fragments that are seed competent (Guix et al., 2018), as well as being highly phosphorylated (Saman et al., 2012), but seed incompetent tau species have also been observed in vesicles (Fontaine et al., 2016). This highlights the lack of consistency in knowledge of this mechanism. Exosomes are implicated as mechanisms of tau spread, especially since transgenic mouse models have shown that highly phosphorylated tau released in exosomes can seed tau aggregation (Polanco et al., 2016), and further that inhibiting exosome production can halt tau spread in (Asai et al., 2015). However, Chai et al. (2012) showed that full length tau can be released at low levels by a mechanism that cannot be blocked by inhibitors of conventional secretory

pathways, and more recently others showed that phosphorylated oligomeric tau can cluster at membranes and be released through the plasma membrane in a process mediated by heparan sulphate proteoglycans (Merezhko et al., 2018), indicating other potential mechanisms of release for tau.

Tau release is also linked to synaptic activity. Tau release is enhanced by stimulated neuronal activity *in vitro* (Pooler et al., 2013; Wang et al., 2017), and *in vivo* (Yamada et al., 2014). Furthermore, optogenetic and chemical stimulation of transgenic mouse neurons enhanced tau spread from donor neurons, causing increased tau pathology in connected neurons *in vivo* (Wu et al., 2016). Similar optogenetic and chemical stimulation of neuronal activity in drosophila showed that phosphorylated human tau is preferentially released compared to relatively unphosphorylated tau species (Ismael et al., 2021). Similarly, in organotypic brain slice cultures, tau release under basal conditions was increased in slices prepared from 3xTg-AD mice, however stimulation with KCl induced further tau release from wild-type but not transgenic slices (Croft et al., 2017). These data indicate that different species of tau may be released by different mechanisms.

1.3.4.2 Tau uptake

Evidence indicates that cells, including neurons, readily internalise aggregated tau seeds. HEK293T cells were shown to internalise and allow seeding of different conformations of aggregated tau that enter through macropinocytosis (Falcon et al., 2015). Tau uptake may be mediated by a group of proteoglycans known as heparan sulfate proteoglycans (HSPGs) that are well conserved and expressed on the surface of neurons as well as other cell types of the brain (Turnbull et al., 2001; Sarrazin et al., 2011). These can interact with protein aggregates including recombinant tau fibrils on the surface of primary neurons, mediating their uptake in a process also indicated to be by macropinocytosis (Holmes et al., 2013). Furthermore, tau internalisation in human iPSC-derived neurons was seen to be regulated by 6-0 sulfation patterns on HSPGs (Rauch et al., 2018), presenting a potential mechanism for cell specific vulnerability to tau uptake. This may be mediated by the cell surface receptor low-density lipoprotein LRP1, which has been found to interact with HSPGs to mediate Aβ clearance in AD (Kanekiyo and Bu, 2014; Liu et al., 2017), at least in astrocytes. Knockdown of LRP1 was shown to block the uptake of both monomeric and oligomeric tau, as well as sonicated tau fibrils, in human neuroglioma cells (Rauch et al., 2020).

1.3.5 Models of tau spread and propagation

There is a body of evidence from *in vivo* models to show that tau spreads and propagates in a prion-like way. The first evidence for this was obtained from a transgenic mouse model expressing mutant human (P301L) FTLD-causing tau, expression of which was restricted to layer II neurons in the entorhinal cortex. Tau aggregated in these cells and was subsequently found to spread trans-synaptically via the perforant pathway to non-mutant tau expressing cells in the hippocampus and other connected regions as the mice aged (de Calignon et al., 2012; Liu et al., 2012).

Tau inclusions with specific filament structure may determine neuronal vulnerabilities and impact tau spread and resulting pathology (Clavaguera et al., 2013). In a mouse model that expresses human wild-type 3R and 4R tau isoforms in appropriate ratios, He and colleagues recapitulated the same disease associated cell type pathology when mice were injected with human tau extracts directly into the brain. This gave rise to the development of tufted astrocytes in PSP tau-injected mice, and astroglial plaques in CBD tau-injected mice (He et al., 2020), suggesting that the pathological conformation of tau is a key driver of transmission in the brain. In non-transgenic mice, injection into the brain of AD patient tau showed spatiotemporal spread and seeding of wildtype mouse tau (Guo et al., 2016). In a follow up model, PSP and CBD patient derived tau was also found to be competent at seeding and spreading through anatomically connected brain regions, although the extent of this spread and its ultimate clearance was found to vary depending on the tauopathy strain injected (Narasimhan et al., 2017). The varying association of tau pathology with astrocytes in different tauopathies shows that their selective vulnerability to certain tau species may play a role in the propensity of tau to spread, as well as the downstream toxic effects that are associated with impaired astrocytic function (Section 1.5.2).

1.3.6 Mechanisms of tau toxicity

As abnormal tau exists in multiple states in tauopathy brain, defining which are the toxic tau species has proved difficult. It seems likely there are various tau species that can cause a multitude of toxic cellular impacts. While tau fibrils deposit around the brain, there is evidence

that soluble tau aggregates, not large fibrils, are toxic species that display seeding and cross-seeding behaviour (Ghag et al., 2018).

There are multiple ways in which tau can influence cell health. The tau posttranslational modifications associated with tauopathies can impair its normal function (see section 1.2.2), for example by inducing detachment from microtubules. This impacts all microtubule associated functions, including cytoskeletal organisation and axon outgrowth, as well as allowing more tau monomers available for aggregation. Other physiological tau functions may be altered, including the protection of DNA & RNA in the nucleus (Violet et al., 2014), long-term depression mechanisms (Kimura et al., 2013) and iron transport (Lei et al., 2012).

Hyperphosphorylation can also cause tau missorting from axons to dendrites, spines and postsynaptic terminals, potentially causing synaptic dysfunction (Thies and Mandelkow, 2007) and loss of spines (Hoover et al., 2010). Indeed, evidence suggests that pathogenic tau may be central to the synaptic loss that is observed in AD and other tauopathies [reviewed in (Wu et al., 2021)]. First, mislocalised tau may rest in the presynaptic terminals and cause a reduction in normal synaptic vesicle release, leading to a reduction in the number of synapses *in vivo* (Decker et al., 2015), and this mislocalisation is observed in both pre- and post- synapses in AD post-mortem tissue (Tai et al., 2014). In a fly model, the N-terminus of tau has been shown to bind the pre-synaptic vesicle protein synpatogyrin-3 and cause stabilisation of vesicles, reducing their motility and altering neurotransmission (McInnes et al., 2018). This finding was also observed in the pre-synapse of PS19 mice that express mutant human P301S tau, where memory defects could be partially rescued by reducing synpatogyrin-3 expression (Largo-Barrientos et al., 2021).

In the post-synaptic compartment, tau acts a scaffold for the Src kinase Fyn, which phosphorylates the NR2B subunit of NMDA receptors, and this can help bind post-synaptic density protein 95 (PSD95), strengthening glutamatergic signalling and enhancing Aβ toxicity (Ittner et al., 2010). Tau has also shown to promote the interaction between the GluA2 subunit of AMPA receptors and PICK1 (protein interacting with C kinase 1), supporting the critical role of tau in regulating AMPAR endocytosis and hippocampal long-term depression (LTD), seen *in vitro* (Yagishita et al., 2015). Tau has also been noted as key for formation of dendritic spines since tau mutations can alter plasticity of cortical dendritic spines in transgenic mice (Hoffmann et al., 2014).

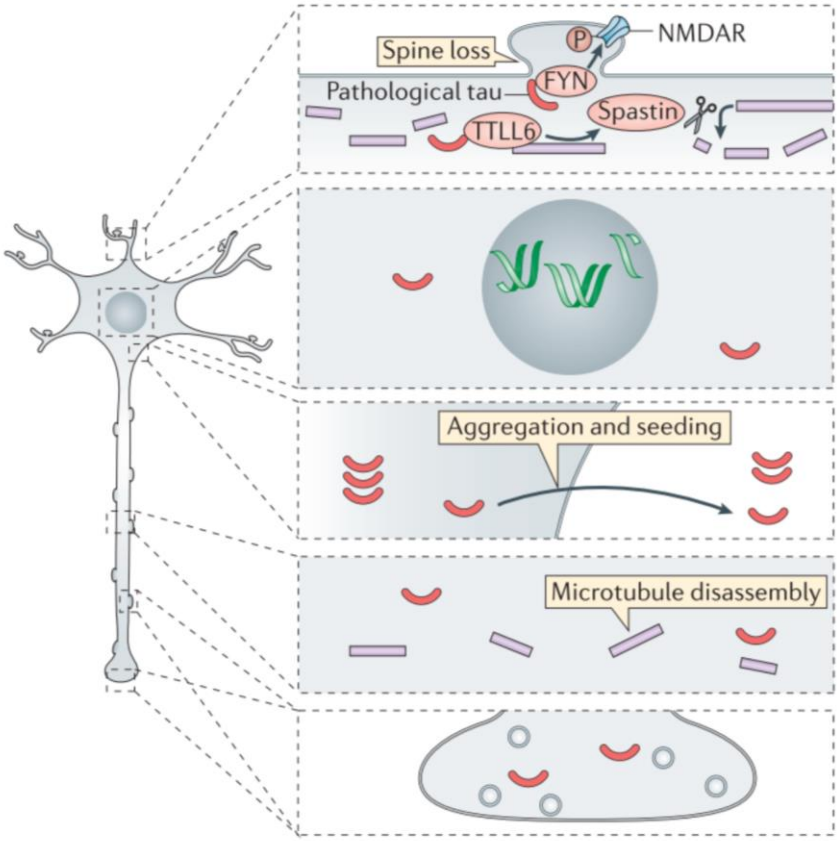

Figure 1.6 Pathogenic tau and its toxic effects on neurons in disease.
Extensive modifications of tau in disease may lead to microtubule disassembly in axons. Mis-localised tau may induce presynaptic dysfunction, leading to synapse loss, and be released and lead to aggregation and seeding as well as disruption at the post synapse. Pathological tau may not be able to enter the nucleus, negating its protective function. Tau may also have a role in strengthening Aβ toxicity by working as a protein scaffold for FYN, which phosphorylates the NR2B subunit of NMDA receptors and stabilises their interaction with PSD95. Figure adapted from Wang and Mandelkow (2016).

In addition, soluble phosphorylated tau species in mouse models has been shown to drive mislocalisation of Nup98, a key component of the nuclear pore complex (Eftekharzadeh et al., 2018), disrupting nucleocytoplasmic transport. Furthermore, this study noted Nup98 as a facilitator of tau aggregation *in vitro*.

Impaired protein degradation pathways are also implicated in the accumulation of tau aggregates. However, evidence also suggests that pathogenic tau may itself impair autophagy-lysosome pathways, amplifying protein degradation impairments to also influence Aβ clearance in AD, as well as general protein clearance pathways crucial for healthy brain function (Wang and Mandelkow, 2012).

1.3.7 Mechanisms of tau clearance

The CNS clears unwanted parenchymal proteins via a glymphatic system that carries cerebrospinal fluid (CSF), as well as vascular pathways through the blood brain barrier (BBB) (Kaur et al., 2021). Dysfunction of the glymphatic system has been linked to AD and other neurodegenerative disorders, traumatic brain injury and stroke (Jessen 2015). In AD, extracellular Aβ undergoes removal via the BBB, interstitial bulk flow (ISF), and then CSF absorption into corresponding systems (reviewed in Tarasoff-Conway et al., 2015). The glymphatic system is indicated to have a large role in Aβ clearance; in a mouse model of AD, soluble Aβ was found to be transported along this route, a process that was impaired by deletion of the astrocyte water channel aquaporin-4 (AQP4) (Iliff et al., 2012) (see 1.4.2). Clearance of extracellular tau may also occur via the glymphatic system, where a novel AQP4 inhibitor was seen to impair CSF-ISF exchange and tau protein clearance in a tauopathy mouse model (Harrison et al., 2020). Reduced glymphatic clearance of tau may therefore potentiate tauopathy disease progression by exacerbating the presence of abnormal, aggregation prone tau that can be internalised and spread by neurons.

At a cellular level, mammalian cells clear proteins by two major pathways – the autophagy-lysosome pathway (ALP), and the ubiquitin-proteasome system (UPS). These have both been implicated in the degradation of aberrant tau to varying degrees (Ihara et al., 2012; Wang and Mandelkow, 2012).

The proteasomal pathway is key for degradation of short-lived misfolded proteins (Wong and Cuervo, 2010), and the canonical pathway involves covalent tagging of a substrate with ubiquitin molecules, then degradation by the 26S proteasome, releasing reusable ubiquitin (Shang and Taylor, 2011), and this is an ATP and ubiquitin dependent process. Other proteasomes such as 20S may be able to digest proteins without ATP or ubiquitin (Jariel-Encontre et al., 2008). Alterations to tau may change their ability to be digested by the proteasome, with phosphorylation of tau by the kinase CaMKII recently being shown to impair proteasomal degradation of tau (Ukmar-Godec et al., 2020). If digested, this cleavage of tau by proteasomes may result in seed competent fragments which help to drive aggregation (Wang and Mandelkow, 2012).

Ubiquitination, particularly within the MTBD, has been detected in isolated insoluble tau fibrils from AD brain (Morishima-Kawashima et al., 1993), as well as soluble misfolded tau (Cripps

et al., 2006). While polyubiquitin chains are a signal for proteasomal degradation (Thrower et al., 2000), most insoluble tau observed in AD brain was only monoubiquitinated (Morishima-Kawashima et al., 1993), which is not normally a sufficient signal for proteasomal degradation (Pickart, 2001). Interestingly, the immune system and ubiquitin system can interact, and in neurodegeneration an immunoproteasome may be induced that is thought to contributes to neuroinflammation (Limanaqi et al., 2020).

The autophagy-lysosomal system of degradation is more complex. At its core, it is a process of delivering unwanted cellular material to lysosomes for degradation and recycling, providing energy and new substrates for synthesis of required molecules. This can be from within cells – autophagosomes, or endocytosis that involves direct processing of substances detected outside of the cell. It involves three separate mechanisms for delivering substrates to lysosomes depending on the size and longevity of these proteins in the cell (Finkbeiner, 2020). Since tau is long lived in cells it would likely be degraded by macroautophagy, and indeed altered tau has been seen to colocalise with lysosomes in post-mortem AD tissue (Ikeda et al., 1998). Inducible cell models have shown that the autophagy-lysosome system is involved in the degradation of soluble and insoluble altered tau (Wang and Mandelkow, 2012), and this is likely the method of degradation where tau phosphorylated at KXGS motifs cannot be degraded by the UPS (Dickey et al., 2007). There is further evidence for autophagy being the main degradation pathway of altered tau (Jiang and Bhaskar, 2020), including observations that reducing autophagy can lead to tau aggregation, as was seen in a transgenic mouse model overexpressing human tau (Hamano et al., 2008), as well as there being evidence for this in primary neurons (Krüger et al., 2012)

If these protein degradation pathways systems are impaired either by genetic predisposition, or by pathogenic tau itself, this could result in an accumulation of phosphorylated tau and amplification of aggregates. Since astrocytes form such a large part of the glymphatic system for CNS waste removal (Jessen et al., 2015), any impact to their function during disease (see section 1.5.1) could further reduce the removal of these seed competent pathogenic tau species from the brain, following their processing.

1.4 Astrocytes

Astrocytes were so named after their observed stellate morphology, first described as the glue ('glia') that surround neurons by Rudolf Virchow in 1846. Now, it is confirmed that astrocytes are one of the most abundant cell types in the CNS (Miller, 2018), critical for normal brain function. Developmentally, they derive from the same lineage as neurons, differentiating from a common pool of neural progenitor cells (NPCs) (Molofsky and Deneen, 2015). They are specified by a myriad of internal and external factors and continue to migrate and proliferate postnatally during development (Freeman, 2010; Molofsky and Deneen, 2015). The result is a heterogenous population of cells with various functions that are crucial for a healthy central nervous system (CNS). Astrocyte function has been greatly elucidated in recent decades (Figure 1.7), overriding the original belief that these were passive cells surrounding the neuronal architecture. This is described in section 1.4.2.

1.4.1 Heterogeneity of astrocytes

Astrocytes have long been broadly categorised by their positions in the cortex and morphologies: interlaminar, protoplasmic, varicose projections and fibrous astroglia (Vasile et al., 2017). Protoplasmic astrocytes are the most abundant type in the human brain, the most complex (covering up to millions of synapses), and the largest. However, there is strong evidence of heterogenous subpopulations of astrocytes within these morphological subcategories, likely defined by a combination of environmental and pre-coded developmental cues (Freeman, 2010; Miller, 2018; Khakh and Deneen, 2019).

More recently, the advent of single cell sequencing and spatial transcriptomic methods in *in vivo* models has provided evidence that subpopulations of astrocytes exist within the brain. Large-area analysis of the cerebral cortex of rodents revealed three major identities of astrocytes based on their gene expression profile that formed a gradient across layers of the cortex, separate from neuronal layering (Bayraktar et al., 2020). This patterning altered slightly with development into adulthood and was similar in human cortex analysis. An unbiased single cell RNA sequencing approach of mouse cortex and hippocampus revealed five major subtypes of astrocytes that were validated by study of their distinct morphologies and spatial positioning (Batiuk et al., 2020). Common markers used to identify astrocytes in IHC and transcriptome analysis are highlighted in Table 2.

Improved measures of astrocyte function may also help to elucidate further subtypes, and it likely follows that different astrocyte populations offer a spectrum of responses during disease (see section 1.5.1). For example, recently it was observed that specific subtypes of astrocytes exist in a preclinical model of multiple sclerosis, with an unsupervised approach revealing decreased expression of nuclear factor erythroid 2–related factor 2 (*Nrf2*) as well as increasing MAF BZIP Transcription Factor G (*Mafg*), which normally acts to repress inflammation (Wheeler et al., 2020). Lysosomal-associated membrane protein 1 (LAMP1) and tumour necrosis factor-related apoptosis-inducing ligand (TRAIL)-positive astrocytes were identified to limit inflammation in the CNS of mice by inducing T cell apoptosis, and their prevalence was dictated by links to the gut microbiome (Sanmarco et al., 2021). Their ability to alter neuroinflammation in response to environmental cues means they likely play a role in neurodegenerative diseases, as discussed below in Section 1.5.1. Alterations in astrocytes leading to their description as being "reactive" are highly heterogenous (Escartin et al., 2021) and this is discussed further below.

Table 1.2 Common markers used to identify astrocytes in the CNS.
Overview of common astrocyte genes, their functions and known expression profile that have been identified in the human brain.

Marker	Function & expression	References
Glial fibrillary acidic protein (GFAP)	Type III intermediate filament, predominantly expressed by astrocytes, important for cytoskeletal function and astrocyte response to injury. Implicated in reactivity changes in neurodegeneration. Regional brain differences in levels of astrocytic GFAP have been observed.	Nawashiro et al., 1996; Hol & Pekny, 2015; Lundgaard et al., 2014; Olabarria and Goldman, 2017.
Vimentin	Type III intermediate filament, also important for astrocyte cellular function and injury response. Shows differential expression patterns in comparison to high GFAP positive astrocytes that may correspond to functional and regional subtypes.	O'Leary et al., 2020;

S100B	Calcium binding protein expressed highly by astrocytes that is dynamically regulated and variably expressed depending on environmental factors, including disease.	Donato et al 2009; Ludwin et al 1976; Moreira 2021
Aquaporin-4 (AQP4)	Water channel highly expressed at the end-feet of astrocyte processes. Key for functioning of the glymphatic waste system of the brain, and for CSF-ISF exchange. Impairment of AQP4 is associated with greater accumulation of toxic protein aggregates in mouse models.	Xu et al., 2015; Harrison et al., 2020; Amiry-Moghaddam et al., 2004; Tarasoff-Conway et al., 2015
Excitatory amino acid transporter (EAAT) 1 & 2	Glutamate transporters, highly expressed by astrocytes and key for glutamate homeostasis in the brain. Both are developmentally regulated, and expression is altered during reactive states in disease and control brain.	Danbolt, 2001; Danbolt et al. 1997; Muñoz-Castro et al. 2022;
Aldehyde Dehydrogenase 1 Family Member L1 (ALDH1L1)	Folate metabolic enzyme that is mainly expressed by astrocytes in the CNS. Cited as a pan-astrocyte marker with little variability during reactive disease induced states.	Yang et al. 2011; Cahoy et al. 2008

1.4.2 Astrocyte functions

Astrocyte metabolic support for neurons comes in the form of neurotransmitter recycling, producing energy substrates and regulating cholesterol levels (Parpura et al., 1994). Astrocytes also uptake glucose, a key energy source for the brain, as seen in positron emission tomography (PET) studies in rats (Zimmer et al., 2017). Glucose can also be sequestered in the endoplasmic reticulum of fetal human astrocytes (Müller et al., 2018). Astrocytes are thought to provide energy to neurons in the form of a lactate shuffle, where stored glucose is converted to lactate for use in neurons (Newington et al., 2013; Magistretti

and Allaman, 2018), and evidence of this transfer via a lactate gradient has been shown *in vivo* (Mächler et al., 2016).

Astrocytes can also provide cholesterol to neurons, a molecule essential for basic neuronal functions and this occurs via APOE lipoproteins (Allaman et al., 2011; Pfrieger and Ungerer, 2011). In this way, astrocytes also interact with microglia, a cell type which also relies on cholesterol for normal physiological function (Bohlen et al., 2017). A mouse model showed the BBB could be negatively impacted by the expression of APOE4 only, which is a major genetic risk factor for AD (Guerreiro et al., 2012; Serrano-Pozo et al., 2021), and this could be counteracted by the expression of APOE3 (Bell et al., 2012).

Astrocytes also play a key role in the vasculature of the brain, where astrocytic end feet make direct contact with blood vessels to help coordinate synaptic activity with blood flow (Iadecola and Nedergaard, 2007; Attwell et al., 2010). Furthermore, astrocytes are involved in regulating the BBB via an upregulation of water channel aquaporin 4 (AQP4) and other transporters and factors released at the neurovascular unit (Lécuyer et al., 2016). *AQP4* expressing astrocytes are also essential to the functioning of the glymphatic system – a CNS specific waste clearance system that promotes efficient removal of soluble proteins (Jessen et al., 2015). Astrocytes can induce anti-inflammatory signalling by the release of sonic hedgehog (Shh), promoting the maintenance of the BBB (Alvarez 2011).

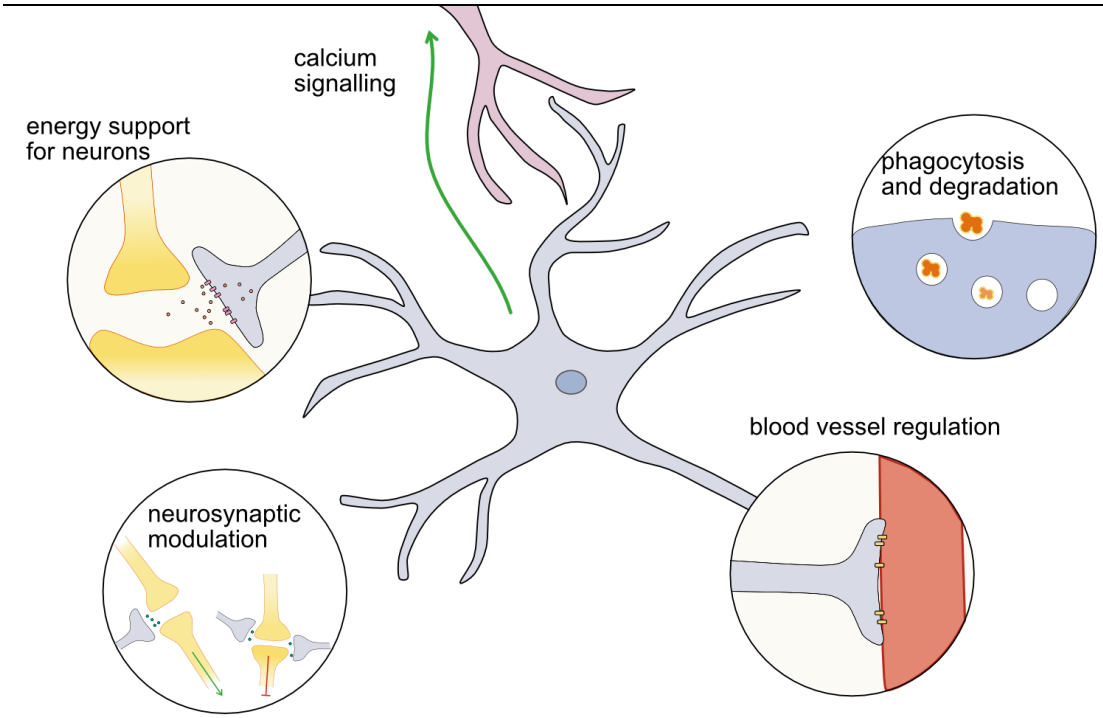

Figure 1.7 Astrocyte functions in the CNS.

Illustration of key astrocyte functions. Astrocytes provide energy support for neurons through lactate after recycling glucose. They associate with neuronal synapses to precisely regulate synaptic transmission, as well as metabolise neurotransmitters and reuptake and release glutamate. Further, they couple synaptic activity with blood flow and regulate the BBB. They also have the ability to degrade cell components and large proteins, along with microglia.

To regulate neuronal synapses, astrocytes can connect to thousands of neurons. Human astrocytes are superior in this ability, with a protoplasmic astrocyte connecting to an estimated 2 million synapses, compared to 90,000 for that of rodent astrocytes (Oberheim et al., 2006). Each neuronal synapse can be modulated, achieved by various cell surface receptors that can sense changes in neuronal activity and modulate neuronal activity by releasing gliotransmitters and gliomodulators (Choi et al., 2014). The multitude of different gliotransmitters that astrocytes can release allow them to control individual synaptic inputs, at both pre and post synaptic levels (Perea et al., 2009). And they can influence other cell types such as microglia to coordinate responses during disease (Vainchtein and Molofsky, 2020). Astrocytes, through their high expression of glutamate transporters, regulate availability of glutamate at the synaptic cleft via regulated uptake and release of glutamate into synaptic spaces (Parpura et al., 1994). This is related to the degree of astrocyte coverage around these neurons, and a lack of coverage can increase extracellular glutamate, affecting activation of presynaptic metabolic glutamate receptors and

downstream neurotransmitter release, as seen in rats (Oliet et al., 2001). Further, astrocytes express K+ channels to help clear K+ ions from the extracellular space around neurons, another route for modulation of membrane potential and excitability of neurons (Lee et al., 2022), and downregulation of K+ channels can lead to neuronal hyperexcitability – linked to neuronal dysfunction in Huntington's disease (Tong et al., 2014) and Parkinson's disease (Chen et al., 2021).

Astrocytes also create a complex calcium signalling network (Bindocci et al., 2017; Santello et al., 2019), which has been shown to be rapid enough to respond alongside neuronal activity changes in mice (Stobart et al., 2018). Astrocytes can mediate neuronal signalling in nearby and far neurons by coordinating calcium signalling and the regulation of glutamate (Mahmoud et al., 2019). The nuances of calcium signalling in astrocytes and how it may be impacted during disease processes is still being elucidated, with improved experimental techniques now helping to better interrogate this cell-cell communication (Semyanov et al., 2020).

1.5 Astrocytes in neurodegeneration

1.5.1 Defining astrocyte reactivity

Astrocyte reactivity is a broad term encompassing many of the changes that astrocytes undergo during diseases of the CNS. It describes an astrocytic response to the pathological environment that arises during neurodegenerative disease, or those caused by insult or injury, such as stroke or chronic traumatic encephalitis (CTE). Several terms have been used over the decades to refer to this astrocytic response. A recent consensus paper suggests 'reactive astrogliosis' or 'astrocyte reactivity' as being broadly acceptable terms for denoting the astrocyte response to pathology, whereby astrocytes have altered gene expression, morphologies, metabolic, biochemical, and physiological functions (Escartin et al., 2021). For clarity, '*astrocyte reactivity'* is the term used in this thesis.

1.5.1.1 Observations from neuropathology

Astrocytes in post-mortem studies are often classified as 'reactive' by their expression of high levels of GFAP, as well as their morphology and/or proximity to neuronal pathology or abnormal protein aggregates such as NFT or Aβ plaques (Serrano-Pozo et al., 2011b). The

number of reactive astrocytes in the vicinity of Aβ plaques in AD increases with age (Vehmas et al., 2003). Furthermore, GFAP-positive astrocytes have also been observed around neurofibrillary tangles (Ikeda et al., 1992; Serrano-Pozo et al., 2011b). Increased GFAP expression in astrocytes is thought to define a hypertrophic response (Vijayan et al., 1991), with large increases in the number and length of GFAP positive processes, (Sofroniew and Vinters, 2010). A spatial study determined that although reactive main processes are thicker, they do not occupy more space than their non-reactive counterparts, nor extend out of their original domains (Wilhelmsson et al., 2006).

It is worth noting, however, that a conclusive marker of astrocyte reactivity has not been determined, and GFAP expression is not consistent across all astrocyte subtypes (Sofroniew and Vinters, 2010), suggesting that using it as a marker for reactivity in post-mortem studies may skew astrocyte analysis in favour of a specific subtype. Therefore, more advanced techniques have sought to define astrocyte reactivity based on gene expression (Liddelow et al., 2017), functional and behavioural changes.

1.5.2 Alterations of astrocyte function

While astrocytes are crucial for normal glutamate function in the brain (see section 1.4.2), alteration to this process can cause excessive glutamate levels and induce excitotoxicity in neurons (Hynd et al., 2004). A deficiency in glutamate transport is associated with AD (Masliah et al., 1996), and more recent evidence has shown a direct link between *EAAT2* knockdown in AD transgenic mice and exacerbated cognitive decline (Mookherjee et al., 2011), which can be rescued when *EAAT2* function is restored (Takahashi et al., 2015). Furthermore, astrocytes derived from AD patients showed decreased glutamate uptake along with reduced expression of glutamate transporters *EAAT1* and *EAAT2* (Liang et al., 2002). A more recent paper showed direct evidence *in vivo* of *EAAT2* downregulation in reactive astrocytes that aligned with impaired glutamate uptake and neuronal dysfunction in the proximity of Aβ plaques in a transgenic AD mouse model (Hefendehl et al., 2016). *EAAT2* expression can be upregulated by an antibiotic, beta-lactam ceftriaxone, and this offers neuroprotection when given to mouse models of ischaemic injury or motor neuron disease, highlighting the contribution of glutamate dysregulation to the progression of neurodegeneration (Rothstein et al., 2005).

Calcium signalling is an important part of astrocyte function and regulation of neuronal activity (Volterra et al., 2014). When dysregulated in astrocytes, this may play a role in functional astrocyte changes, and Aβ has been shown to enhance calcium signalling *in vitro* (Abramov et al., 2003; Lee et al., 2014), as well as near Aβ plaques in AD mouse models (Kuchibhotla et al., 2009), potentially by the upregulation of P2Y1 receptors (Delekate et al., 2014). Enhanced Ca+ waves in astrocytes can also increase the release of glutamate, ATP and GABA, therefore having downstream impacts on multiple astrocyte functions including glutamate homeostasis (Lee et al., 2022). Reactive astrocytes may play a role in GABA-mediated memory loss (Jo et al., 2014). Further, the adenosine receptor A_{2A} was found to be increased in the astrocytes of AD brain, and suppression of A_{2A} in an APP-based AD mouse model rescued memory deficits in aged mice (Orr et al., 2015), suggesting not only key role of astrocytes in memory regulation, but that their alteration during AD contribute to neurodegeneration.

Using advanced transcriptome techniques in an amyloid based model of AD, researchers identified a subpopulation of disease-associated astrocytes that appeared early and increased with disease progression (Habib et al., 2020). This population was associated with Aβ plaques and may represent a dynamic population that is protective in the first response but becomes detrimental upon chronic exposure to a diseased brain environment by the adoption of inflammatory and neurotoxic phenotypes. A similar population appeared in older mice and aging human brains, suggesting shared genetic and environmental factors play a role in generating this subtype of astrocytes.

Tau may have a differing impact on astrocytes. In a tau-based mouse models of neurodegeneration, α2-Na+/K+ adenosine triphosphatase (α2-NKA), seen to be upregulated in post-mortem brain, was increased in mouse models and its inhibition or knockdown suppressed neuroinflammation and the accumulation of tau pathology (Mann et al., 2022). A broader investigation into astrocyte reactivity induced by tau or Aβ pathology in mouse models showed a spectrum of upregulated risk factor genes and distinct reaction profiles when comparing the two models (Jiwaji et al., 2022). In the tauopathy model they saw upregulation of a subset of previously reported AD related genes that differed from those altered in APP mice, indicating a difference in astrocytic response to pathological tau compared to that of Aβ. This work suggests that abnormal protein accumulation in neurodegeneration does not have a common effect on astrocyte reactivity and function, but

rather is specific to the protein accumulations to which astrocytes are exposed. Given the differences in astrocytic tau pathology observed in different tauopathies (Table 1.3), it could be speculated that these differential responses could be extrapolated to the different tau filament structures observed in distinct tauopathies (Section 1.3.3).

Astrocytes may also play a role in coordinating defences against the toxic proteins that accumulate in dementias. In a mouse model, astrocytes release IL3 that activates microglia, priming them to clear amyloid plaques (McAlpine et al., 2021). The complement system, important in innate immune defence (Ricklin et al., 2016), also plays a role in astrocyte-microglia communication, where acute C3 release from astrocytes can activate microglia via C3aR to induce microglial phagocytosis (Lian et al., 2016).

1.5.3 Astrocyte contribution to tau spread

Because astrocyte have been shown to harbour tau inclusions in tauopathies, and as they are connected to neurons synaptically, it follows that they are well positioned to contribute to the spread of tau pathology. Indeed, early evidence of prion-like spread of tau between neurons in mouse models noted the presence of PHF1-positive human tau in GFAP-positive astrocytes in the dentate gyrus of mice following the spread of human tau from its site of restricted expression in the entorhinal cortex (de Calignon et al., 2012).

1.5.3.1 Astrocyte internalization of tau aggregates

As discussed previously, astrocytes not only surround extracellular NFT 'ghost' tangles (Perez-Nievas and Serrano-Pozo, 2018), but also harbour tau inclusions in AD and other tauopathies, indicating they can internalize these aggregates. This process may be mediated by mechanisms of endocytosis.

Broadly speaking, endocytosis is a distinct process of cells taking up macromolecules and particles through their outer phospholipid bilayer (Cooper, 2000). There are specific types of endocytosis related to the mechanisms and size of the particles that are internalised. Pinocytosis allows for uptake of smaller, marcomolecules and is often receptor mediated process. Phagocytosis is a specialised form of endocytosis for the engulfment of large particles that includes cells and cellular debris. Emerging evidence shows that astrocytes can internalize cells and large proteins by phagocytic mechanisms (Konishi et al., 2022), in

addition to receptor mediated uptake of smaller molecules. For example, astrocytes also express several heparan sulphate proteoglycans (HSPGs) that may mediate this process (Turnbull et al., 2001). Primary astrocytes exogenously expressing transcription factor EB (TFEB), a master regulator of lysosomal biogenesis, can internalise tau fibrils in a HSPG-dependent manner (Martini-Stoica et al., 2018). Smaller tau proteins can, however, be internalised independent of HSPGs (Perea et al., 2019). HSPGs can also vary the length of their glycosaminoglycan chains and sulfation patterns, and because this can vary between astrocytes and neurons (Tselnicker et al., 2014), it may provide a potential mechanism for selective uptake of different tau fibrils and cell type vulnerability.

HSPGs have previously been observed to facilitate Aβ uptake and degradation in astrocytes by interacting with LRP1, a low-density lipoprotein receptor (LDLR) (Kanekiyo and Bu, 2014; Liu et al., 2017). Knockdown of LRP1 in neuronal cells blocked uptake of both monomeric and oligomeric tau, while partially inhibiting uptake of sonicated tau fibrils (Rauch et al., 2020). Whether or not LRP1 impacts the uptake of tau in astrocytes remains to be seen.

1.5.3.2 Can astrocytes contribute to tau spread?

Human astrocytes express low levels of tau (Kahlson and Colodner, 2015; Perea et al., 2019), raising the question of whether this tau can be recruited after internalization of seed competent tau fibrils. If the intracellular tau is degraded by lysosomes, as has been shown previously *in vitro* for preformed tau fibrils (Martini-Stoica et al., 2018), then this may not be the case. However, the ability of astrocytes to degrade different forms of pathogenic tau has not been investigated extensively.

Astrocytes may indirectly contribute to the spread of tau pathology by a dysregulation of their functions related to the BBB and glymphatic clearance system. AQP4, as previously mentioned, is expressed by astrocyte endfeet and is essential for these systems in the CNS (Benarroch, 2007), and has a demonstrated important in Aβ clearance (Iliff et al., 2012), as well as in ameliorating neurofibrillary tau pathology in a mouse model of CTE (Iliff et al., 2014).

The transmission of pathogenic tau from astrocyte to neurons, and indeed between astrocytes, requires further study. Furthermore, how the range of pathogenic tau species may cause varying responses remains a key area of investigation. This is important not only

in understanding the complete mechanism of tau spread throughout tauopathy brain but may also uncover new routes of therapeutic intervention.

Table 1.3 Overview of astrocyte associated tau pathology in tauopathies.

The common descriptors of tau pathology in astrocytes that have been observed in postmortem human brain, including details of the subcellular localisation of tau inclusions in affected astrocytes.

Disease	PiD	PSP	CBD	AGD	GGT	ARTAG	AD	PART	CTE
Hallmark astrocytic tau pathology	Ramified	Tufted	Astrocytic plaques	Thorn-shaped & granular fuzzy/bush-like	Globular inclusions	Thorn-shaped & granular fuzzy	*None*	*None*	Astrocytic tangles and some thorn-shaped astrocytes.
Cellular localisation of astrocytic tau inclusions	Asymmetric 3R (predominant) or 4R tau inclusions in cell bodies & proximal processes.	Symmetric 4R tau inclusions in proximal processes.	4R tau in distal processes and end feet; thread-like processes are also common.	4R tau inclusions and diffuse staining in cell bodies & proximal-distal processes.	4R globular tau in cell bodies & proximal processes.	4R tau inclusions and diffuse staining in cell bodies & proximal processes.	*n/a*	*n/a*	Irregular p-tau lesions (around small vessels).

1.6 Aims & Objectives

It is evident that astrocytes play a role in tauopathy progression. Yet, it is not known how they contribute to tau spread, the key process underlying the spread of pathology in the brain. This project specifically aims to elucidate how astrocytes respond to different tau species, their readiness to internalise tau fibrils and their capacity to degrade these aggregates, how this impacts their function and interactions with neurons. The hypothesis underlying this work is that astrocytes internalise human tau, with differing responses to different forms of tau in distinct tauopathies.

The thesis has the following main aims:

1. To determine the association of astrocytes with tau pathology in a mouse model of tau spread.
2. To establish a human astrocyte culture model with which to study human tau internalisation by astrocytes.
3. To examine the impact of tau uptake on astrocyte morphology and function.
4. To determine the impact of astrocytic tau uptake on astrocyte support for neurons.

2 Materials & Methods

All reagents were purchased from ThermoScientific, UK or Sigma-Aldrich Company Ltd., Dorset, UK unless otherwise stated. Stock solutions and buffers were prepared using ultrapure H_2O from an Elga Maxima Purification System (Veolia Water Ltd., London, UK).

2.1 Postmortem human brain

Post-mortem human brain samples were obtained from the London Neurodegenerative Diseases Brain Bank/Brains for Dementia Research at King's College London. All human issue collection and processing were carried out under the regulations and licensing of the Human Tissue Authority, and in accordance with the UK Human Tissue Act, 2004.

Table 2.1 Post-mortem brain sample details.
Sex, age at death (years), post-mortem delay (PMD) (hours), brain region used and pathological diagnosis of human brain samples. All samples are from temporal cortex except *PiD which was obtained from premotor cortex.

Diagnosis	Sex	Age (years)	PMD (h)	Case notes
Cases from which aggregated tau was isolated for injection into mice				
CTRL	F	92	17	Non diseased, Braak I
CTRL	F	55	12	Non-diseased, Braak I
CTRL	M	83	24	Non-diseased, Braak I
AD	F	94	29	Braak VI, ApoE 3/4
AD	F	84	<24	Braak V, ApoE 4/4
AD	F	97	12	Braak V, ApoE 3/4
AD	F	69	16	Braak VI, Apo E3/4
AD	F	84	36	Braak V/VI, ApoE 4/4
AD	F	82	32	Braak VI, ApoE 3/4
PSP	M	71	16	PSP
*PiD	M	61	73	PiD, Extensive glial pathology
Cases used to isolate tau aggregates for astrocyte treatment				

CTRL 1	M	77	11	Non-diseased
CTRL 2	M	86	6	Non-diseased
CTRL 3	F	55	12	Minimal tau pathology consistent with HP-tau stage
AD 1	M	88	46	AD, Braak VI
AD 2	M	81	74	AD, Braak VI
AD 3	M	72	5	AD, Braak VI with marked amyloid angiopathy
AD 4	F	97	12	AD, Braak V
AD5	F	87	48	AD. Braak VI with moderate amyloid angiopathy
AD 6	F	74	19	AD, Braak VI with moderate amyloid angiopathy Type 1, moderate cerebrovascular disease
PSP 1	F	84	9	PSP
PSP 2	M	65	16.5	PSP
PSP 3	F	75	48	PSP
PiD 1	F	93	17.5	PiD (temporal lobe type), vascular dementia and AD ageing changes
PiD 2	F	67	38.5	PiD
PiD 3	M	66	17	PiD

2.1.1 Preparation of human brain homogenates

Frozen control and tauopathy human brain was prepared as described in (Clavaguera et al., 2014). Briefly, tissue was homogenised at 200 mg/mL in sterile phosphate buffered saline (PBS: 140 mM NaCl, 2.68 mM KCl, 12.54 mM Na_2HPO_4, 1.98 mM KH_2PO_4 in ultrapure H_2O, adjusted to pH 7.4) with a Tissue Master 125 handheld homogeniser (Omni International, Kennesaw, GA, USA) and briefly sonicated (Output 3, 10 seconds on a Sonics Vibra Cells (Jencons PLC, East Grinstead, UK)) before centrifugation at 3,000 x *g* (av) for 10 minutes at 4°C with an Eppendorf 5415R desktop centrifuge (Eppendorf, Hamburg, Germany). The supernatant was collected and sterilised by passing through a 0.2 µm sterile filter (Corning Inc., Corning, NY, USA). 0.5-1 mL aliquots of each sample were stored at -80°C until

required. Characterisation and quantification of tau was achieved by SDS-PAGE and western blotting. Briefly, known amounts of recombinant tau ladder (Covance Inc, Princeton, USA) representing tau standards were loaded into gels alongside known volumes of human brain samples diluted 1:1 in 2X sample buffer (National Diagnostics, Hull, UK). Following SDS-PAGE and immunoblotting, the intensity of tau signal in the recombinant tau ladder was quantified and used to create a standard curve correlating amount of tau, in ng, with band intensity. Using the formula $x=y-c/m$ where x=amount of tau, y=intensity, c=y-intercept and m=gradient, the amount of tau in the entire lane for each human brain sample in ng/µL was estimated.

2.1.2 Isolation of sarkosyl insoluble tau

Sarkosyl was used to extract insoluble tau from postmortem human brain using a method adapted from that of Greenberg & Davies (1990). Briefly, samples were weighed and homogenised at 100 mg/mL in homogenisation buffer composed of Tris-Buffered Saline (TBS: 50 mM Tris-HCl, 150 mM NaCl in ultrapure H_2O, adjusted to pH 7.4) containing 2 mM Ethylene glycol-bis(β-aminoethyl ether)-N,N,N′,N′-tetraacetic acid (EGTA), 10% (w/v) sucrose, and Protease Inhibitor Cocktail 'Complete Mini EDTA-free' and PhosSTOP tablets (1 tablet per 10 mL solution) (Roche; Basal, Switzerland). Tissue was homogenised using a handheld tissue master 125-watt lab homogenizer (Omni International; Kennesaw, GA, USA) until smooth in consistency. Samples were centrifuged at 20,000 x g at 4°C for 20 min. Part of the resulting supernatant was collected as the low-speed supernatant (LSS). The remainder was used for sarkosyl extraction: sarkosyl (Sigma-Aldrich, St. Louis, MO, USA) was added to a total of 1% (v/v) in the LSS and samples were nutated on a shaker at RT for 30 min. Samples were then centrifuged at high speed (100,000 x *g*) using Beckman Coulter Optima MAX-XP Ultracentrifuge (Beckman Coulter; CA, USA) with TLA-55 rota at 18°C for 1 hr. The high-speed supernatant was collected, and the resulting sarkosyl-insoluble (SI) pellet was washed in homogenisation buffer containing 1% sarkosyl. The pellet was re-spun at 100,000 x *g* and all remaining supernatant carefully removed. The resulting SI pellet was resuspended in sterile-filtered Dulbecco's PBS (Thermo Fisher Scientific, MA, USA) at 100 µL per 1000 µL of initial low-speed supernatant used for sarkosyl extraction. The resuspended pellet was sonicated using a Bandelin Sonopuls HD 2070 (BANDELIN electronic GmbH & Co, Berlin, Germany) for 3 x pulses set at 10% power. The resulting solution could be used directly for tau spiking experiments or mixed with 2 x sample buffer

(National Diagnostics, Hull, UK) for western blotting after measuring concentration against known rTau standards (see section 2.1.1). Samples were *not* re-sonicated following freeze-thawing between experiments.

2.2 Mice

All animal work was conducted in accordance with the UK Animals (Scientific Procedures) Act 1986 and the European Directive 2010/63/EU under UK Home Office Personal and Project Licenses and with agreement from the King's College London (Denmark Hill) Animal Welfare and Ethical Review Board (AWERB). Animal work was conducted by a previous PhD student, Matthew Wade who held a personal licence and all work was conducted under, and in accordance with, the project licence held by Professor Wendy Noble. Samples generated from this work were used in this thesis.

Human tau (htau) mice were purchased from The Jackson Laboratory, Bar Harbor, ME, USA and bred in-house. Htau mice were generated by mating 8c mice which express the entire human tau gene under the control of the human MAPT promoter (Duff et al., 2000) with tau knockout (KO) mice generated by targeted disruption of the Mapt gene by insertion of enhanced green fluorescent protein into Mapt exon 1 (Tucker et al., 2001). Htau mice are hemizygous for the full-length human tau gene and express all six tau isoforms of human tau in the absence of endogenous tau. WT mice of an identical background strain (C57Bl/6J) were used as controls.

2.2.1 Injection of mice with tau extracts from postmortem human brain

Male and female wild-type and htau mice of 2.5-3.5 months of age were intraperitoneally injected with control or tauopathy brain extracts totalling 2-3 µg tau using a Myinjector Insulin U-1000 27-gauge needle (Terumo, Tokyo, Japan). The injected material was thawed and warmed to body temperature before injection. Mice received two injections of 100µl, one week apart, according to methods described by (Clavaguera et al., 2014). Initial quantification of tau content in samples was performed to establish that the total amount of injected tau protein would be 2µg. However, subsequent reanalysis established that extracts from control, PSP and PiD extracts were more concentrated than first established, and that

3μg tau proteins were injected. Additional controls included untreated age-matched htau and WT mice, some of which were littermates of those treated. Mice were closely monitored for changes in weight and health following injection. Mice were aged to 18 months before being killed by cervical dislocation prior to tissue collection.

2.2.2 Collection of mouse brain tissue

Mice were killed by cervical dislocation. The brain was removed and one hemisphere was separated into cortex, hippocampus and remaining brain, all of which were snap-frozen on dry-ice. The other hemisphere was drop-fixed in fixation solution (16 % (w/v) paraformaldehyde (Alfa Aesar, Haverhill, MA, USA) diluted 1:3 in PBS to give a 4 % (v/v) working solution), for 24 hours at ambient temperature, followed by an additional 24 hours in 2 % fixation agent (16 % (w/v) paraformaldehyde (Alfa Aesar, Haverhill, MA, USA) diluted 1:7 in PBS) at ambient temperature. Following fixation, the fixation reagent was removed by washing in three changes of PBS for 30 minutes each at ambient temperature, and the brains were stored long-term in cryoprotectant solution (30 % (v/v) ethylene glycol (Santa Cruz Biotechnolgies Inc., San Diego, CA, USA), 15 % (w/v) sucrose, 0.05 % (w/v) NaN_3 in TBS) at 4 °C. The fixed brain hemispheres were sectioned on a Microm 430 freezing-stage microtome (Microm International, Walldorf, Germany) as 40 μm coronal sections which were stored long-term in cryoprotectant solution [30 % (v/v) ethylene glycol (Santa Cruz Biotechnolgies Inc., San Diego, CA, USA), 15 % (w/v) sucrose, 0.05 % (w/v) NaN_3 In TBS] at 4°C.

2.2.3 Preparation of mouse brain lysates and isolation of sarkosyl-insoluble tau

Mouse brain was homogenised as described in Section 2.1.2. The sarkosyl-insoluble pellet was resuspended in a volume of 2X sample buffer (National Diagnostics, Hull, UK) equal to a tenth of the volume subject to ultracentrifugation. Samples were stored at -20 °C until required.

2.3 Cell Culture

All media reagents and consumables used in cell culture were manufactured and supplied by Thermo Fisher Scientific™ (MA, USA) under the Gibco™ brand. All cell culture plates used were Nunc™ branded, manufactured and supplied by Thermo Fisher Scientific™.

2.3.1 iPSC maintenance

The iPSC line used in this study (CTR_M3_36S) was received as a donation from Prof. Deepak Srivastava at KCL, previously generated from hair-root derived keratinocytes of a healthy control male, as described in (Cocks et al., 2014). Consent for storage of tissue and iPSCs and explicit consent for use in subsequent research was obtained by the original lab, following the guidelines of the UK Human Tissue Act 2004. Specific Research Ethics Committee approval is not a legal requirement for generating iPSCs from human donor tissue. .

iPSCs were maintained in StemFlex™ medium at approximately 0.25 mL/cm^2 and incubated in hypoxic conditions (37°C; 5% O_2; 5% CO_2). Nunc plates were pre-coated with LDEV-Free Reduced Growth Factor Basement Membrane Matrix (Geltrex™) at 1:100 in Dulbecco's Modified Eagle Medium (DMEM)/F12 medium at approximately 0.125 mL/cm^2. Plates were incubated at 37°C for 1 hr and Geltrex™ solution was aspirated before use. To maintain healthy cultures, cells were passaged at 80-95% confluency. Media was aspirated and cells were washed with Hank's balanced salt solution (HBSS, no Calcium/Magnesium) and then covered with Versene™ solution at 0.5 mL/cm^2 for 5 minutes at 37°C. Cells were then dislodged using a 5 mL serological pipette, and cell solution moved to a centrifuge tube of prewarmed (37°C) DMEM/F-12 medium at twice the volume of Versene™ solution used. Cells were then centrifuged at room temperature (RT) for 3 min at 190 x *g*. Excess solution was aspirated and cell pellets were gently resuspended in StemFlex™ medium with added RevitaCell™ supplement (1:100) to aid cell survival. Cells were replated at between 1:2 and 1:4 ratio. After 24 hours, cell media was changed for fresh StemFlex™ medium, and medium was then changed every 48 hours until cells were confluent and required further passaging.

2.3.2 Differentiation of iPSCs into Neural Progenitor Cells (NPCs)

NPCs were induced from iPSCs using the Gibco™ PSC Neural Induction Medium system. iPSCs were grown in Geltrex™ coated 6-well Nunc™ plates as detailed in 2.3.1. After iPSCs reached 15-25% confluency (**day 1**), media was aspirated and replaced with 2.5 mL/well of pre-warmed Neural Induction Medium (NI medium) composed of Neurobasal Medium and Neural Induction Supplement (1:50), and cells were moved to a non-hypoxic incubator (37°C; 20% O_2; 5% CO_2).

Cells were maintained in NI medium for 7 days: On **day 3** media was changed for fresh NI medium at 2.5 mL/well. On **day 5**, media was changed at double the volume to 5 mL/well. On **day 7** media was changed, at which point cells were reaching confluency and were ready for passaging from **day 8** onwards.

Cells were passaged by aspirating medium and dissociating cells with room temperature StemPro™ Accutase™ solution, added at 0.125 mL/cm^2 for 5 minutes at 37°C. Cells were then gently dislodged using a p1000 pipette, and the resulting cell solution was moved to a centrifuge tube containing prewarmed (37°C) DMEM/F-12 medium at twice the volume of Accutase™ solution used. Cells were pelleted by centrifugation at 190 x *g* for 2 min, and then resuspended gently in Neural Expansion Medium (NE medium) composed of equal ratios of Neurobasal® Medium and Advanced™ DMEM/F-12 medium with Neural Induction Supplement (1:50). Upon passaging, RevitaCell™ supplement was added to media (1:100) to aid cell survival. Cells were replated at an expanded 1:3 ratio onto Geltrex™ coated 6-well Nunc™ plates (plates coated as described in Section 2.3.1). Media was exchanged with fresh NE media the day after plating and then every 48 hours until NPCs were confluent for the next passage. NPCs were passaged 4 times at which point they were used for future differentiation or cryopreserved for future use (see Section 2.3.6 for cryopreservation method).

2.3.3 Differentiation of NPCs into astrocytes

NPCs were plated at low density onto Geltrex™ coated (detailed in 2.3.1) 6-well Nunc™ plates at 15,000 cells/cm^2 in NE media with added RevitaCell™ supplement (1:100). After 24 hours, media was replaced with Astrocyte Medium (ScienCell, CA, USA) at 2 mL/well (**day 1**). Astrocyte Medium is composed of basal medium, fetal bovine serum (FBS) (1:50)

and astrocyte growth supplement (1:100). Media was again replaced after a further 24 hours, and then every 48 hours at 2.5 mL/well. After approximately 6 days as cells began to reach confluency (90%+) they were passaged at the same density, using the same method as described in 2.3.2 but with the appropriate Astrocyte Medium. From day 30, fetal bovine serum was removed from the Astrocyte Medium. At this point, cells could be passaged at a 1:3 ratio approximately once per week. Cells were grown in this way and expanded up to day 120. Day 60 cells were cryopreserved (see 2.3.6) for future assays.

2.3.4 Differentiation of NPCs into neurons

Nunc™ Cell-Culture treated plates (6-well or 96-well Black/Clear Bottom) were coated with Gibco™ Poly-D-Lysine solution at 140 µL/cm^2. Plates were left at RT for 1 hr, and then washed with sterile ultrapure H_2O at 4x the volume of poly-d-lysine used. Wells were aspirated and left to evaporate at RT for 1 hr. Cells were then coated with Laminin from Engelbreth-Holm-Swarm murine sarcoma basement membrane (Sigma-Aldrich, MO, USA) using a 10 µg/µL solution made up in ice cold DMEM/F-12 medium and plated at 112 µL/cm^2. Plates were incubated at 37°C for a minimum of 1 hr to overnight. Laminin solution was aspirated prior to neuron plating.

For terminal plating of NPCs into neurons, cells were counted and plated at low density as a single cell suspension (17,000 cells/cm^2). Cells were plated in Neurobasal™ Plus Medium that is composed of a base Neurobasal™ Plus Medium with B-27 Plus supplement (1:50) and GlutaMAX™ Supplement (1:100). Additional RevitaCell™ supplement (1:100) was added to aid cell survival during plating. To aid differentiation, the γ-secretase inhibitor DAPT (Sigma-Aldrich, MO, USA) was added at 10 µM along with 200 µM L-ascorbic acid (Sigma-Aldrich, MO, USA). CultureOne™ Supplement was also added (1:100) to reduce unwanted neural progenitor proliferation. Cells were kept in this media for 7 days, and media was changed with 70% aspiration to prevent neuron exposure to air. Media was changed at 100 µL/well volumes for 96-well plates, and 2 mL/well for 6-well plates. Media was changed on day 2, 4 and 6. After 7 days, DAPT and L-ascorbic acid were removed from the media. To maintain neurons, media was changed every 72 hours.

2.3.5 Plating of differentiated astrocytes for tau spiking assays

Cryopreserved day 60 astrocytes were thawed as described in **Section** 2.3.7. Astrocytes were thawed onto Geltrex™ coated 6-well Nunc™ plates as detailed in 2.3.1, or onto Nunc™ Cell-Culture treated 96 well black optical bottom plates coated with Gibco™ Poly-D-Lysine solution at 140 µL/cm^2 (as described in 2.3.4), and then coated with 50 µL Geltrex™ as described in 2.3.1. Astrocytes were counted using a haematocytometer and plated at 15,000 cells/cm^2 in astrocyte media. For experiments lasting in excess of 7 days, cells were plated at 7,500 cells/cm^2 and treated with 5 µM 1-β-D-Arabinofuranosylcytosine (AraC) (Sigma-Aldrich, MO, USA) for 24 hrs to reduce proliferation. 24 hrs after plating, cells were ready for experiments.

2.3.6 Cryopreservation of cells

The cryopreservation of all cell types used during this project was performed in the same way. Once cells reached 80-100% confluency, media was aspirated and the cells were dissociated by adding room temperature StemPro™ Accutase™ (or Versene™ in the case of iPSCs) solution at 0.125 mL/cm^2 and incubating for 5 minutes at 37°C. Cells were then gently dislodged using a p1000 pipette, and the resulting cell solution was moved to a centrifuge tube containing prewarmed (37°C) DMEM/F-12 medium at twice the volume of Accutase™ solution used. Cells were spun down at 190 x *g* for 2 min. The resulting pellet was resuspended in the maintenance medium for the appropriate cell type made up with 10% dimethyl sulfoxide (Sigma-Aldrich, MO, USA). Cells were thoroughly resuspended at approximately 1 mL per well of 6-well plate (scaled up or down accordingly). The resulting cell suspension was instantly transferred into cryovials at 1 mL per vial. Vials were quickly moved to Corning™ CoolCell™ LX Cell Freezing Vial Containers (Corning, NY, USA) and then to -80°C freezers. After a minimum of 24 hours and maximum of 7 days, vials were transferred to liquid nitrogen storage containers for long term storage at approximately -170°C.

2.3.7 Plating of cryopreserved cells

All cell types were thawed in the same way. Cell vials were retrieved and stored on dry ice prior to use. Vials were then thawed quickly in a Lab Armor Bead heat bath at 37°C. The cell suspension was moved into a 15 mL centrifuge tube and pre-warmed (37°C) DMEM/F-12

medium was added dropwise to at least twice the volume of the cell suspension. The resulting cell suspension was pelleted by centrifugation at 190 x *g* for 2 min in benchtop centrifuge. The media supernatant was aspirated, and the resulting pellet was resuspended in the appropriate media with added RevitaCell™ supplement (1:100) to aid cell survival.

2.4 Internalisation of human tau by iPSC-astrocytes

2.4.1 Quantification of human brain-derived tau

The concentration of tau in sarkosyl-insoluble pellets was calculated by blotting for total tau (Dako Tau antibody) after SDS-PAGE separation of proteins against known concentrations of recombinant human tau (Human Tau Protein Ladder, 6 isoforms; Sigma-Aldrich, MO, USA; Cat# T7951) as described in Section 2.1.1.

2.4.2 Tau treatment in iPSC-astrocytes

Sarkosyl-insoluble tau that had previously been sonicated in sterile PBS (section 2.1.2) was added to Astrocyte Medium (ScienCell, CA, USA; Cat# 1801) at a tau concentration of 0.1 ng/µL (or median equivalent volume in control derived samples). This concentration was chosen as sufficient tau to measure uptake in majority of cells without excess, after pilot experiments (data not shown) with varying concentrations were tested, based on (unpublished) recommendations from other lab groups. Tau-containing medium was added to day 60 iPSC-astrocytes at 80 µL/well for 96-well plates, 600 µL/well for 12-well plates or 1200 µL/well for 6-well plates or. Cells had been plated at 5,000, 90,000 or 180,000 cells/well respectively the previous day from cryopreserved stocks, plates were coated with Geltrex™ as described previously, as well as Poly-D-lysine for optical 96-well plates. Astrocytes were incubated in tau-containing medium for 1, 3, 5 or 7 days for 7-day time course experiments, and all astrocytes were fixed at end timepoint in ice cold methanol for 5 min at -20°C.

For examination of tau degradation after 7 days, day-60 iPSC astrocytes were plated at 2,500 cells/well in Nunc™ 96-well optical pates and treated with AraC for 24 hours to reduce excessive proliferation over time. After, tau-containing media was added at 80 µL/well for 7 days. 7-day time point was fixed in 70 µL/well of ice-cold methanol for 5 min at 20°C. For later timepoints, media were aspirated, cells washed in Astrocyte medium, and then replaced

with fresh Astrocyte medium at 80 µL/well. 200uL of sterile water was added to surrounding empty wells in order to reduce evaporation over time. For day 14 astrocyte plates cells were fixed as detailed above. Other day 21 timepoint astrocytes were washed and replaced with fresh astrocyte media as above and fixed at day 21 in methanol as detailed above. Astrocytes were immunolabelled as per section 2.5.3.

2.4.3 Astrocyte conditioned media

Day-60 iPSC astrocytes were plated in Geltrex™ coated 12-well plates at 90,000 cells/well and the next day were treated with tau-containing astrocyte media, as detailed in 2.4.2, for 5 days. Cells were then washed in Astrocyte media to remove residual tau, remaining media was aspirated and replaced with Neurobasal™ Plus Medium at 600 µL/well. After 3 days media was collected and added to pre-plated day 7 neurons in Nunc™ optical 96-well plates (as detailed in 2.3.4) at 80 µL/well for 3 days. At this point, cells were fixed in ice-cold methanol for 5 min at -20°C as describe previously, using 80% partial media changes to be careful not to expose neurites to air. Neurons were immunolabelled as per section 2.5.3.

2.5 Immunostaining

2.5.1 Immunohistochemistry of human tissue

Formalin-Fixed Paraffin-Embedded brain (7 µm) sections were prepared by technicians at the London Neurodegenerative Diseases Brain Bank. To remove paraffin, slides were rested on heat blocks set to 95°C for 30 sec. They were then submerged in pure xylene for 2 x 5 min, followed by 2 x 5 min in 100% ethanol. They were then washed for 5 min in ultrapure H_2O.

A common antigen retrieval step was used for all antibodies in this project. Slides were submerged in sodium citrate solution (10 mM trisodium citrate dehydrate (VWR, Radnor, PA, USA), 0.05 % (v/v) Tween-20 in ultrapure H_2O, pH 6.0) in a covered microwaveable container and microwaved at full power for 6 min. After cooling, slides were microwaved twice at low power for 5 min. Slides were then washed twice by submerging in TBS for 5 min.

Blocking of non-specific binding was achieved by adding 100-400 µL (depending on size of the section) of blocking solution composed of TBS with 10% v/v normal goat Serum (NGS, Sigma-Aldrich, MO, USA; Cat# G9023), and was incubated for 1 hr at RT. Where possible,

a hydrophobic circle was drawn on the slide around the tissue to allow for easy application of solutions. The blocking solution was gently tapped off and replaced with primary antibody made up in blocking solution (See Table 2.2). Slides were incubated with primary antibodies in humidified chambers at 4°C overnight. The next day, the primary antibody solution was removed and slides washed twice in TBS for 5 min. Appropriate secondary antibodies (see Table 2.3) prepared in blocking solution were added to sections and incubated in a humidified chamber at RT for 1 hr while protecting from light.

To reduce autofluorescence slides were washed twice in TBS and incubated with sudan black solution for 10 min. Sudan black solution was prepared by mixing 300 mg Sudan Black B high purity stain (Thermo Fisher Scientific™; MA, USA) in 100 mL 70% ethanol and filtering twice to remove impurities. Slides were washed twice for 10 min in TBS. Nuclei were stained by incubating with Hoescht 3342 (Thermo Fisher Scientific™; MA, USA) diluted 1:1000 in TBS for 10 min. Slides were washed in TBS prior to coverslipping with ProLong™ Gold Antifade Mountant (Thermo Fisher Scientific™; MA, USA).

2.5.2 Immunohistochemistry of free-floating mouse brain sections.

Free floating brain sections were washed in PBS and TBS for 5 min to remove cryoprotectant. Slices were then permeabilised in 0.25% (v/v) triton-x-100 in 1 X TBS (TBS-T) for 30 min at RT. Non-specific antibody binding was blocked by incubating sections in 5% (v/v) NGS in TBS-T for 1 hour at RT. Primary antibodies were prepared in 1% blocking solution and added to sections for overnight incubation in a high humidity chamber at 4°C. Sections were washed with TBS on a gentle rocker for 30 min (x3) and then incubated with secondary antibodies diluted in 1% NGS in TBS-T for 2 hours at RT. Following washing, sections were mounted onto Superfrost Ultra Plus slides using Flouromount-G™ with DAPI (Thermo Fisher Scientific; MA, USA).

In order to reduce further non-specific binding, mouse sections treated with mouse derived antibodies were incubated with M.O.M.® (Mouse on Mouse) Blocking Reagent for 2 hours according to the manufacturer's instructions (Vector Laboratories, CA, USA), utilising approximately 3- 4 drops of M.O.M reagent in 2.5 mL of 1 X TBS.

2.5.3 Immunocytochemistry

Cells grown on Nunc™ Cell-Culture treated plates were fixed by removing 70% of remaining media, replacing with ice-cold pure methanol and incubating at -20°C for 5 min. Wells were then washed twice with double the amount of Dulbecco's PBS containing calcium and magnesium (DPBS w/ Ca^{2+}/Mg^{+}) (Thermo Fisher Scientific; MA, USA). Care was taken not to expose cells to air. Plates were stored at 4°C until ready for use.

Non-specific antibody binding was blocked by incubating wells with blocking solution containing 5% v/v NGS (Sigma-Aldrich, MO, USA) in DPBS w/ Ca^{2+}/Mg^{+} for 1 hr at RT at 50 µL per well of a 96-well plate. Blocking solution was then removed and primary antibodies diluted in blocking solution were added at 50 µL per well of a 96-well plate. See Table 2.2 for list of antibodies and appropriate dilutions. Cells were incubated in primary antibody solution overnight on a gentle rocker at 4°C. Primary solution was removed, wells were washed twice in DPBS w/ Ca^{2+}/Mg^{+}, and secondary antibodies made up in blocking solution were added for 1 hr at RT (see Error! Reference source not found.). Wells were then washed twice in DPBS w/ Ca^{2+}/Mg^{+} and counterstained with Hoescht 33352 (Thermo Fisher Scientific™; MA, USA) diluted 1:1000 in DPBS w/ Ca^{2+}/Mg^{+} for 10 min at RT. Cells were washed a final two times and stored in DPBS w/ Ca^{2+}/Mg^{+} at 4°C until ready for imaging.

2.5.4 Image acquisition

Imaging was performed at the Wohl Cellular Imaging Centre at King's College London, Denmark Hill campus.

Images of plate grown cell cultures were captured on a confocal Opera Phenix high content screening system (Perkin Elmer; MA, USA) using a 20X dry lens and covering up to 25 fields per well. Images were taken after laser excitation of Alexa Fluor® (Thermo Fisher Scientific; MA, USA) fluorophores using a laser at wavelengths of 385 nm, 488 nm, 561 nm or 640 nm. Images were taken and analysed using Harmony High-Content imaging and analysis software.

All images of plate grown astrocytes were imaged as a Z-stack over 10 heights 1.0 µm apart in order to determine tau contained within cells. The 20X air lens had a NA of 0.4, and set to 'Binning 1' this gives an effective Z resolution of 6.4 µm for 488 channel (GFAP) and 8.1 µm for 647 channel (AT8). This appeared sufficient to judge that tau was indeed internalised

within the astrocyte and not bound to the membrane. Internalisation has also been confirmed by pilot data that utilised 40X lens (Data not shown), with a Z resolution of 2.8-3.3µm, and demonstrated clear AT8 positive signal within the cell volume of approximately 15 µm.

For analysis, a maximum projection image of collapsed Z-stack was used. All plates used Hoescht 33342 to detect nuclei, and GFAP immunolabelling to detect astrocytes (see 2.7 for antibody list). GFAP was chosen as a general astrocyte marker as it was seen to label all iPSC-astrocytes in culture (data not shown) and its expression is relatively uniform across cell body compared to ALDH1L1 and S100B, enabling the best cell detection with Harmony software. A third channel was utilised for phospho-tau AT8 immunolabelling, in order to visualise tau aggregates and distinguish between the endogenous astrocytic tau. In some experiments, a fourth channel was used to measure S100B immunolabelling and measure endogenous astrocyte changes and association with internalised tau aggregates. Channels were imaged sequentially to avoid bleed-through.

Images of slide mounted sections were captured on either the Inverted Nikon Ti-E Live Cell 3 Camera Microscope (Nikon; Tokyo, Japan), or the Upright Confocal Nikon A1RHD2 microscope, at 20X or 40X magnification using a dry lens. Nikon Elements software was used to process and export the images. See 2.7 section for antibodies used. Fluorescent channels were imaged sequentially to avoid bleedthrough.

2.5.4.1 Astrocyte analysis from mouse tissue using ImageJ

Fiji ImageJ software (Schindelin et al., 2012) was used to trace the astrocytes after images were obtained from slide mounted brain sections as detailed above. Astrocyte tracing was completed by using the Simple Neurite Tracer located in the included Neuroanatomy Plugin.

2.5.4.2 Image pipeline analysis of iPSC-astrocytes on Harmony software

For astrocyte tau uptake imaging analysis, cells were identified by 'Find Nuclei' function using nuclear staining (Hoechst 33342). Intensity and morphology properties of nuclei were calculated, and 'Select Population' function was trained using the 'Linear Classifier' method to separate small, round, high intensity nuclei as 'Dying cells' (Kerr, 1971; Kerr et al., 1972) and large, dull less round nuclei as 'Healthy cells', in order to avoid detection of apoptotic nuclei and false detection of cells. The outline of astrocytes were identified by

immunofluorescence of GFAP labelling (see section 2.7 for antibodies used for ICC) and through the 'Find Cytoplasm' function of Harmony analysis pipeline of nuclei detected as 'Healthy cells'.

For internalised tau detection, AT8 intensity (maximum, average) was detected within the outlines of GFAP positive astrocytes using the 'Calculate intensity properties' function. 'Find Spots' was also used to detect larger aggregates relative to background, and from this volume and intensity properties of these aggregates could be calculated, including intensity of GFAP and S100B channels.

Astrocytes were distinguished into 'High AT8' and 'Low AT8' by a 'Select Population' function and trained by 'Linear Classification' method that took into account detected AT8 spot properties, the relative number of spots per area of cells, and AT8 intensity properties of cells as a whole. These populations could then be used for separate analysis of GFAP and S100B intensity properties.

'Calculate Morphology Properties' function was used to calculate size and roundness of detected astrocytes in determined cell populations.

2.6 SDS-PAGE and Western blotting

2.6.1 Protein assays

The protein concentration of samples from human post-mortem tissue, organotypic brain slices or cell lysate was measured using the BCA Protein Assay Kit [Pierce, USA) according to the manufacturer's instructions. A BSA standard consisting of eight known protein concentrations was freshly prepared in the corresponding homogenisation/lysis buffer at concentrations ranging from 0-2 mg/mL. In brief, duplicate samples were appropriately diluted (typically 1/5 for human samples and 2/5 for cell lysates) in lysis buffer directly into a 96-well plate. Reagent A was mixed with reagent B at a ratio of 70:6. 100 µL of the solution were added into each well and the plate was covered with aluminium foil. Samples were incubated at 37 ºC for 30 min. The absorbance was then measured at 592 nm using a microplate reader (Clariostar, BMG Labtech) and values were extrapolated from the standard curve generated using the MARS analysis software (BMG Labtech) to determine protein concentration in mg/mL.

Tissue homogenates were diluted in the corresponding homogenisation buffer to ensure an equal protein concentration across different samples. For immunoblotting, approximately 18 µg of human homogenates or samples of mouse brain were loaded per well.

2.6.2 Sodium dodecyl sulphate-polyacrylamide gel electrophoresis (SDS-PAGE) and western blotting

Unless otherwise stated, all western blotting reagents and equipment were manufactured and provided by Thermo Fisher Scientific (MA, USA) under the Invitrogen™ brand.

Samples were prepared in 2 X Sample Buffer or NuPage sample buffer and reducing agent. Samples were heated at 95°C on a heating block for 5 min to denature proteins and samples were loaded into NuPAGE™ Bis-Tris 4-12% precast gels in the XCell SureLock™ Mini-Cell system and run with MOPS-SDS (1X) or MES-SDS (1X) running buffer. Gels were run at a constant 120V voltage until bands reached bottom of the gel. A protein ladder (3 µL) Precision Plus Protein™ WesternC™ Blotting Standards (Bio-Rad; CA, USA) was added to the first well.

Gels were moved to an XCell II™ Blot Module for transfer in transfer buffer (2 mM Tris-Base, 192 mM glycine, 20 % methanol) onto an Amersham™ Protran® 0.45 µm nitrocellulose membrane (Cytiva; Amersham, UK) at constant 0.3 A for 1 hr while keeping the module cold.

Non-specific antibody binding on membranes was blocked by incubation with Intercept® (TBS) Blocking Buffer (LI-COR Biosciences; NE, USA) for 1 hr at RT. Membranes were incubated with primary antibodies (Table 2.2) diluted in Intercept® (TBS) Blocking Buffer with 0.1% (v/v) Tween® 20 (Sigma-Aldrich, MO, USA) overnight at 4°C. Membranes were washed three times for 5 min each on a shaker in TBS with 0.1% Tween® 20 (TBS-T). Secondary antibodies (Table 2.3) were diluted 1:5000 in Intercept® (TBS) Blocking Buffer with 0.1% (v/v) Tween® 20 and incubated with membrane for 1 hr at RT. Membranes were washed thrice on a shaker for 5 min in TBS-T and a final time in TBS only (to remove detergent that may cause autofluorescence). Membranes were imaged using the Odyssey CLx Imager (LI-COR Biosciences; NE, USA). A semi-quantitative analysis of band densitometry was performed manually by selecting each detected lane. Background

readings for each sample were subtracted automatically using Image Studio Lite (LI-COR Biosciences; NE, USA).

2.7 Antibodies used in this thesis

Table 2.2 Primary antibodies.

Primary antibodies detailed with their clonality (polyclonal/monoclonal), target protein, host species, manufacturer/catalogue number and the typical dilution used for immunofluorescence of plated cells (ICC) or slide mounted tissue (IHC) or SDS-PAGE western blotting (WB).

Antibody	Target	Host	Clonality	Manufact. (cat#)	Dilution used		
					ICC	IHC	WB
GFAP	Glial fibrillary acidic protein	Rb	Poly	Agilent Dako; CA, USA (Z0334)	1:500	1:500	1:1000
GFAP	Glial fibrillary acidic protein	Ch	Poly	Thermo Fisher Scientific™; MA, USA; (PA1-10004)	1:500	1:500	1:1000
S100β	S100 calcium binding protein B	Rb	Poly	Proteintech Group; IL, USA; (15146-1-AP)	1:500	1:500	-
ALDH1L1	aldehyde dehydrogenase 1 family, member L1	Rb	Poly	Proteintech Group; IL, USA; (17390-1-AP)	1:500	-	1:1000
Tau	Tau protein (all isoforms)	Rb	Poly	Agilent Dako; CA, USA (A0024)	1:500	1:500	1:2000
AT8	Phospho-Tau (Ser202, Thr205)	Ms	Mono	Thermo Fisher Scientific™; MA, USA; (MN1020)	1:300	1:300	1:1000
PHF1	Phospho-tau	Ms	Mono	Peter Davies;	1:300	1:500	1:1000

	(Ser396, Ser404)			Feinstein Institute Medical Research (NY, USA)			
MC1	Tau (conformation dependent)	Ms	Mono	Peter Davies; Feinstein Institute Medical Research (NY, USA)	1:300	1:300	-
T22	Specifically recognises tau oligomers and fibrils but not monomeric tau.	Rb	Poly	Merck Millipore, Billerica MA, USA (ABN454)		1:250	
RD3	3R Tau (amino acids 209–224)	Ms	Mono	Merck Millipore, Billerica MA, USA(05-803)			1:500
LAMP1	lysosomal-associated membrane protein 1	Rb	Poly	Proteintech Group; IL, USA; (21997-1-AP)	1:500	-	-
GLAST (EAAT1)	solute carrier family 1 (glial high affinity glutamate transporter), member 3	Rb	Poly	Proteintech Group; IL, USA; (20785-1-AP)	1:500	-	-
EAAT2	solute carrier	Rb	Poly	Proteintech Group; IL,	1:500	-	-

	family 1 (glial high affinity glutamate transporter), member 2			USA; (20785-1-AP)			
β-actin	beta-actin (amino acids 1-100)	Ms	Mono	Abcam Plc., Cambridge, UK (ab8226)			1:5000
GAPDH	Mouse, rat and human glyceraldehyde 3-phosphate dehydrogenase (GAPDH)	Ms	Mono	Santa Cruz Biotechnologies Inc., Santa Cruz, CA, USA (sc-32233)			1:1000

2.7.1 Secondary antibodies

Table 2.3 Secondary antibodies.

Secondary antibodies detailed with their clonality (polyclonal/monoclonal), target species immunogen, host species, manufacturer/catalogue number and the dilution used for immunofluorescence of plated cells (ICC) or slide mounted tissue (IHC) or SDS-PAGE western blotting (WB).

Antibody	Target	Host	Clonality	Manufact. (cat#)	dilution used		
					ICC	IHC	WB
Goat anti-Mouse,	Mouse IgG	Goat	Poly	Thermo Fisher Scientific™;	1:500	1:500	-

Alexa Fluor 680				MA, USA; (A-21057)			
Goat anti-Rabbit, Alexa Fluor 568	Rabbit IgG	Goat	Poly	Thermo Fisher Scientific™; MA, USA; (A-11011)	1:500	1:500	-
Goat anti-Rabbit, Alexa Fluor 488	Rabbit IgG	Goat	Poly	Thermo Fisher Scientific™; MA, USA; (A-11034)	1:500	1:500	-
Goat anti-Chicken, Alexa Fluor 568	Chicken IgY	Goat	Poly	Thermo Fisher Scientific™; MA, USA; (A-11041)	1:500	1:500	-
IRDye® 680RD Goat anti-Mouse	Mouse IgG	Goat	Poly	LI-COR Biosciences; NE, USA; (926-68070)	-	-	1:5000
IRDye® 800CW Goat anti-Rabbit	Rabbit IgG	Goat	Poly	LI-COR Biosciences; NE, USA; (926-32211)	-	-	1:5000
IRDye® 680RD	Rabbit IgG	Donkey	Poly	LI-COR Biosciences;	-	-	1:5000

Donkey anti-Rabbit			NE, USA; (926-68073)			
IRDye® 800CW Donkey anti-Goat	Goat IgG	Donkey	Poly	LI-COR Biosciences; NE, USA; (926-32214)	-	-	1:5000

2.8 Gene expression analysis

All reagents used for the following methods, unless otherwise stated, were made and supplied by Thermo Fisher Scientific™ (MA, USA) under the Invitrogen™ brand. All consumables and reagents used were molecular grade and certified nuclease and RNAase/DNAase free.

2.8.1 Cell lysis

Cells were quickly washed in pre-warmed DMEM/F-12 to remove cellular debris. Cells were then lysed with TRIzol™ Reagent (cat# 15596026) at approximately 0.4 mL reagent per 1 x 10^5 cells, which equates to approximately 0.5 mL reagent per confluent well of a 6-well plate. After 30 sec, the solution was pipetted up and down to homogenise cells. Lysates were collected in 1.5 mL microcentrifuge tubes and stored at -80°C.

2.8.2 RNA extraction of cell lysates

Cell lysates were transferred (maximum 1.4 mL, minimum 0.3 mL) to a Phasemaker™ Tube (cat# A33248) which had been pre-spun at 1000 x *g* for 60 seconds. To this, 100 µL of 1-Bromo-3-chloropropane (BCP) was added (Sigma-Aldrich; MO, USA) per 1 mL of lysate (minimum 100 µL BCP). Tubes were shaken vigorously by hand for 10 sec, and incubated at room temperature (RT) for 5 min. Tubes were then centrifuged in a cooled (4°C) benchtop centrifuge at 16,000 x *g* for 10 min. The top clear aqueous layer was then transferred to a 1.5 mL microcentrifuge tube. To help visualise the RNA pellet, 1 µL of RNA grade glycogen was added. To this, RT isopropanol was added at 500 µL per 1 mL of original lysate used. Tubes were vortexed and RNA allowed to precipitate for 60 min at RT. The tubes were then

centrifuged at 16,000 x g for 15 min at 4°C. Supernatants were discarded and the white RNA pellets washed twice with 80% (v/v) ethanol in nuclease free water. After the final wash, the supernatant was carefully removed, and the tubes left open on a 40°C heating block for 5 min to allow for any remaining ethanol to evaporate. To the pellet, 21.5 µL of nuclease free water was added. Tubes were spun down and placed on a heating block at 50°C for 5 min to aid solubilising of RNA. Samples was stored at -80°C. The RNA concentration and purity of the resulting samples was determined using the NanoDrop™ One/OneC Microvolume UV-Vis Spectrophotometer. Pure RNA has an absorbance ratio of A280/A260 of 2.0 approximately, whereas the A260/A230 ratio should be above 2.0 [T042-Technical Bulletin, Thermo Scientific].

2.8.3 Reverse transcription

Purified RNA was reverse transcribed into complementary DNA (cDNA) using Maxima H Minus First Strand cDNA Synthesis kits with dsDNase (cat# K1681) using between 1 and 5 µg of RNA. The protocol was carried out as per manufacturer instructions, without the use of random hexamer primers. Briefly, RNA normalised to 1 µg that had previously been quantified on the NanoDrop™ One was incubated with DNAase to remove any residual genomic DNA, and then mixed with oligo(dT)18, 10 mM dNTP Mix and nuclease free water and incubated as per manufacturer instructions to generate cDNA, which was then diluted 5-fold in nuclease free water and stored at -20°C until required. In subsequent qPCRs, 2 µL or 1 µL was used per reaction in 96-well or 384-well plates respectively.

2.8.4 Primers for RT-qPCR

The following primers were designed to cover the majority of isoforms of each gene of interest as determined using the USSC Genome Browser Gateway (Kent et al., 2002) with the 2013 Human genome assembly. Primers were ordered from Integrated DNA Technologies (IA, USA) as purified 25 nmole DNA Oligo powder which were then hydrated to 100 µM using nuclease-free water. Primers were stored at -20°C for long term storage (+6 month) or at 4°C for short term use. Primers were diluted to 5 µM for use in subsequent qPCR reactions.

Table 2.4 Primer sequences.
Forward and reverse primer sequences for each gene used in qPCR.

Gene	Forward (5' – 3')	Reverse (5' – 3')
0N MAPT	GCTGGCCTGAAAGCTGAAG	ATCGCTTCCAGTCCCGTCT
1N MAPT	CAACAGCGGAAGCTGAAGAA	GTGACCAGCAGCTTCGTCTT
2N MAPT	ACTCCAACAGCGGAAGATGT	GTGACCAGCAGCTTCGTCTT
3R MAPT	AGGCGGGAAGGTGCAAATA	GCCACCTCCTGGTTTATGATG
4R MAPT	CGGGAAGGTGCAGATAATTAA	TATTTGCACACTGCCGCCT
ALDH1L1	CCAAAGTCCTGGAGGTTGAA	TAACTCCAGGCCATCACACA
B-ACTIN	TCGTGCGTGACATTAAGGAG	AGGAAGGAAGGCTGGAAGAG
C3	AAAAGGGGCGCAACAAGTTC	GATGCCTTCCGGGTTCTCAA
CRYAB	GCCTGGAGAAGGACAGGTT	ATGTTTTCCATGCACCTCAA
EAAT1	TCAAGTTCTGCCACCCTACC	AATGAAAATGGCAGCCAAAG
EAAT2	TCAGTCAATGTTGTGGGTGA	GTTGCTTTCCCTGTGGTTCT
GAPDH	AGCCTCAAGATCATCAGCAA	CTGTGGTCATGAGTCCTTCC
GFAP	GAGTCCCTGGAGAGGCAGAT	GTAGGTGGCGATCTCGATGT
IL3	GACAAGCTGGGTTAACTGCTC	GTCTTCCCCATTGAGGTTGT
LCN2	CTCCACCTCAGACCTGATCC	TGGTGGCATACATCTTTTGC
LRP1	CTTGCATCAGCCCACACC	GCCAGCCCTTTGAGATACAG
MAP2AB	AAACTGCTCTTCCGCTCAGACACC	GTTCACTTGGGCAGGTCTCCACAA
MAPT	GTCGAAGATTGGGTCCCT	GACACCACTGGCGACTTGTA

NRF2	GCGACGGAAAGAGTATGAGC	GTTGGCAGATCCACTGGTTT
OCT4	TTGGGCTCGAGAAGGATGTG	GTGAAGTGAGGGCTCCCATA
PAX6	GCCAGAGCCAGCATGCAGAACA	CCTGCAGAATTCGGGAAATGTCG
S100β	AAAGAGCAGGAGGTTGTGGA	CGTGGCAGGCAGTAGTAACC
SOX9	AGGTGCTCAAAGGCTACGAC	GCTTCTCGCTCTCGTTCAGA
SERPIN3A	CGTGGTGGAGCTGAAGTACA	GCCCAGCTGGAGAAGTATGT
STAT3	GGCATTCGGGAAGTATTGTCG	GGTAGGCGCCTCAGTCGTATC
TFEB	CCAGAAGCGAGAGCTCACAGAT	TGTGATTGTCTTTCTTCTGCCG
TUJ1	CCCGTTATCCCAGCTCCAATATGCT	ATGGCTTGACGTGCGTACTTCTCC

2.8.5 RT-qPCR

Real time quantitative polymerase chain reaction (RT-qPCR) experiments were performed using PowerUp™ SYBR™ Green Master Mix on the QuantStudio™ 7 Flex Real-Time PCR System. For 96-well PCR plates, each reaction consisted of 10 µL master mix, 2 µL of 5 µM primers (forward and reverse primers combine) and 2 µL of cDNA product, normalised previously by equal RNA concentration used in the RT step. 8 µL of nuclease free water was added for a total 20 µL reaction volume. For 384-well PCR plates, quantities were halved for a total of 10 µL reaction volume.

Analysis of gene expression was performed using the comparative CT method relative to a control sample, using the equation of $2\Delta\Delta C_T$ = [(CT gene of interest – Ct internal controls) sample A – (Ct gene of interest – Ct internal control) sample B] with average of two internal control genes β-ACTIN and GAPDH. The fluorescence threshold was set automatically by the proprietary QuantStudio™ Real-Time PCR Software v1.7.1, utilising a 'baseline threshold algorithm' that subtracts a baseline component and sets a threshold in the exponential region of the Amplification Plot. No template controls (NTC) were used to check for contamination

or primer-dimer amplification and 'Undetermined' Ct values were confirmed in NTCs before proceeding with analysis of sample data. Any undetermined Ct values in sample data therefore indicated no detectable gene expression. Gene expression was measured relative to a control sample (iPSC or untreated astrocytes or human postmortem brain) that showed some detectable expression (a valid Ct value). The melt curve was used to confirm only one product was created during the PCR run.

Run method was as follows:

Hold stage: 50°C for 2 min (1.6°C/s). 95°C for 2 min (1.6°C/s). PCR Stage (40 cycles): 95°C for 15 sec, 60°C for 15 sec, 72°C for 1 min (1.6°C/s). Melt Curve Stage: 95°C for 15 sec (1.6°C/s), 60°C for 1 min (1.6°C/s), 95°C for 15 sec (0.15°C/s).

2.9 Data analysis and statistics

All data in this thesis was statistically analysed using GraphPad Prism 9.0 software (La Jolla, USA). To detect differences between three or more groups according to the sample distribution, either non-parametric Kruskal-Wallis H test with Dunn's post-hoc analysis or one-way analysis of variance (ANOVA) with Holm-Šidák's test for multiple comparisons was used. These tests were chosen to maximise power without the need to generate confidence intervals in the case of the Holm-Šidák's test. An unpaired student's t-test or Welch's *t*-test was used to evaluate differences between two groups under the assumption of equal or unequal variances, respectively. For analysis of data with more than one independent variable, analysis was performed by two-way ANOVA with post-hoc Holm-Šidák's test for multiple comparisons. All data in this thesis were presented as mean ± standard error of the mean (SEM), unless replicates were not available for a given data point. The number of biological independent experiments (n) can be found in the figure legends. For iPSC-astrocyte experiments, n refers to separate experiments performed on independently differentiated astrocytes from one control iPSC line. Results were considered statistically significant when p-value <0.05. Asterisks indicate the degree of statistical differences as follows: *p<0.05, **p< 0.01, ***p< 0.001, ****p<0.0001.

3 Astrocyte association with pathological tau seeds *in vivo*

3.1 Introduction

The tau that is deposited in tauopathies has unique filament structures (Shi et al., 2021) that may determine spreading patterns during disease because of cell- and region- specific vulnerability to different types of tau (Jucker and Walker, 2018) (see section 1.3.4). It is therefore important to study the pattern and cell-type localisation of pathogenic tau aggregates to develop an understanding of the causes of this regional vulnerability to tau in different diseases. For this purpose, this lab developed a new mouse model of tau spread utilising htau mice. Htau mice express the entire wild-type human tau gene in the absence of endogenous mouse tau (Andorfer et al., 2003). Alternative splicing leads to the expression of both 3R and 4R isoforms, in contrast to adult wild-type mice that have predominantly 4R tau and very little 3R tau expression (McMillan et al., 2008), and this is important when studying tau seeding since tau may need a similar substrate to seed further aggregation (Goedert et al., 2017). Htau mice show the progressive accumulation of hyperphosphorylated tau with age, followed by the deposition of aggregated tau inclusions in somato-dendritic regions of neurons (Andorfer et al., 2003, 2005). This correlates with increased tau associated protein kinases (Kelleher et al., 2007). Htau mice also exhibit evidence of synaptic dysfunction by 12 months of age that is also age-dependent, and is related to deficits in object recognition and spatial memory (Polydoro et al., 2009). A robust impact on food-borrowing behaviour in these mice has also been observed (Geiszler et al., 2016).

To examine regional vulnerability to tau, htau and wild-type mice of an identical genetic background were intraperitoneally injected with tau extracts isolated from postmortem tauopathy (AD, PiD, PSP) and non-diseased control brain. These tauopathies were selected since they display different characteristics. Pathological deposits of tau are first observed in the transentorhinal cortex in AD, then later in the medial and basal temporal lobes, neocortical regions and later the sensory and motor cortex (Braak et al., 2006). In Pick's disease, tau pathology also begins in the entorhinal cortex and particularly the dentate gyrus as well as neocortical regions, spreading to subcortical regions and brainstem nuclei, and the primary motor cortex and nuclei of the medulla, while severe cases can also show tau

pathology in the visual cortex and sometimes in the cerebellar granular layer and white matter of the brainstem (Irwin et al., 2016a). For most PSP cases, tau pathology is first observed in the subthalamus, substantia nigra and globus pallidus, propagating to neocortical and midbrain areas, well as cerebellum, and cortical regions are affected late in disease (Kovacs et al., 2020). Interestingly, tau pathology in astrocytes is prominent in PSP in the form of tufted astrocytes, often preceding neuronal tau pathology in some brain regions, and this disease shows mainly 4R tau inclusions (Kovacs, 2020). Astrocyte involvement in PiD is also common, with astrocytic plaques a defining feature of disease, and in this case it is predominantly 3R tau that is deposited. Glial tau pathology in AD is not a common pathological feature, although tau accumulations in hilar astrocytes has been reported in the dentate gyrus (Richetin et al., 2020b). The unique spreading patterns and cytopathology in these tauopathies prompted this exploration of regional susceptibility to different pathological tau deposits in mice, and study of astrocyte association with the pathological tau deposits.

The rationale for the approach used for this work was based on previous publications showing that intraperitoneal injection of tau aggregates isolated from mice expressing mutant human P301S tau, into mice expressing wild type human tau, resulted in the deposition of tau aggregates in the brain (Clavaguera et al., 2013). Moreover, others showed that similar experiments with Aβ resulted in brain Aβ deposition that was attributed to Aβ entering the bloodstream and crossing into the brain through the (leaky) blood-brain-barrier (Eisele et al., 2010). This suggested that tau entry into the brain via a similar random route might allow investigation of specific regional vulnerabilities to tau aggregates isolated from different tauopathies. Interestingly, preliminary data suggested that tau burden is increased in the cerebellum/brainstem when tau from PiD and PSP, but not AD, brain was injected compared to untreated mice or those injected with control human brain extracts. In the cortex, mice injected with AD, PiD and PSP extracts showed increased presence of tau aggregates compared to controls, whereas no overt changes were noted in the hippocampus. This therefore suggests regional vulnerability to different forms of tau.

The samples collected from this study were further analysed to examine the association of astrocytes with tau deposition resulting from the spread of pathogenic tau seeds from the periphery into the CNS. Previously, direct brain injection of post-mortem brain tissue from PSP and CBD cases was found to induce astrocyte tau inclusions in non-transgenic mice, in

contrast to AD case derived tau (Narasimhan et al., 2017). Interestingly, a follow up study demonstrated that glial tau pathology spread through connected oligodendrocytes, but not astrocytes, in a neuronal tau knockout model (Narasimhan et al., 2020). This suggests that astrocyte tau pathology (Narasimhan et al., 2017) is due to astrocyte uptake of neuronal tau aggregates. Another human tau expressing mouse model also showed PSP and CBD induced tau pathology within astrocytes following seeding of human tauopathy strains, but again this did not result when AD brain tau was directly injected into the brain (He et al., 2020). The propagation in all these models was induced by intracerebral injections, which pre-determines the initial site of tau deposition and the origin of spread. In contrast, the model analysed in this chapter will allow for analysis of tau spread induced by indirect entry, which is predicted to allow random tau entry via a leaky blood-brain-barrier, with vulnerable neurons accumulating tau deposits.

The overarching aims of this chapter were to:

- Characterise the human brain tissues from which tau extracts were obtained by western blot.
- Investigate the brain regions in which tau deposits accumulate by western blot and immunohistochemistry.
- Examine features of the astrocyte response to tau pathology, including measurements of cell numbers, morphology, and markers of astrocyte reactivity.

3.2 Methods

All methods are described fully in Chapter 2.

Briefly, 3-4-month-old mixed gender htau or WT mice received injections of tauopathy human brain extract into the intraperitoneal cavity (see Figure 3.1 for overview). Treatment protocols were based on those previously published by Clavaguera *et al.* (2013). WT treated mice, mice injected with control human brain extracts, and untreated mice were used as controls. The tauopathy brain extracts were prepared from a single PSP case, expected to have a relative abundance of 4R tau aggregates, a single PiD case, where 3R tau aggregates are abundant, and AD, where approximately equal proportions of 3R and 4R tau are expected (see 1.3.3 for details). Mice were aged until they were 18 months old and

sacrificed. The brain was bisected with half being drop-fixed in 4 % (v/v) paraformaldehyde, prior to sectioning for immunohistochemistry (2.5.2). Sections were labelled with antibodies against tau and astrocytes, as indicated below, and imaged using a Nikon A1R confocal microscope (2.5.4). Images were exported and astrocytes analysed using the Fiji plugin for ImageJ (2.5.4.1). The other hemibrain was snap frozen for biochemical assessment following crude dissection into brainstem/cerebellum, hippocampus, and cortex. Tissue samples were processed to isolate sarkosyl-insoluble tau (2.1.2), a process that yields a low-speed supernatant (LSS, total), sarkosyl-soluble high-speed supernatant (HSS) and sarkosyl-insoluble (SI) pellets that contain aggregated tau (Noble et al., 2003). These were used for western blotting.

Figure 3.1 Schematic overview of workflow.

Schematic showing the experimental design. Tau extracted from the temporal cortex of tauopathy (AD, PiD or PSP) and control human post-mortem brain was homogenised in PBS, sterile filtered, normalised for total tau content, and then injected interperitoneally into wild-type or hTau mice at 3-4 months of age. Mice were aged until 18-months and brains taken for biochemical and immunohistochemical (IHC) analysis, focusing on 3 regions - cortex, hippocampus, and the brainstem/cerebellum.

3.3 Results

3.3.1 Characterisation of human tauopathy cases used for injection

Although some initial characterisation of the human brain samples used in this study had previously been conducted, it was important to further examine their main features prior to the rest of the investigations conducted in this chapter. This may allow characteristics of the postmortem tau extracts to be linked with changes induced in mouse brain.

Therefore, the human tauopathy samples were examined by western blot and IHC. Prior to western blotting, samples were processed using standard methods to isolate sarkosyl-insoluble tau (2.1.2). This method, first described by Greenberg and Davies (1991), isolates tau aggregates on the basis of its insolubility in the detergent sarkosyl. Others have shown that tau isolated in this fraction is filamentous and labels by immuno-gold EM with antibodies against phosphorylated tau (Noble et al., 2003). The protocol involves homogenising tissue at 100mg/ml and first isolates a low-speed supernatant (LSS), to which sarkosyl is added, and following ultracentrifugation a sarkosyl-soluble and sarkosyl-insoluble pellet (SI) are collected. The proportion of insoluble tau fraction is calculated relative to the amount of tau in the LSS fraction for each sample. Here, samples from the LSS and SI were examined by western blot using antibodies against total tau (DAKO), tau phosphorylated at Ser396/404 (PHF1) and an antibody specific to 3R tau isoforms (Figure 3.2b). An antibody against Aβ (6E10) was also used to confirm Aβ enrichment in AD, but not PSP, PiD or control cases. β-actin was used as a loading control.

Western blotting with an antibody that detects total (phosphorylated and non-phosphorylated) tau (DAKO) showed several bands of tau between approximately 46-68kDa, as expected (Kelleher et al., 2007). These correspond to individual tau isoforms that are differentially phosphorylated or otherwise modified (Guo et al., 2017). All tauopathy samples demonstrated strong bands in both LSS and SI fractions, with tau in the SI fractions indicating the presence of aggregated sarkosyl-insoluble tau. High molecular weight bands in this fraction are indicative of tau that is extensively modified and/or aggregated. Sarkosyl-insoluble tau from the AD case showed three strong bands of approximately 60-68kDa, which has been previously reported (Sergeant et al., 2005). In contrast, sarkosyl-insoluble tau from the PiD and PSP cases showed relatively lower proportions of sarkosyl-insoluble tau, with more motile, lower kDa, bands. When an antibody that specifically detects tau phosphorylated at Ser396/404 (PHF1), an epitope known to be highly phosphorylated in AD (Hanger et al., 2007) was used, the SI in all tauopathy cases was found to be enriched in phosphorylated tau relative to the LSS. No PHF1+ve tau was detected in samples from the control case. β-actin showed that the concentration of protein in LSS from all samples was approximately equivalent. An antibody against 3R tau was also used since the relative abundance of tau isoforms differs between tauopathies, with AD and PiD tau neuropathology involving 3R tau, unlike PSP (Reid et al., 2020). Immunolabelling with the 3R tau antibody

gave signals for all samples in the low-speed supernatant, as expected. 3R tau was also found to be enriched in the SI fraction from AD and PiD, but not PSP. This is in-keeping with knowledge that tau filaments in AD contain both 3R and 4R forms of tau (Goedert et al., 1989a) that PiD aggregates are predominantly 3R tau (Dickson, 2001; Kovacs et al., 2017), and that 4R tau accumulates in PSP (Dickson et al., 2007; Kovacs et al., 2020). Finally, Aβ was only detected in the LSS and SI of AD samples, as expected.

In the human tauopathy and control brain sections analysed, tau pathology and associated astrocytes were briefly characterised (Figure 3.2b). In control non-diseased brain, GFAP positive astrocytes were observed in the absence of clear AT8 positive tau aggregates. For AD, GFAP positive astrocytes were seen along with AT8 positive structures resembling neurites or NFTs, and some astrocytes were observed in the presence of these tau aggregates, suggesting that astrocytes might respond to tau. In PiD sections, rounded AT8 positive structures are observed, which resemble the rounded 'ballooned' neuronal bodies (Pick bodies) that are a hallmark of PiD pathology in the cortex (Dickson, 2001). Astrocytes appear ramified, as is often described in PiD (Irwin et al., 2016a), and some show co- or close- localisation to AT8. In PSP, GFAP positive astrocytes localised in the proximity of AT8 positive structures, and there were clear examples of GFAP- and AT8- positive tufted astrocytes, which are a characteristic feature of PSP (Nishimura et al., 1992; Dickson et al., 2007).

3.3.2 Characterisation of tau aggregate burden in mice peripherally injected with tauopathy brain extracts

Tau aggregates in AD, PSP and PiD arise and spread from distinct brain regions, as described in the introduction to this chapter (3.1). To determine if peripheral injection of tauopathy extracts into mice recapitulates this regional deposition, the LSS and SI fractions from the cortex, brainstem + cerebellum and hippocampus of peripherally injected wild-type and htau mice were analysed.

Running htau samples by western blot (Figure 3.3a) revealed, as expected, that total tau was present in the LSS of all brain regions for all treatment conditions. PHF1 tau was also present in the LSS of all mice including untreated, and this is expected since mice are known to accumulate phosphorylated tau by 9 months of age (Andorfer et al., 2003). For all brain regions, the amount of total and PHF1+ve tau in the SI fraction appeared to be at higher

levels in control brain extract- and tauopathy brain extract- injected mice compared to untreated mice. In the brainstem/cerebellum, SI tau appeared strongest in the PiD and PSP injected mice. This is contrast to the hippocampus of PiD and PSP extract injected mice, where SI PHF1 +ve tau appeared at lower levels than was observed in mice injected with AD or control brain extracts. β-actin was present as expected in all LSS fractions, and at lower levels in the SI fraction.

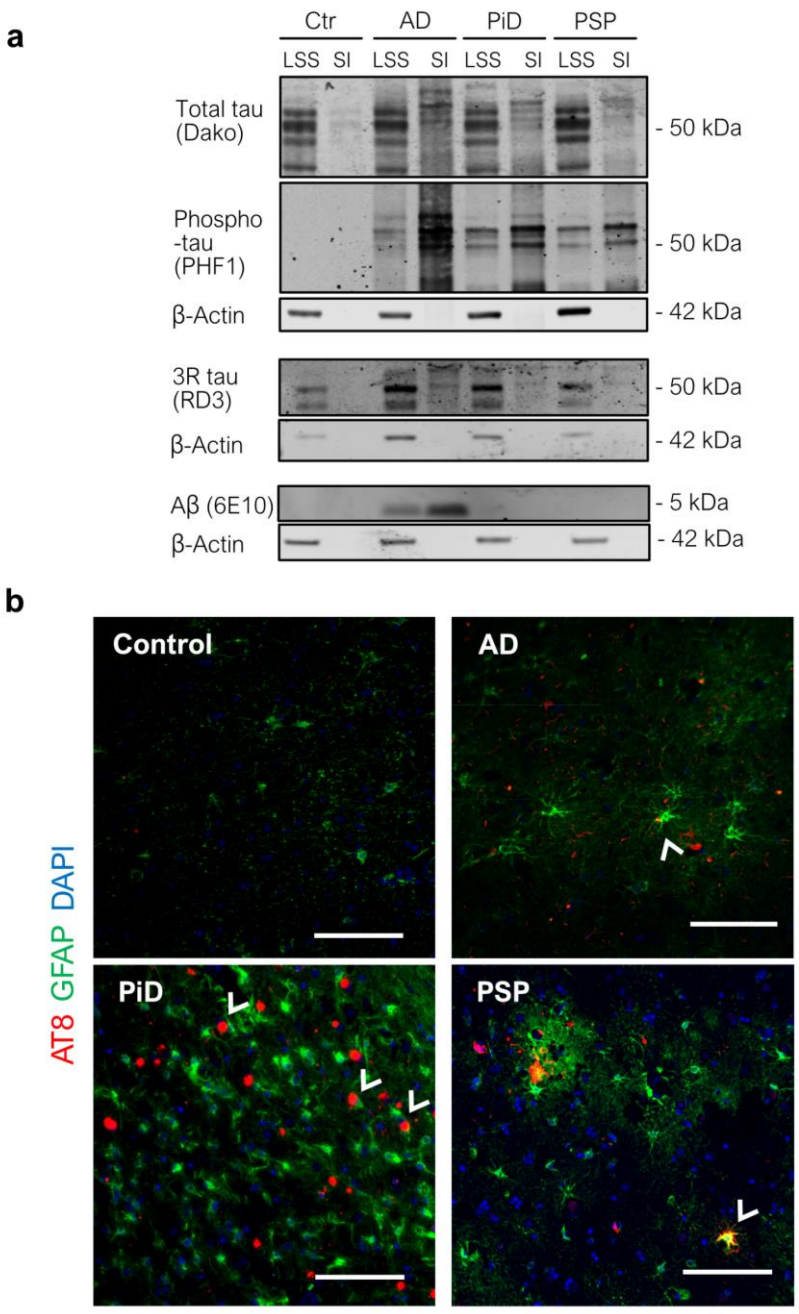

Figure 3.2 Characterisation of human brain tissue used to isolate brain extracts for injection into mice

(**a**) Western blots of the low-speed supernatant (LSS) and sarkosyl insoluble (SI) fraction from human post-mortem control (Ctr), AD, PiD and PSP brain probed with antibodies against total tau (DAKO), phosphorylated tau (Ser396/Ser404) detected by the PHF1 antibody, 3-repeat (3R) tau detected with the RD3 antibody and Aβ (6E10). β-actin was used as a loading control. kDa markers are indicated. (**b**) Representative immunohistochemistry of brain sections from the same cases immunolabelled with the AT8 antibody against phosphorylated tau (Ser202/Thr202) and the astrocyte marker GFAP. Images show merge plus counterstain with DAPI. White arrows indicate examples of astrocyte association with AT8 in AD and PiD and a tufted astrocyte in PSP. White scale bar is 100 μm. n=1.

To quantify the amount of aggregated tau in each sample, the amount of total tau in the SI fraction was quantified relative to the amount of total tau detected in the LSS of the same sample (Figure 3.3b), as previously described (Noble et al., 2003; Kurbatskaya et al., 2016). Data are shown relative to values for control human brain extract-injected samples. In the cortex, the quantified data shows that there are higher levels of aggregated tau relative to total tau for all mice injected with tauopathy brain extracts relative to control brain injected mice, which showed similar levels to untreated mice. A Kruskal Wallis one-way ANOVA analysis indicated that tauopathy injection significantly altered the presence of aggregate tau ($H(4) = 16.19$, $p = 0.003$), and Dunn's pairwise comparison revealed significant increase following injection of htau mice with AD and PSP extracts, relative to control brain injections ($p = 0.017$ and 0.036 respectively). In the brainstem and cerebellum, a significant increase in aggregated tau was observed in mice injected with PiD and PSP extracts relative to control. Again, Kruskal-Wallis one way ANOVA analysis revealed that aggregated tau present in the brainstem + cerebellum was significantly increased following injection of htau mice ($H(4) = 19.11$, $p = 0.0007$), and Dunn's pairwise comparison indicated this was significant in PiD and PSP injected mice ($p = 0.037$ and 0.028 respectively). While mice injected with AD and control extracts showed higher aggregate levels than untreated mice, this was not statistically significant. These data indicate that PiD and PSP tau preferentially stimulated tau accumulation in the brainstem/cerebellum. In the hippocampus, while there was a small increase in aggregated tau in all tauopathy brain extract injected mice, this was not significant for any tauopathy type and was highest for mice injected with control extracts, indicating that tau pathology does not accumulate in the hippocampus in this model, at least not to an extent that it can be detected by these methods.

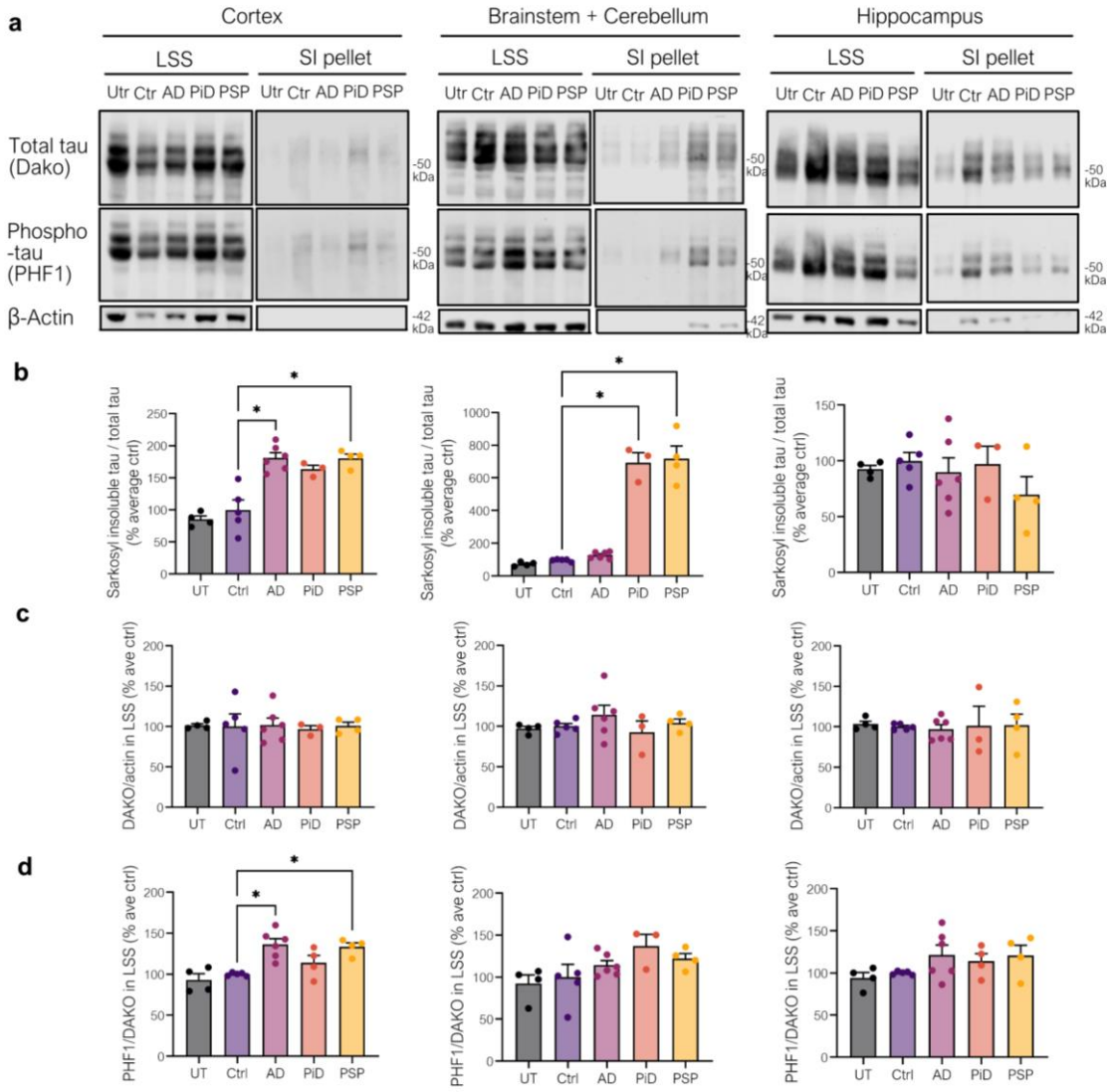

Figure 3.3 Htau mice show regional accumulation of aggregated tau following peripheral injection with tauopathy brain extracts.

Representative western blots of low-speed supernatants (LSS) and the sarkosyl insoluble (SI) pellet from the cortex, brainstem+cerebellum and hippocampus of htau mice intraperitoneally injected at 3-4 months of age with extracts from control (Ctr), AD, PiD or PSP postmortem brain or left untreated (Utr) and aged to 18 months (**a**). Samples were immunoblotted with antibodies against total tau (Dako) and tau phosphorylated at Ser396/Ser404 (PHF1). β-actin was used as a loading control. kDa markers are indicated. Bar charts show (**b**) the amount of tau in the sarkosyl insoluble fraction relative to tau amounts in the LSS for each sample as a measure of tau aggregation, (**c**) the amount of total tau in the LSS relative to β-actin as a measure of total tau amounts in each sample, and (**d**) the levels of phosphorylated (PHF1) relative to total tau in the same sample to determine relative tau phosphorylation. Tau bands running between 35kDa and 75kDa were included in quantification. Data is shown as percentage change from control brain extract-injected mice. Data is mean +/- SEM. N= 4 (UT), 5 (Ctrl), 6 (AD), 3 (PiD), 4 (PSP). Data were analysed using non-parametric Kruskal Wallis ANOVA with Dunn's multiple comparison to the control-injected group. *p<0.05.

The amount of total tau within the LSS was also determined relative to β-actin within the same sample (Figure 3.3c). This allowed evaluation of changes in overall tau levels following peripheral injection of tauopathy brain extracts. In the cortex, while there appeared to be a slight increase in total tau in AD and PSP extract- injected mice, this was variable and was not significantly altered when a one-way ANOVA was conducted. Similarly in the brainstem/cerebellum there was a negligible increase in tau following tauopathy brain extract injection. In the hippocampus, tau levels in PiD extract injected mice appeared slightly reduced while those injected with PSP extracts showed an increase, however again these changes were not significant. This data suggests that overall levels of tau are not altered following peripheral injection of mice with tauopathy or control brain extracts.

To determine if the phosphorylation of tau is altered, blots were probed with an antibody against tau phosphorylated at Ser396/404 (PHF1). Tau phosphorylation at this site is known to increase in htau mice with age (Kelleher et al., 2007). In the cortex, when the amount of PHF1+ve tau was normalised to total tau amounts in the LSS, Kruskis-Wallis one-way ANOVA indicated that tauopathy injection significantly altered the presence of PHF1+ve tau ($H(4) = 15.23$, $p = 0.0043$), and Dunn's pairwise comparison revealed a significant increase following injection of htau mice with AD and PSP extracts, relative to control brain injected mice ($p = 0.0122$ and 0.0459 respectively). PiD extract injected mice also showed a higher average amount of PHF1 tau, but this was not significantly different from controls, likely owing to higher levels of variation in the small number of samples. In the brainstem and cerebellum, there were no changes in PHF1 levels in PiD or PSP extract injected mice, as might have been expected since there was an increase in sarkosyl-insoluble tau in these samples. Levels of PHF1 in mice injected with control brain extracts in this region were similar to those in untreated mice, while tauopathy extract injected mice showed more variation, although without significant changes relative to controls. In the hippocampus, the average amount of PHF1 tau was higher in control and tauopathy extract injected mice. However, large SEM indicates that these levels were variable, and again one-way ANOVA showed no significant changes in PHF1 tau in the hippocampus after tauopathy injection.

Overall, these results indicate that aggregated tau accumulates in the CNS of htau mice following peripheral injection of tauopathy brain extract. Regional variation was apparent,

with the brainstem/cerebellum showing selective accumulation of tau aggregates following PiD and PSP extract, but not AD extract injection, and this is in keeping with pathological analysis showing that the brainstem and cerebellum are particularly vulnerable in PSP (Kovacs et al., 2020) and can even be affected in late stage PiD (Irwin et al., 2016a), whereas for AD this is often spared (Braak et al., 2011). The apparent alteration in tau aggregation in the brainstem/cerebellum of PSP and PiD injected mice appears in the absence of increases in tau phosphorylated at Ser396/404. The results further indicate that the cortex shows accumulation of tau aggregates following peripheral injection with all tauopathy brain extracts (AD, PiD and PSP), particularly for AD and PSP, and this correlated with increased tau phosphorylation at Ser396/Ser404, suggesting this may have been a mechanism for tau aggregation considering that PHF1 tau is associated with paired helical filaments (Otvos et al., 1994). Areas of the cortex are affected in postmortem tissue of all tauopathies examined here (Kovacs et al., 2020). The hippocampus appeared largely unaffected by tauopathy brain extracts, even though this is an area particularly affected in AD (Braak et al., 2011) and sometimes in PSP and PiD (Irwin et al., 2016a; Kovacs et al., 2020).

To determine if endogenous mouse tau is readily recruited by human tau seeds, wild-type mice were injected in parallel with htau mice and samples from these mice were analysed as described above (Figure 3.4).

Samples of LSS and SI from each brain region of wt mice were characterised by western blot (Figure 3.4a). As expected, there were no discernible tau bands in the SI fraction of any brain region, although a low intensity smear was apparent in some cases. In the LSS, total tau amounts were consistent between untreated mice and those injected with human brain extracts. Tau phosphorylated at S396/404 was observed at low levels in all brain regions, in keeping with previous findings from aged wt-mice, at least in the hippocampus (Torres et al., 2021). There were no differences in tau phosphorylation between groups.

Again, the results were quantified and are presented relative to control injected mice. The ratio of total tau to actin was measured to detect any changes in total tau levels after human brain extract injection (Figure 3.4b). In the cortex, mice injected with PSP and PiD extracts showed a somewhat reduced tau level, but this was not significantly lower than levels in control brain extract injected mice. In the brainstem + cerebellum, and hippocampus, tau levels were unchanged between groups. The ratio of phosphorylated (PHF1+ve) tau to total

tau in the LSS was measured for each brain region (Figure 3.4c). Overall, the relative abundance of PHF1 tau was unchanged between groups for all brain regions. A small decrease in PHF1 levels were observed in the cortex of mice injected with PSP extracts, but one-way ANOVA indicated that there was no significant effect of treatment. This data indicates that peripheral injection of tauopathy brain extract were not sufficient to induce increased tau phosphorylation in wt mice, at least not at the single time point examined here.

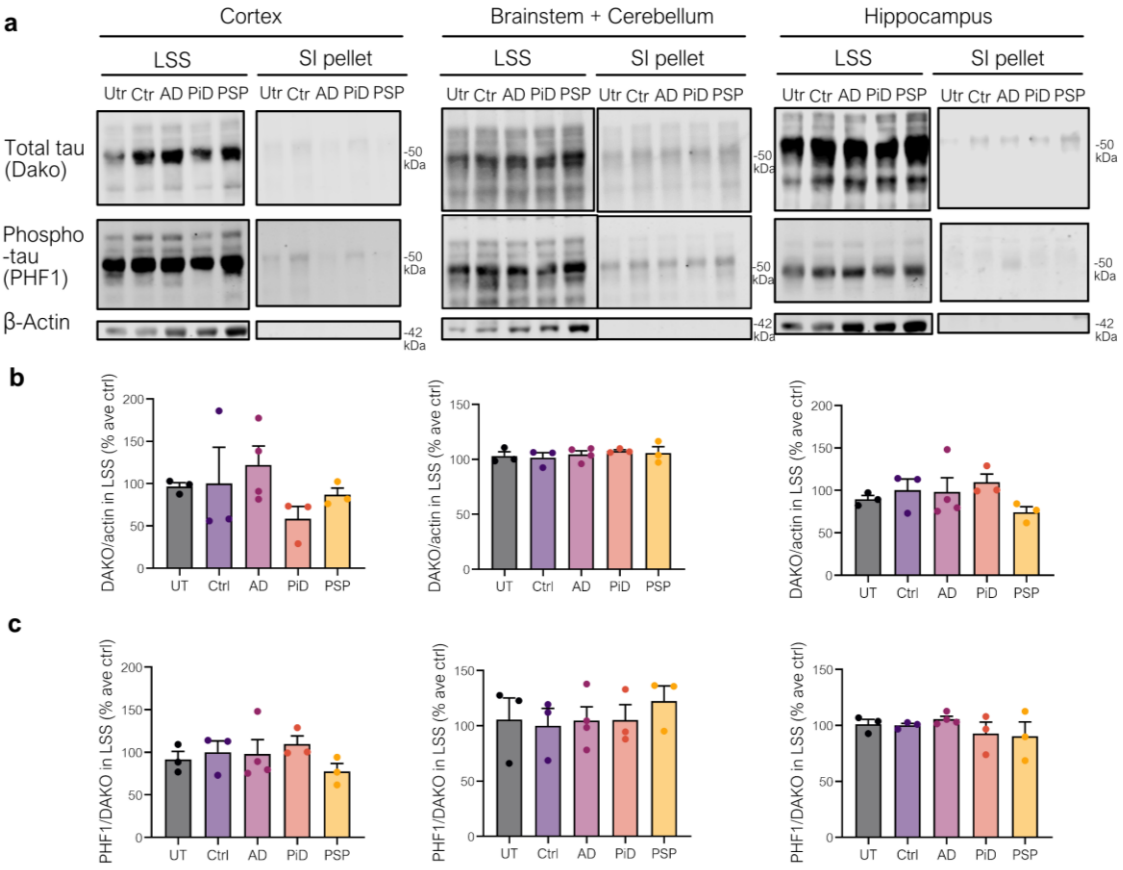

Figure 3.4 Wt mice show no changes in tau following injection with tauopathy brain extracts.

Representative western blots of low-speed supernatants (LSS) or sarkosyl-insoluble tau (SI) from three brain regions (cortex; brainstem+cerebellum; hippocampus) of wild-type mice injected with AD, PiD, PSP and control human brain extracts or left untreated (**a**). Blots were immunoblotted with an antibody against total tau (Dako) and phospho-tau (Ser396/Ser404) (PHF1). Bar charts show the amount of (**b**) total tau in the LSS relative to β-actin and (**c**) the ratio of PHF1 tau to total tau. Tau bands running between 35kDa and 75kDa were included in quantification. Data in graphs is normalised to show percentage change from control brain extract- injected mice. Data is mean ± SEM. N= 3 (UT), 3 (Ctrl), 4 (AD), 3 (PiD), 3 (PSP). Data were analysed using non-parametric Kruskal Wallis ANOVA with multiple comparisons to the control-injected group. *p<0.05.

Overall, these results demonstrate that peripheral injections of human tau extracted from tauopathy brain can cause increases in tau aggregation and tau phosphorylation in the brain of aged mice that express human tau, but not in mice only expressing mouse tau (wt mice). Moreover, there appeared to be some brain region specificity that was dependent on the tauopathy type from which the brain extract was derived. The mechanism behind these regional differences was not the focus of this project but are worthy of further exploration. Regardless, this data shows characterisation of a unique *in vivo* model with which to investigate the association of astrocytes with different types of tau pathology in affected brain regions.

3.3.3 Investigating the association of astrocytes with tau aggregates

Astrocyte reactivity (often referred to as [reactive] astrogliosis) is common in mouse models of tauopathy (Zamanian et al., 2012; Sidoryk-Węgrzynowicz and Struzyńska, 2019; Spanos and Liddelow, 2020; Jiwaji et al., 2022) and in postmortem tauopathy brain (Osborn et al., 2016; Garwood et al., 2017). These observations are substantiated by a growing body of evidence suggesting that altered astrocyte responses in tauopathies contribute to disease progression (Kovacs, 2020; Reid et al., 2020). This laboratory has previously shown a reactive astrocyte response in htau mice (Garwood et al., 2011) and this has also been observed in other tauopathy mouse models in which mutant human FTD-causing tau is expressed (Schindowski et al., 2006). To investigate if indicators of astrocyte reactivity are associated with the deposition of tau aggregates, hemi brains were drop fixed in 4 % (v/v) paraformaldehyde and sectioned in the coronal plane at 40μm. These were used to examine a) the regional deposition of modified tau, and b) glial fibrillary acidic protein (GFAP) as a marker of (reactive) astrocytes, by immunofluorescent labelling. Sections were selected that contained the cortex, brainstem and cerebellum, and hippocampus and these were matched across animals. Misfolded tau was labelled with the MC1 antibody that recognises a discontinuous epitope of residues 7-9, 313-322 amino acids, according to 2N4R tau numbering (Jicha et al., 1997). This allows detection of a conformational change in tau that is thought to precede tangle formation (Weaver et al., 2000). Sections were also labelled with the T22 antibody that specifically recognises oligomeric tau but not monomeric or filamentous tau (Lasagna-Reeves et al., 2012).

MC1-positive tau inclusions were observed in the majority of htau mice injected with tauopathy brain extracts tauopathy (Figure 3.5). Labelling in the hippocampus also revealed large numbers of GFAP positive astrocytes in both untreated, and all control extract-injected and tauopathy extract-injected mice, indicating a high presence of astrocytes in this region and in keeping with reports that astrocytes are present at high density in the mouse hippocampus (Keller et al., 2018). MC1 staining was relatively sparse in this region, although some neuritic and spheroid-like MC1 positive structures were present in sections from mice injected with PiD, PSP and AD brain extracts. These were less common in control brain extract-injected and untreated mice. GFAP+ve astrocyte processes were often seen to associate with these MC1-positive structures. T22 labelling for oligomeric tau indicated some granular structures that were sporadic and present in all treatment conditions, but predominantly in mice injected with AD and PiD extracts.

In the cortex, GFAP positive astrocytes were less abundant than in the hippocampus, in keeping with published cell densities in this region (Keller 2018). In AD and PID extract injected mice, relatively more GFAP +ve cells were often observed and these appeared more fibrous than in the PSP injected mice, which may indicate an increased GFAP response and cytoskeletal rearrangement in response to these sources of tau. More MC1-positive tau structures were observed in the cortex relative to the hippocampus, and these were present in all groups. A selected high magnification image (Figure 3.6) in the cortex of PSP-extract injected mice shows one area where GFAP positive astrocytes surround MC1-positive spheroid-like structures. This close proximity may indicate an astrocytic response to the accumulation of these pre-fibrillar tau structures. Co-localisation with astrocytes was difficult to interpret. T22 labelling in this region revealed similar granular structures as found in the hippocampus, but with the addition of spheroid-like structures that may overlap with neuronal cell bodies. The appearance of these structures appeared lower in untreated mice compared to those injected with tauopathy brain extracts. GFAP +ve cells were observed in the presence of T22 labelled structures, but co-localisation was not common. Control injected cortical sections were not available for T22 analysis, and due to time limitations, it was not possible to include this data here.

Immunolabelling of the cerebellum revealed high levels of GFAP-positive astrocytes in all treatment groups, with no obvious differences in morphology between untreated mice and those injected with tauopathy brain extracts. This is in keeping with high astrocyte marker

expression being previously reported, particularly on the outer layers of the folding cerebellar structure (Luo et al., 2018). Rounded MC1 speheroid-like structures were observed in all treatment groups including the untreated group, however they appeared more abundant in tauopathy extract injected mice, especially in the mice injected with PSP extracts. Astrocytes could be seen localised near some MC1+ve structures, as shown in a higher magnification image from the cerebellum of a mouse injected with PiD extract (Figure 3.6). However, astrocytes were not always found localised around MC1+ve structures.

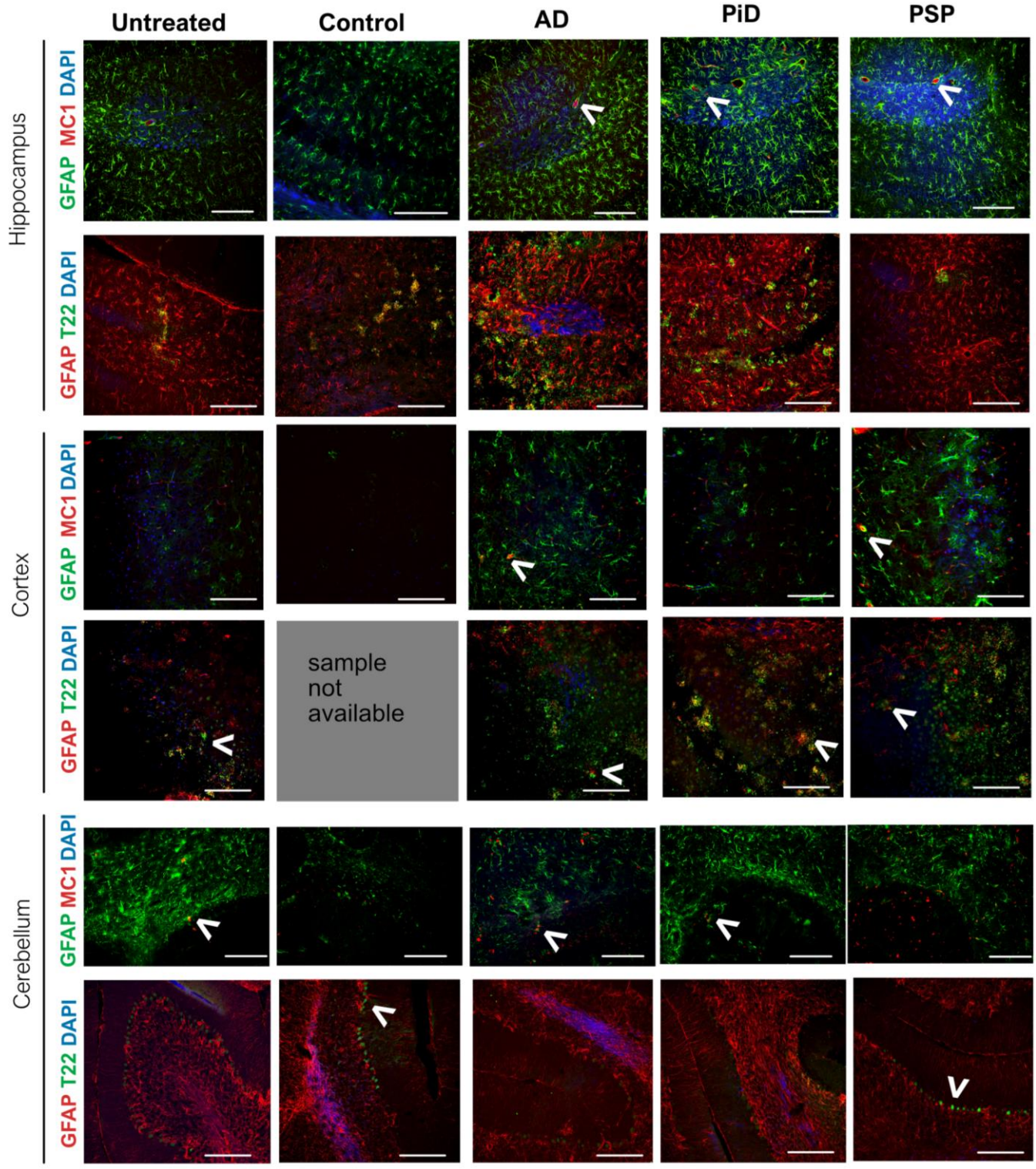

Figure 3.5 Representative immunofluorescent labelling of GFAP-positive astrocytes and misfolded or oligomeric tau in htau mice injected with tauopathy brain extracts relative to controls.

Sections containing the hippocampus, cortex or cerebellum from htau mice that were injected with control or tauopathy brain extracts or left untreated were immunolabelled with antibodies against (GFAP) and either tau in an abnormal conformation (MC1) or oligomeric tau (T22). White arrow heads indicate examples of astrocyte association with abnormal tau. Nuclei were stained with DAPI merged images are shown. White scale bars: 100 μm.

Again, T22 was observed in spheroid-like structures that may overlap with neuronal cell bodies. As highlighted in Figure 3.6, GFAP positive astrocytic processes can be seen to envelop some of these T22 positive tau structures. The T22 labelling in the cerebellum did not reveal the same granular structures as were observed in other brain regions but did reveal T22-positive GFAP-negative cell bodies that ran along the perimeter of cerebellum. As highlighted in Figure 3.6, GFAP-positive astrocytic processes can be seen to envelop some of T22 positive tau structures in PSP extract injected mice, where particularly high levels of T22 positive cells which may indicate accelerated tau pathology.

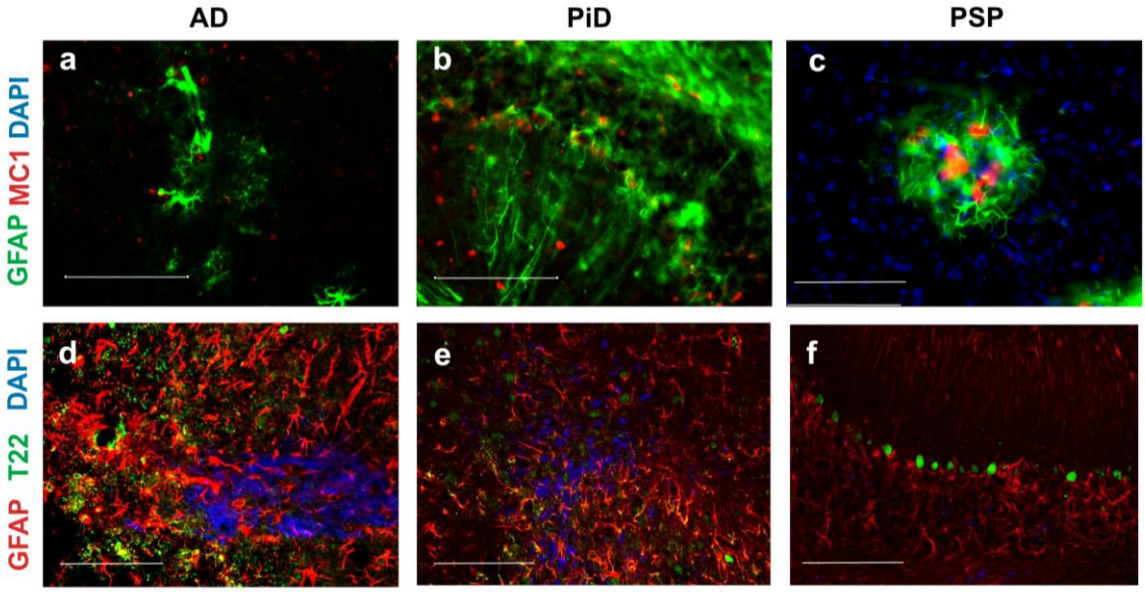

Figure 3.6 Selected high-magnification immunofluorescent labelling of GFAP-positive astrocytes and misfolded or oligomeric tau in htau mice injected with tauopathy brain extracts.

Sections containing the cortex (a, c), cerebellum (b, f), hippocampus (d), or brainstem (e) from htau mice injected with tauopathy brain extracts and immunolabelled with antibodies against (GFAP) and either tau in an abnormal conformation (MC1) or oligomeric tau (T22). Nuclei were stained with DAPI (blue). Merged images are shown. Selected areas of astrocyte association with tau pathology are represented here. White scale bars: 100 μm.

Others have reported that tau aggregates can accumulate in the brains of wild-type mice following injection into the brain of tauopathy brain extract, and this recreates classic glial pathology (Guo et al., 2016; Narasimhan et al., 2017). To investigate how this compares with peripheral injection in wild-type mice, sections were examined by IHC (

Figure 3.7) as described above for htau mice. Immunofluorescence labelling revealed similar abundance of GFAP +ve astrocytes in the hippocampus as was observed in htau mice, which is expected in this region that has been reported to have higher ratio of astrocytes to neurons compared to the cortex (Keller et al., 2018). Similar to the htau mice, there were minimal MC1 positive structures, indicating that the hippocampus is not affected by tauopathy brain extract injection into the periphery, as previously indicated by lack of increased tau aggregation in this region (section 3.3.2). T22 labelling again showed granular structures, as with htau mice, that may indicate areas of pre-tangles or extracellular tau oligomers. While astrocytes overlap in these areas and may be responding to the tau oligomers, it is difficult to interpret a direct response to abnormal tau in this region due to the high numbers of astrocytes in the hippocampus.

In the cortex of wild-type injected mice, GFAP positive cells are observed in all treatment conditions, as with htau mice. Similarly, some MC1 positive structures can be observed, with both spheroid-like structures that may represent tau accumulation within axons, and long thin structures that could localise with neurites but may also represent blood vessel walls labelling, as has been seen previously with MC1 labelling in mouse tissue (Bennett et al., 2018). Astrocyte processes may converge around these areas in some cases suggesting that some of the longer MC1 processes may indeed be blood vessels. As some MC1 positive structures are present in untreated wildtype mice, questions remain as to whether wild-type mouse tau begins a process of misfolding with age. Considering that PHF1 tau associated with paired helical filaments has been observed in the hippocampus of aged mice (Torres et al., 2021), it is possible that tau begins to misfold even in wild-type mice with age. Interestingly, MC1 labelling appeared stronger in the cortex of wt mice following injection with PiD and PSP extracts, suggesting that tauopathy injections may increase misfolded tau in the cortex of these mice, although western blotting did not show any changes in tau

phosphorylation in these animals. T22 labelling revealed similar granular structures as observed in htau mice and this was lowest in mice injected with PSP and control brain extracts, which was also the case in htau mice.

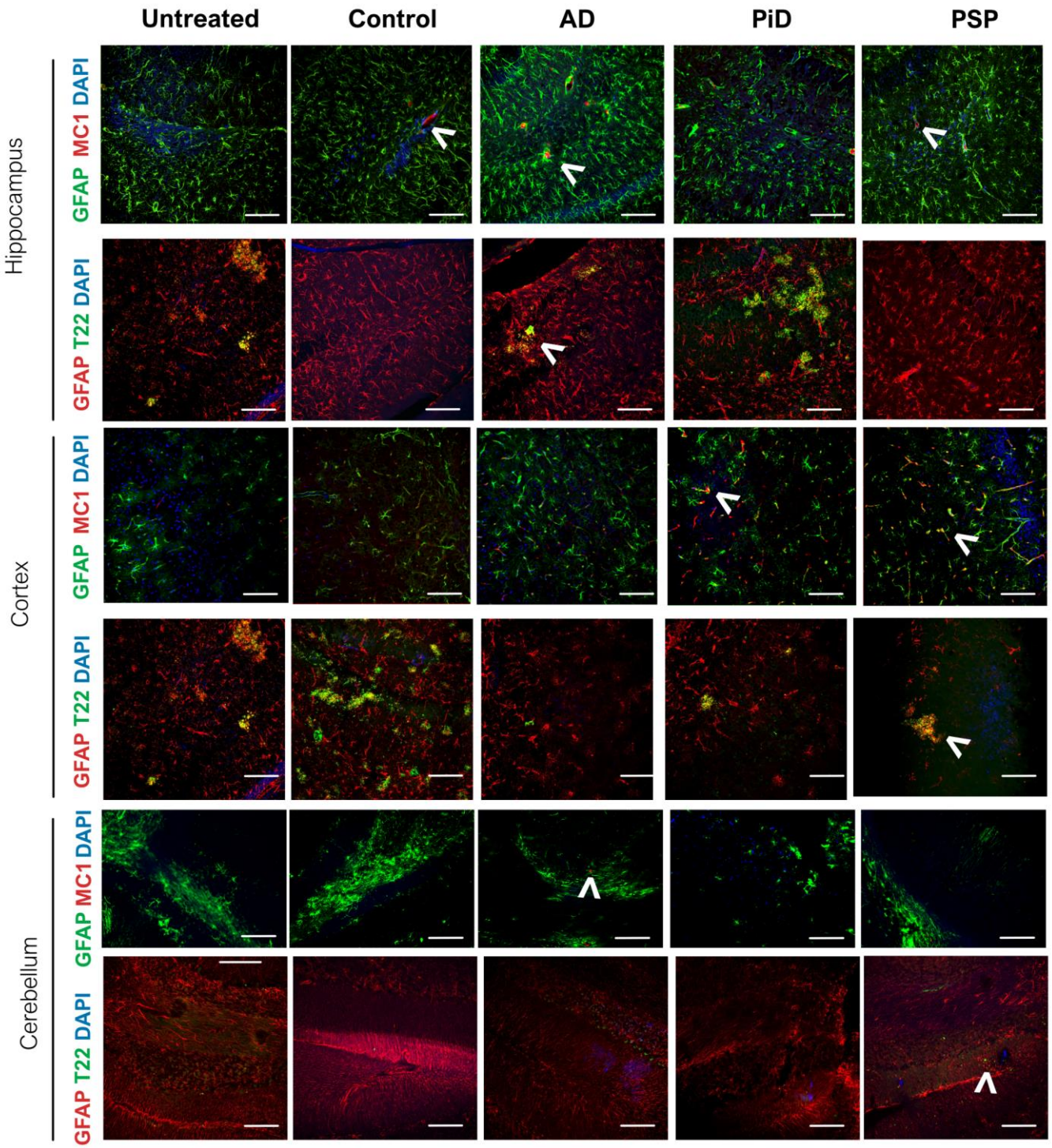

Figure 3.7 Representative immunofluorescent labelling of GFAP-positive astrocytes and misfolded or oligomeric tau in wild-type mice injected with tauopathy brain extracts relative to controls.

Sections containing the hippocampus, cortex or cerebellum from wild-type mice injected with control or tauopathy brain extracts or left untreated were immunolabelled with antibodies against astrocytes (GFAP) and either tau in an abnormal conformation (MC1) or oligomeric tau (T22). Nuclei were stained with DAPI merged images are shown. White arrow heads indicate examples of astrocyte association with abnormal tau. White scale bars: 100 μm.

In the cerebellum, the abundance of GFAP positive cells was similar to those observed in htau, and were as expected in this region (Keller et al., 2018; Luo et al., 2018). MC1 labelling was rare, however some T22 labelling was observed particularly in the neuronal bodies also observed to be immunoreactive in htau mice, but not to the same intensity.

Overall, these images demonstrate evidence of some astrocyte association with pathological tau aggregates, perhaps indicating their ability to respond to the presence of abnormal tau. Therefore, astrocytes were examined more closely for changes that may indicate a reactive state.

3.3.4 Changes to astrocytes after tauopathy injections

The data presented above suggests astrocytes may respond to the deposition of abnormal tau. Indeed, astrocytes are observed to undergo changes during tauopathy progression (Kovacs, 2020; Reid et al., 2020), including adopting a reactive astrocyte response (Garwood et al., 2017; Escartin et al., 2021) and they may also proliferate in response to changes in the local brain environment (Yong et al., 1991).

To examine the abundance of astrocytes, cortical lysates from treated and control htau and wild-type mice were used to assess changes in astrocyte proteins (Figure 3.8). An antibody against Aldehyde Dehydrogenase 1 Family Member L1 (ALDH1L1) was used, which is a folate metabolic enzyme (Krupenko, 2009) that has been noted as a pan-astrocyte marker in the mammalian CNS (Yang et al., 2011) that labels more astrocytes than are detected with antibodies against GFAP (Cahoy et al., 2008). Immunoblotting for the ALDH1L1 antibody revealed bands at approximately 99kDa, corresponding to the predicted molecular weight of this protein. The faint band below may represent a lower molecular weight isoform of ALDH1L1. The levels of ALDH1L1 appeared to be quite variable between and within groups. Total intensity of ALDH1L1 band was quantified relative to levels of GAPDH as a housekeeping protein, within the same sample. While the average of ALDH1L1 levels were lower in tauopathy extract injected mice compared to control extract injected, for both wt and htau mice, the results were variable and there were no significant differences between groups. This data indicates that there are likely no changes in astrocyte numbers in the cortex in response to human tau extracts. ALDH1L1 levels appeared to be comparatively higher in htau relative to wild-type mouse samples, although these were run on separate blots and could not be properly compared. It should be noted that for wild-types, only two

samples from each group were included due to lack of available samples, and so formal statistical analysis could not be performed.

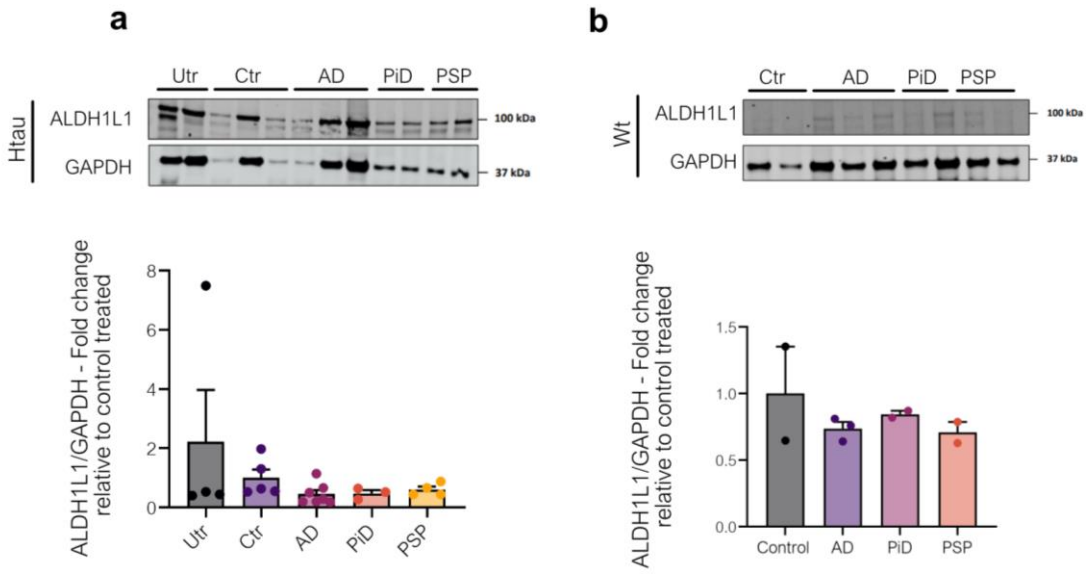

Figure 3.8 Levels of ALDH1L1 in htau and wild-type mice injected with tauopathy or control brain extracts.

The low-speed supernatant (LSS) from mouse cortex was immunoblotted with an antibody against the pan-astrocyte marker ALDH1L1. The prominent band was quantified at around 99 kDa for quantification of (**a**) htau and (**b**) wt mice that had been peripherally injected with brain extract from Alzheimer's disease (AD), Pick's disease (PiD) or progressive supranuclear palsy (PSP) compared to non-diseased control (Ctr) brain or left untreated (Utr). Data is presented as mean ± SEM. N= 3-5 (Htau), N=2 (WT). Wild-type untreated mice samples were unavailable for analysis.

Because increased GFAP expression is often associated with astrocyte reactivity (Middeldorp and Hol, 2011; Brenner, 2014; Garwood et al., 2017), and is not a pan-astrocyte marker as with ALDH1L1 (Yang et al., 2011), the relative expression of GFAP was determined relative to that of ALDH1L1 to determine if there are changes in astrocyte reactivity. Again, lysates from the cortex were examined by western blot GFAP was quantified by bands between 45-50 kDa which represent multiple isoforms of GFAPIn htau mice, there was considerable variation within the control extract and untreated groups, and tauopathy extract injected mice did not show any significant changes in proportion of GFAP relative to ALDH1L1. In wt mice, limited samples were available, and those analysed indicated a decrease in the relative abundance of GFAP expression after tauopathy brain

extract injections compared to control. However, it was difficult to draw firm conclusions from this limited data set.

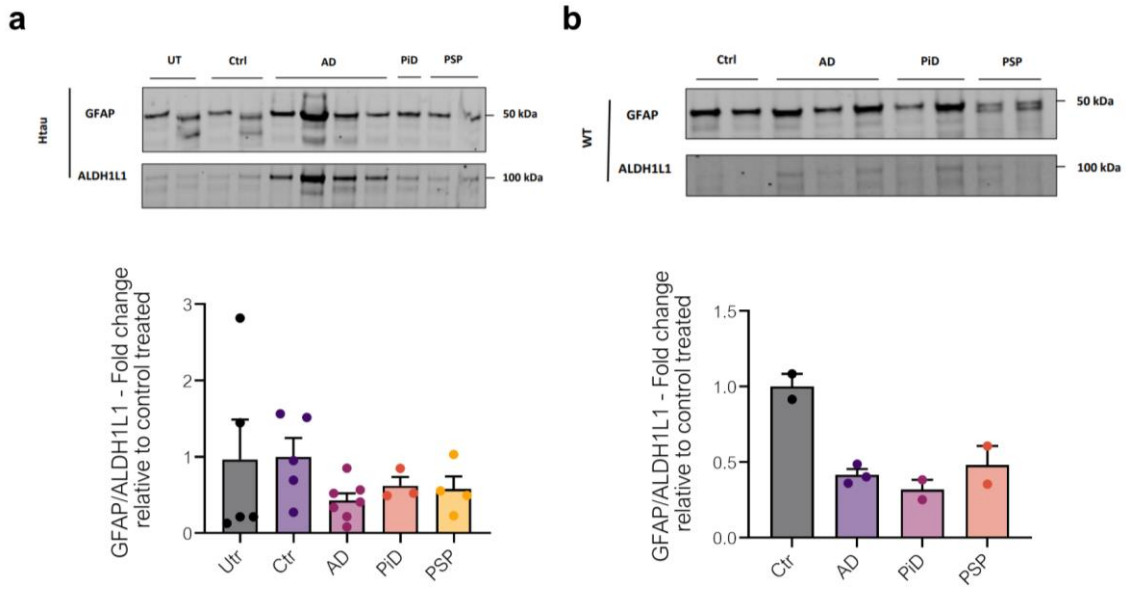

Figure 3.9 Relative expression of GFAP in htau and wild-type mice injected with tauopathy or control brain extracts.

The low-speed supernatant (LSS) of mouse cortex was immunoblotted with antibodies against reactive (GFAP) and total astrocytes (ALDH1L1). All isoform bands were quantified for GFAP between 45-50 kDa, where as the prominent higher band for ALDH1L1 was quantified at around 99 kDa. Samples were analysed for (**a**) htau and (**b**) wt mice that had been peripherally injected with brain extract from Alzheimer's disease (AD), Pick's disease (PiD) or progressive supranuclear palsy (PSP) compared to non-diseased control (Ctr) brain extract or left untreated (Utr). Data is presented as mean ± SEM for n=3-5 (htau) and n=2 (wild-type) mice. Wild-type untreated samples were unavailable for analysis.

The number of GFAP-positive cells in immunolabelled htau and wt sections containing cortical and hippocampal brain regions was next determined (Figure 3.10). GFAP-positive cells were detected and counted utilising the Fiji Image J plug in (method 2.5.4.1), and the density of GFAP-positive astrocytes was determined as number of cells per mm^3. In the hippocampus, higher astrocyte numbers were observed in untreated htau mice compared to untreated wt mice. This was also replicated in the cortex, although a two-way ANOVA with multiple comparisons did not reveal any significant differences between region or genotype (or an interaction). This apparent increase in astrocyte numbers in untreated htau mice compared to wt mice was also indicated by stronger ALDH1L1 banding in cortical lysates, as mentioned previously (Figure 3.8), although a direct western blot comparison between

untreated htau and wild-type mice was not performed. Nonetheless, this suggests that the expression of human tau may increase the number of reactive astrocytes present in tau transgenic mouse brain compared to wt mice as previously demonstrated by others (Garwood et al., 2011).

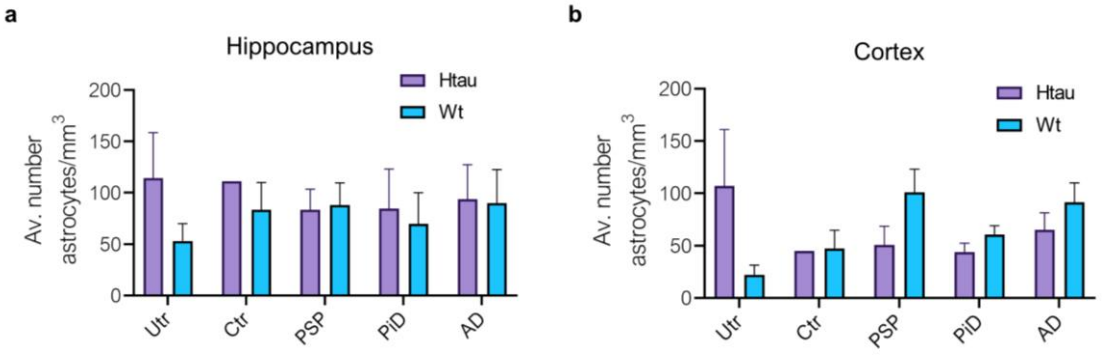

Figure 3.10 Numbers of GFAP+ve cells in htau and wild-type mice injected with control and tauopathy brain extracts.

GFAP positive cells were counted in (**a**) the hippocampus or (**b**) combined ventral, medial and dorsal areas of the cortex in hemi-brains from htau and wt mice peripherally injected with brain extract from Alzheimer's disease (AD), Pick's disease (PiD) or progressive supranuclear palsy (PSP) compared to non-diseased control (Ctr) brain extracts or left untreated (Utr). Data is presented as mean ± SEM. N=2 except for n=1 for ctr extract-injected htau mouse).

In the cortex of wt mice, astrocyte numbers were increased on average in groups injected with human brain extracts, and were highest for those injected with PSP and AD extracts (Figure 3.10b). Apart from these two treatment conditions, there were no apparent differences in the number of astrocytes between wt and htau mice between groups in either the cortex or hippocampus. This may suggest that astrocyte numbers are not significantly altered by tauopathy brain extract injections, and that possible variability between the selected sections is responsible for variations in data.

These results indicate that there may be a difference in astrocyte numbers between wt and htau mice in the regions examined. The reduction in astrocyte numbers in the cortex of htau mice after control or tauopathy brain extract injection indicates that astrocytes may be negatively regulated or even become atrophic and die in response to human brain injections. However, only limited conclusions can be drawn from this small dataset. In wt mice, this trend is reversed, with an average increase in astrocyte numbers following injection with human brain extracts. This may indicate that wt mice respond to human extracts by

increasing astrocyte proliferation. For htau mice, it may be that higher levels of tau pathology in this region (as confirmed in section 3.3.2) causes a reduction in astrocyte numbers in mice at this age point.

Finally, functional changes in astrocytes are sometimes associated with changes to their morphology, including increased number of processes and branching that has been described as ramification (Schiweck et al., 2018). Therefore, astrocytes were examined for morphological changes indicative of this transition to a reactive state. Astrocytes were analysed by utilising a basic neurite tracker in the Fiji plug in for ImageJ (Schindelin et al., 2012) to count processes and their features. GFAP positive astrocytes with high numbers of processes (≥6), dubbed 'ramified', were counted as a percentage of the total number of astrocytes detected in the cortex and hippocampus (Figure 3.11a).

In the hippocampus, the number of astrocytes classified as 'ramified' were similar between untreated htau and wt mice, suggesting that this astrocyte morphological type is not altered in this region by human tau expression. The numbers of ramified astrocytes varied depending on the source of the brain extract injected. In htau and wt mice, injection with control brain extracts appeared to reduce the numbers of ramified astrocytes, whereas in animals injected with PSP extracts there was an apparent increase in ramified astrocyte numbers compared to mice injected with control extracts. In mice htau mice injected with AD extracts, there appeared to be higher number of 'ramified' astrocytes, whereas numbers in wt mice remained similar to untreated or control extract injected htau mice. Mice injected with PiD extracts showed no changes across groups in the number of ramified astrocytes. These trends were replicated when analysing the average number of processes per astrocyte (Figure 3.11b). Two-way ANOVA revealed no significant impact of injection type or genotype on either the percentage of ramified cells or the average number of processes, and there was no genotype x treatment interaction. This is perhaps expected, considering that tauopathy brain extract injection into htau or wt mice did not affect tau aggregation or phosphorylation in the hippocampal region (see section 3.3.2).

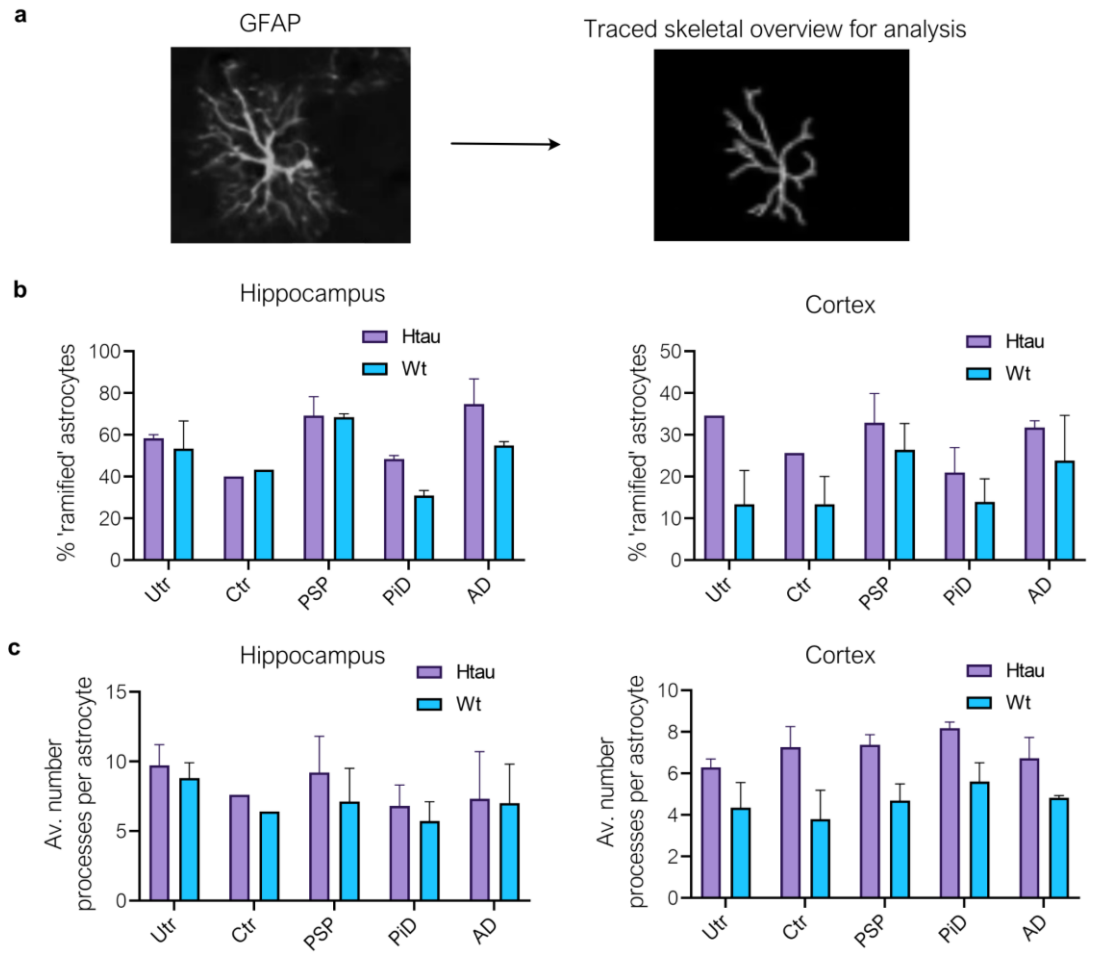

Figure 3.11 Assessing astrocyte morphology in htau and wild-type mice following injection with control or tauopathy brain extracts.

GFAP positive cells were counted in the hippocampus and cortex in GFAP-immunolabelled sections from htau and wt mice peripherally injected with brain extract from Alzheimer's disease (AD), Pick's disease (PiD) or progressive supranuclear palsy (PSP) compared to non-diseased control (Ctr) brain extracts or left untreated (Utr). (**a**) Analysis of astrocyte "skeleton" was used to categorise astrocytes as ramified or non-ramified based on their number of processes. (**b**) This data was quantified and is shown expressed as a percentage of total number of astrocytes analysed in that region. (**c**) Average number of processes per astrocyte was determined based on this analysis. Data is mean+/-SEM. N=3.

In the cortex there was a clearer distinction between the percentage of 'ramified' astrocytes in htau and wt mice, with untreated wt mice showing 13.3 % ± 8.15 of ramified astrocytes, compared to 34.5 % ± 0.12 in htau mice. This indicates that expression of human tau alone is sufficient to increase the number of astrocyte processes in the cortex. This likely reflects hypertrophied astrocytes that have previously been described in tau transgenic mouse brain (Garwood et al., 2011). A similar difference was observed in mice injected with control brain

extracts. For htau mice injected with tauopathy brain extracts, the percentage of 'ramified' astrocytes did not appear to increase following tauopathy brain extract injection compared to control extract injected or untreated mice. In wt mice, only injection with PSP and AD extracts appeared to increase the number of astrocytes, while the results were highly variable between groups. Indeed, a two-way ANOVA showed no significant impact of injection type or mouse genotype on the percentage of 'ramified' astrocytes in either the hippocampus or the cortex, and there was no interaction between parameters. Analysis of the average number of processes (Figure 3.11b) did, however, reveal a stronger disparity between htau and wt mice in all treatment conditions. However, there was not a clear increase in number of processes in tauopathy extract injected mice compared to control extract injected mice. A two-way ANOVA analysis found that mouse genotype had a statistically significant impact on the average number of astrocyte processes in the cortex ($p = 0.0009$), however pairwise comparison did not indicate statistical differences due to specific brain extract injections.

These results indicate that astrocytes are altered in htau mice relative to wt mice. There is evidence of increased overall astrocyte numbers, as well as increased number of astrocyte processes in htau mice, especially in the cortex. This was also observed in untreated mice, so was not as a result of injection with human brain extracts. Overall, these data show that astrocytes appear to respond to chronic exposure to a tauopathy brain environment, but that human tauopathy brain extracts were not sufficient to exacerbate these changes.

3.4 Discussion

This chapter aimed to investigate the association of astrocytes with tau pathology in a novel mouse model of tau spread. This model used a transgenic mouse expressing the entire wild-type tau gene on a mouse tau knockout background (htau line, Andorfer et al., 2003) to investigate selective regional vulnerability of the mouse CNS to different forms of tau. Htau mice were chosen for this purpose, since unlike most mouse lines which only express 4R forms of mouse, wild-type or mutant human tau (Noble et al., 2010), htau mice show developmental regulation of tau splicing and express all six isoforms of human tau in the adult CNS. This is critical since it is believed that tau efficiently seeds physiological forms of only similar forms of tau (Jucker and Walker, 2018). Intraperitoneal injection was selected since to understand selective vulnerability, it is critical that the origin of tau spread was not pre-

determined by injection site. It was therefore important that the spread of tau pathology was carefully characterised in order to properly delineate any alterations in astrocyte pathology and association with tau pathology that might be observed.

3.4.1 Human tauopathy brain extracts can induce the deposition of tau aggregates in specific regions of htau mouse brain

Biochemical analysis determined that peripherally injection of human brain extracts from tauopathy cases was able to induce increased deposition of pathological forms of tau in some areas of mouse brain, and this was somewhat related to the source of tau that was injected and that suggested regional vulnerability to different tau species (3.3.2). For example, it was found that tau from PiD and PSP brain, but not AD brain, induced increased tau pathology in the brainstem/cerebellum of htau mice relative to mice injected with control human brain extracts and untreated mice. In PSP, the brainstem and cerebellum are some of the most affected brain regions that show significant accumulation of pathological tau species (Kovacs, 2020), suggesting that these areas are particularly vulnerable to tau species isolated from PSP in preference to AD brain, or that they are less efficient in degrading and clearing tau deposits. However, in PiD this area of the brain is not commonly associated with tau pathology (Dickson, 2001), although there are some reports that it is affected at later stages of disease (Irwin et al., 2016a). In humans, the cerebellum expresses lower levels of foetal tau isoforms (0N3R), and lower levels of tau overall compared to other brain regions (Trabzuni et al., 2012). However, a recent analysis suggests that total levels of tau expression (and α-synuclein expression) are poorly correlated with vulnerability to these protein aggregates (Praschberger et al., 2022). It is unknown if this translates into mice, but it is interesting that this region was vulnerable to PSP tau, in which 4R forms of tau accumulate. Why PiD tau showed a similar pattern of deposition is somewhat puzzling, however, biochemical analysis of tau from the cases used for mouse injections showed similarities in the profile of tau from PSP and PiD brain, without the clear distinction between 4R and 3R tau, respectively, that would be expected. Indeed, the banding profile of the PiD and PSP cases were virtually indistinguishable. Analysis of the human samples used to inject mice indicated that 3R tau was present in the sarkosyl insoluble fraction of AD brain, but much less so in tau extracted from the PSP cases, which was unexpected. Still, although 3R tau is the predominant isoform of tau deposited in PiD disease fold (Reid et al., 2020), it does not prohibit 4R tau being incorporated in aggregates, and PiD cases are also highly variable

and may also contain converging tau aggregate pathologies (Dickson, 2001; Irwin et al., 2016b).

The heterogeneity of astrocytes in the mouse brain, as has been demonstrated in recent studies (Bayraktar et al., 2020; Batiuk et al., 2020), also may play a role in how different brain regions respond to increased tau seeds that have entered after tauopathy injections. Batiuk et al found distinct populations of astrocytes in the mouse cortex and hippocampus, with unique gene expression and morphologies, likely leading to functional difference and which may provide evidence of differential astrocyte subtype response, and which ultimately impacts tau spread in this model.

Tau shows considerable molecular heterogeneity between and within disease states, and it has been suggested that there are different "strains" of human tau that can have different biological outcomes (Kaufman et al., 2016). For example, some strains of "atypical" PiD tau show similar biochemical and functional properties to PSP tau, and this may explain the similarity in regional vulnerability between these two disease states of tau, in this chapter.

It is important to consider the route of tau entry in this model. Intraperitoneal injections avoid the direct exposure of one area of the brain to exogenous tau seeds as if often the case in tau spread mouse models, and allows exploration of vulnerability of different brain regions. There was confidence that this approach would be successful since others had previously shown that CNS tau aggregation occurred following intraperitoneal injection of tau isolated in the same way from mice expressing mutant forms of human tau into mice expressing wild-type human tau (Clavaguera et al., 2013). However, this means that the route of entry of endogenous tau seeds is not well defined. One possible route is a leaky blood-brain barrier, where previous work by others showed that intraperitoneal injection of beta-amyloid species into mice resulted in tau spread into the brain via the bloodstream in a random pattern as a result of blood-brain barrier (BBB) permeability (Eisele et al., 2010). A previous study demonstrated that mutant human tau expressed in mice was able to induce BBB damage, a phenotype that could be reversed by repressing tau expression utilising the tetracycline induction of this model (Blair et al., 2015). A more recent study found that Lipopolysaccharide (LPS), an inflammation inducer that is found to be elevated in the hippocampus of AD patients (Zhao et al., 2017), could cause BBB integrity to be weakened and mediate the spread of injected human mutant P301L tau from the mouse medial

entorhinal cortex (Liu et al., 2020). This provides evidence that other molecules alongside tau that may be present in the LSS fraction injected could compromise the blood brain barrier, providing a pathway for the entry of specific tauopathy aggregate strains that are present in the injected homogenate. However, while there is a lack of study on how the innate pathology of htau mice causes disruption of the BBB over time, it is difficult to estimate the contribution of this or undetermined factors from the tauopathy injections that may be causing BBB dysfunction. Still, it appears plausible that this is a route of entry for the injected seed-competent tau species.

While the lack of 3R tau in wt mice may also prevent tau seeding occurring in these mice, differences in the ability of tau to spread from the periphery into the CNS between transgenic and wt models is also worth considering and may be worth determining for future studies. Indeed, if there are any inherent differences in BBB integrity between 4-month-old wt and htau mice at the timepoint of injection in these experiments, this may contribute to the lack of increased tau burden observed in the brains of wt mice by 18 months.

In addition to tau being able to enter the brain via the blood-brain barrier, it is possible that enteric nervous system (ENS) neurons in the gut may be able to uptake and spread tau seeds. Indeed, tau expression in myenteric plexus neurons in the ENS has been described (Lionnet et al., 2018; Prigent et al., 2020). This may also be an explanation for why this region shows significant tau accumulation following peripheral injection, at least for PSP and PiD tau, since projections from the enteric nervous system converge on the brain stem via the vagus nerve and spinal cord (Furness, 2012). However, the absence of tau modifications or aggregation in tau from the ENS of PSP cases may argue against this route (Lionnet et al., 2018). While it is possible that pathogenic tau seeds injected into the peritoneal cavity can seed neuronal tau through neuronal connections in the enteric nervous system, and/or enter through the blood brain barrier or lymphatic system into the brain, this may reduce the amount of human derived pathological tau seeds that mouse brains are directly exposed to. Whichever is the route of entry, this may also create a new where some brain regions are preferentially exposed to tau seeds depending on their route of entry into the CNS.

The fraction used to inject mice is not enriched for tau aggregates, and so it is also feasible that a myriad of other factors from the tauopathy homogenate could induce a pro-inflammatory environment which speeds up the tau aggregation that naturally occurs in htau

mice (Andorfer et al., 2003). As mentioned above, LPS can induce BBB dysfunction (Liu et al. 2020), and this may be present in the brain homogenate from AD cases as it has been seen in AD patients (Zhao et al. 2017). It is known that astrocytes can release cytokines in response to a pro-inflammatory environment, communicating with other cell types such as microglia (Vainchtein and Molofsky, 2020) that may alter the ability of htau mice to tackle the tau pathology that develops with age. If such factors are present in the tauopathy brain lysate injected into mice, they may not only affect BBB integrity, but may be able to trigger such responses in the mouse brain. Further, this could have consequences for mechanisms such as kinase activity, which when altered could lead to an increase in tau pathology as has been noted previously in htau mice (Kelleher et al., 2007).

Therefore, although injected tauopathy extract can increase tau burden in the cortex and brainstem/cerebellum of htau mice in this model, peripheral injection may reduce the amount of tauopathy specific conformations of tau that can spread when compared to intracranial injections, and this may affect the appearance of astrocyte pathology.

3.4.2 Mouse astrocytes show muted response to peripherally injected tauopathy extract but may be altered by the presence of genetically expressed human tau.

Regardless of the pathways that lead to increased tau aggregation, this model provided a unique and interesting tool with which to examine the association of astrocytes with tau pathology, and to begin to explore whether there are differing astrocyte responses to different forms of tau. Brain sections were examined for the presence and extent of GFAP positive astrocytes in relation to tau deposits. Immunolabelling with antibodies against misfolded tau (MC1) and oligomeric tau (T22). In some areas GFAP positive astrocytes were seen to surround tau deposits. While there was only rare evidence of astrocytic tau inclusions as is common, at least in PSP (Kovacs et al., 2020) the IHC data suggested that astrocytes are physically responding to tau pathology, and that their motility towards neurons harbouring tau inclusions might suggest their involvement in tau uptake and spread or clearance.

Astrocyte abundance was found to increase in htau mice compared to wt mice, along with the number of astrocytic processes, and this may indicate a global astrocyte change that is associated with the expression of human tau in this model and the resulting tau pathology. The observed lack of consistent increase in astrocyte numbers after tauopathy brain extract

injection is in line with a previous report that did not determine an increase in proliferation in hippocampal astrocytes in post-mortem AD hippocampus (Marlatt et al., 2014), or cortex (Pelvig et al., 2003). It may be that proliferation occurs sporadically depending on disease state and other molecular and cellular factors. How astrocyte proliferation differs in other tauopathies is yet to be explored.

Astrocytes were examined for disease associated changes in terms of their morphology and protein expression of reactivity markers by IHC and western blot. This did not reveal any significant reactivity changes in astrocytes from mice injected with tauopathy brain extracts compared to those injected with control brain extracts or untreated mice. While there may have been some variation between morphological types of astrocytes between untreated, control brain extract and tauopathy brain extract injected mice, it was difficult to make a firm conclusion since the sample size used for this analysis was limited. Because tufted astrocytes containing tau inclusions formed primarily of 4R Tau are a hallmark of PSP (Dickson et al., 2007; Kovacs et al., 2020), especially in the cortex which was shown to accumulate tau pathology in experimental htau mice, and ramified astrocytes are often seen in Pick's disease (Dickson, 2001), recapitulation of such astrocyte morphological features might be expected in this model, as has been observed in previous studies in mice (Clavaguera et al., 2013; He et al., 2020). However, these studies differ from the work presented here since tauopathy extracts were injected directly into the brain, and the pattern of spread and neurons first affected were pre-determined. In contrast, the intraperitoneal injection approach used in this thesis could potentially be a limiting factor for the spread of tau, as discussed above.

It is also worth considering that only a single time point after intraperitoneal tau extract injections were examined in this work and it is possible that tau had accumulated in other regions prior to the regional pattern determined in this work. If this was the case, it would suggest that tau is efficiently cleared from resilient brain regions and accumulates, in a tau species specific manner, only in vulnerable brain regions. This would suggest that there are regional differences in the ability of neurons to degrade specific species of tau. There is evidence to support this notion. Evidence from postmortem AD brain shows that tau clearance pathways, including the ubiquitin proteasome system and macroautophagy are likely defective (Nixon and Yang, 2011). Moreover, experimental evidence shows that disease-associated forms of tau directly affect these clearance pathways (Piras et al., 2016).

Of direct relevance to this work, recent studies have shown that there is defective tau clearance in two models of tau spread (Blaudin de Thé et al., 2021) that was indicated by colocalization of misfolded tau with p62, a cargo protein which binds to autophagy substrates and that should be degraded with them. That p62 associated with tau deposits is evidence that autophagy is disrupted upon the accumulation of pathological tau in circuits involved in tau spread.

3.4.3 Limitations of htau mouse experiments

While the peripheral injections of this model sought to remove the clear bias of injection into a specific brain region, it also makes it difficult to track the spread of tau as there are multiple entry points (as discussed above). This is coupled with the fact that the injected brain extracts were not labelled, and it was impossible to distinguish human tau from extracts from the human tau expressed by htau mice. If tau injected tau was tagged, this would aid this distinction, however this would likely require a recombinant tau aggregate which are different to the unique tau confirmations that are found in tauopathy brain (Shi et al., 2021).

The results in this chapter represent changes observed 14 months after injection into 4-month-old mice. This may lead to over generalised conclusions on the spread of tau from the periphery and ignores how other brain regions may have been affected at earlier time points. Indeed, it would be interesting to observe monthly changes to determine how the initial injection altered tau accumulation and astrocyte response, and how this might change the regional accumulation of tau pathology in htau or wt mice with age.

Additionally, the assessment of other pathological criteria are missing from this model. While it is known that htau mice show behavioural and cognitive changes by 12 months (Polydoro et al., 2009; Geiszler et al., 2016), these were not examined in this study. Of particular interest would have been to determine if motor deficits resulted from PSP (and indeed the AD) extract injected mice, where the cerebellum/brainstem was most affected. For PSP at least, this is a common clinical criterion (Dickson et al., 2007). Furthermore, this analysis could have been performed without the need to sacrifice further mice. Neuronal health was also not measured in this mouse model. Synaptic function is impaired in htau mice with age (Polydoro et al., 2009), and so alterations after tauopathy injection would have been interesting to examine.

Finally, inherent issues exist with utilising mouse antibodies to label proteins in mice, where mouse secondary antibodies can bind to endogenous mouse immunoglobins. While care was taken to reduce this in IHC, including utilising a mouse background reduction kit (2.5.2), it may not have eliminated all background labelling. Indeed, some of the staining observed in wild-type mice may be indicative of blood vessel staining, although this may be genuine pathology (Bennett et al., 2018). MC1 has been observed to exhibit non-specific binding in mouse samples, at least in western blotting despite it not being recommended for use in western blotting since this disrupts the discontinuous epitope detected by this antibody (Petry et al., 2014), but this may not necessarily translate to IHC. PHF1 does, however, show incredibly high specificity (Petry et al., 2014; Li and Cho, 2020).

3.4.4 Conclusions

The results in this chapter demonstrate a varied astrocytic response to increased tau burden in htau mice injected with tauopathy brain extracts. While astrocytes can be seen to localise near abnormal tau, and thus are in a physiological position to respond to the tau, they do not demonstrate markers of reactivity that might draw parallels with the well-established reactive phenotype of astrocytes in tauopathy brain. Mouse astrocytes differ from human astrocytes, including in their size and number of processes, therefore they may be less adapted to the task of internalising and spreading tau from and to connected neurons. To examine astrocyte capacity for pathogenic tau uptake, it is important to isolate these factors in a new model. Thus, in the next Chapter, a human cultured astrocyte model is established for exploration of the astrocyte response to tau aggregates isolated from post-mortem human AD brain.

4 Establishing and characterising human astrocyte cultures

4.1 Introduction

Human astrocytes differ from their non-primate mammalian counterparts. Although their basic functions are the same (Section 1.4.2), they are more complex in several aspects. First, adult human (and non-human primate) astrocytes are larger, with a threefold increase in diameter and tenfold more processes compared to rodent astrocytes (Oberheim et al., 2006). Humans also have distinct mature astrocyte subtypes that are not found in rodents in the form of layer 1 interlaminar and layer 5-6 polarised astrocytes (Oberheim et al., 2006). More recently, the true heterogeneity of mammalian astrocytes is beginning to be elucidated (Miller, 2018; Batiuk et al., 2020; Bayraktar et al., 2020) (section 1.4.1), including discoveries about the unique neural stem cell niche from which astrocytes subtypes are derived (Allen et al., 2022). It is reasonable to suggest that astrocyte subtypes specific to humans may also exist that are not found in rodents. Functionally, human astrocytes are better able to mediate calcium signals, and their engraftment into mice can improve long-term potentiation and memory (Han et al., 2013). Human astrocytes may thus play a more complex role in disease progression than it is possible to study using rodent models. Indeed, a heterogenous response of astrocytes to disease is also being revealed (Barbar et al., 2020; Wheeler et al., 2020; Sanmarco et al., 2021) (Sections 1.5). It is therefore advantageous to utilise *human* cells to develop an astrocyte model in order to investigate their ability to internalise pathological tau aggregates.

Culturing primary astrocytes from human brain has obvious complications. Successful methods have been developed to culture human neural cells from tissue biopsies removed during neurosurgery (Spaethling et al., 2017). However, this is challenging and efforts in our laboratory to culture astrocytes from brain cancer resections ran into problems when the cultures became over-ran with presumed cancer cells. Other methods involve isolating and culturing astrocytes from post-mortem tissue collected soon after death, and others have shown that this is feasible (Re et al., 2014), and is without the risk of culturing mutated cells from cancerous biopsy tissue. However, this was again attempted in our laboratory and ultimately the postmortem interval in the UK is too long (generally 12 hours plus) to yield viable cells.

Induced pluripotent stem cells (iPSCs) provide a potentially limitless source of human stem cells with minimal ethical consideration in comparison to embryonic derived stem cells. A specific combination of transcription factors, often referred to as the 'Yamanaka' factors after one of the scientists that discovered them (Takahashi and Yamanaka, 2006), allows reprogramming of human somatic cells into a naïve pluripotent state (Antosiewicz-Bourget et al., 2007), from which they can be differentiated into nearly any cell type of the body.

Differentiating specific neural cell types from iPSCs requires an understanding of the complex developmental signalling pathways of the mammalian nervous system. Attempts to induce such changes require exogenous signals in the form of small molecules and transcription factors in order to push cells down a specific fate. Successful protocols to differentiate iPSCs into neural cell types have been established that mimic developmental pathways, inhibiting SMAD signalling pathways (Chambers et al., 2009a) and cells can be induced to further differentiate into functional neurons that display cortical markers (Shi et al., 2012a).

Historically, differentiating astrocytes from a neural intermediate has been a convoluted processes with a resulting astrocyte population that is heterogenous in nature (Krencik et al., 2011; Shaltouki et al., 2013). However, more recent efforts have successfully streamlined the differentiation process and created a 30-day protocol for differentiating iPSCs into functional astrocytes from iPSCs, with the differentiated astrocytes recapitulating functional and transcriptional characteristics of human foetal astrocytes (TCW et al., 2017). These iPSC-astrocytes are immunoreactive with traditional astrocyte markers ALDH1L1 (Cahoy et al., 2008), glutamate transporters EAAT1 and EAAT2 (Rothstein et al., 1994), as well as vimentin (Schnitzer et al., 1981). Gene expression analysis using qPCR confirmed the expression of *GFAP* and *S100B* (Ludwin et al., 1976), *AQP4* (Hubbard et al., 2015), and *APOE* (Boyles et al., 1985). Variations in lineage marker expression observed in these hiPSC, as well as in human primary foetal astrocytes, are thought to demonstrate intercell variability, and/or differences in regional patterning (TCW et al., 2017). The authors also demonstrated a similar transcriptional pattern to human foetal astrocytes through RNA-sequencing, and the gene expression profile correlated well with foetal human cortical brain tissue data from the *Allen BrainSpan Atlas of the Developing Human Brain*. A cell-type specific cluster analysis showed that the iPSC-astrocytes more particularly resemble hippocampal or cortical astrocytes, rather than other cell types of the developing human

brain. Their analysis also pointed at a quiescent, rather than reactive, set of astrocytes, when compared to an RNA-seq data set from murine astrocytes exposed to 'proinflammatory' or' immunoregulatory' conditions (Zamanian et al., 2012).

An alternative method is the differentiation of induced NPCs into astrocytes. The preparation of induced-NPC derived astrocytes (iNPC-As) includes a rapid induction of donor fibroblasts into neural progenitor cells, using the 'Yamanaka' factors for induction to NPCs, followed by culture in media that preferentially supports astrocytes in order to induce astrocyte differentiation from donor fibroblasts (Gatto et al., 2020). This rapid induction protocol allows astrocytes to retain some of the cell ageing characteristics of the donor fibroblasts (Gatto et al., 2020). RNA-seq data suggests that these cells closely resemble adult human astrocytes in their overall transcriptome that correlates with the age of the donor (Gatto et al., 2020), however specific astrocytic genes were not analysed in this work.

The aim of this chapter is to optimise the protocol established in TCW et al. (2017) to generate consistent pools of astrocytes for experimentation. It was also important to characterise astrocytes beyond the 30-day differentiation timepoint established in this paper to examine relevant changes in gene expression and cell morphology with increasing differentiation time. Comparisons were also made with iNPC-astrocytes, as a model with an aged cell phenotype. Throughout these experiments, iPSC-astrocytes cells were tested for their viability after cryopreservation to enable viable stores of cells to be utilised for future chapters of this PhD thesis.

4.2 Methods

Methods are fully described in Section 2.1.2. Briefly, a previously published protocol (TCW et al., 2017) was used as a starting point for differentiating astrocytes from human iPSCs. A control human iPSC line from a neurotypical male (CTR_M3_36S), which had previously been characterised for pluripotency potential and ability to differentiate into neuronal lineages (Cocks et al., 2014) (Robbins et al., 2018), was used for this work.

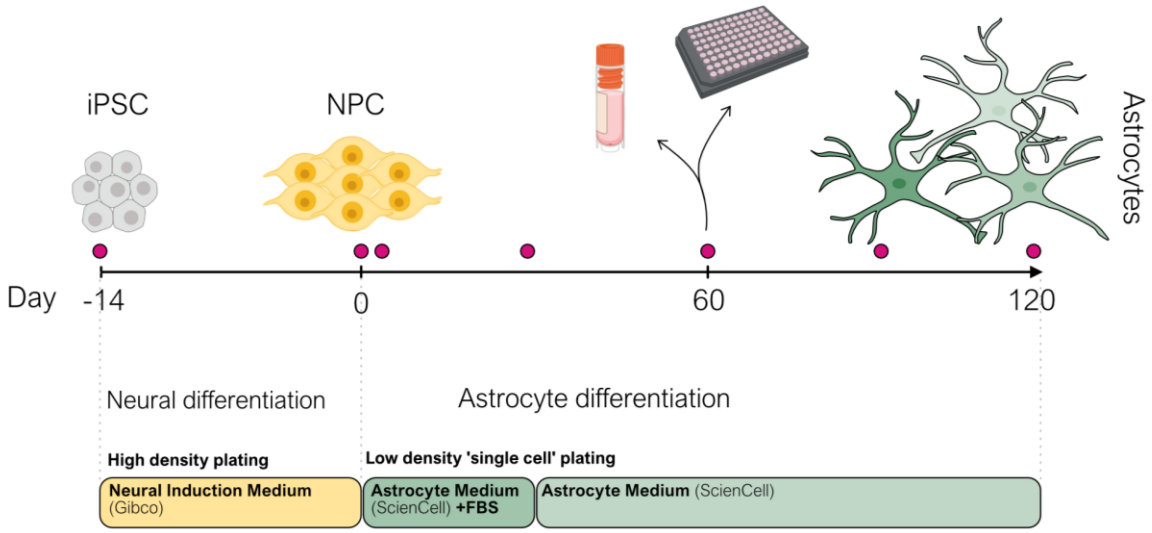

Figure 4.1 Summary of the astrocyte differentiation protocol.

iPSCs were plated in Neural Induction Medium (Gibco), passaged at confluency for 2 weeks to generate neural progenitor cells. These are plated as a single cell suspension in Astrocyte Medium (ScienCell), passaging before cells reach confluency as required. After 30 days, FBS was removed from the medium. At day 60, cells were cryopreserved for future use NPCs and day 30 astrocytes can also be cryopreserved for expansion of stocks at later time points. Samples were taken at various timepoints (red dots) for characterisation.

Neural progenitor cells (NPCs) were first generated from iPSCs using a commercially available kit (Gibco™ PSC Neural Induction Medium, Thermo Fisher Scientific™ (MA, USA) (cat# A1647801) (Yan et al., 2013) that contains bovine serum albumin (BSA), small molecules and products inhibiting GSK and Transforming growth factor β (TGFβ) pathways (manufacturer communication). The induction process results in a homogeneous pool of 'primitive' neural progenitor cells (Figure 4.6a) that retain inducible positional cues from brain development, allowing derivation into region specific neuronal subtypes. For example, GABA neurons from forebrain, dopaminergic neurons from midbrain, and motor neurons from hindbrain have been differentiated from this pool of cells (Yan et al., 2013). These NPCs have further been seen to differentiate into different cell types of the CNS (Martín-Maestro et al., 2019; Liang et al., 2020).

NPCs were then plated at low density in a single cell suspension to promote glial differentiation (Section 2.3.3) in a commercially available medium designed to support human astrocytes (ScienCell, CA, USA; Cat# 1801). This media does *not* contain any small molecules to modify cell signalling pathways.

Cells were cultured until 80% confluent and passaged at a 15,000 cells/cm^2 until day 30. After which, FBS was removed from the media (Figure 4.1). Cells continued to be passaged when they reached approximately 90% confluency. Cell lysates for RNA, protein analysis or cells fixed for ICC were collected at 30-day intervals. Cell batches were frozen, stored in liquid nitrogen vessels (-170°C), and periodically tested for viability following cryopreservation. NPC stocks were cryopreserved for generation of new astrocyte batches and future neurons, and astrocyte stocks were cryostored for future use at 30-day intervals, up to day 60, after which cryo-viability began to decline.

4.3 Results

4.3.1 Characterisation of astrocyte identity by gene and protein expression

Astrocytes are crucial for normal brain development (Clarke and Barres, 2013) and functioning of the CNS (see section 1.4.2). As they mature, they alter their expression of several genes, many of which are critical for key physiological functions in the CNS (Molofsky and Deneen, 2015). Therefore, it was important to characterise iPSC-astrocyte gene and protein expression throughout the differentiation protocol to ascertain an appropriate astrocyte timepoint from which to perform experiments.

Astrocytes in the adult human brain have a number of unique physiological functions (Section 1.4.2) and specific genes are used to identify astrocytes including *GFAP* and *S100B* (Ludwin et al., 1976), *ALDH1L1* (Cahoy et al., 2008) and the glutamate transporters *EAAT1* and *EAAT2* (Rothstein et al., 1994), amongst others. RNA was collected at different timepoints from iPSC stage to iPSC-astrocyte (Figure 4.1), namely iPSC stage, NPC stage, early astrocyte differentiation (day 1 in astrocyte media), day 30, the timepoint characterised in TCW et al. (2016), and at 30-day intervals up to day 120. The expression of key astrocyte genes was examined using qPCR. Samples were normalised for RNA concentration, and then reverse transcribed to generate cDNA to be used for qPCR (Figure 4.3). Gene expression for each sample was normalised to two housekeeping genes *βACTIN* and *GAPDH* and calculated relative to expression in iPSC using the comparative C_T method (2.8.5). No template controls determined background expression and confirmed expression in cell samples (see Methods 2.8.5). The log values of these data were calculated and

analysed for statistical differences. The levels of some proteins encoded by these genes were validated by immunocytochemistry (Figure 4.4 & Figure 4.5).

It was important to first determine that iPSCs and NPCs lose their pluripotent and progenitor phenotype once they differentiate into astrocytes (Figure 4.2).

Oct4 is a transcription factor required to maintain the self-renewal capacity and pluripotency potential of embryonic stem cells (Nichols et al., 1998; Loh et al., 2006), and is one of the Yamanaka factors used to induce pluripotency of iPSCs (Takahashi and Yamanaka, 2006). Oct4 levels were therefore examined (Figure 4.2a). As expected, *OCT4* expression was dramatically reduced at all time points measured relative to iPSC, indicating an instant loss of pluripotency as cells are pushed into an ectodermal cell fate. Gene expression was > 1000-fold lower than measured in iPSCs in all samples measured, and this low level of expression was maintained with further time in culture. A one-way ANOVA indicated that differentiation significantly affected *OCT4* expression ($F(2.530, 8.010) = 242.9$, $p<0.0001$), and Sidak's post-hoc multiple comparison test for multiple pairwise comparisons to (1) iPSC and (2) NPC stages revealed that *OCT4* expression was highly significantly reduced at all timepoints relative to iPSC, while there was no significant difference between NPC and subsequent differentiation timepoints. This indicates that *OCT4* expression was robustly downregulated as cells are differentiated, as expected (Kehler et al., 2004; Wu and Schöler, 2014).

Pax6 is a transcription factor important for progenitor identity, cell cycle and fate in the developing mammalian brain (Ericson et al., 1997; Estivill-Torrus et al., 2002). *PAX6* expression was increased in NPC and iPSC-astrocytes relative to iPSC but showed a general decrease in expression in iPSC-astrocytes with increased differentiation time (Figure 4.2b). Expression peaked at NPC stage with 961.1 ± 49.5 – fold change increase in expression relative to iPSC, as is expected considering that *PAX6* expression is strongly correlated with neural progenitor cell identity (Ericson et al., 1997; Estivill-Torrus et al., 2002; Cvekl and Callaerts, 2017). A one-way ANOVA showed a significant impact of differentiation on *PAX6* expression ($F(1.351, 4.503) = 93.19$, $p<0.003$), and Sidak's multiple comparisons showed that expression was significantly higher in iPSC-astrocytes relative to iPSCs. Comparison relative to NPC showed that *PAX6* expression after 1 day of astrocyte differentiation was significantly decreased, as well as at day 90. While the overall trend was of decreasing PAX6

expression after differentiation into astrocytes, there still appeared to be high levels of expression of *PAX6* during astrocyte differentiation, suggesting that *PAX6* still plays a role in astrocyte identity. Indeed, *PAX6* has been observed to continue being expressed in some populations of GFAP positive astrocyte-like cells of the rat dentate gyrus (Nacher et al., 2005), as well as GFAP positive radial glial like cells in the subgranular zone (Maekawa et al., 2005). It seems that Pax6 is highly dynamic and multifunctional in regulating proliferation and differentiation of astrocytes (Osumi et al., 2008), and this is reflected in changes observed here.

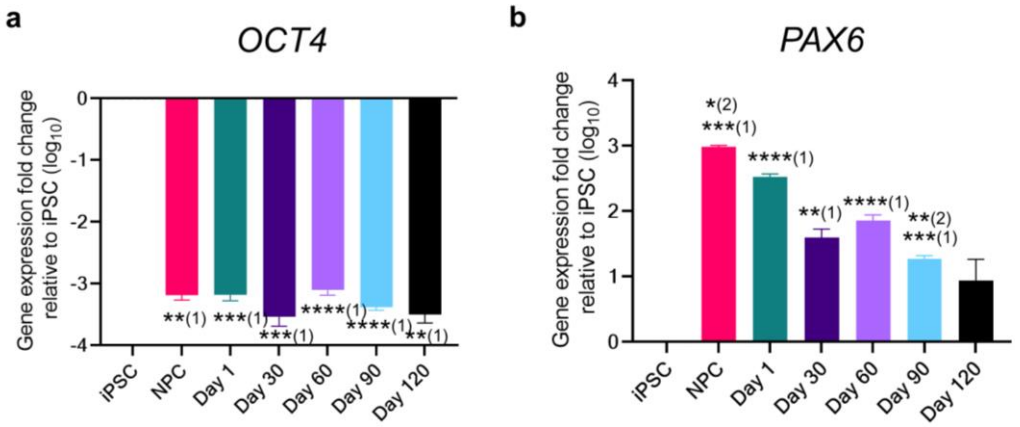

Figure 4.2 Decreased progenitor and increased neural precursor gene expression after iPSC differentiation into astrocytes.

Gene expression of the pluripotency marker *OCT4* significantly decreased after differentiation into NPCs and iPSC-astrocytes (**a**). Neural progenitor identity (*PAX6*) (**b**) significantly increased at NPC stage and thereafter decreased during iPSC-astrocyte differentiation. mRNA gene expression (2^-ΔΔCt) data relative to iPSCs was transformed to $\log_{10}$ for analysis/graphing and presented as mean ± SEM, using one-way ANOVA with repeated measures and Holm-Šidák's pairwise multiple comparisons to iPSC and NPC, denoted by (1) and (2) respectively (***** $p < 0.05$, ****** $p < 0.01$, ******* $p < 0.001$, ******** $p < 0.001$). n = 3-6 separate astrocyte differentiations from a common iPSC line.

Astrocytes are developmentally regulated by the transcription factor Sox9 (Kang et al., 2012), and overexpression of this transcription factor has been shown to aid the induction of astrocyte differentiation from rodent somatic cells (Caiazzo et al., 2015) and is sufficient on its own to induce conversion to an astrocyte fate in human cells (Neyrinck et al., 2021). It was therefore of interest to examine *SOX9* expression during astrocyte differentiation from iPSC.

SOX9 expression was increased at all timepoints relative to iPSC, and all iPSC-astrocytes showed higher levels relative to NPC (Figure 4.3a). A one-way ANOVA revealed that increasing differentiation time had a significant effect on gene expression (F (1.328, 4.428) = 19.68, p=0.0077). Šidák's multiple comparisons test revealed that *SOX9* was significantly higher in day 60 and day 120 astrocytes. Astrocyte expression was not significantly higher than NPCs. *SOX9* expression peaked at day 60, perhaps indicating high levels of activity in the developmental signalling pathways that the transcription factor Sox9 interacts with at this time (Kang et al., 2012). High levels of *SOX9* expression at NPC stage are expected, as this transcription factor is necessary and sufficient to induce and maintain adult neural stem cells (Scott et al., 2010). *SOX9* expression is also expected to be increased by notch signalling during astrocyte differentiation, as this has been observed as a crucial lineage determination step for glial cell induction (Martini et al., 2013). Higher variability in the data with increasing differentiation time may indicate there is variation in the level of *SOX9* expressed by individual astrocytes, and this may be representative of changes in developmental cues with time. Expression appears much higher from differentiation day 60 onwards, perhaps indicating upregulation of Sox9 related pathways for determining glial lineage, although this is difficult to interpret owing to the large effects that Sox9 has on downstream lineage pathways (Jo et al., 2014a).

Aldehyde dehydrogenase 1 family member L1 (*ALDH1L1*) is a gene that encodes the protein 10-formyltetrahydrofolate dehydrogenase – a folate metabolic enzyme that irreversibly converts 10-formyltetrahydrofolate to tetrahydrofolate and CO_2 (Krupenko, 2009). Although expressed in various mammalian tissues (Krupenko and Oleinik, 2002), it has been described as a pan-astrocyte marker in the mammalian CNS (Yang et al., 2011), able to label more astrocytes than GFAP since GFAP levels may only be detectable in "reactive" astrocytes (Cahoy et al., 2008), although this may differ *in vitro*. Therefore, ALDH1L1 expression was assessed during astrocyte differentiation (Figure 4.3b). Expression of *ALDH1L1* at NPC stage was relatively indistinguishable from that of iPSCs, appeared reduced one day after the differentiation protocol started, and only showed an increase in expression from day 30. A one-way ANOVA showed a significant impact of differentiation time on *ALDH1L1* expression (F (1.256, 4.185) = 30.32, p=0.041). Interestingly the data shows that *ALDH1L1* expression was reduced at day 1 of differentiation relative to iPSC, although not significantly. This reduction may be expected, as although *ALDH1L1* is

expressed by postnatal neural stem cells (Foo and Dougherty, 2013), it is also expressed by iPSCs, and can show reduction in expression during early stages of astrocyte differentiation (Szabo et al., 2021). Indeed, the data in Figure 4.3b show that at day 60 after differentiation do astrocytes show a significant increase in ALDH1L1 expression relative to iPSCs. This increase appeared to be maintained although the data were variable, and results were not significant at later time point. Overall, there is a trend of increasing *ALDH1L1* expression with extended astrocyte differentiation time. Large variability at day 90 and other time points may indicate some inconsistencies in *ALDH1L1* expression at this timepoint, and increasing the sample size may have provided more consistent data.

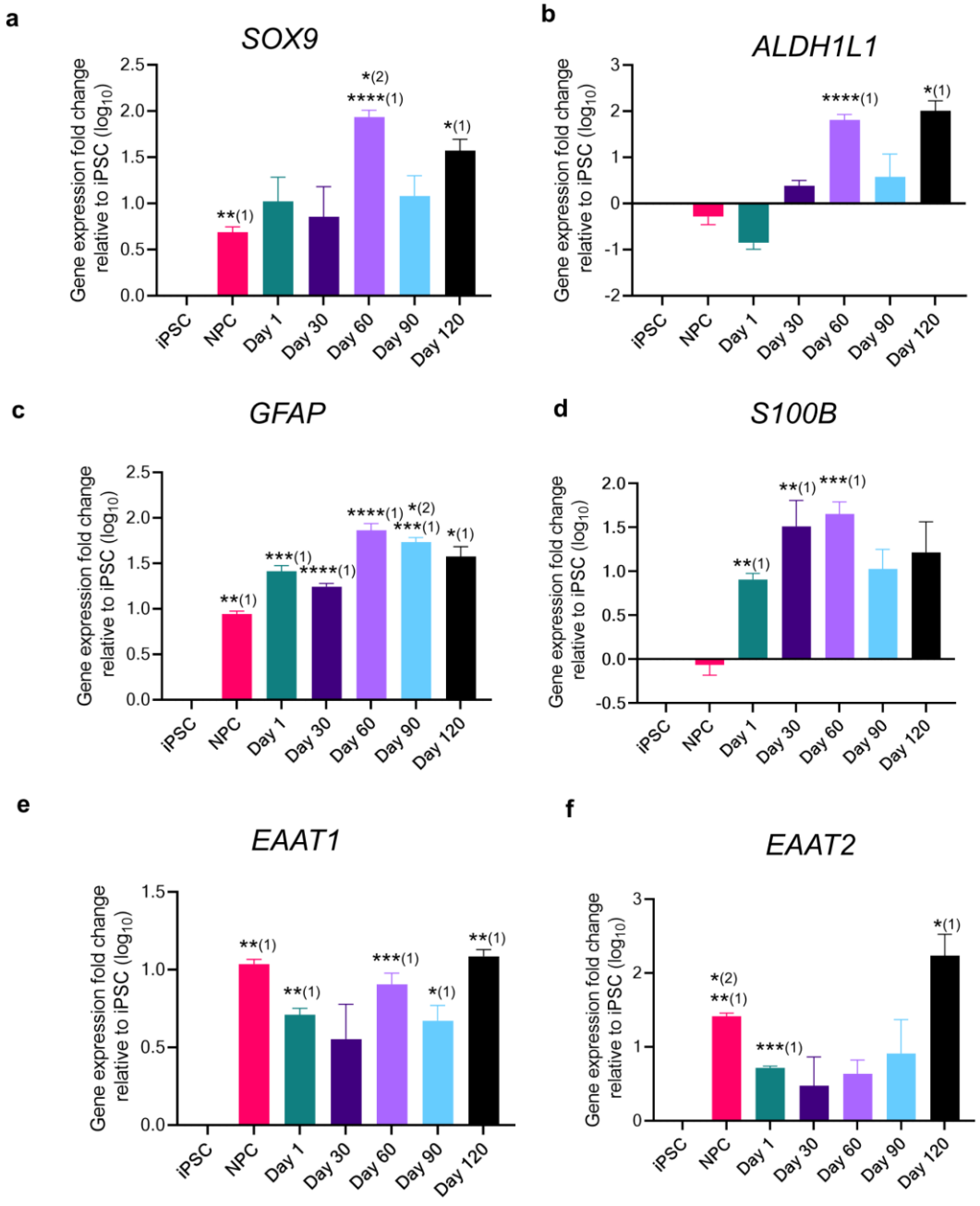
a
SOX9
Gene expression fold change relative to iPSC (log10)
**(1)
*(2)
****(1)
*(1)
iPSC
NPC
Day 1
Day 30
Day 60
Day 90
Day 120
b
ALDH1L1
****(1)
*(1)
c
GFAP
**(1)
***(1)
****(1)
****(1)
*(2)
***(1)
*(1)
d
S100B
**(1)
**(1)
***(1)
e
EAAT1
**(1)
**(1)
***(1)
*(1)
**(1)
f
EAAT2
*(2)
**(1)
***(1)
*(1)

Figure 4.3 Increased expression of key astrocyte markers during iPSC differentiation into astrocytes.

Bar charts show common genes expressed by astrocytes. (a) SOX9, (b) ALDH1L1, (c) *GFAP*, and (d) *S100B* are significantly increased relative to iPSC at longer differentiation times. Expression of the glutamate transporters (e) *EAAT1* and (f) *EAAT2* increase after differentiation relative to iPSCs. n = 3-6 separate astrocyte differentiations from a common iPSC line. Data is presented as mean fold change of gene expression (2^-ΔΔCt) relative to iPSC (value 0). Data is transformed to $\log_{10}$ for analysis/graphing and presented as mean ± SEM, using one-way ANOVA with repeated measures and Holm-Šidák's pairwise multiple comparisons to iPSC and NPC, denoted by (1) and (2) respectively (***** $p < 0.05$, ****** $p < 0.01$, ******* $p < 0.001$, ******** $p < 0.001$). n = 3-6 separate astrocyte differentiations from a common iPSC line.

GFAP is an intermediate filament that may have been crucial in evolution of the CNS, where it coincided with the emergence of different glial cells in primitive fish (Apple, 2013). Intermediate filaments have several roles as key components of the cytoskeleton, including structural support, acting as a scaffold for organelles and other proteins, and mechanosensing changes in the environment (Lowery et al., 2015). GFAP knockout mice are viable show alterations in hippocampal and cerebellar physiology, including altered long-term potentiation, suggesting that GFAP is key for these complex neurological processes (Mccall et al., 1996; Shibuki et al., 1996). Moreover, GFAP null mice do not recover from head injury as readily as wild-type mice, indicating the importance of GFAP in the astrocyte response to injury (Nawashiro et al., 1998). GFAP is expressed exclusively in the CNS and PNS (Uhlén et al., 2015) and is primarily associated with astrocytes (Hol and Pekny, 2015), although it is expressed in progenitor like cells including radial glia that can differentiate into neurons as well as astrocytes (Levitt and Rakic, 1980), and neural progenitors of the adult mouse forebrain (Garcia et al., 2004). There are regional differences in astrocyte *GFAP* expression, and it is widely accepted that white matter astrocytes have higher levels of GFAP than grey (Lundgaard et al., 2014; Olabarria and Goldman, 2017). As at least 6 major isoforms of GFAP are now known to be expressed in the CNS, with GFAPα being the predominant isoform in astrocytes (Messing and Brenner, 2020), although GFAPδ expression has also been noted in developing as well as adult mouse astrocytes (Mamber et al, 2012). Isoforms can also be generated by alternative splicing, uncommon in other intermediate filaments (Hol and Pekny, 2015). To avoid isoform bias when analysing *GFAP* expression here, qPCR was performed using a set of primers that were designed to span all isoforms (Table 2.4).

The gene expression data analysed here shows that *GFAP* expression in iPSC-astrocytes was increased relative to iPSCs at all differentiation time points (Figure 4.3c). This appeared highest at longer astrocyte differentiation time points when compared to NPC, particularly from day 30. A one-way ANOVA confirmed that time of differentiation had a significant impact on *GFAP* expression ($F(1.364, 5.910) = 156.4$, $p<0.0001$), and Šidák's multiple comparisons tests showed that GFAP expression was significantly increased in all iPSC-astrocytes compared to iPSCs. GFAP expression in NPC and astrocytes differentiated for 1 day only is expected since GFAP is known to be expressed in neural progenitor cells (Garcia et al. 2004). GFAP expression is expected to be higher as astrocytes age, considering observations *in vivo* (Hol and Pekny, 2015; Vasile et al., 2017), although how this is mirrored in *in vitro* conditions is yet to be determined, as it is possible that culture conditions can affect cytoskeletal behaviour (Barooji et al., 2021).

S100β encodes one member of the S100 family of proteins that can bind calcium and help regulate various cell functions, both intra- and extra- cellularly (Donato et al., 2009). Although S100β expression is not unique to astrocytes, being expressed in a variety of cells not just in the CNS (Donato et al., 2009), including oligodendrocytes (Hachem et al., 2005), retina cells (Rambotti et al., 1999) and muscle cells (Arcuri et al., 2002), it has still been historically used as an astrocyte marker in the brain (Ludwin et al., 1976), and its levels are correlated with the maturation of astrocytes from neural stem cells in the mouse CNS (Raponi et al., 2007). Therefore, its expression was examined during differentiation of iPSC-derived astrocytes (Figure 4.3d).

S100B levels did not appear largely altered between iPSC and NPC, and this is in line with GFAP-expressing neural progenitor cells of the subventricular zone that were observed not to express S100B (Raponi et al., 2007). Expression was much higher at the start of astrocyte differentiation, and this level of expression was largely maintained through each subsequent astrocyte differentiation timepoint. Expression was observed to be highest at day 30 and 60 of astrocyte differentiation. A one-way ANOVA confirmed that differentiation time had a significant impact on *S100B* expression ($F(1.891, 8.196) = 15.67$, $p=0.0017$), and pairwise multiple comparisons demonstrated a significant increase in *S100B* expression in all iPSC-astrocytes up to day 60 relative to iPSCs, which were most significant at day 30 and 60. Variations in S100B expression at different astrocyte timepoints may be down to environmental cues, as S100B expression can be easily altered by environment (Donato et

al., 2009). More experimental repeats at higher time points may prove significant for astrocytes of this differentiation age. Overall, however, these data demonstrate a consistently elevated *S100B* expression as iPSCs differentiate into astrocytes.

The uptake of glutamate is fundamental to the role of astrocytes in the CNS, being crucial for glutamate homeostasis at synaptic junctions (Mahmoud et al., 2019). Excitatory amino acid transporters (EAATs) are sodium-dependent transporters responsible for the majority of extracellular glutamate uptake (Rose et al., 2018), predominantly through EAAT1 and EAAT2 (known as GLAST and GLT-1 respectively in rodents) (Lehre and Danbolt, 1998; Eulenburg and Gomeza, 2010), which are the main glutamate transporters expressed by mammalian astrocytes (Danbolt, 2001). EAAT1/GLAST was observed to be expressed by radial glia and immature astrocytes in the developing mouse forebrain and cerebellum postnatally (Shibata et al., 1997), while also predominantly being expressed by mature astrocytes in the CNS (Schmitt et al., 1997; Lehre and Danbolt, 1998). Some expression, although relatively reduced, has been observed in microglia and oligodendrocytes in primary rodent cultures (Kondo et al., 1995). EAAT2/GLT-1 is less expressed during early development (Furuta et al., 1997; Ullensvang et al., 1997; Schreiner et al., 2014), but is highly expressed by mature astrocytes in the CNS (Rothstein et al., 1994). It was therefore important to examine the expression profile of these two transporters during astrocyte differentiation from iPSCs since these are linked with key astrocyte functions.

EAAT1 expression was elevated at all differentiation timepoints relative to iPSC expression (Figure 4.3e). This appeared highest at NPC and day 120. A one-way ANOVA analysis confirmed that length of differentiation significantly affected *EAAT1* expression ($F(1.471, 4.905) = 14.98$, $p=0.0097$), and pairwise comparison revealed that all iPSC-astrocytes (except day 30) showed significantly higher *EAAT1* expression compared to iPSC. High expression levels of *EAAT1* at NPC stage might be expected considering that *EAAT1*/GLAST is expressed in immature GFAP expressing radial glia cells in the developing mouse spinal cord (Shibata et al., 1997) and ependymal neural cells of rat brain (Schmitt et al., 1997). In the developing mouse hippocampus, *EAAT1* expression in GFAP positive cells increases after birth (Schreiner et al., 2014), and high expression at day 120 may indicate that further increases in expression might be expected had astrocytes been differentiated for longer. Overall, these results demonstrate a high expression of *EAAT1* with astrocyte differentiation.

Expression of *EAAT2* was lower in comparison, although a similar pattern of expression was observed, with highest levels of *EAAT2* being observed in NPC and astrocytes differentiated for 120 days (Figure 4.3e). A one-way ANOVA indicated that length of differentiation time significantly alters EAAT2 expression ($F(1.944, 6.480) = 6.863$, $p=0.0255$), although pairwise comparisons revealed this was significantly increased at NPC and day 1. The data indicates increased expression at all astrocyte stages, peaking at day 120, however this was not significant, perhaps due to variability in repeats at each time point. High expression is expected as astrocytes mature with time, and *in vivo,* higher levels of *EAAT2* expression correlate with later developmental stages as observed previously in rat brain (Rothstein et al., 1994), and further in mice brain where expression has been seen to peak around 20-25 days postnatally (P20-25) (Schreiner et al., 2014). This contrasts with *EAAT1* that peaked in astrocytes around P3-5 in this study. With highest *EAAT2* levels observed at day 120 astrocytes here, this may indicate that astrocytes are relatively immature and will continue to express higher levels of *EAAT2* if differentiated for longer.

Immunocytochemical labelling of ALDH1L1 protein in iPSC-astrocytes differentiated for 1, 30 and 60 days (Figure 4.4) demonstrated the presence of ALDH1L1 protein at all stages, including in astrocytes differentiated for only 1 day, indicating that this protein is also expressed to a lesser extent in progenitor and stem cell like cells, in agreement with the results from qPCR. ALDH1L1 showed a predominantly cytoplasmic localisation and was abundant in branches in astrocytes differentiated for 60 days, as described by others in mouse cortical cells (Yang et al., 2011). Overall, these data are in broad agreement with previous reports (Szabo et al., 2021.; Foo and Dougherty, 2013; Molofsky et al., 2013).

Immunocytochemical labelling of GFAP proteins using a polyclonal antibody that is not specific to any one isoform (Agilent Dako; CA, USA (Cat# Z0334)) demonstrated relatively high expression of GFAP from Day 1 after differentiation from NPC to Day 60 post-differentiation (Figure 4.4), as confirmed by gene expression data. In day 60 astrocytes, GFAP showed high cytoplasmic expression that tended to decrease with distance from the nucleus but was also visible in astrocyte processes. While expression of GFAP was relatively consistent, rare cells did express dramatically higher GFAP expression, and this may be representative of astrocyte subtypes within these cultures (Figure 4.4). As GFAP expression is altered in response to environmental cues (Messing and Brenner, 2020), resulting in variable GFAP expression within localised populations of astrocytes *in vivo* (Oberheim et al.,

2006), it may be expected that there is astrocyte heterogeneity in cultures. Nonetheless, GFAP appeared to highlight all cells in culture, and thus this antibody was used as a general astrocyte marker for subsequent experiments (Figure 4.5, Figure 4.4 and Figure 4.6).

Immunocytochemical analysis of astrocytes differentiated for 1, 30 and 60 days confirmed EAAT2 protein expression (Figure 4.5). EAAT2 was localised to the cell soma with patches of high expression across cells, and higher expression was particularly apparent in astrocytic processes by 60 days of astrocyte differentiation (Figure 4.5, bottom panel). This is in line with previous EAAT2 analysis in mouse astrocytes of the hippocampus, where immunoreactivity did not cover whole cell soma and discrete clusters of expression was observed in perivascular endfeet (Schreiner et al., 2014). Indeed, time in culture after passaging and the number of astrocytic processes put out by astrocytes may strongly influence *EAAT2* expression.

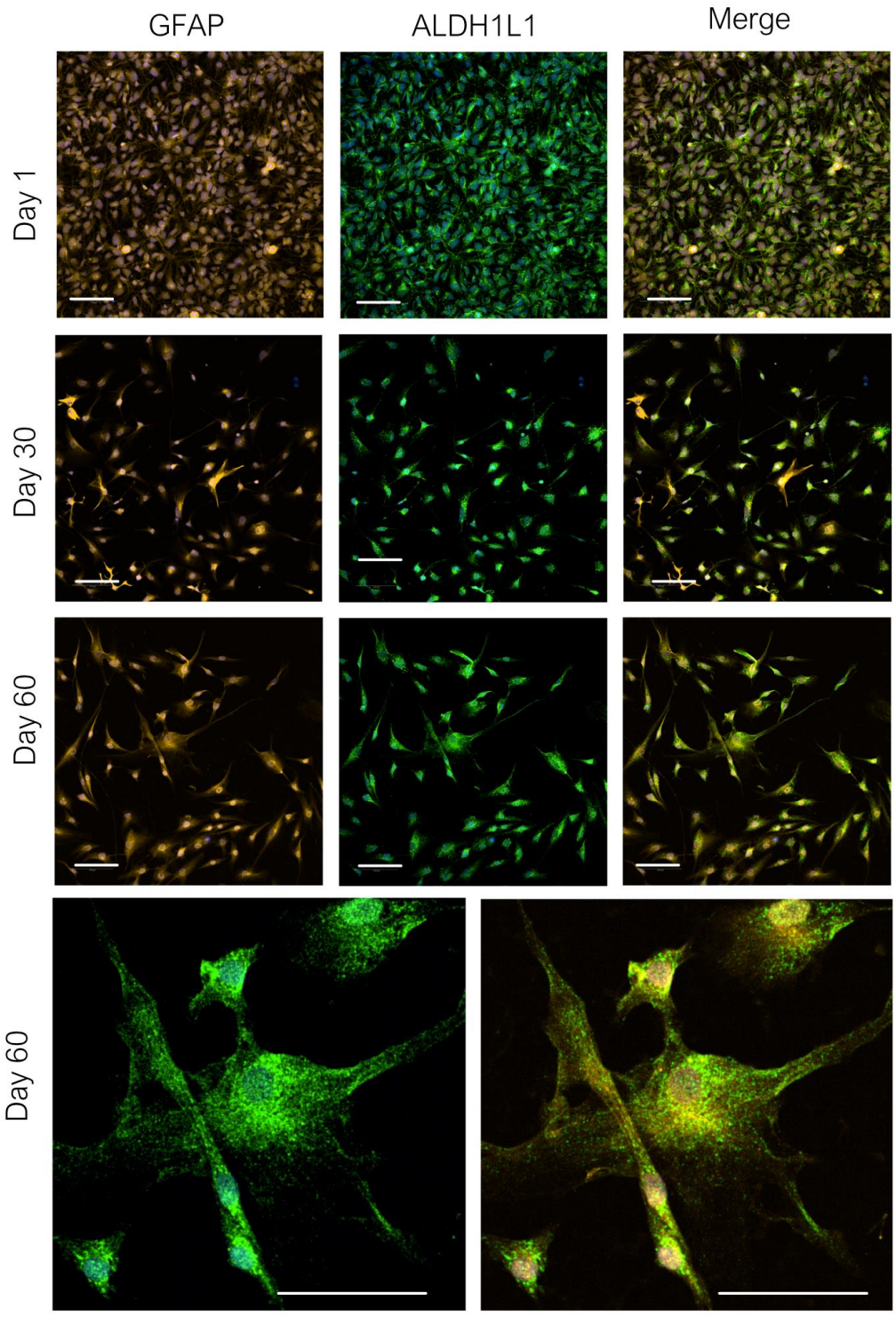

Figure 4.4 Immunocytochemistry of ALDH1L1 and GFAP during astrocyte differentiation.
Representative images of ALDH1L1 labelling (green) in astrocytes differentiated for 1, 30 and 60 days. Astrocytes expressed ALDH1L1 at all time points. An antibody against GFAP was also used to label astrocytes (yellow). Higher magnification images shown for day 60. Nuclei were labelled with Hoechst 33342. White scale bar = 100 µm. N=3.

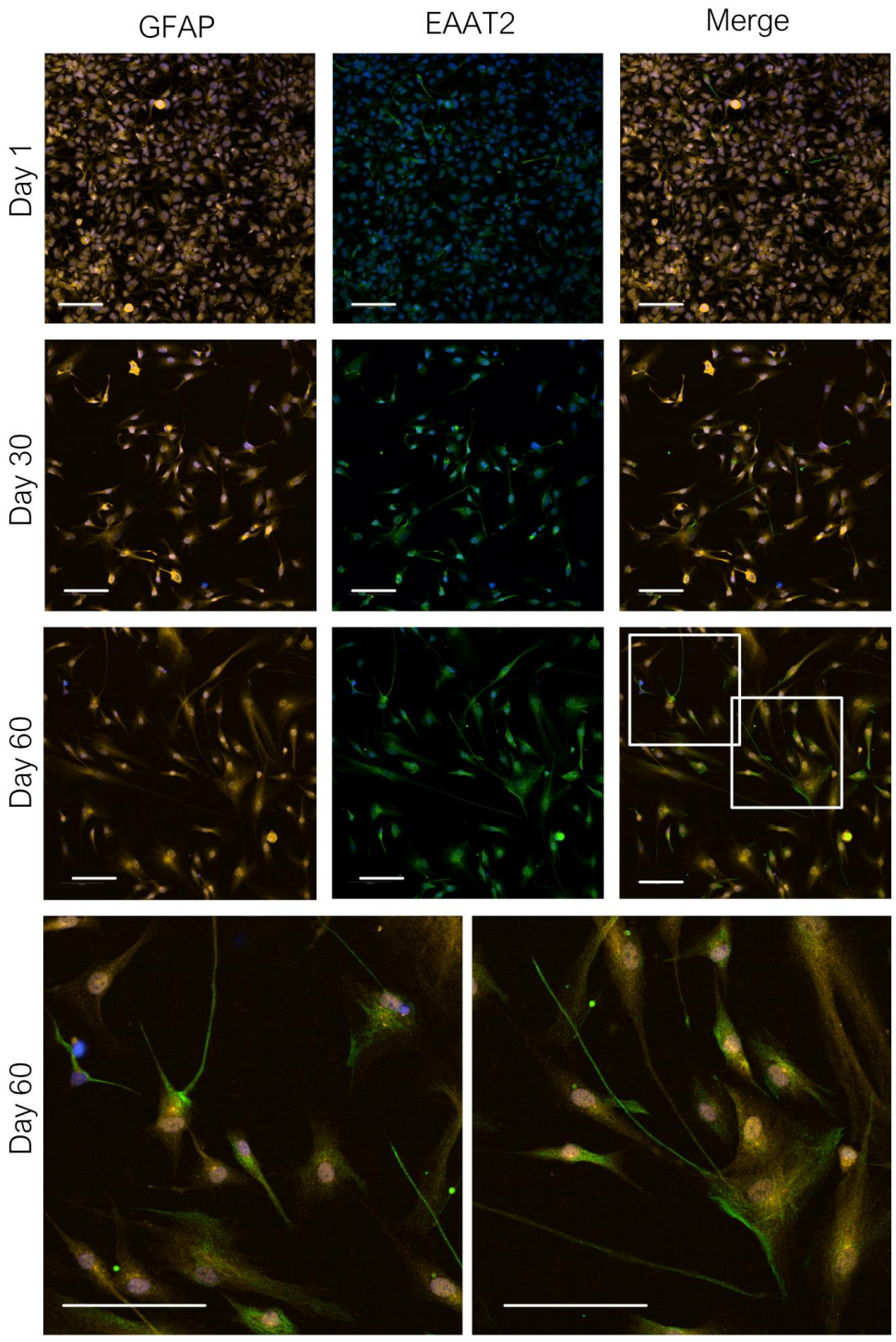

Figure 4.5 Expression of EAAT2 during astrocyte differentiation from iPSC.

Representative images of iPSC-derived astrocytes immunolabelled with an antibody against EAAT2 (green) at different timepoints of differentiation from iPSC. Cells were also immunolabelled using an antibody against GFAP (yellow). Nuclei are stained with Hoechst 33342. Astrocytic processes, as highlighted in the bottom panel (magnified from white boxes above), show relatively high levels of EAAT2 protein. White scale bar = 100 µm. N=3.

As a whole, with increasing astrocyte differentiation time, these data demonstrate an increase in the expression levels of genes found in mature astrocytes, as well as a relative decrease in markers or pluripotency and precursor states which appear broadly in line with changes expected during development.

4.3.2 Astrocyte morphological changes with time in culture

Astrocyte morphology is observed to change during development (Freeman, 2010). Postnatally, they initially extend long filopodial processes that can overlap with nearby astrocytes (Bushong et al., 2004). With time, their processes are refined to occupy unique spatial domains and their processes are closely associated with synapses (Bushong et al., 2004). They have also been seen to increase in size during this post-natal period (Nixdorf-Bergweiler and Albrecht, 1994).

While different astrocyte morphologies exist in the iPSC-derived astrocytes that have been established (Figure 4.4 & Figure 4.5), which may represent heterogeneity within the same population, general trends can be captured by high-throughput image analysis. To this purpose, cell size and cell roundness were analysed in NPCs and astrocytes differentiated for 1- 60 days. Cells were immunolabelled with an antibody against GFAP and nuclei were stained with Hoechst 33342. The Perkin Elmer Opera Phenix imaging system was used to capture images. Cell detection and analyses of characteristics was performed using Harmony software. Cell sphericity was measured as an average of cells per well, with 1 representing a perfect circle. Neural progenitors are typically small and round (Figure 4.6a), and thus demonstrated the highest cell roundness (Figure 4.6c). With longer times of astrocyte differentiation, there was a consistent decrease in cell roundness, likely attributed to an increase in the number of astrocytes putting out projections. Interestingly, the average cell size of astrocytes also increased with differentiation time (Figure 4.6d). While cells differentiated for more than 60 days were not included in this analysis, a representative phase contrast image of day 120 astrocytes demonstrates the further increase in size that may occur in some astrocytes, along with increased number of processes.

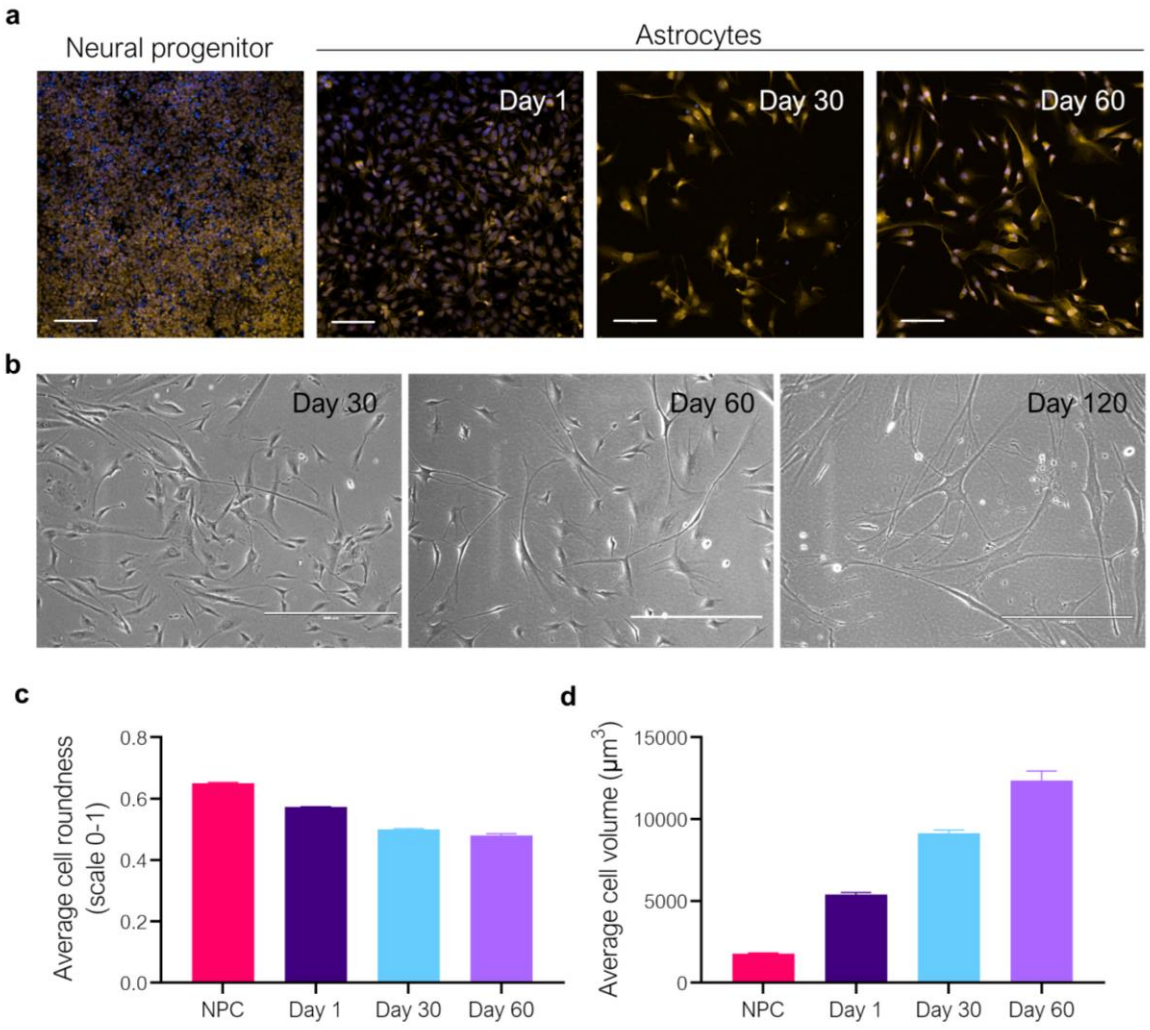

Figure 4.6 Changes to astrocyte morphology with differentiation time.

(**a**) Captured images from NPCs and astrocytes differentiated for 1, 30, and 60 days and immunolabelled with an antibody against GFAP were analysed for morphological changes using Harmony software. Nuclei were stained with Hoechst 33342 (blue). White scale bar is 100µm. (**b**) Phase contrast images of astrocytes in culture demonstrate changes in cell size and complexity with time in culture (white scale bar = 400 µm). Cells were analysed in 3D using Z-stacks of GFAP immunostaining for both (**c**) cell roundness (scale 0-1 with 1 being a perfect circle) and (**d**) cell volume (μm^3) Data is mean ± SEM. n = 3-6 separate astrocyte differentiations from a common iPSC line.

4.3.3 MAPT expression in hiPSC-derived astrocytes

Although tau is primarily expressed by neurons (Binder, 1985), in humans it is now known to be expressed at lower levels in glial cells, including astrocytes (Zhang et al., 2014; Darmanis et al., 2015; Seiberlich et al., 2015; McKenzie et al., 2018), and to a greater extent than found in rodent astrocytes (Zamanian et al., 2012).

The expression of tau in astrocytes has implications for the spread of pathogenic tau in the brain, where current understanding implies that endogenous tau molecules in astrocytes have the potential to be seeded by tau filaments (Jucker and Walker, 2018; Vogels et al., 2019). Therefore, astrocytes were examined for *MAPT* expression by qPCR (Figure 4.8) and immunocytochemistry (Figure 4.7). Since the isoforms of tau expressed may also be important for the ability of tau to be seeded (Clavaguera et al., 2013), previously published primer sequences (Table 2.4) (Spicakova et al., 2010) were used to detect the N-terminal inserts and microtubule binding domains that together comprise the six major isoforms of tau in the adult human CNS (Figure 1.4). Gene expression was calculated relative to a positive control which was RNA isolated from post-mortem human adult temporal cortex (Figure 4.8). Note that due to sample availability and time constraints, data was not available for NPC or day 120 astrocytes as with previous qPCR characterisation.

To first look at presence and/or cell distribution of tau, cells were immunolabelled with a polyclonal tau antibody that is not isoform specific (Figure 4.7). Interestingly at NPC stage, tau highlighted long processes that were not apparent following labelling of cells with GFAP antibodies or phase contrast imaging, and this was the predominant tau protein expression, with lower levels observed in cell soma. At day 1 of differentiation reduced numbers of these processes were observed, which likely reflects that cells are plated at lower density in astrocyte media. With longer times of differentiation into astrocytes, tau is observed in the cell soma of astrocytes with some showing high expression in processes by 30 days post-differentiation. Tau expression was quite high in perinuclear regions and was more diffuse in other regions of the cytoplasm, and by 60 days of differentiation tau was less obvious in astrocyte processes. Expression of tau in astrocyte and neural progenitor cells has not previously been well characterised, but high levels of tau expression in NPC processes and immature (day 1) astrocyte processes are in line with evidence that tau is important in neurite outgrowth (Knops et al., 1991; Yuan et al., 2008). It is likely that these do not represent

neurons since the selection medium used does not support neuronal differentiation. Moreover, cells co-labelled with GFAP.

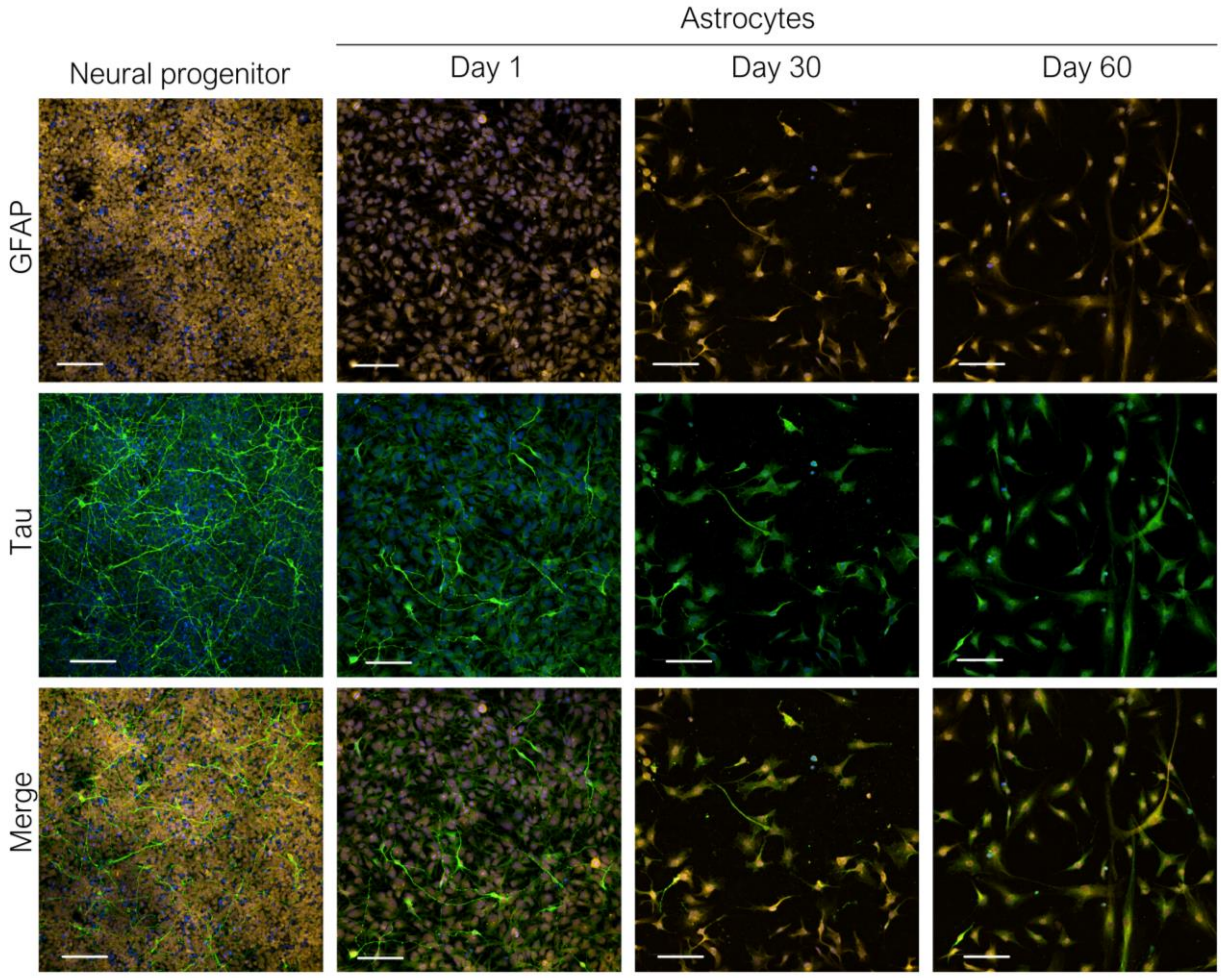

Figure 4.7 Expression of tau protein with differentiation of astrocytes from iPSC.
A non-isoform specific antibody for tau protein (Agilent Dako; CA, USA (Cat# Z0334) was used to look at tau protein levels (green) in NPCs and astrocytes differentiated for 1, 30, and 60 days. GFAP was used to label all astrocytes (yellow) and nuclei were stained with Hoechst 33342 (blue). White scale bar = 100 µm. n=3.

The mRNA expression of *MAPT* in astrocytes was then examined to validate ICC data. *MAPT* was expressed at all astrocyte differentiation timepoints, correlating with ICC data, but as expected, expression of all tau isoforms and overall *MAPT* expression was drastically lower relative to measurements from a reference human brain sample (Figure 4.8a). *MAPT* expression was relatively higher in astrocytes differentiated for 1, 30 and 60 days. However, levels returned to similar levels as in iPSC by 90 days of differentiation. A one-way ANOVA was performed and showed that length of differentiation had a significant effect on *MAPT*

expression ($p<0.0001$). Pairwise comparisons to day 1 iPSC-astrocytes using Šidák's multiple comparison tests showed that *MAPT* expression was significantly reduced in iPSC-astrocytes by 90 days of differentiation compared to 1 day. This indicates there may be an initial increase in *MAPT* expression as astrocytes differentiate which is then reduced as astrocytes mature. *MAPT* is known to undergo developmental regulation generally throughout the CNS (Kosik et al., 1989; Hefti et al., 2018), so it follows that astrocyte expression of tau may also be regulated, although this is an area that requires more research.

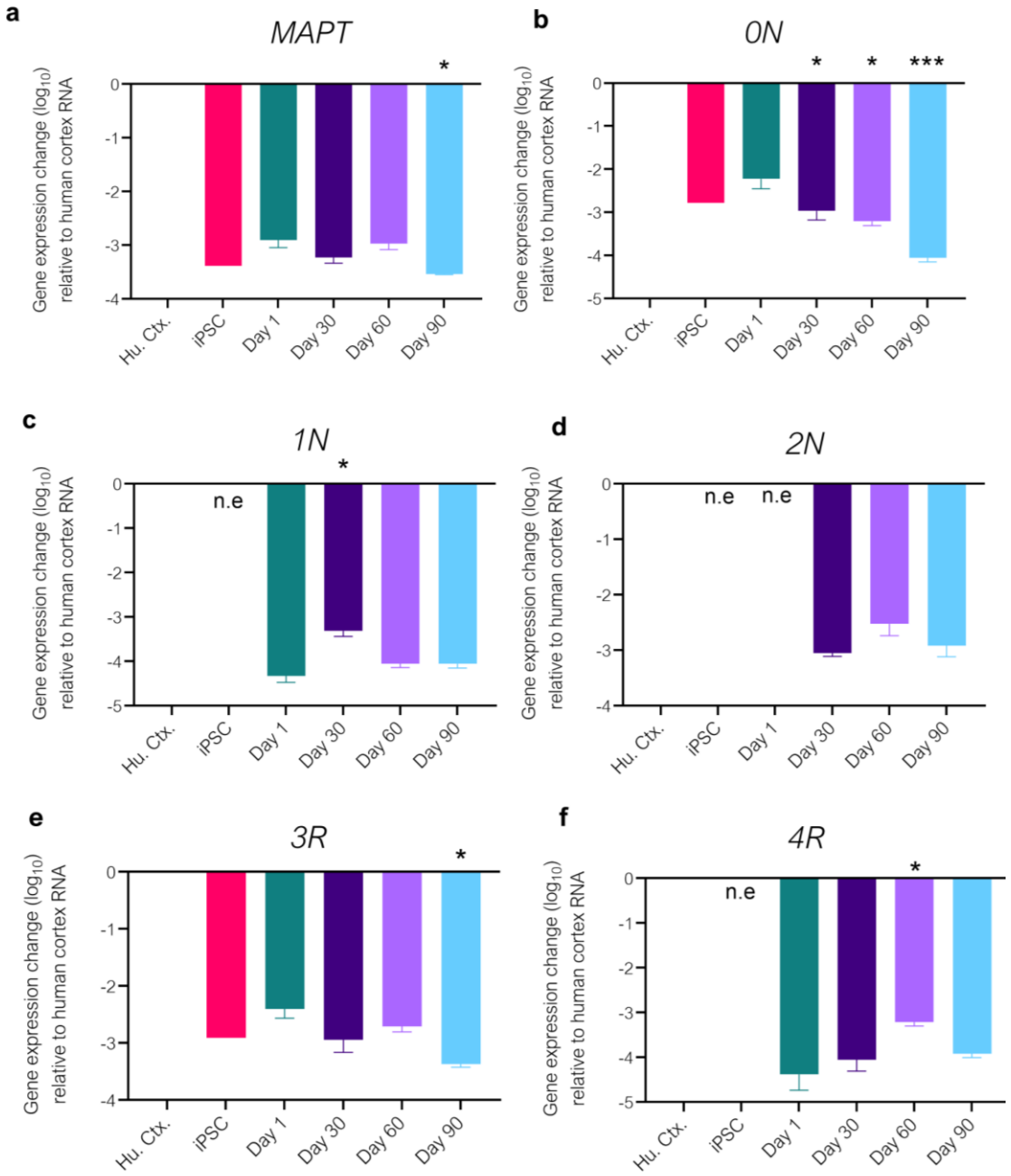

Figure 4.8 MAPT isoform expression changes with astrocyte differentiation.

The expression of **(a)** all *MAPT* isoforms as well as individual tau domains **(b)** 0N, **(c)** 1N, **(d)** 2N, **(e)** 3R and **(f)** 4R were assessed by RT-qPCR. **0N** expression, for example, indicates the presence of 0N3R and/or 0N4R tau isoforms, and likewise for other tau isoform primers (**1N** = 1N3R / 1N4R; **2N** = 2N4R / 2N4R; **3R** = 1N3R / 2N3R / 0N3R; **4R** = 0N4R / 1N4R / 2N4R). Data presented as mean fold change in gene mRNA expression (2^-ΔΔCt) relative to mRNA from human control temporal cortex of post-mortem brain (normalised value 0). Data is transformed to $\log_{10}$ for analysis and presented as mean ± SEM, using one-way ANOVA with Šidák's pairwise multiple comparisons to day 1 astrocytes. * $p \leq 0.05$, ** $p \leq 0.01$, *** $p \leq 0.001$. n = 3 separate astrocyte differentiations from a common iPSC line for day 1 – 90 astrocytes, n = 1 for iPSC and the human brain sample used for comparison.

Specific primers were used in order to determine relative expression of tau isoforms. Primers that are specific for 0N tau isoforms were used to determine the relative expression of tau isoforms with no N terminal domains (Figure 4.8b). All differentiation timepoints expressed some level of 0N, indicating expression of this isoform even if it was highly lowered compared to human brain RNA. Expression of this isoform appeared relatively highest at day 1 of astrocyte differentiation, with one ANOVA showing significant decreases with longer times of differentiation. Pairwise Šidák's multiple comparisons analysis showed significant differences in 0N *MAPT* expression between astrocytes differentiated for 30, 60 and 90 days relative to astrocytes differentiated for 1 day. To determine if this expression correlates with 3R or 4R tau isoforms, primers specific for those isoforms (Figure 4.8e & Figure 4.8f) were examined. No expression of 4R tau at iPSC stage was detected, but there were low levels of 3R tau, indicating that iPSCs express only 0N3R tau at low levels. This may be expected considering that 0N3R tau isoforms are associated with early stages in development (Goedert et al., 1989; Kosik et al., 1989), and it is feasible that low-level 0N3R expression may occur in pluripotent stem cells which are readily induced into ectoderm lineage (Yan et al., 2013), but how much mRNA is translated into tau protein in these cells is unknown.

For day 1 astrocytes, 3R expression was the highest in comparison to other differentiation time points, indicating that again 0N3R is expressed. This was also the case for astrocytes differentiated for 30 and 60 days. At day 90 of differentiation, 3R tau expression was significantly lower than observed at day 1, indicating a reduction in 0N3R tau by this time point that may correlate with a maturity in astrocytes, as 0N3R tau isoforms are the predominant isoform at foetal stages of development (Kosik et al., 1989; Hefti et al., 2018). This reduction in 0N3R tau with differentiation time also appears to broadly correlate with an increase in 4R tau expression (Figure 4.8f), as day 60 and 90 astrocytes show relatively higher levels of 4R tau which is significantly higher at day 60 relative to day 1. This indicates

that 0N4R tau isoforms are expressed in astrocytes as they differentiate and may be a sign of *MAPT* developmental regulation as astrocytes mature.

1N tau expression (Figure 4.8c) was not detected in iPSCs but was again expressed at low levels at day 1 of astrocyte differentiation. This appeared to increase significantly to its highest relative level at day 30 of astrocyte differentiation, reducing to a stable level at day 60 and 90. This indicates that 1N3R isoforms are also expressed as astrocytes develop, and this may be a transient expression at this 30-day timepoint as it appears to decrease at subsequent timepoints. 1N4R isoforms may also be expressed at some astrocyte differentiation time points, with highest levels being detected at differentiation day 60 and 90, as indicated by both 1N and 4R tau expression (Figure 4.8f).

2N tau isoforms were not detected prior to day 30 of astrocyte differentiation (Figure 4.8d), and this is expected considering 2N4R, the longest tau isoform, is associated with adult brain tissue (Hefti et al., 2018), being rarely detected before P0 in mice (Liu and Götz, 2013). The presence of 2N tau indicates that full length 2N4R tau, as well as 2N3R tau, can be expressed in these astrocytes as they differentiate past day 30. Differentiation day 60 astrocytes appear to show highest expression of 2N tau, although this is not significantly different from day 30 when tested for pairwise comparisons after one-way ANOVA was found to show a significant effect of differentiation time on 2N expression ($p=0.0044$).

Overall, these data represent a change in the pattern of tau isoform expression with differentiation from iPSC to day 90 astrocytes. Limited tau isoforms and higher levels of foetal associated tau (0N3R) at early differentiation stages appears to reduce as astrocytes age, and by day 90, 1N, 2N, 4R and smaller amounts of 3R tau were observed, and this likely represents an increase in the number of tau isoforms expressed by these cells, with 1N4R and 2N4R tau likely the most highly expressed. Thus, astrocytes appear to show developmental regulation of tau isoform expression as previously reported for iPSC-derived neurons (Sposito et al., 2015). However, while it could take several months or even years (Sposito et al., 2015) for 4R forms of tau to be expressed by control iPSC-neurons, 4R tau was observed in iPSC-astrocytes at detectable levels after 60 days. In future studies it will be important to confirm that these data correspond to protein levels by western blotting.

On the basis of all characterisation experiments, it was decided that day 60 astrocytes represent the most robust and time-efficient timepoint for future use.

4.3.4 Comparing iPSC-astrocytes to human induced NPC derived (iNPC) astrocytes

The establishment of iPSCs from human somatic cells places them in a developmentally and epigenetically naïve state (Patterson et al., 2011), also resetting their age associated changes (Miller et al., 2013). As tauopathies are neurodegenerative diseases primarily associated with age, this begs the questions as to whether an ageing phenotype is required to model and investigate neurodegenerative changes including the uptake and spread of tau. Thus, an alternative astrocyte model, in which some molecular aging-like changes are retained, was considered. These cells were first compared to iPSC-derived astrocytes.

Previously, a method was established for the rapid induction of donor fibroblasts into neural progenitor cells (dubbed iNPCs) and 7-day differentiation into astrocyte-like cells (iNPC-Astrocytes) (Gatto et al., 2020). Interestingly, astrocytes derived from the fibroblasts of aged donors retained many of the aged cell associated characteristics compared to those derived from young donors, including nucleocytoplasmic shuttling differences, altered oxidative stress response, and overall transcriptional differences, as well as a reduced ability to support neurons in co-culture after pro-inflammatory stimuli (Gatto et al., 2020).

In collaboration with Professor Laura Ferraiuolo at the Sheffield Institute for Translational Neuroscience, some iNPC-astrocyte lines were investigated. These cells were characterised and compared to iPSC-derived astrocytes. First, the expression of key genes, as described above for iPSC-astrocytes, were investigated in two iNPC-astrocyte cell lines (155v2 and CS14) that were derived from healthy control adult donors. These were compared with iPSC-astrocytes differentiated for 60 days (Figure 4.9a).

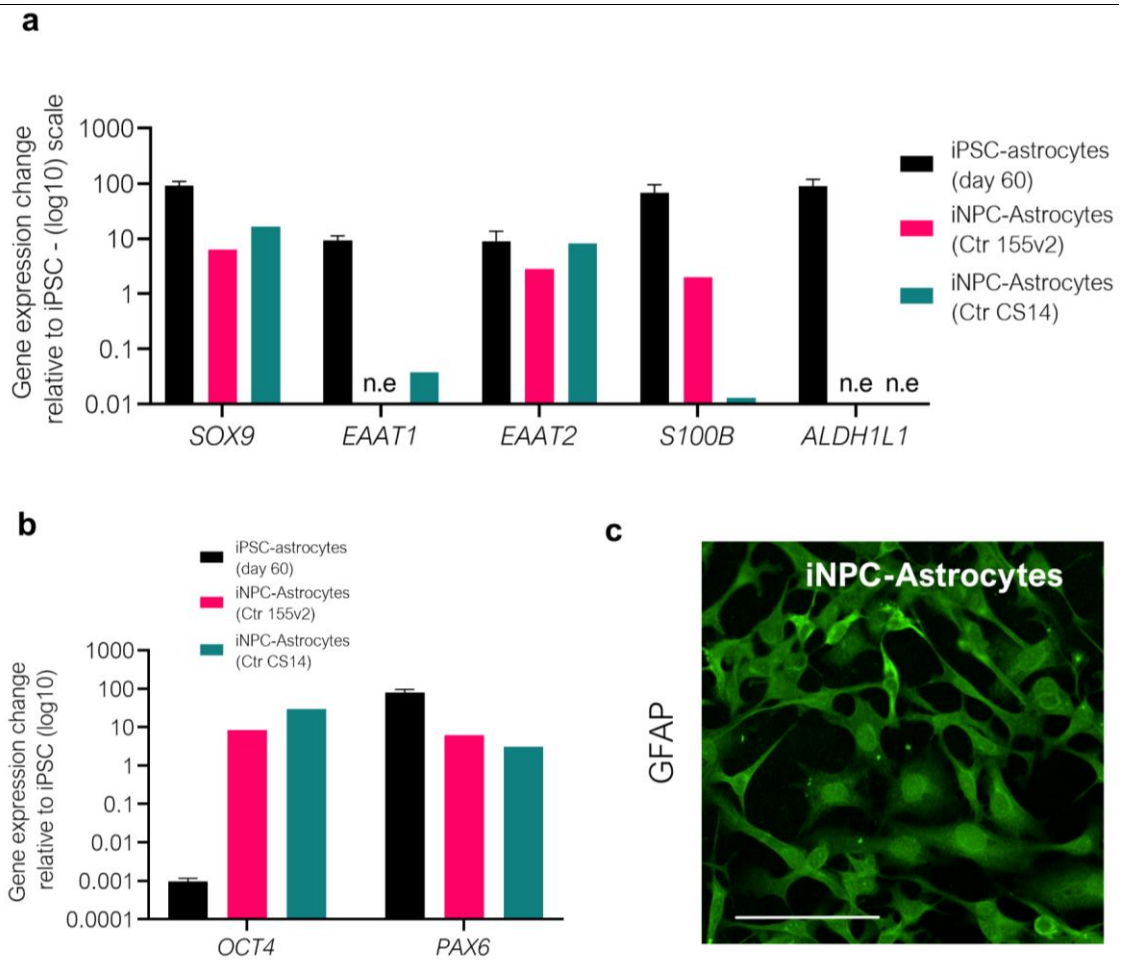

Figure 4.9 Comparison of iNPC-astrocytes and iPSC-astrocytes.

Two iNPC-Astrocyte cell lines were analysed for gene expression of key astrocyte markers compared to their expression in iPSC-astrocytes that were differentiated for 60 days **(a)**Stem cell and neural progenitor markers OCT4 and PAX6 were also examined (**b**) Example of iNPC-Astrocytes in culture immunolabelled with an antibody against GFAP (green), (**c**) Gene expression data is presented as fold change relative to iPSC and presented on a logarithmic scale, ± SEM where possible. N=3 for iPSC-astrocytes, n=1 for each iNPC-Astrocyte cell lines. n.e = no detectable expression.

In both iNPC-Astrocyte cell lines, *SOX9* expression was higher relative to iPSC stage and comparatively similar to iPSC-derived astrocytes (Figure 4.9a), suggesting that these cells are also undergoing Sox9 related transcriptional changes as would be expected as this reflects developmental pathways related to astrocyte development (Kang et al., 2012), but this could also be latent expression from neural progenitor cell induction, as Sox9 can induce and maintain neural stem cells (Scott et al., 2010).

EAAT1 expression was either lower (CS14) than iPSC stage or not detectable (155v2) in iNPC-Astrocyte lines, in contrast with iPSC-derived astrocyte *EAAT1* expression. *EAAT2* expression, however, was relatively increased in both iNPC-Ast cell lines in line with iPSC-astrocytes. While EAAT2 is associated with astrocytes (Rothstein et al., 1994), it is also expressed in neural stem cells (Furuta et al., 1997; Ullensvang et al., 1997; Schreiner et al., 2014), and therefore does not automatically confer astrocyte phenotype. Other key astrocyte markers were also examined.

S100B expression was inconsistent between iNPC-Ast lines, reduced in CS14 while similar to iPSC stage in 155v2. *ALDH1L1* was not detectable in either iNPC-astrocyte lines. As this marker is often used as pan-astrocyte protein and is widely associated with astrocytes, the lack of detectable expression is difficult to interpret. Some level of expression of ALDH1L1 has been detected at NPC stage of iPSC differentiation into astrocytes (Figure 4.3b), albeit lower than iPSC, this indicates that cells are retaining neural progenitor like phenotype.

The presence of GFAP was demonstrated by immunocytochemistry (Figure 4.9c) while *GFAP* gene expression data was not available. Its presence is not necessarily indicative of an astrocyte phenotype, however, this GFAP antibody has been shown to label iPSC derived astrocytes at all stages of iPSC-astrocyte differentiation, including NPC (Figure 4.4).

Surprisingly, iNPC-Astrocytes retain a considerable level of *OCT4* expression (Figure 4.9c), with an 8.4-fold and 29.8-fold increase in expression relative to iPSC stage in 155v2 and CS14 lines, respectively. This is in stark contrast to the marked reduction in *OCT4* observed when astrocyte differentiation is initiated, and as would be expected when cells differentiate. This may indicate residual *OCT4* expression due to the use of retroviral induction of *OCT4* in fibroblasts used to generate cell lines (Meyer et al., 2014), where retroviruses are known to integrate into the host genome and cause residual expression issues after reprogramming (Hu, 2014). Conversely, the iPSC line used in this project utilised Sendai viral vectors for reprogramming that do not require genome integration and are rapidly cleared after transduction (Beers et al., 2015).

PAX6 expression is increased relative to iPSC stage at 6.2-fold and 3.1-fold increase relative to iPSC but was comparatively lower than iPSC-astrocytes differentiated for 60 days, which had an average *PAX6* expression 80-fold higher relative to iPSC stage. This suggests that

iNPC-Ast may be undergoing different developmental regulatory processes that may distinguish them from iPSC derived astrocytes.

Overall, these results demonstrate an expression pattern of astrocyte related genes that is not consistent with iPSC-derived astrocytes. The lack of *ALDH1L1* expression, very low *EAAT1* expression and relatively low and inconsistent *S100B* expression, suggest these cells are developmentally immature, even though they have been shown to retain aging-like features (Gatto et al., 2020). Further differences in *SOX9* and *PAX6* expression suggest different regulatory processes that may be responsible for these differences in astrocyte marker expression. Further, unwanted *OCT4* expression may be contributing to downstream signalling processes.

This analysis suggests that while iNPC-astrocytes might be a useful tool in that they may allow investigation in an aged cellular environment, the evidence here suggest they are immature astrocytes in comparison to iPSC-derived astrocytes, which is a major disadvantage for study of pathogenic tau uptake. Therefore, these cell lines were not routinely used in future experiments.

4.4 Discussion

4.4.1 Summary of results in this Chapter

These results confirm that astrocytes can be differentiated from human iPSC as described in TCW et al. (2017). Interestingly, these results demonstrate that with increased time in culture, these iPSC-derived astrocytes further mature and show increases in astrocytic gene expression (Figure 4.3) and morphological changes akin to astrocyte maturity (Figure 4.6). The main findings were as follows:

- iPSC-derived astrocytes express appropriate genes that are indicative of an astrocyte phenotype.
- iPSC-derived astrocytes display increased expression of appropriate astrocyte associated markers with longer differentiation time, while losing their pluripotency and reducing progenitor related gene expression.

- iPSC derived astrocytes display morphological changes with age, including changes in size and process number, as a further indicator of astrocyte maturity with time in culture.
- iPSC-derived astrocytes express *MAPT* and show regulated splicing of *MAPT* isoforms as they differentiate, that are associated with a maturing developmental stage.
- iPSC-derived astrocytes show more faithful astrocyte gene expression in comparison to iNPC-astrocytes.

4.4.2 Characterisation & heterogeneity of iPSC-astrocytes

GFAP (Levitt & Pasko 1980), S100B (Ludwin et al., 1976) and *ALDH1L1* (Cahoy et al., 2008), which encode three common proteins used for marking astrocytes in brain tissue, were examined during this characterisation. There appeared to be a general trend of increasing astrocyte related gene expression with differentiation time up to day 120 analysed, although this was not a linear relationship. Astrocyte samples were not collected at all timepoints for every differentiation repeat, and so less data was available for day 90 and 120 astrocytes, and this may go some way to explaining the differences in significance at these timepoints when analysing gene expression relative to iPSC. It may be that increasing data at these timepoints would give greater insight into the variability and consistency at later astrocyte differentiation stages.

ALDH1L1 expression was highest relative to iPSC from day 60 of astrocyte differentiation onwards, peaking at day 120. The upregulation of *ALDH1L1* has been seen to correspond to the reduced proliferative potential of these cells in the developing CNS (Anthony and Heintz, 2007), although postnatal ALDH1L1 heterogeneity of expression has been observed in astrocytes depending on CNS region they are derived, including a potential parallel upregulation of expression with *EAAT2* in some cells (Yang et al., 2011). Indeed, this may be the case with day 120 astrocytes which also showed highest *EAAT2* expression. Thus, even though *ALDH1L1* expression was highest at the longest astrocyte differentiation time point analysed, a consistent increase in *ALDH1L1* may not be expected. It would be interesting to observe if *ALDH1L1* expression stabilises at high levels with further time in culture, or if it is altered further.

For *S100B*, expression did not increase after day 60. However, *S100B* expression has been noted to be strongly impacted by environmental factors (Donato et al., 2009), with complex environmentally influenced transcriptional regulation evident where cell types such as cultured microglia can express *S100B* in the right context (Ellis et al., 2007). This may explain why even though *S100B* expression generally increased after astrocyte differentiation, the variability between repeats at each time point was high.

Glutamate transporters *EAAT1* and *EAAT2* were increased in astrocytes relative to iPSC at all time points studied but did not exhibit the general trend of increasing expression with astrocyte differentiation time as with astrocyte markers discussed above. It is also worth noting that the expression of *EAAT2* was more variable. This is in line with reports in developing rodent brains that showed variations in *EAAT1* and *EAAT2* homologue (GLAST and GLT-1) expression in the developing brain (Schreiner et al., 2014). Researchers noted that *EAAT1* steadily increased during the first 2 weeks of postnatal development, but that the peak of *EAAT2* expression was delayed by 10 days. The data presented in this thesis somewhat agrees with these findings, since at the latest timepoint studied (day 120) iPSC-astrocytes showed a significant increase in *EAAT2* expression relative to that measured in day 60 astrocytes. Schreiner et al. (2014) also noted a heterogeneous pattern of EAAT2 expression in astrocytes, depending on where cells were located in the hippocampus. They also noted particular EAAT2 expression patterns at the end feet of astrocytes, which may be analogous to the expression of EAAT2 in astrocytic processes that was observed here (Figure 4.5). As EAAT2 has also previously been seen to correlate with synaptic activity (Swanson et al., 1997), the variation observed in these cultures is not unexpected. *EAAT1* expression, on the other hand appears to be fairly constant in the CNS (Mahmoud et al., 2019), and the *EAAT1* expression shown in this chapter reflected this, where differences between time points were less pronounced than with EAAT2 expression.

If developmental cues are in effect, it is possible that with further time in culture, astrocytes may show higher and more stable EAAT2 expression. It is also worth noting that time after passaging – how long have astrocytes have been attached to the plate before sample collection – may also play a role in EAAT2 expression, since its regulation may be modulated by connections with other astrocytes in culture. This was not always accounted for when planning sample collection at each timepoint. Astrocytes maintained for 120 days, for

example, often had longer in culture after passaging due to their decreased proliferation and reduced requirement for frequent passaging.

At each time point, a range of astrocyte morphologies were observed, as has recently been reported by others using the same protocol (Barbar et al., 2020). This paper identified CD49f as a useful marker of functional and reactive astrocytes, and the authors noted that these cells displayed heterogeneity of astrocyte morphology that is consistent with morphologies observed in the iPSC-derived astrocytes here. This may indicate that subtypes of astrocytes exist within the same culture that may show variations in gene expression levels. Indeed, while trends observed in this chapter point to overall maturation of astrocyte phenotype with age, it is important to remember that gene expression analysis are performed on whole populations of astrocytes. Some variability between replicates could potentially be related to this heterogeneity in the cell populations. This may be the case for the variability in *SOX9* expression observed here. Sox9 is considered to be a master transcription factor regulator of astrogliogenesis important for both induction of astrocyte differentiation (Caiazzo et al., 2015; Neyrinck et al., 2021), but that also remains upregulated with its cofactor nuclear factor-I A (NFIA) to coregulate a subset of genes during the differentiation of astrocytes (Kang et al., 2012). It is possible that levels of Sox9 expression that may vary between cells (for unknown environmental reason in culture) could alter cell phenotypes and also morphology of these astrocytes, and the variation in *SOX9* expression seen here may be evidence of intercellular variability within cultures and at different timepoints. In a recent fate-mapping study of astrocyte diversity in mouse cortical development (Allen et al., 2022), the authors found variable expression of Sox9, among other astrocyte markers, in morphologically defined astrocyte subtypes using Patch-seq, further pointing to molecularly defined astrocyte subtypes that can develop from the same niche. It is yet to be determined if this is replicated through differentiation *in vitro*, but variations in morphology as well as in global gene expression observed in the iPSC-astrocyte cultures in this chapter suggest that subtypes may develop.

Overall, expression of *GFAP, S100B, ALDH1L1, SOX9* were significantly increased at day 60 astrocytes relative to iPSC and NPC, and this was also higher than was measured following 30 days of differentiation. This data justified the decision to culture astrocytes for longer periods of time than was reported in the original protocol (TCW et al., 2017). Day 120 astrocytes, although they demonstrated the highest levels of mature astrocyte gene

expression and morphology, were not practical to use in experimental assays. When deciding on a timepoint to utilise for future experimental assays, it was important to balance indicators of astrocyte maturity with the practicality of cell culture work. Therefore, day 60 astrocytes were chosen on the basis of their high maturity and relative ease of storage and use in culture.

4.4.3 Tau expression in astrocytes

The results in this chapter demonstrate that *MAPT* is expressed by human iPSC-derived astrocytes. Interestingly, the *MAPT* isoform profile was observed to shift from primarily being the foetal 0N3R isoform of tau at 1 day after differentiation, to expression of 1N, 2N and 4R isoforms from day 30 onwards, indicating a switch to more mature isoform expression with increasing times of astrocyte culture and development. It is interesting that 4R and full-length tau were upregulated in the astrocytes used in this project, which is not common in control iPSC-derived neurons, which have previously seen to only express 0N3R tau for the first 100 days in culture (Sposito et al., 2015). It is curious to note that iPSC lines derived from FTD patients with 10 + 16 mutations in MAPT could also express 0N4R tau early on, highlighting developmental regulation can be overwritten by disease associated mutations. In a more recent study, researchers demonstrated that elevated 4R tau persisted in astrocytes derived from iPSC patients with a similar *MAPT* 10+16 intronic mutation, and that this expression became deviated from neurons derived from the same cell line, indicating differential MAPT regulatory mechanisms in astrocytes compared to neurons (Setó-Salvia et al., 2022). The authors analysed astrocytes at 140 and 300 days in vitro (DIV), with tau protein levels being detected at this later timepoint. It is unclear whether RNA or protein was absent at earlier timepoints, or these data were not reported. The authors utilised a different differentiation protocol compared to the one in this project (Andrea 2013), and this may represent a less efficient astrocyte differentiation process, as was the justification for utilising the efficient protocol as thoroughly tested in TCW et al. (2016). A more thorough analysis of *MAPT* isoform expression and protein expression with extended cultures would be interesting.

4.4.4 Comparison of iPSC-astrocytes and iNPC-astrocytes

iNPC-Astrocytes were found not to share a similar expression profile of astrocytic genes to iPSC-derived astrocytes. The lack of ALDH1L1 expression is surprising considering low levels of expression were detected in iPSCs. It is possible that the cell type from which iNPC-

Astrocytes are derived played a role. The human protein atlas indicates that skin derived fibroblasts express low levels of ALDH1L1 (0.9 nTPM (transcripts per million)), or none at all depending on the fibroblast cluster that was defined in this analysis (for comparison, the value for astrocytes was 92.7 nTPM) (Karlsson et al., 2021a). Therefore, perhaps fibroblasts used to derive iNPC-astrocytes did not contain residual expression of this protein and that the rapid differentiation protocol used was not sufficient to induce this.

Still, iNPC-astrocytes do express comparable levels of the gene encoding the Sox9 transcription factor, so it seems likely that these cells are undergoing some transcriptional changes related to neural stem cells or indeed astrocytes. It may be that these cells, taken approximately 12 days after iNPC induction into astrocytes, were at too early stage in this protocol to induce expression of *ALDH1l1*, along with *EAAT1*. *EAAT2* expression was relatively similar to day 60 iPSC-derived astrocytes, and this may be due to environmental reasons in culture, as discussed previously. Indeed, the morphology of iNPC-Astrocytes (Figure 4.9c) appeared more similar to early (day 1) iPSC-astrocytes (Figure 4.4), indicating that they may be more neural progenitor like in their phenotype. NPC expression of EAAT2 was higher than observed in most iPSC-astrocytes (Figure 4.3f), and this may correlate with levels of expression in iNPC-Astrocytes.

Interestingly, for iNPC-astrocytes, high levels of mRNA expression of the pluripotency transcription factor Oct4 are present, even at levels exceeding that of the iPSC line used to generate astrocytes in this chapter. This suggests there is some residual expression of one of the 'Yamanaka' factors that were used to rapidly induce fibroblasts into neural progenitors. This may be explained by the authors use of retroviral vectors, as described in (Meyer et al., 2014), to transduce these cultured fibroblasts. Retroviruses integrate into the host genome and are known to cause residual expression issues after reprogramming (Hu, 2014), among other issues, and this may also be responsible for unidentified downstream transcriptional issues as cells differentiate. In contrast, the iPSC line used in this chapter utilised a Sendai virus transduction protocol for reprogramming that does not require host genome integration and is cleared rapidly. This ensures that the cell lines differentiated from the iPSCs used in this study can be induced with small molecules without complication of pluripotency related gene expression interfering with signalling pathways.

Overall, the data here point to incomplete differentiation of iNPC-astrocytes towards an astrocyte phenotype. This may be in part down to the choice of vector for transduction creating unwanted transcription factor expression, altering signalling pathways. It may also be a product of the rapid nature of this protocol, preventing full astrocyte differentiation from occurring. While an ageing cell phenotype would have been beneficial for assays in this study, the astrocyte phenotype was not comparable to iPSC derived astrocytes and would have therefore made direct experimental comparisons difficult.

4.4.5 Culturing & cryopreserving iPSC-astrocytes

The viability of cells during cryopreservation was qualitatively tested every 30 days. For iPSC, NPC, day 30 and day 60 astrocytes, it was determined that cells can be cryopreserved (Section 2.3.6) and revived (Section 2.3.7) with high levels of cell survival. Cells that were differentiated for 90 days showed reduced cell survival after passaging, and this translated into reduced viability when they were revived after cryopreservation. This worsened when cells were maintained for 120 days, and passaging at even low ratios (1:1) still resulted in minimal cell survival (qualitative observations). This could be down to a number of factors. An increase in the number of processes and the observed reduction in the proliferative capacity of astrocytes meant that cells may not be robust enough to survive passaging or freeze/thawing procedures. Indeed, astrocytic processes may be more sensitive to environmental changes, inducing apoptosis more readily than astrocytes in the population that still retain some proliferative ability. Future experiments may more rigorously test how time in culture, between passages and overall differentiation time of these astrocytes affects their viability. Moreover, how astrocyte-like morphology changes with these parameters may impact this. Therefore, it is important to maintain consistency in culture times and astrocyte age when performing experimental assays in future chapters.

4.4.6 Limitations and future work

The GFAP expression determined in this chapter covered all isoforms to avoid bias, as noted previously. However, this may not have taken into consideration the fact that astrocytes express specific isoforms of GFAP (Mamber et al., 2012; Messing and Brenner, 2020), and therefore the analysis may be skewed towards isoforms expressed by neural stem cells, for example. While the developmental regulation of GFAP isoform expression in astrocytes is still unclear (Messing and Brenner, 2020), it would be of interest to test for changes to

specific astrocyte associated isoforms with increasing astrocyte differentiation time to determine if these are upregulated.

While it was interesting to observe changes in *MAPT* and related isoform gene expression, time was not available to determine if this correlated with detectable protein expression of tau and/or its specific isoforms. Previous work has shown that tau protein expression was detectable at later timepoints than *MAPT* mRNA expression in iPSC derived astrocytes (Setó-Salvia et al., 2022), indicating that longer culture times may be needed to examine protein expression, and particularly to distinguish between isoforms. Further, differences in alternative splicing of tau mRNA in astrocytes compared to neurons are unknown and may also play a role in protein levels.

The range of astrocyte morphologies observed in culture are reminiscent of similar morphologies highlighted by previous published work utilising the same protocol (Barbar et al., 2020), but also indicate that heterogeneity may exist within cultures that could have downstream impact on assays developed in later chapters. It would be interesting to examine this in more detail, specifically how differences in gene expression may manifest in astrocytes of different morphologies. Single cell RNA sequencing would allow unbiased examination of this, and especially if stratified cell types could be correlated with the results of tau-based assays developed in subsequent chapters.

While the iPSC line used here has been extensively characterised and used in multiple studies (Cocks et al., 2014; Robbins et al., 2018), ideally this astrocyte protocol would be taken through at least three control iPSC lines to determine that astrocyte characterisation is consistent between cell lines. However, with this protocol having been replicated with multiple lines in the original study (TCW et al., 2016), this suggests that the extended protocol developed here would fare well across multiple iPSC lines. Utilising mutant iPSC lines from patients with MAPT mutations, for example, might be interesting to explore especially in regard to MAPT isoform expression.

4.4.7 Conclusions

Overall, the results in this chapter present a protocol for generating human astrocytes that can be grown for extended periods in culture, stored cryogenically, and demonstrate a robust astrocyte phenotype with respect to gene and protein expression, while also

demonstrating morphological changes consistent with astrocyte development. Astrocytes differentiated for 60 days were cryopreserved and thawed for the development of tau uptake and astrocyte reactivity assays that are described in future chapters.

5 Internalisation of post-mortem human brain derived tau aggregates by iPSC-derived astrocytes

5.1 Introduction

Evidence from post-mortem tauopathy tissue indicates that astrocytes associate with aggregated tau to a varying extent, depending on the disease (Kovacs, 2020; Reid et al., 2020). As summarised in Table 1.3, in some tauopathies, modified forms of tau are deposited within astrocytes, and all tauopathies show indications of astrocyte reactivity. This, coupled with our current understanding of different tau fibril structures (Shi et al., 2021) and tau spreading patterns (Vogels et al., 2019) in tauopathies, suggests that conformational differences in tau aggregates, or specific tau modifications (Dujardin et al., 2020) may influence the readiness of astrocytes to internalise and/or degrade and extrude tau. It is now known that the conformational structure of induced recombinant tau is not equivalent to that of human derived tau aggregates (Zhang et al., 2019), and therefore it is important to study tau seeding and spread in model systems using physiological forms of human tau aggregates.

Early evidence of trans-synaptic tau spread in a mouse model in which FTD-causing mutant (P301L) human tau was selectively expressed in layer 2 neurons in the medial entorhinal cortex (de Calignon et al., 2012; Liu et al., 2012) also implicated astrocytes. PHF1-immunoreactive tau was detected in GFAP+ve astrocytes that do not express human tau in this model, following tau spread from the entorhinal cortex to the hippocampus of aged mice (de Calignon et al., 2012). Indeed, it has now been observed that astrocytes have the ability to phagocytose large proteins (Söllvander et al., 2016). The mechanisms by which tau uptake is mediated are still being investigated. Heparin sulfate proteoglycans expressed by astrocytes among other cell types of the brain (Turnbull et al., 2001; Sarrazin et al., 2011) may mediate the update of specific tau species, similar to the mechanisms by which they facilitate the uptake of infectious prion proteins (Schonberger et al., 2003; Horonchik et al., 2005). More recently, alterations in HSPGs with respect to glycosaminoglycan chain length and sulfation patterns have been observed to regulate tau uptake in HEK293T cells, as well as in iPSC-derived neurons and mouse brain slice cultures (Rauch et al., 2018; Stopschinski et al., 2018). Interestingly, astrocytes have been found to internalise tau monomers in a

HSPG-independent manner (Perea et al., 2019), whereas tau fibrils were taken up in a HSPG-dependent manner by primary astrocytes (Martini-Stoica et al., 2018). Moreover, in primary astrocytes, blocking HSPGs with heparin did not prevent uptake of recombinant tau fibrils. Instead, the authors discovered an integrin αV/β1 receptor that mediates tau uptake, activating integrin signalling and downstream pro-inflammatory pathways (Wang and Ye, 2021).

Other cell surface receptors expressed by astrocytes are also implicated in tau uptake. LDL receptor related protein 1 (LRP1), a member of the low-density lipoprotein receptor family, can facilitate Aβ uptake and degradation in astrocytes (Kanekiyo and Bu, 2014; Liu et al., 2017). Knocking down LRP1 was found to impede uptake of monomeric and oligomeric tau, but only partially inhibited the uptake of sonicated tau fibrils, strongly suggesting that there are selective mechanisms governing the astrocytic internalisation of physiological and disease-associated forms of tau uptake (Rauch et al., 2020). Section 1.5.3.1 summarises potential methods of tau internalisation.

Previous characterisation of the human iPSC-derived astrocytes used in this project demonstrated the phagocytic capacity of these cells, in a manner that was equivalent to primary human foetal astrocytes and microglia (TCW et al., 2017). These astrocytes were also able to enhance the phagocytic capacity of microglia in a co-culture environment (TCW et al., 2017), indicating their capacity to release cytokines for crosstalk with microglia, as is known to occur in health and disease (Skripuletz et al., 2013; Liddelow et al., 2020). Astrocytes are able to degrade large proteins through common autophagy and protein degradation pathways (Section 1.3.7). Evidence of autophagic clearance by astrocytes in neurodegeneration is apparent in mouse models of Alexander disease, where abnormal GFAP accumulates within cells. Autophagy mediated clearance of Aβ aggregates has also been demonstrated in astrocytes from mice, where APOE determined Aβ clearance efficiency (Simonovitch et al., 2016). Furthermore, TDP43 aggregates were found to be cleared more rapidly when iPSC-derived astrocytes were treated with autophagy-inducing small molecules (Barmada et al., 2014).

Therefore, the capacity of astrocytes to uptake and degrade is tau likely has important implications for tau spread. This chapter aimed to investigate the efficiency and timeframes

by which iPSC-astrocytes internalise and/or clear tau extracted from different post-mortem human tauopathy brains.

5.2 Methods

All results and samples used are fully detailed in Chapter 2. Key methods for post-mortem sample preparation and cell culture assays used in this chapter are summarised below.

Frozen post-mortem tissue blocks were obtained from the London Neurodegenerative Diseases Brain Bank (King's College London). Cases were selected that had a diagnosis of tauopathy (AD, PiD and PSP) with extensive tau pathology, together with tissue from age-matched controls with no neurodegenerative disorders.

Protocols for extractions are detailed in Methods Section 2.1.2. Briefly, homogenised brain was centrifuged at 4°C at 20, 000 x g and the resultant low-speed supernatant (LSS) collected. This contains both sarkosyl-soluble and -insoluble tau. The LSS was incubated with 1% sarkosyl for 1 hr and then centrifuged at high speed (100, 000 x g) for 1 hr. The resulting high-speed supernatant was collected, and the sarkosyl-insoluble (SI) pellet was washed and collected. This contains tau aggregates.

Low-speed supernatants were sonicated at 10% power for 3 pulses using a Bandelin Sonopuls HD 2070 (BANDELIN electronic GmbH & Co, Berlin, Germany) for 3 x pulses set at 10% power, sterile filtered using Millex-GS Syringe Filter Unit (Merck Group, Darmstadt, Germany) with 0.22 µm pore size. This mimics the preparation of samples that were used to inject htau and WT mice (Chapter 3). The SI fraction was resuspended in sterile-filtered PBS (Thermo Fisher Scientific™, MA, USA) at 100 µL per 1000 µL of initial LSS used for homogenisation, and these were also sonicated in PBS as above. Samples were examined by SDS-PAGE against recombinant human tau (rTau) standards of known concentrations. Blots were probed with an antibody against total tau. A standard curve was generated using the signal intensity of the recombinant tau. The concentration of tau in each sample was determined by plotting the intensity of total tau signals for each sample against a line of best fit for rTau standards. Samples of LSS were normalised to 0.025 ng/µl tau in Astrocyte medium. For the SI fraction, tau content in AD samples was diluted to 0.1 ng/µl tau concentration in Astrocyte media. There is very little (if any) sarkosyl-insoluble tau in control

samples and therefore the sarkosyl-insoluble samples from control cases were diluted to the median dilution value used for AD cases.

For tau spiking assays (see section 2.4), astrocytes were plated from cryo-preserved day 60 stocks at approximately 5,000 cells/well for 96 well or 180,000 cells/well for 6 well plates. For assays longer than 7 days, cells were plated at half density to avoid overcrowding as a result of proliferation over time. Cells were cultured for 1 day to acclimatise before tau spiking into culture medium, Astrocyte Medium (ScienCell, CA, USA) was removed and replaced with Astrocyte Medium premixed with appropriate concentration of extracted tau solution. Cells were fixed in ice cold methanol for 5 min at -20oC before ICC, or lysed in TRIzol™ Reagent (Thermo Fisher Scientific™, MA, USA) for future RNA extraction.

5.3 Results

5.3.1 Characterisation of human samples used for tau spiking into astrocyte cultures

To provide a general characterisation of the samples being used in spiking experiments, the low speed supernatant (LSS), which contain all forms of tau (monomers and abnormally aggregated/phosphorylated tau), high speed supernatant (containing sarkosyl-soluble tau) and sarkosyl-insoluble (SI) pellets containing tau aggregates from control, AD, PiD and PSP temporal cortex were separated by SDS-PAGE and immunoblotted using antibodies against total tau (Agilent Dako; CA, USA; cat# A0024) and tau phosphorylated at Ser396/404 (PHF1, Peter Davies, Feinstein Institute of Medical Research, NY, USA) (Table 2.2).

All cases showed a cluster of tau bands from approximately 46-64 kDa in the LSS fraction as expected (Atherton et al., 2014), although the levels of tau detected varied between cases and diseases, with two of the three PiD cases showing low overall levels of total tau. There were no immediately apparent differences in banding pattern between diseases with the total tau antibody. This might have been expected since both 3R and 4R tau accumulates in AD, whereas 4R tau is predominantly deposited in PSP and 3R tau in PiD (Guo et al., 2017). However, AD cases demonstrate a hallmark smear that is indicative of high levels of post-translational modifications to tau (Kurbatskaya et al., 2016). This was more apparent when blots were probed with an antibody against tau phosphorylated at Ser396/404 (PHF1). None of the control samples showed reactivity against the PHF1 antibody, and the levels of

phosphorylated tau also appeared lower in 2 out of 3 PiD cases and all PSP cases. However, differences in the banding pattern were apparent, with PSP cases showing PHF1 immunoreactive bands of approximately 60-64kDa that were present in the AD samples, but less apparent in PiD cases. Similarly, the PiD cases showed bands of approximately 50kDa that were also in AD, but absent from PSP. These might be indicative of phosphorylated 4R and 3R tau in PSP and PiD, respectively.

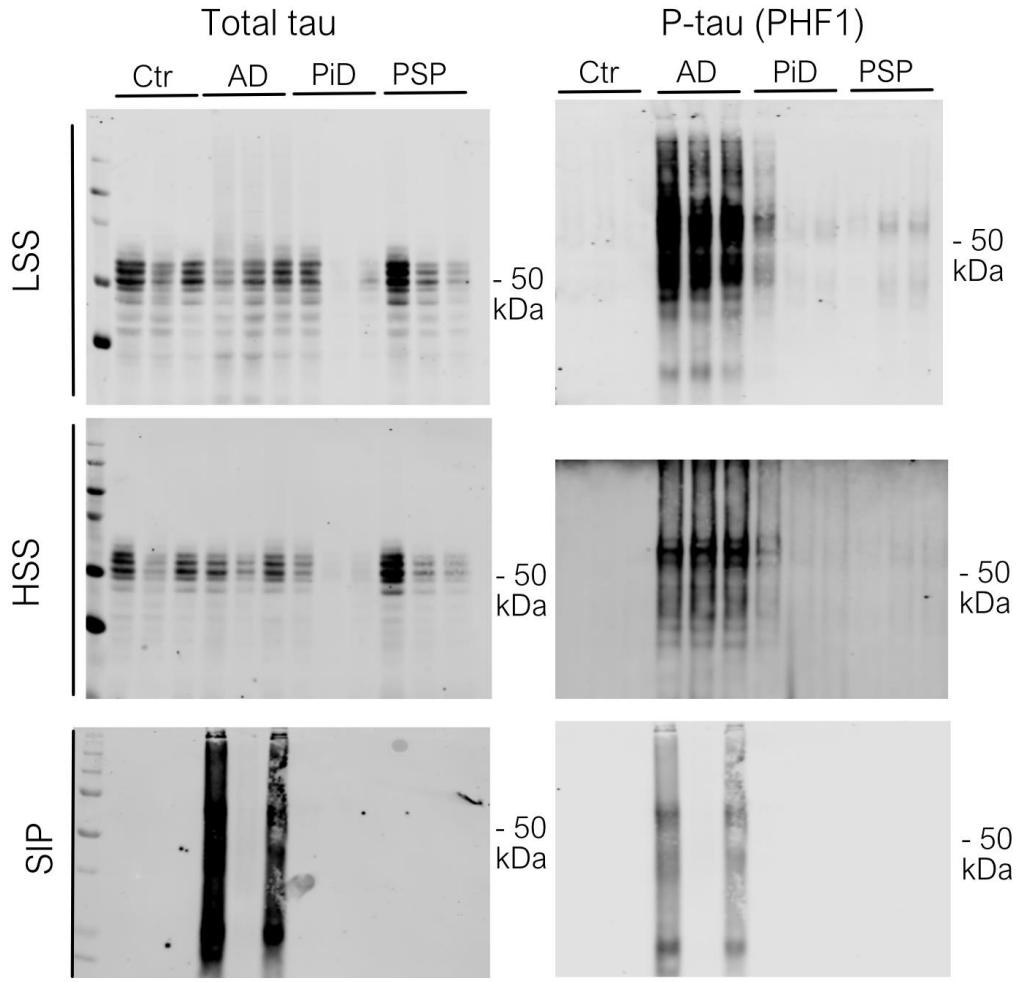

Figure 5.1 Characterisation of sarkosyl-soluble and insoluble tau in temporal cortex samples from human postmortem control and tauopathy brain.

Post-mortem temporal cortex from control (Ctr), AD, PSP and PiD brain was fractionated using a protocol that yields a low speed supernatant (LSS) containing sarkosyl-soluble and insoluble tau, a high speed supernatant (HSS) containing only sarkosyl-soluble tau and a sarkosyl insoluble pellet (SIP) containing tau aggregates (Greenberg and Davies, 1990). Samples from each fractionation step were immunoblotted using antibodies against total tau and tau phosphorylated at Ser396/Ser404 (PHF1). N=3 ctrl, AD, PSP, PiD. Molecular weight markers are indicated on the right of each blot, and protein ladder on the left of total tau blots.

The high-speed supernatant (HSS) demonstrated similar levels and banding patterns of total and PHF1-immunoractive tau as was found in the LSS from the same sample. Particularly when blotted with the PHF1 antibody, a smear of tau was apparent for AD, PSP and PiD suggesting that there are multiple forms of modified and phosphorylated tau in this fraction of tauopathy brain samples.

There was a marked difference in the amount of sarkosyl-insoluble (aggregated) tau between cases (Figure 5.1, bottom row). A high intensity smear was apparent for two out of three AD cases when blots were probed with antibodies against total tau and PHF1. The other AD case showed dramatically lower amounts of sarkosyl-insoluble tau, although some was present in this lane at high contrast levels (not shown). Aggregated tau was not detected in control, PiD or PSP cases, although the smearing apparent with the PHF1 antibody in the HSS fraction, and that sarkosyl-insoluble tau can be isolated from PSP and PiD, suggests that there is aggregated tau in these samples, but at levels below the threshold of detection. This highlights the variability within and between tauopathies. However, these data suggest that, at least for the cases used here, that the inherent solubility of tau aggregates derived from PiD and PSP cases is different, as suggested by others (Wray et al., 2008) and that considerable amounts of tissue would be required to isolate sufficient sarkosyl-insoluble tau aggregates from some cases to ensure that equivalent levels of aggregated tau were used to spike astrocyte cultures.

To start with, since the LSS fraction is equivalent to the tau extracts used to inject wild-type and htau mice (Chapter 3), samples of this fraction were used to spike the culture medium of iPSC- astrocyte cultures that were established and characterised as described in Chapter 4.

5.3.2 Preliminary tau spiking experiments

To determine if tau is internalised by astrocytes, as suggested by the results in Chapter 3, the low-speed supernatant of each control or tauopathy case was normalised for tau content (Methods Section 2.4.1) and added to iPSC-astrocyte culture medium. Pre-plated 60-day old iPSC-astrocytes had their culture media replaced with astrocyte medium spiked with LSS samples from control, AD, PiD and PSP cases (3 separate cases of each). Astrocytes were returned to the incubator for 48 hours, after which time, cells were fixed in methanol and immunolabelled with antibodies against GFAP to reveal astrocytes and AT8 which detects

tau phosphorylated at Ser202/Thr205. PHF1 was found not to be as robust for immunostaining, and AT8 worked poorly on western blots, so it was not possible to use the same phospho-tau antibodies for both ICC and WB as was desired. Nevertheless, both AT8 and PHF1 detect tau that is abnormally phosphorylated in AD (Hanger et al., 2009). Plates were imaged using an Opera Phenix plate reader (Perkin-Elmer, MA, USA). Images were analysed using Harmony software to detect cell nuclei by Hoechst staining, and GFAP labelling to identify astrocyte cell outline, and within each cell outline measurements of AT8 intensity were taken.

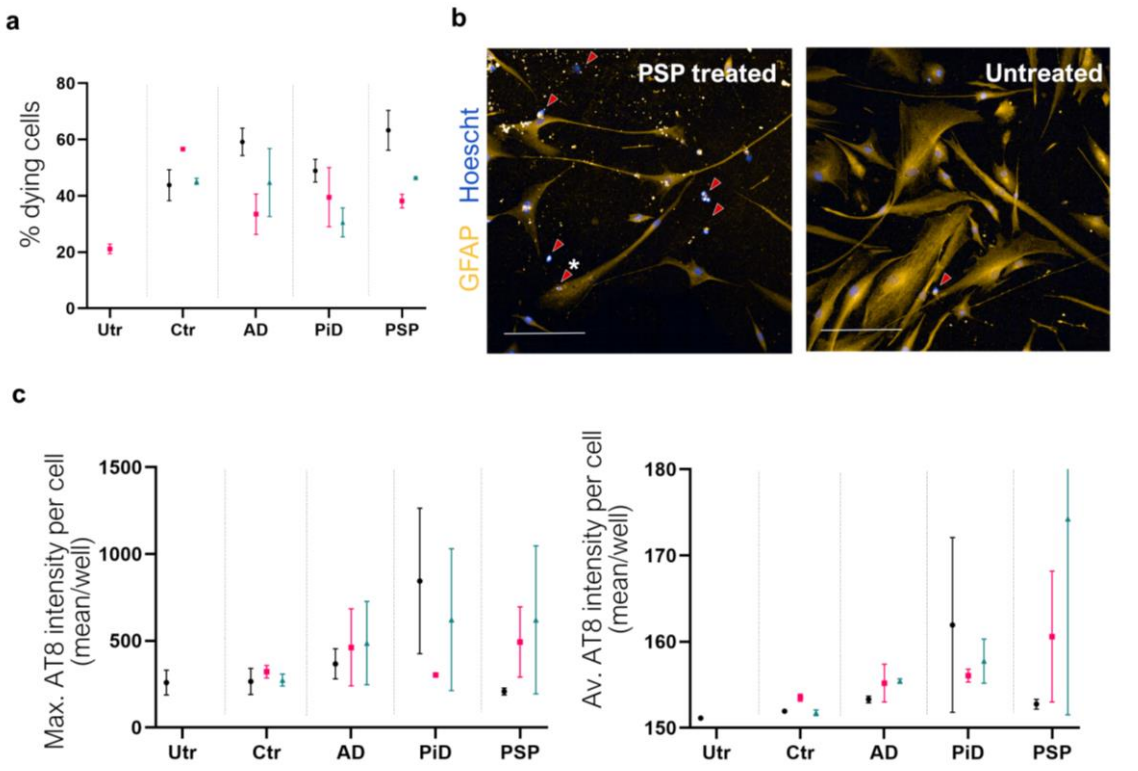

Figure 5.2 Astrocytes spiked with soluble and insoluble tau (LSS fraction) of human control and tauopathy brain show decreased viability and minimal tau uptake.

Characteristics of 60-day iPSC-astrocyte cultures following 48-hour treatment with 0.025 ng/µl tau from control (ctr), AD, PiD or PSP brain lysates relative to cells left untreated (utr). (**a**) Analysis of Hoechst 33342 stained nuclei revealed a higher proportion of dying cells in iPSC-astrocyte cultures spiked with 0.025 ng/µl tau control or tauopathy LSS compared to untreated cells. (**b**) A representative image of iPSC-astrocytes treated with the LSS from one PSP case compared to untreated astrocytes demonstrates the impact of LSS spiking on cell viability. Red arrows indicate bright condensed nuclei representing dead or dying cells. Red arrow with * indicates a dead cell likely engulfed by another astrocyte. (**c**) Measurement of AT8 intensity per remaining cell indicates some uptake of p-tau by astrocytes, as assessed using maximum or average AT8 intensity inside cells as a readout. Distinct accumulations of tau aggregates were not readily distinguishable in the images. N=3 for ctr, AD, PiD, PSP. N=1 for Utr. Data plotted is mean ± SEM of 3 biological replicates. Scale bar = 100 µm.

After treatment with LSS, regardless of whether this was from control or tauopathy samples, astrocytes appeared sparser compared to untreated wells (Figure 5.2b). Therefore, an analysis pipeline was created to quantify the proportion of dead or dying cells in each well. This was based on the appearance of nuclear staining in these wells. During apoptosis, 'apoptotic bodies' are formed that involve the condensation of nucleus and cytoplasm (Kerr, 1971; Kerr et al., 1972) and can contain primarily condensed nuclear chromatin without many cytoplasmic elements. In such cases, the nucleus, as labelled by Hoescht 33342

(Thermo Fisher Scientific™; MA, USA), which fluoresces only when bound to adenine-thymine regions of DNA, condenses, and becomes brighter. This is in contrast to the larger, duller nuclei of healthy cells. A linear classification system that utilises the pre-calculated size, intensity and roundness of Hoechst-stained nuclei was trained by machine learning to split cells into 'healthy' and 'dead or dying cells' (methods section 2.5.4.2). The resulting data indicated that the cells treated with LSS of either control or tauopathy cases, showed reduced cell viability compared to untreated cells (Figure 5.2a). The average number of dying cells in untreated cultures was 21.11 ± 0.9 % whereas the same measure in astrocyte cultures spiked with tauopathy or control brain LSS were all higher, ranging from 30.5 ± 4.8 % to 63.1 ± 6.2%. This indicates that factors present within the brain sample, and/or factors involved in the process of extraction, are harmful to iPSC-astrocytes in culture, regardless of any pathological tau species present.

AT8 positive fragments or fibril like structures were not clearly visible in the astrocyte cultures. Instead, the average AT8 intensity and the maximum AT8 intensity present within GFAP positive astrocytes were determined as indicators of the uptake of pathological tau species (Figure 5.2c). Interestingly, there was some evidence of tau uptake in these astrocytes after treatment with LSS from tauopathy brain. In cells spiked with LSS from two of three control cases, there were no increases above baseline (untreated), with the third demonstrating a small increase in average and maximum AT8 intensity per cell. In contrast, when cultures were spiked with LSS from each of the tauopathy cases, a higher average and maximum intensity of AT8 immunoreactivity was observed per cell. However, the data was very variable, even for the two technical replicates assessed for each case. Moreover, there was no clear association between cases with higher levels of PHF1 or sarkosyl-insoluble tau on either cell viability or the intensity of AT8 within astrocytes. Nevertheless, these data suggest that phosphorylated tau species isolated from post-mortem tauopathy brain can be internalised by iPSC-astrocytes.

However, it is likely that the concentration of these tau species is not high enough to determine a significant and consistent uptake in tau. Furthermore, based on the results in Figure 5.2a, it is likely that increasing the amount of LSS used would result in higher cell death, and inevitable difficulty in analysing tau uptake and its impact on astrocytes. Although these experiments were designed to supplement the data shown in Chapter 3, using tau extracts that were prepared in the same way, this proved technically challenging. Therefore,

the sarkosyl insoluble fraction was used in subsequent experiments as a source of high concentrations of disease associated tau aggregates for interrogating tau uptake and downstream astrocyte responses.

5.3.3 Characterisation of further AD cases for tau extraction

Since the AD cases showed the most consistent isolation of tau aggregates, it was decided to focus on AD brain-derived tau for subsequent experiments. Tau shows considerable molecular heterogeneity between AD cases, and certain post-translational modifications have been found to correlate with enhanced seeding activity and more severe clinical outcomes (Dujardin et al., 2020). It was therefore of interest to examine any differences in the uptake of aggregated tau isolated from distinct AD cases.

Brain samples from the temporal cortex of six late Braak stage AD cases were processed using the method detailed in Section 2.1.2. The sarkosyl-insoluble fraction was characterised by western blotting using an antibody against total tau (Table 2.2). Recombinant human tau of known concentration was used to generate a standard curve and determine the concentration of tau aggregates within each sample. The recombinant human tau ladder showed six clear bands, representing the six isoforms of human tau expressed in the adult human CNS. In contrast, aggregated tau from AD brain presented as three main bands. These are the same isoforms, but that have been differentially modified such that they co-migrate on SDS-PAGE (Hanger et al., 1991). A number of higher molecular weight species that likely represent modified tau oligomers, and lower kDa bands representing cleaved tau fragments, were also observed. This data showed that aggregated tau could be isolated from each of these cases using sarkosyl. The abundance of aggregates relative to tissue weight varied between samples, but tau aggregate concentration was normalised prior to tau spiking experiments as described above.

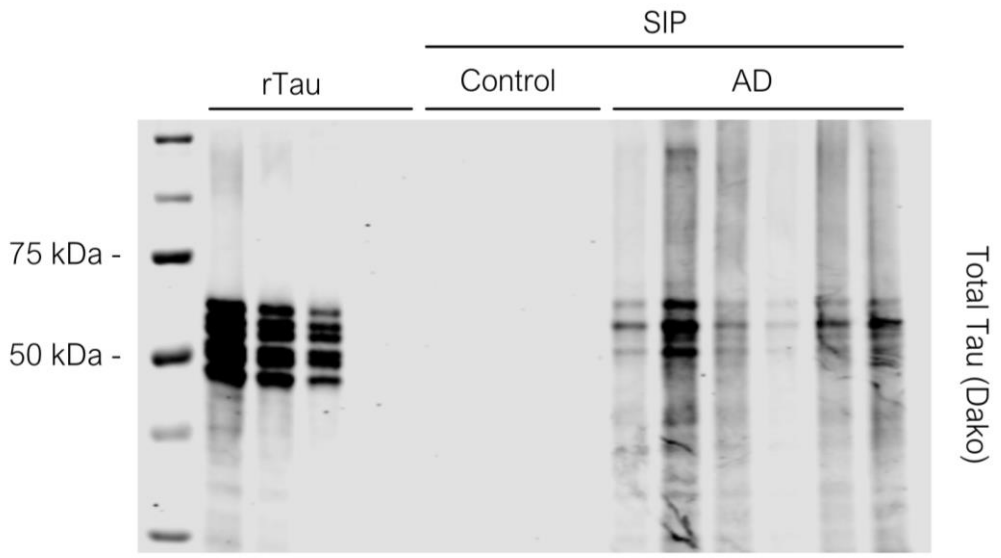

Figure 5.3 Sarkosyl-insoluble tau from AD cases used for tau spiking assays relative to control brain samples and human recombinant tau ladder.

The sonicated sarkosyl-insoluble pellet (SIP) extracted from 6 AD and 3 control brain samples were processed by SDS-PAGE and immunoblotted using an antibody against total tau. A recombinant human tau ladder, containing six isoforms of human tau, was diluted in sample buffer and loaded at known concentrations of 6.0, 2.7 and 1.3 ng/µL, next to sample buffer only representing 0 ng/µL tau. The intensity of tau immunoreactivity of the standards was used to generate a standard curve from which the amount of tau in each tauopathy sample was calculated.

Formaldehyde-fixed paraffin-embedded sections of temporal cortex from the same cases were also immunohistochemically labelled using antibodies against AT8 and GFAP (Figure 5.4 & Figure 5.5). In control cases, no prominent AT8 staining was observed (Figure 5.4). In contrast, in all AD cases, some AT8 immunoreactivity was apparent, although the extent of AT8 immunoreactivity varied between cases (Figure 5.5). Some mature NFT structures were apparent, for example in AD3 (marked by filled arrowhead), with this and surrounding larger tau fibrils perhaps being examples of 'ghost' tangles. Here, clear astrocyte association is observed with these phospho-tau structures, which astrocytes are known to associate with (Perez-Nievas and Serrano-Pozo, 2018). In other cases, smaller AT8 positive tau fibrils are clearly visible and these are likely associated with neuronal cell bodies or neurite processes (marked by arrowhead), as are typically described in AD (Wharton et al., 2016). This is indicative of variation in the extent of tau pathology that is typically observed between human cases with the same diagnosis and similar Braak staging (Lowe et al., 2018; Singleton et al., 2021; Vogel et al., 2021). All cases used here were Braak stage VI with the exception of AD

4 which was Braak stage V. In addition to the clear association of GFAP positive astrocytes with large areas of AT8 positive tau fibrils, there is also sometimes overlap with AT8 pathology (both marked by asterisks), which may indicate tau internalisation by these astrocytes.

There is no clear correlation between the size and quantity of AT8 tau aggregates and the level of tau in the SI fraction of the corresponding AD samples (Figure 5.3). While it may be expected that samples with higher concentration of SI tau correlate with high AT8 tau in sample sections, as both are from the temporal cortex, conclusions are difficult to draw considering the small sample sizes used. Ideally, extensive analysis of multiple sections from these cases, including for sarkosyl extraction, would be required to investigate any correlation between these parameters.

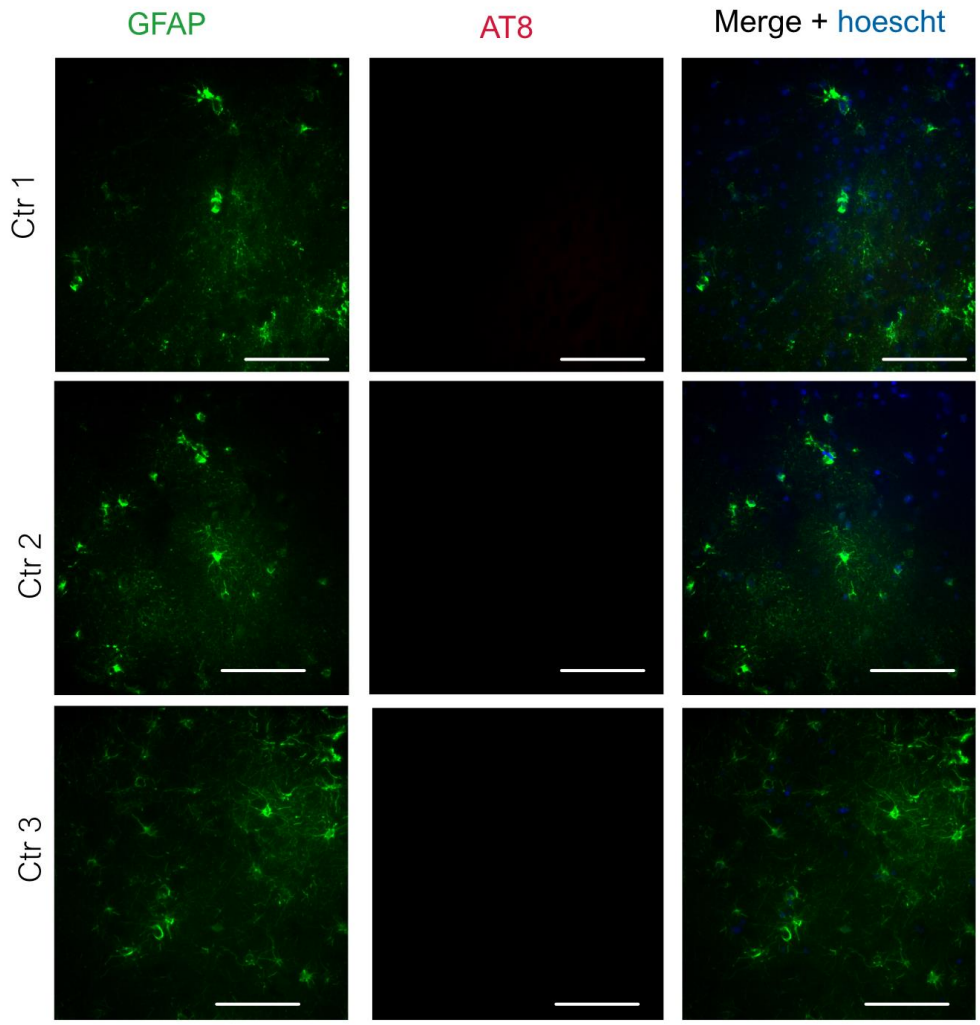

Figure 5.4 IHC of control brain sections shows minimal AT8 immunoreactivity.

Representative brain sections from the temporal cortex of control post-mortem brain were immunostained with an antibody against GFAP to label astrocytes (green) and tau phosphorylated at Ser202/Thr205 (AT8, red). Hoechst 33342 was used to stain nuclei (blue). None or minimal AT8 positive structures were observed. N=3.

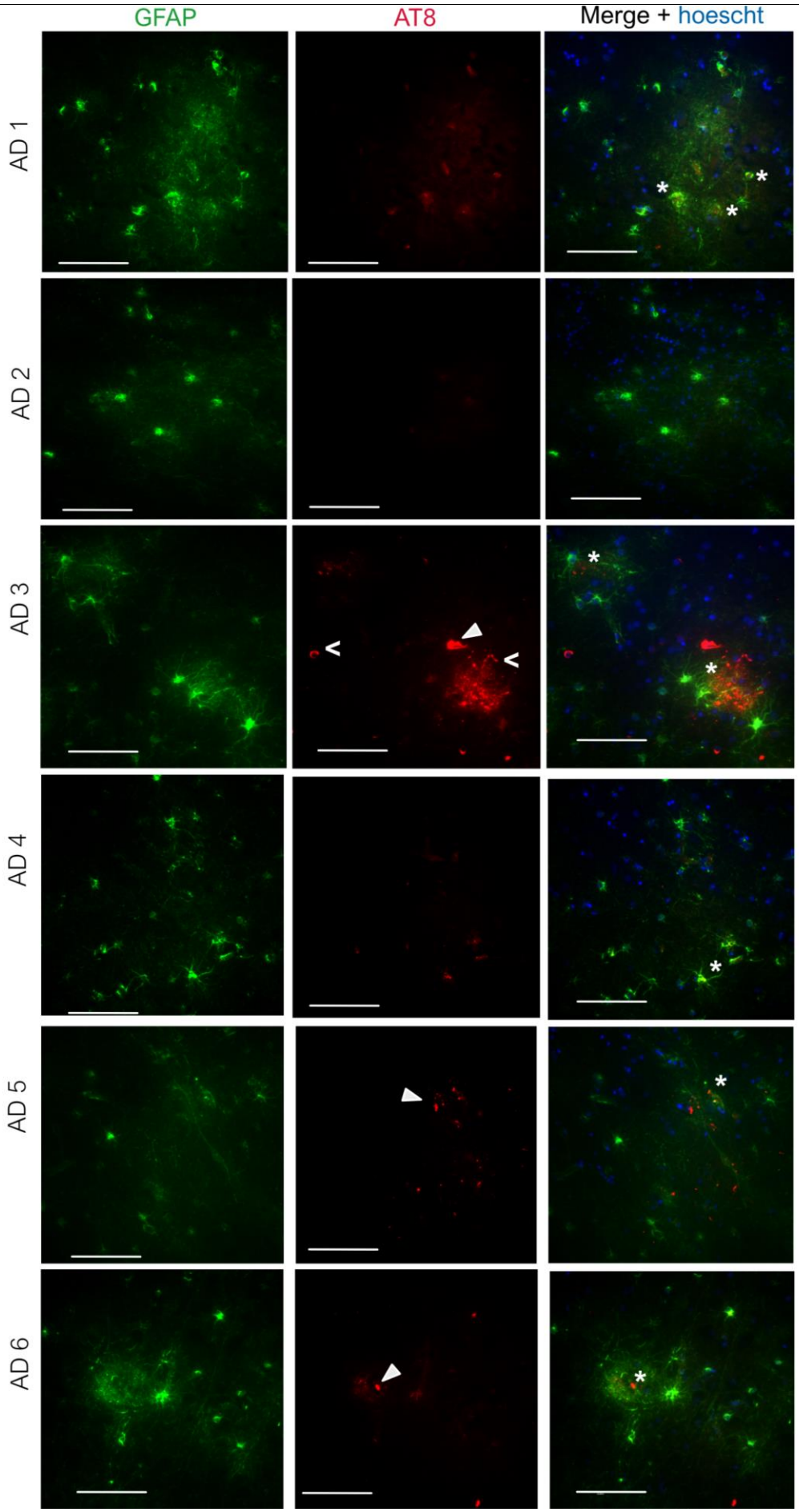
GFAP
AT8
Merge + hoescht
AD 1
AD 2
AD 3
AD 4
AD 5
AD 6

Figure 5.5 IHC of AD brain sections showing AT8 immunoreactivity.

Representative brain sections from the temporal cortex of AD post-mortem brain were immunostained with antibodies against GFAP to label astrocytes (green) and tau phosphorylated at Ser202/Thr205 (AT8, red). Hoechst 33342 was used to stain nuclei (blue). Examples of mature NFT marked with filled arrowhead, open arrowhead indicates examples of neuropil threads and smaller less 'mature' aggregates, and asterisks indicate examples of astrocyte association or overlap with aggregated tau structures. Scale bar = 100 μm. n=6.

Overall, the characterisation of AD cases here demonstrates classic tau pathology, and consequently the cases were considered suitable for aggregated tau is suitable for subsequent tau uptake experiments in iPSC-astrocytes.

5.3.4 Astrocyte internalisation of aggregated tau from AD cases

Having successfully isolated aggregated tau from AD brain, the next step was to determine if astrocytes internalise human AD brain-derived sarkosyl-insoluble tau aggregates. 60-day old, cryopreserved iPSC-astrocytes were plated at 5,000 cells/well in 96-well optical plates, and after one day astrocyte culture medium was removed and replaced with astrocyte media containing sarkosyl insoluble aggregated tau derived from these six AD cases at equivalent concentrations, as well as equivalent volume of the sarkosyl insoluble fraction from three control cases. Astrocytes were exposed to tau from these different AD and control cases for different lengths of time to determine the rate of tau internalisation (Fig. 5.9A). Exposure was for 1, 3, 5 or 7 days without media changes, after which cells were fixed at the same end point. Following fixation of cells with methanol, astrocytes were visualised after ICC using an antibody against GFAP, as the characterisation performed in Chapter 2 revealed that GFAP was expressed consistently by all astrocytes. Confocal images were taken on a high throughput imaging system (Opera Phenix; Perkin Elmer, MA, USA) as a Z-stack to ensure that labelled tau aggregates were within the cytosol and not membrane bound. Tau aggregates were immunolabelled with the AT8 antibody as this antibody was found to label tau aggregates previously (Figure 5.5).

For these experiments, maximum AT8 intensity per cell was measured since tau uptake should sufficiently increase the AT8 intensity from background levels. This was quantified as average per cell in each well. Average AT8 cell intensity was also measured, and while it mirrored maximum AT8 intensity, the disparity was less pronounced, likely due to the size of the cell compared to the size of the tau aggregate internalised. Therefore, maximum AT8 intensity was considered a better output for indication of tau uptake. These experiments were

repeated in astrocytes that had previously been characterised after 3-6 independent differentiations from a three separate pools of NPC generated from one iPSC control line. As detailed in Chapter 3, astrocyte changes were relatively consistent across independent differentiation into astrocytes. In the tau uptake experiments described here, there were 2 technical replicates (individual wells). Data is presented as fold change of AT8 maximum intensity relative to untreated cells, in order to account for natural variability of immunolabelling intensities between experimental repeats.

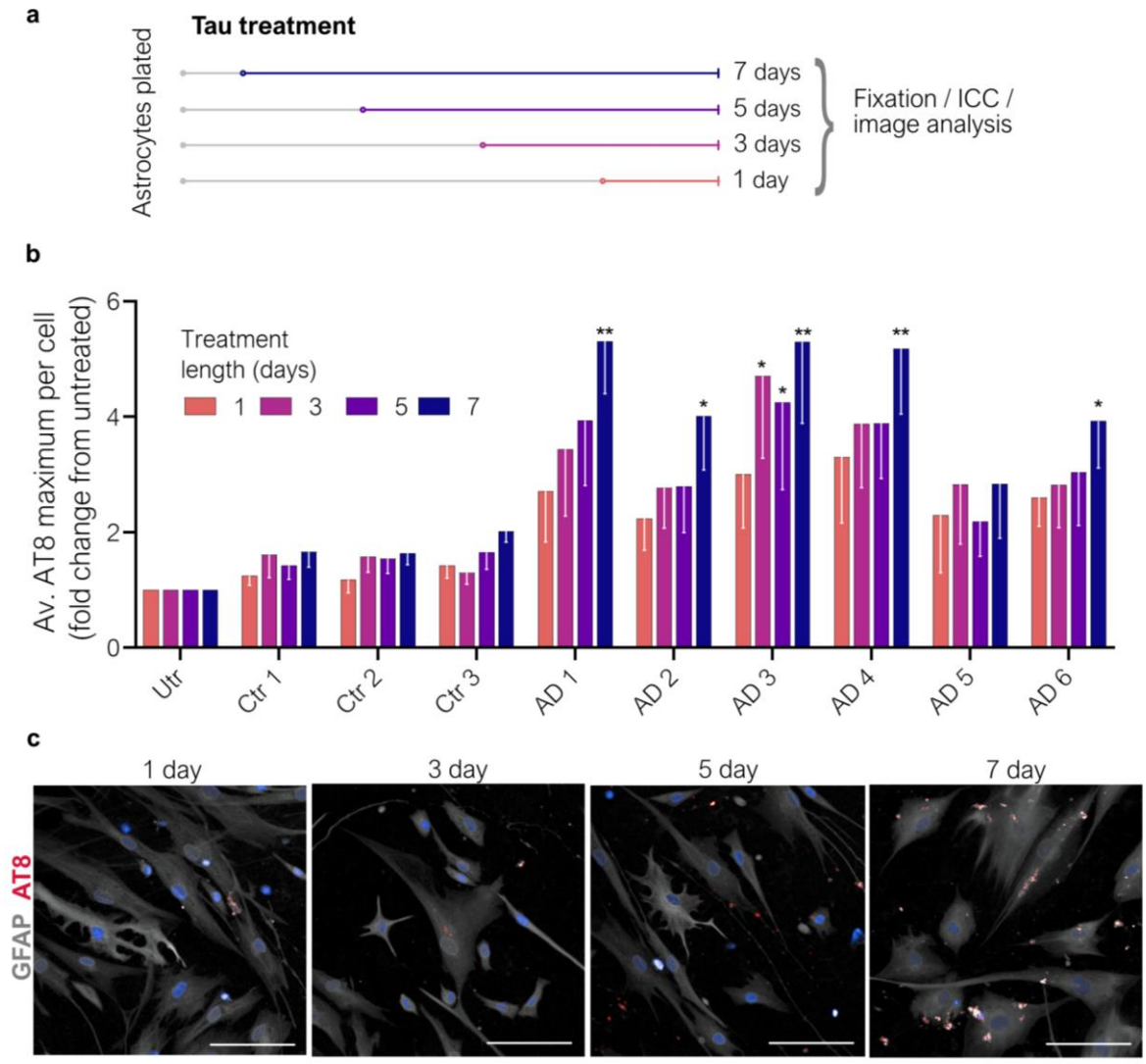

Figure 5.6 AT8 intensity within astrocytes increases with time following exposure to AD brain-derived tau aggregates for up to 7 days.

60-day iPSC-astrocytes were exposed to 0.1 ng/µL of human AD brain derived tau aggregates or equivalent volumes of control samples. Some astrocytes were left untreated. (**a**) Schematic overview of the experimental design. (**b**) The maximum AT8 intensity per cell was measured and the average value for each well was normalised to the same measure in untreated astrocytes. The graph shows relative fold changes for all cases 1-, 3-, 5- or 7-post exposure. (**c**) Representative images of tau aggregate uptake depicted by AT8 immunolabeling (red) in astrocytes labelled with GFAP (grey). A two-way ANOVA showed treatment and time effects, but no interaction of treatment and time. Holm-Šidák's multiple comparisons test for pairwise differences was performed relative to untreated cells at each treatment length. Data is mean ± SEM (internal white error bars). N=4 (independent astrocyte differentiations, performed in duplicate. * $p < 0.05$, ** $p < 0.01$

A low intensity signal for AT8 was measured in untreated iPSC-astrocytes that was consistent between timepoints (Figure 5.9B). Although human astrocytes express small

amounts of endogenous tau (Zhang et al., 2014; Karlsson et al., 2021b), as shown in Section 4.3.3 for iPSC-astrocytes, this is unlikely to be AT8 positive, and so this signal is presumed to represent background levels of fluorescence. Astrocytes exposed to all control samples showed slightly elevated AT8 signal relative to untreated cells from 1 day after exposure, that increased slightly with increasing incubation time. While tau aggregates were not detected in these samples by western blot, it is possible that small amounts of tau aggregates were present but below the level of detection. Indeed, tau is known to aggregate in aged brain (Wharton et al., 2016).

In astrocytes exposed to aggregated tau from postmortem AD brain, each case showed higher average AT8 intensity per cell relative to cells exposed to control samples and those left untreated, following 1-day of exposure. For cells treated with the majority of tau extracts (AD 1, 2, 3, 4, 6), the average maximum AT8 intensity per cell further increased with extended incubation time, with 7-day exposure resulting in the maximum levels of AT8 intensity inside cells, indicating that astrocytes appear to either internalise tau in a slow time frame, or that the internalised tau aggregates are seeding endogenous tau within astrocytes. AD 5 showed a slightly different pattern, with increased tau intensity observed at 3 days relative to one day, but then AT8 levels appeared to plateau from 3-7 days post-exposure. The reason for this different profile is not clear since this case appeared similar to the others when analysed by western blot and ICC.

A two-way ANOVA was performed on the data set depicted in Figure 5.6b, to analyse the effect of case and length of treatment on tau uptake, as indicated by the average maximum AT8 intensity per astrocyte. This revealed that there was not a statistically significant interaction between the effects of case and length of treatment ($F(27, 120) = 0.284$, $p = 0.999$). Simple main effects analysis showed that both time ($p = 0.0111$) and case ($p<0.0001$) had a significant effect on maximum AT8 intensity. Afterwards, Holm-Šidák's multiple comparisons test was performed to indicate significant changes relative to untreated astrocytes. For nearly all AD cases (except AD 5), there was a significant increase in the average AT8 maximum per astrocyte when compared to untreated. Control cases did not show a significant increase relative to untreated controls. AD 3 also showed significantly increased AT8 additionally at days 3 and 5, indicating that tau uptake of this tau is either more efficient, or that endogenous tau is efficiently recruited by AD 3 tau seeds once internalised. The maximum AT8 signals after 1 day of treatment with AD 3 treatment was

high but not as high as AD 4, for example, which in turn did not show the same level of AT8 intensity at longer treatment time. This indicates further that AD 3 tau may have inherent properties that allow for more efficient uptake and/or endogenous tau seeding. It is interesting to note that the corresponding brain section analysed by IHC for AD 3 (Figure 5.5) tau showed the highest levels of mature tau fibrils and astrocyte association. This may be further evidence that the pathogenic tau species here have properties that make them better to be seeded and potentially spread tau, although this would require a more thorough examination of molecular heterogeneity of the tau species involved. Furthermore, cells treated with AD 5 showed an increase in AT8 that was not significant at day 7, and did not increase with length or time. This could indicate the properties of tau from this AD case prohibit tau uptake in astrocytes, or are less able to seed endogenous tau in astrocytes, or were quickly degraded by astrocytes once internalised. IHC analysis of this sample did show some tau pathology near astrocytes (Figure 5.5), but it appeared less abundant in comparison to other AD cases.

Together, these data show that astrocytes can internalise tau aggregates that are isolated from postmortem human AD brain. The intensity of AT8 labelling within astrocytes generally increased with longer periods of exposure, although some case specific variability is indicated in the data. Astrocytes also have the ability to degrade proteins and peptides, including Aβ (Ries and Sastre, 2016; Yamamoto et al., 2018) as well as dead or damaged nearby synapses and cells (Wakida et al., 2018; Sanchez-Mico et al., 2020), and the astrocytes in these studies showed pH changes that indicate lysosomal degradation of cellular debris. A key question thus remans – how do astrocytes process these tau aggregates after tau uptake? To begin to answer this question, it was first important to determine if astrocytes show clearance of tau aggregates over time. To this end, a longer-term assay was developed to look at the abundance of internalised tau over longer periods of time.

5.3.5 Astrocyte retention of internalised tau aggregates with extended time in culture.

As summarised in Figure 5.7a, three separate 96-well plates of 60-day iPSC-astrocytes had their astrocyte culture medium removed and replaced with astrocyte medium containing aggregated tau from AD brain and equivalent control volumes, while some were left untreated, as per the experiment described above. After 7 days of exposure, one plate was

fixed while others were washed to remove residual tau and replaced with fresh tau-free astrocyte medium. These plates were maintained for an additional 7 or 14 days prior to fixation. This allowed retention of internalised tau within astrocytes to be examined in an environment when there is no extracellular tau to be internalised. Cells were fixed, immunolabelled and imaged, and the images analysed as described above.

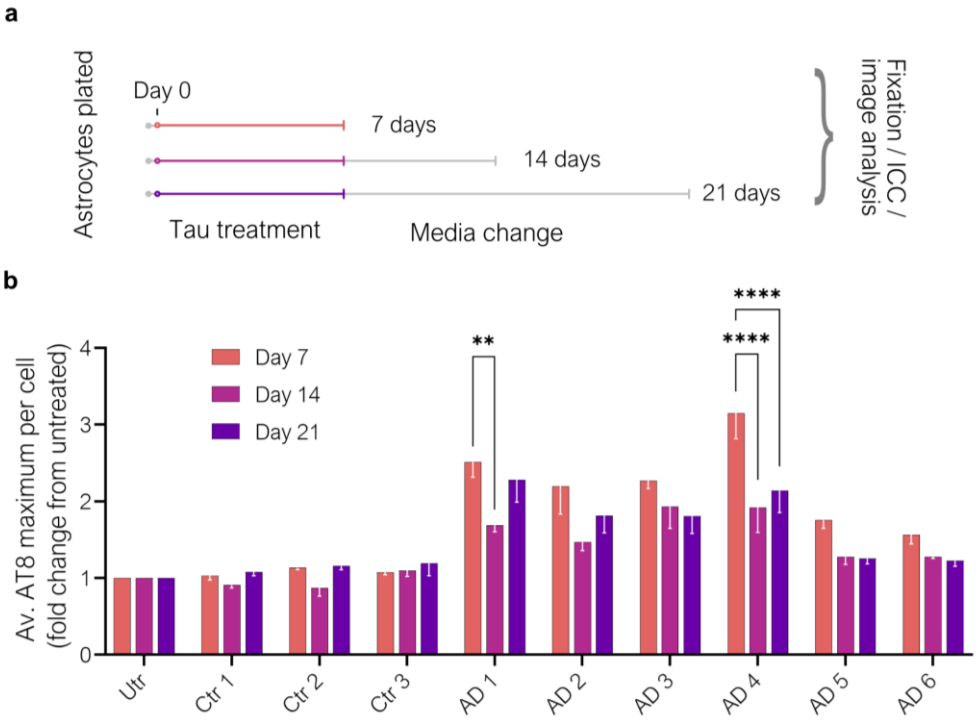

Figure 5.7 Alterations in AT8 intensity within human astrocytes following exposure to AD brain tau aggregates for up to 21 days.

Schematic overview of the experimental design shown in (**a**): three sets of 60-day iPSC-astrocytes were exposed to 0.1 ng/µL of human AD brain derived tau aggregates or equivalent volumes of control samples. Some astrocytes were left untreated. After 7 days, one set of astrocytes were fixed, tau-containing medium was removed from the other cells, and this was replaced with fresh astrocyte medium. These cells were fixed at either day 14 or 21 with no further media changes. (**b**) Graph displays the average of the maximum intensity of AT8 labelling per cell in each well, relative to untreated cells. Astrocytes showed greatest AT8 immunoreactivity 7 days following tau aggregate exposure. A two-way ANOVA was performed confirming statistical significance of time and case on AT8 intensity, and pairwise comparisons were performed by Holm-Šidák's' multiple comparisons test relative to day 7 in each treatment condition. Data is mean ± SEM. N=4 (independent differentiations), each of which was performed in duplicate. * $p < 0.05$. ** $p < 0.01$. *** $p < 0.001$, **** $p < 0.0001$.

Similar to the data presented in Figure 5.6, a low intensity signal for maximum AT8 intensity was detected in untreated iPSC-astrocytes that was consistent between timepoints (Figure 5.7b), representing background fluorescence. Values were normalised to this and are shown as fold change from untreated. Astrocytes exposed to all control samples again showed small increases in AT8 immunoreactivity relative to untreated astrocytes that were not largely altered with increasing incubation time.

Astrocytes exposed to AD tau aggregates all showed higher AT8 immunoreactivity than cells exposed to control brain samples or those that were untreated. The intensity of AT8 intensity in astrocytes exposed to AD brain tau aggregates peaked in astrocytes exposed to tau for 7 days (Figure 5.7b). A two-way ANOVA was performed on this dataset, to analyse the effect of case and time on tau uptake, as indicated by the average maximum AT8 intensity per astrocyte. This revealed that there was a statistically significant interaction between the effects of case and time ($F(18, 90) = 1.872$, $p = 0.0284$). Simple main effects analysis showed that both time ($p<0.0001$) and case ($p<0.0001$) had a significant effect on maximum AT8 intensity.

Following removal of the aggregated tau containing medium and further incubation of the astrocytes for 7 days, there was a decrease in maximum AT8 immunoreactivity in all astrocytes exposed to AD brain tau. In astrocytes that were cultured in tau-free medium for 14 days after original 7-day tau medium exposure (day 21), two main patterns of changes in AT8 immunoreactivity relative to the 14-day timepoint were observed. In astrocytes exposed to tau from AD cases 3, 5 and 6, the intensity of intracellular AT8 labelling remained relatively stable compared to the 14-day time point. In contrast, astrocytes exposed to tau aggregates from AD cases 1, 2 and 4 demonstrated an increase in maximum astrocyte AT8 levels at day 21 compared to day 14. A post-hoc Holm-Šidák's multiple comparisons test was performed to highlight significant changes in AT8 intensity for each case with time, relative to day 7. AD 1 showed significant decrease in AT8 intensity at day 14 only, but at day 21 there appeared to be a large enough recovery to remove this significant decrease. AD 4 showed the highest reduction in AT8 intensity with time at both day 14 and 21. This may indicate AD4 tau is less able to seed endogenous iPSC-astrocyte tau once internalised, and/or that astrocytes are more efficient at degrading these specific tau species. Indeed, these results overall indicate that while internalised tau appears to be reduced once internalised in all AD cases, variations in the subsequent reduction or recovery indicates that

specific properties of these aggregates may confer how astrocytes process tau and their seeding potential. Variation between AD cases in the post-translational modification and seeding potential of tau as has been indicated previously by post-mortem studies and *in vitro* (Wesseling et al., 2020; Kamath et al., 2021). This is further corroborated by the statistical interaction between the effect of time and case on astrocyte internalisation of tau, which suggests that these variables are affected by one another. It is worth noting that the average number of cells was not altered between time points (data not shown), suggesting that these changes were not due to cell death or proliferation changes with increasing time in culture.

Overall, this data suggests that the rate of tau uptake and/or clearance is dependent on characteristics of the tau extracted from each case. To determine if the changes in AT8 intensity over time equated to a reduction or increase in the size of tau aggregates within astrocytes, images from these astrocytes were analysed using a spot detection protocol that detects high AT8 intensity regions relative to background and calculates them as spot regions. The properties of these spots can be analysed, allowing the average volume of AT8 puncta to be measured and compared across time points (Figure 5.8).

A low level of AT8 spot volume was detected in untreated astrocytes that remained consistent across timepoints, indicating the level of background detected in this analysis. Control treated astrocytes also showed a low volume of AT8 spots that was only marginally higher than untreated and in keeping with a slight increase in AT8 intensity observed in data analysed previously (Figure 5.6 & Figure 5.7), again suggesting some level of AT8-positive tau present in control samples that might be expected where some tau aggregation is known to occur in non-diseased brains (Wharton et al., 2016). In contrast, AD treated astrocytes demonstrated the highest levels of total spot area after 7-day treatment, which again decreased following removal of tau treatment media as previously described with AT8 intensity. A two-way ANOVA was also performed on this dataset, to analyse the effect of case and time on total AT8 spot area within cells. This revealed that there was a statistically significant interaction between the effects of case and time ($F(18, 90) = 3.10$, $p = 0.0002$). Simple main effects analysis showed that both time ($p<0.0001$) and case ($p<0.0001$) had a significant effect on total AT8 spot area.

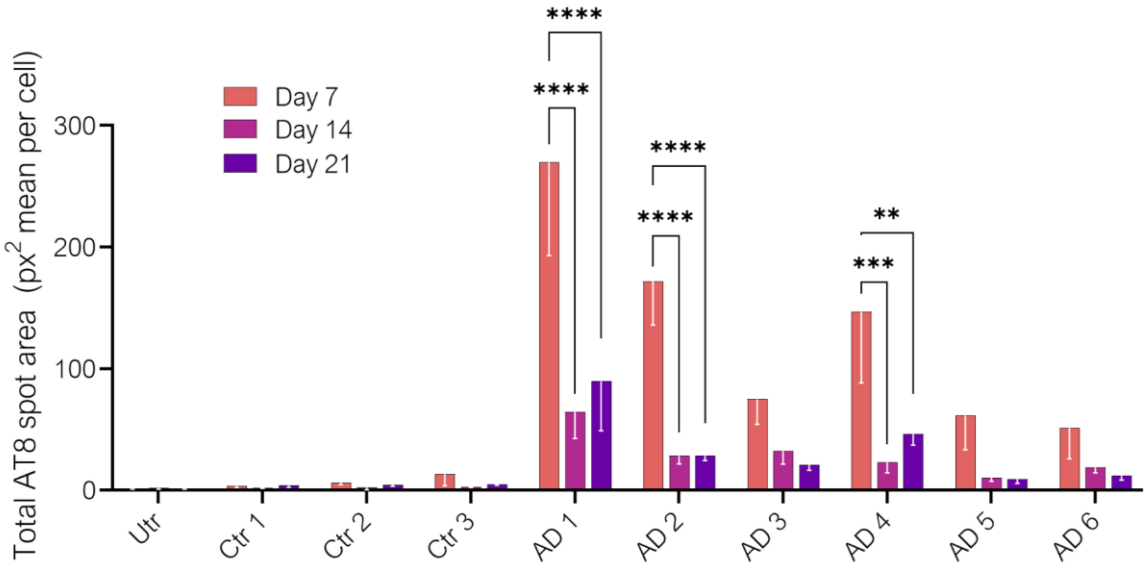

Figure 5.8 Aggregate area is decreased following 7-day tau treatment.

Tau retention assay data shown in Fig. 5.7 was analysed for area of internalised tau aggregates at each timepoint for AD treated and control treated as well as untreated day-60 iPSC-astrocytes. Detected AT8 positive spot regions in astrocytes was reduced at day 14 and day 21 after initial 7-day AD tau treatment. A two-way ANOVA was performed confirming statistical significance of time and case on AT8 intensity, and pairwise comparisons were performed by Holm-Šidák's' multiple comparisons test relative to day 7 in each treatment condition. Data is mean ± SEM. N=4 (independent differentiations), each of which was performed in duplicate. ** $p < 0.01$. *** $p < 0.001$, **** $p < 0.0001$.

Similar to AT8 intensity measurements, all AD treated astrocytes saw a large reduction in total spot area after tau treatment removal at day 14. A post-hoc Holm-Šidák's multiple comparisons test was performed to highlight significant changes in AT8 spot area for each case over time, as was done previously for AT8 intensity. Here, results showed a significant reduction in spot area at day 14 in astrocytes treated with AD 1, AD 2 and AD 4. This was not apparent in AT8 intensity measurements with AD 2, and a greater decrease was apparent in AD 1 and 4. This suggests that the maximum AT8 intensity is indicative of a decrease in the volume of AT8 positive tau aggregates, but the reduction in aggregate area is more significant than first indicated by AT8 maximum intensity changes. It seems likely that maximum AT8 intensity is a better indication of the density of tau fibrils, which would likely cause a higher AT8 immunofluorescence.

For astrocytes that were kept a further 7 days in tau-free astrocyte media until day 21, the spot area appeared relatively stable in most cases and remained significantly decreased for AD 1, AD 2 and AD 4, as for day 14. AD 1 and AD 4 again showed a recovery of AT8 spot volume, and in AD 4 this meant that spot area at day 21 was not as significantly decreased compared to day 14, relative to day 7. This suggests that some level of tau seeding may occur in this case.

However, for AD 1 a large recovery of AT8 aggregate volume from day 14 to 21 was not observed as with measurements for AT8 intensity. Variability at these time points suggest that tau aggregate size at day 21 was not largely increased. It may be the case that *density* of AT8 positive tau aggregates are increased at day 21 in AD1 treated astrocytes, as indicated by AT8 max intensity data (Figure 5.7), but that the total volume of these fibrils has not increased to a detectable change. AD 4 treated on the other hand did show an increase at day 21 relative to day 14 that may indicate an increase in the size of tau aggregates and a propensity for rapid tau seeding of this case derived AD tau, as indicated by AT8 intensity data. While AD2 AT8 intensity was increased at day 21 relative to day 14, this was not the case with total spot area, and remained fairly stable. AD 3, 5 and 6 followed a similar pattern to their respective AT8 max intensity values.

This data provides more evidence that there may be two patterns of tau retention after uptake depending on the AD case form which tau was derived. While it seems that astrocytes are able to reduce the intensity and volume of tau aggregates they internalise from all cases, they do not appear to be able to completely remove tau to within control or untreated levels within the time frame examined. This suggests that there may be tau aggregates that are not degradable by astrocytes, or that astrocytes require extended periods to achieve this. Further, the recovery in tau volume and intensity indicated in AD1 and AD4 treated astrocytes may indicate tau seeding of endogenous astrocytic tau is masking or overcoming removal of tau aggregates, and that seeding may preferentially or more efficiently occur with specific AD tau species, as has been seen with post-mortem AD tau fibrils seeded with recombinant tau monomers *in vitro* (Kamath et al., 2021).

5.4 Discussion

5.4.1 Summary of results

This chapter investigated the uptake of pathological forms of human brain tau by human iPSC-derived astrocytes. The main findings are that:

- hiPSC-astrocytes efficiently internalise human tau aggregates
- There is variation in the rate of internalisation and clearance of tau isolated from different AD cases
- Internalised human tau may be able to seed further aggregation.
- There are different patterns in tau clearance/seeding rates that may reflect molecular heterogeneity in brain tau, but this is yet to be determined.

5.4.2 Isolation of aggregated tau from different tauopathies

Isolation of tau aggregates from different tauopathies demonstrated that there may be intrinsic differences in tau aggregates from different tauopathies that alters their solubility in sarkosyl and therefore their ability to be isolated using the method used here. The protocol used was optimised to extract tau aggregates from AD tissue (Greenberg and Davies, 1990) and it was expected to be efficient in extracting pathogenic tau from other tauopathies. Indeed, the results shown in Chapter 3 indicated that sarkosyl-insoluble tau aggregates can be isolated from PSP and PiD brain as well as AD brain, however the cases used in this Chapter did not yield much, if any, insoluble tau. Tau fibrils from PiD and PSP have a core comprised of 3R or 4R tau, respectively (Figure 1.5) (Shi et al., 2021) and the fold itself is different from that in AD and this may confer differences in solubility. A major structural difference in these folds is the outward exposure of microtubule binding domain R3 in AD and PiD folds, which is conversely shielded in PSP fold to form the central layer (Shi et al., 2021). This may alter the overall charge and hydrophobicity of tau, and ultimately its solubility in sarkosyl. Indeed, in their paper, Shi et al. (2021) describe an alternative process for isolating PSP and AGD tau fibrils which differs from the extraction protocol used to extract aggregates from PiD and AD brain. Optimisation of tau extraction for multiple tauopathies was, however, beyond the scope and time limitations of this project.

5.4.3 Rates of astrocyte uptake of AD tau and implications for tau uptake mechanisms

The intensity of tau aggregates increased with time of exposure, up to 7 days tested, suggesting that this is not a rapid process of internalisation. The exact process of internalisation was not tested in this chapter, but potential mechanisms are described in Section 1.5.3.1. The data in this chapter that indicate slow uptake are in line with previous studies that observed astrocyte phagocytosis is a slow process (Lööv et al., 2015), and less efficient than that of microglia (Magnus et al., 2002; Konishi et al., 2022). Lööv et al. (2015) previously found that while engulfed material by macrophages converged with lysosomes within 5 hr, astrocyte engulfed cellular material did not fuse with lysosomes until after 3 days, and it took up to 2 weeks for astrocytes to degrade the ingested dead cells (Lööv et al., 2015). While it is not clear whether or not tau is internalised by phagocytosis and/or by other receptor mediated endocytosis mechanisms suggested by others (Holmes et al., 2013; Rauch et al., 2018), it is worth considering that the process of phagocytosis involves several steps, including detection of the particle for digestion. Astrocyte phagocytosis ability has been emphasised in the uptake and clearance of Aβ (Wyss-Coray et al., 2003; Basak et al., 2012; Li et al., 2014), and so it is reasonable to assume similar processes may be involved in the astrocyte uptake of large tau fibrils. It has also been shown that astrocytes can phagocytose apoptotic cells (Wakida et al., 2018). In the experiments shown in this chapter, apoptotic cells were identified and were present in all treatment conditions. This offers another indirect route of pathogenic tau internalisation if the apoptotic cell had already internalised tau aggregates. Further, other studies have shown that astrocytes are able to engulf neuronal synapses (Lee et al., 2020), which can harbour pathological tau species (Robbins et al., 2021), presenting further mechanisms by which astrocytes can internalise pathological tau.

This selectivity of astrocytes for digestion targets is not well understood, but the evidence in this chapter demonstrates that astrocytes do not actively prevent the uptake of AD tau, as all six AD derived tau samples were readily internalised by these astrocytes. This is interesting because pathogenic tau inclusions are not often seen in AD post-mortem tissue and are more commonly associated with other tauopathies (Kovacs, 2020; Reid et al., 2020), as well as other neurodegenerative diseases such as ALS (Velebit et al., 2020) and Parkinson's disease (Tsunemi et al., 2020) . However, evidence of astrocytic tau inclusions in AD is now emerging, with post-mortem tissues showing 3R tau inclusions in hilar

astrocytes of the dentate gyrus, which altered astrocyte mitochondrial dynamics and synaptic function when modelled in mice (Richetin et al., 2020b). Whether this tau was internalised and/or accumulated from aggregation of endogenous astrocytic tau, is yet to be determined. However, the evidence in this project confirms in principle the ability of human astrocytes to internalise AD tau aggregates.

5.4.4 Astrocyte ability to degrade tau

A longer-term assay was utilised in this chapter to probe if and how long astrocytes take to degrade internalised tau after an initial 7-day treatment period. The data here indicates that astrocytes begin a process of degradation during this timeframe that starts to reduce astrocytic tau aggregates towards baseline levels. Potential mechanisms of tau clearance are explored in Chapter 1 (Section 1.3.7), and further explored in Chapter 6. While proteasomal pathways may play a role, specific phosphorylation of tau has shown to impair this mechanism of degradation in a non-cellular *in vitro* model (Ukmar-Godec et al., 2020). Likely is the involvement of the autophagosome-lysosomal system of degradation, which is known to be involved in the degradation of soluble and insoluble altered tau (Wang and Mandelkow, 2012), and indeed there is post-mortem evidence of altered tau interacting with lysosomes in AD tissue (Ikeda et al., 1998). Exploring the specific mechanisms of degradation of tau aggregates in astrocytes is an interesting area of future exploration.

AT8 spot area detection indicated that the size of tau aggregates in astrocytes was reduced extensively during the first 7 days post tau exposure, whereas a further 7 days was not able to reduce the remaining volume of aggregates. This may be in line with normal astrocytic degradation and clearance processes that have been shown to be slower than microglia clearance mechanisms (Magnus et al., 2002), and also in studies that have shown that astrocytes store ingested cellular material rather than degrading it completely (Lööv et al., 2012). It remains to be seen if astrocytes are able to clear all ingested tau at longer time frames.

If some AD tau aggregates are internalised as phagosomes and undergo a process of maturation and degradation, they must also be resolved. Phagocyte resolution has not been studied extensively, and the processes of reabsorbing into the cell are not well understood (Levin et al., 2016). It is possible that if the tau aggregates are not able to be degraded completely by the hydrolases and acidic environment of the phagolysosome (Levin et al.,

2016), then it is likely that aggregated tau will remain in the cytosol of astrocytes as the phagosome membrane and other digestible components are recycled phagolysosome (Levin et al., 2016; Kishore et al., 2020). This may be what is observed in the astrocytes that retain tau aggregates two weeks following exposure. While the reduction in AT8+ve tau aggregates after tau is removed from culture medium was observed to occur across a 2-week period, there is still evidence that astrocytes harbour tau inclusions which indicates that it is difficult for astrocytes to completely process the ingested material. If astrocytes are unable to degrade tau completely, then it is possible that tau may interfere with the phagosome resolution process that is crucial for regeneration of lysosomes and subsequent degradative capacity of astrocytes (Lancaster et al., 2021).

5.4.5 Evidence for internalised AD tau to seed astrocytic tau

Astrocytes exposed to tau from some, but not all of the AD cases showed an increase in internalised tau 2 weeks following tau removal that was greater than observed only one week after tau was removed from media. This may indicate the ability of internalised tau to seed the endogenous tau that is known to be expressed in these astrocytes from characterisation data in Chapter 4. There is evidence for this in primary mouse neurons, where AD derived tau fibrils were able to recruit endogenous mouse tau into these aggregates (Guo et al., 2016), as well as a tau biosensor cell system that saw AD brain lysate induce recombinant tau aggregation as well as seed mutant human tau in a transgenic mouse model (Kaufman et al., 2017). While this has not been explored in astrocytes, the data here suggests that in some AD cases, seeding process may be possible in astrocytes. Specific tau seeding assays are required to determine if endogenous astrocytic tau can easily be incorporated into the internalised tau aggregates.

5.4.6 Variations in AD tau uptake/clearance

The data here shows that when exposed to tau derived from all AD cases, astrocytes show a similar pattern of slow, increasing tau uptake over a 7-day time course, and reduction in tau in the 7 days following the removal of treatment followed by either a plateau or increase. There was also variability in the amount of tau internalised between astrocytes exposed to tau from different AD cases, as indicated by spot size and AT8 maximum data. For some cases, such as AD3, this is consistent with the tissue samples of the AD cases examined in Figure 5.5, where high tau pathology near astrocytes observed in AD 3 brain sections may

correlate with the high tau internalisation and low reduction in AT8 intensity or AT8 aggregate volume seen long term compared to other AD tau used. In cases such as AD5 and 6, measures of tau uptake were lower overall, and this may correlate with low AT8 seen in these sections. However, correlations that can be made with single brain sections are limited considering that tau pathology may vary considerably, even within brain regions such as the temporal cortex here that are broadly affected by tau pathology. The amount of tau aggregates used for spiking were normalised, so these differences are likely not a result of differences in tau concentration. Rather, it is possible that variability between the specific properties or modifications to tau in each AD case resulted in different rates of internalisation, degradation, and possibly seeding. Indeed, this variation in the properties of tau derived from different AD cases has previously been observed experimentally, where the seeding competence of patient derived tau aggregates varied and correlated with biochemical differences observed between different AD tau species (Kamath et al., 2021), and this molecular diversity of tau can also contribute to clinical heterogeneity in AD patients (Dujardin et al., 2018), highlighting the differences this can make on cell toxicity. The authors of this study went on to demonstrate tau seeding of isolated high molecular weight tau species could be correlated with specific tau phosphorylation sites (Dujardin et al. 2020). How this may impact the uptake of tau in astrocytes is yet to be determined but remains an interesting topic for future investigation.

5.4.7 Limitations and future work

The initial aim of this work was to determine if the same type of tau extracts isolated from tauopathy brain that showed peripheral transmission in htau mice (Chapter 3) were internalised by human astrocytes. Although no obvious tau fibrils were observed, exposure of cells to these extracts gave some evidence that tau is being internalised by some of the cells. However, it also demonstrated a toxic effect as indicated by the number of altered nuclei that are reminiscent of cells that have undergone apoptosis. This highlights the difficulty in using a general tissue homogenate that is not enriched for tau, as it likely contains various cytomodulating factors that have an apparent toxic effect on cells and that are difficult to control. Therefore, this strategy was not pursued and instead this work focussed on tau aggregates.

AT8 was utilised as a phospho-tau antibody that labels aggregated tau fibrils (Li et al., 2020; Gandhi et al., 2015), in order to distinguish between the endogenous tau expressed by the astrocytes. An image Z-stack was acquired and 3D reconstruction of astrocytes by GFAP immunolabelling to measure internal AT8 (see section 2.5.4 for microscopy details). The final resolution appeared sufficient to distinguish between internal and membrane bound AT8 positive tau aggregates. However, reducing the numerical aperture (NA) by utilising a 20X water lens instead of the 20X air lens, or a higher objective such as 40X, would have provided significantly higher resolution. This may have allowed for more certainty when analysing internalised tau proteins in the Opera Phenix high throughput system. Nonetheless, previous pilot data had been conducted (data not shown) at higher magnification, and thus higher resolution, that demonstrated clear internalisation of aggregated tau proteins when utilising the same antibody labelling. Furthermore, the gradual increase in AT8 volume and intensity within astrocytes over a 7-day time course (Fig. 5.6), and subsequent decrease in AT8 levels after removal of tau (Fig. 5.7) may be in line with slow phagocytic tau internalisation process of large proteins (Wakida et al., 2018; Paul et al., 2013). While care could be taken in future experiments to maximise the NA and subsequent resolution along of the image, without compromising analysis pipelines, as well as exploring the stripping of surface bound tau aggregates, it seems likely based on the discussion points above that tau aggregates were indeed internalised by astrocytes in these experiments.

While rates and ability of tau internalisation was explored, the next step is clearly to investigate specifically how different mechanisms contribute to tau uptake. HSPGs, for example, that have been routinely implicated in tau uptake in neurons (Holmes et al., 2013; Rauch et al., 2018; Yamada and Hamaguchi, 2018) could investigated by blocking this pathway through specific HSPG inhibitors or competitive binding partners, to elucidate its impact on tau uptake.

A key area of interest would also be the differences in tau derived from other tauopathies, such as PSP and PiD that were explored in Chapter 3. Evidence suggests astrocytes have a different relationship with pathological tau species in these tauopathies (Kovacs, 2020; Reid et al., 2020), and therefore repeating these experiments in this tau, once properly isolated, would be interesting to observe as this could be explain differences in tau uptake and rates of degradation that the assays developed in this chapter explore.

5.4.8 Conclusions

The data presented in this chapter confirm that human iPSC-astrocytes can internalise AD brain derived tau aggregates, and that degradation of these internalised proteins is apparent given enough time in culture. Key questions remain as to the cellular impact that this tau internalisation has on astrocyte structure and behaviour, and whether this may be detrimental to the cells they interact with in normal brain physiology. This will be explored in the next chapter.

6 Human astrocyte response to AD derived tau uptake

6.1 Introduction

While results from the previous chapter confirm the ability of iPSC-astrocytes to internalise tau aggregates, how they process the tau and the impact of tau internalisation on astrocyte function is yet to be determined. This chapter therefore aims to investigate how astrocytes respond to tau once internalised.

Astrocyte reactivity, as described in detail in Section 1.5.1, is a common phenotypic change in astrocytes in response to environmental changes in neurodegenerative diseases. There are myriad factors that have the potential to contribute to astrocytes acquiring this 'reactive' state. The intermediate filament GFAP is often correlated with astrocytes being in a reactive state, in part because high GFAP-positive astrocytes are often observed around neurofibrillary tangles (Ikeda et al., 1992; Serrano-Pozo et al., 2011b), and this is thought to define a hypertrophic response (Vijayan et al., 1991) correlated with an increase in the number of GFAP positive processes (Sofroniew and Vinters, 2010). S100B, another protein associated with astrocytes, has recently been associated with suppressing aggregation of both Aβ (Cristóvão et al., 2018) and of tau (Moreira et al., 2021). As both of these are highly expressed in the human iPSC-astrocytes characterised in Chapter 3, their expression and association with tau was examined here.

Various pathways are also involved in astrocyte reactivity. The JAK-STAT3 pathway has emerged as a central regulator of astrocyte reactivity and while multiple pathways govern this signalling, STAT3 is common to many of them (Ceyzériat et al., 2016). *GFAP* is also known to be a target gene of STAT3 (Herrmann et al., 2008; Wanner et al., 2013; Levine et al., 2016), and STAT3 is also linked to the complement cascade which plays a large role in regulating proinflammatory pathways and regulating innate immunity (Ricklin et al., 2016), especially through the C3 molecule which is upregulated in AD brain and may play a negative role in neurodegeneration, where its deficiency could mitigate neuronal loss in mutant tau mice as well as amyloid transgenic mouse models (Wu et al., 2019). Other genes that are commonly associated with reactive astrocytes, such as SERPINA3 – a peptidase inhibitor linked to inflammation (Vanni et al., 2017), and LCN2, a lipophilic protein that can induce neuronal cell death (Bi et al., 2013) were examined. Both proteins are secreted by astrocytes

and are markers of astrocyte reactivity (Zamanian et al., 2012). Conversely some genes such as NRF2 have been associated with a cryoprotective state in disease models, where astrocyte specific expression reduces Aβ deposition and phospho-tau accumulation in mutant tau and APP/PS1 knockin transgenic models (Jiwaji et al., 2022)

Astrocytic degradation of tau is also one of the key questions stemming from the clearance of internalised AD tau that was observed in Chapter 5. As discussed in the previous chapter and Introduction Section 1.3.7, the autophagosome-lysosomal degradation pathways are a likely route for tau degradation as they are have previously been implicated in clearance of Aβ in primary mouse astrocytes (Simonovitch et al., 2016), and TDP43 clearance in iPSC derived astrocytes is accelerated when autophagy is increased with small molecules. Lysosome formation is also important for the degradation of particles internalised by astrocytes (Lööv et al., 2015), and therefore it is worth investigating *TFEB* which a master regulator of lysosomal biogenesis (Sardiello et al., 2009; Settembre et al., 2011), as an indicator of upregulation in this process. Uptake mechanisms of tau into astrocytes are also important to investigate, and as such LRP1, a receptor associated with the selective uptake of tau in human neuroglioma cells (Rauch et al., 2020), that is observed to mediate astrocytic clearance of Aβ in primary astrocytes, is also worth investigating.

Investigating these factors after AD tau uptake and clearance in human iPSC-astrocytes will give some indication as to the impact that pathogenic tau uptake can have on astrocyte reactivity, their ability to support neurons, and indications of how astrocytes process tau.

6.2 Results

6.2.1 Alterations in GFAP after tau uptake

Increased levels of GFAP has been correlated with AD pathology (Middeldorp and Hol, 2011; Hol and Pekny, 2015). Therefore, changes in overall GFAP protein expression in human iPSC-astrocytes was examined in 60-day iPSC-astrocytes exposed to 0.1 ng/µL tau aggregates from AD brain or equivalent control brain extracts for 1, 3, 5 or 7 days, relative to untreated human iPSC-derived astrocytes (Figure 6.1). iPSC-astrocytes were immunolabelled with antibodies against GFAP and phospho-tau (AT8, Ser202/Thr205)

(Figure 6.1a). Harmony software was used to determine the average and maximum GFAP intensity per cell (Figure 6.1b, c). This initial analysis was conducted independently of whether or not the astrocytes showed tau aggregate internalisation. A two-way ANOVA was performed to measure the effect of length of treatment and case (AD or control) on average GFAP intensity per astrocyte. The results indicated that there was not a significant interaction between the effects of case and treatment length on average GFAP intensity in cells ($F(27, 120) = 0.231$, $p > 0.999$). A simple main effects analysis showed that both case ($p = 0.036$) and treatment length ($p = 0.009$) did have a significant effect on average GFAP intensity in cells. A post-hoc Holm-Šidák's test for multiple comparisons did not find any significant changes relative to untreated cells. Interestingly, astrocytes treated for 7 days showed the lowest levels of GFAP compared to shorter treatment lengths. This was true also in astrocytes exposed to (aged) control brain extracts, suggesting that it is likely exposure to some age-related factor present in both control and AD extracts that is inducing changes in GFAP. While not being significant different from controls, there was a trend towards increased average GFAP intensity in astrocytes exposed to tau aggregates from AD cases 3 and 4 relative to untreated cells.

Maximum GFAP intensity per cell was also analysed in order to determine if astrocytes displayed areas of higher GFAP expression that did not impact average GFAP expression across the cell (Figure 6.1c). As before, a two-way ANOVA was performed to measure the effect of length of treatment and case (AD or control) on maximum GFAP intensity per astrocyte. The results indicated that there was not a significant interaction between the effects of case and treatment length on average GFAP intensity in cells ($F(27, 120) = 0.183$, $p > 0.999$). A simple main effects analysis showed that both case ($p = 0.273$) and treatment length ($p = 0.214$) did *not* have a significant effect on maximum GFAP intensity in cells. A post-hoc Holm-Šidák's test for multiple comparisons did not find any significant changes relative to untreated cells. Similar to average GFAP intensity measurements, astrocytes exposed to tau aggregates from AD case 4 also demonstrated the highest maximum GFAP levels, although this was not a significant difference when compared to either untreated or control brain extract-treated astrocytes. However, the GFAP maximum appeared to vary less between cases and length of treatment, only increasing 1.32-fold from the mean in AD 4, compared to 1.54-fold increase in average GFAP in the same condition. This perhaps

suggests that changes to astrocyte GFAP intensity occurs largely to the astrocyte as a whole, and peak intensity of GFAP within astrocytes does not vary as much.

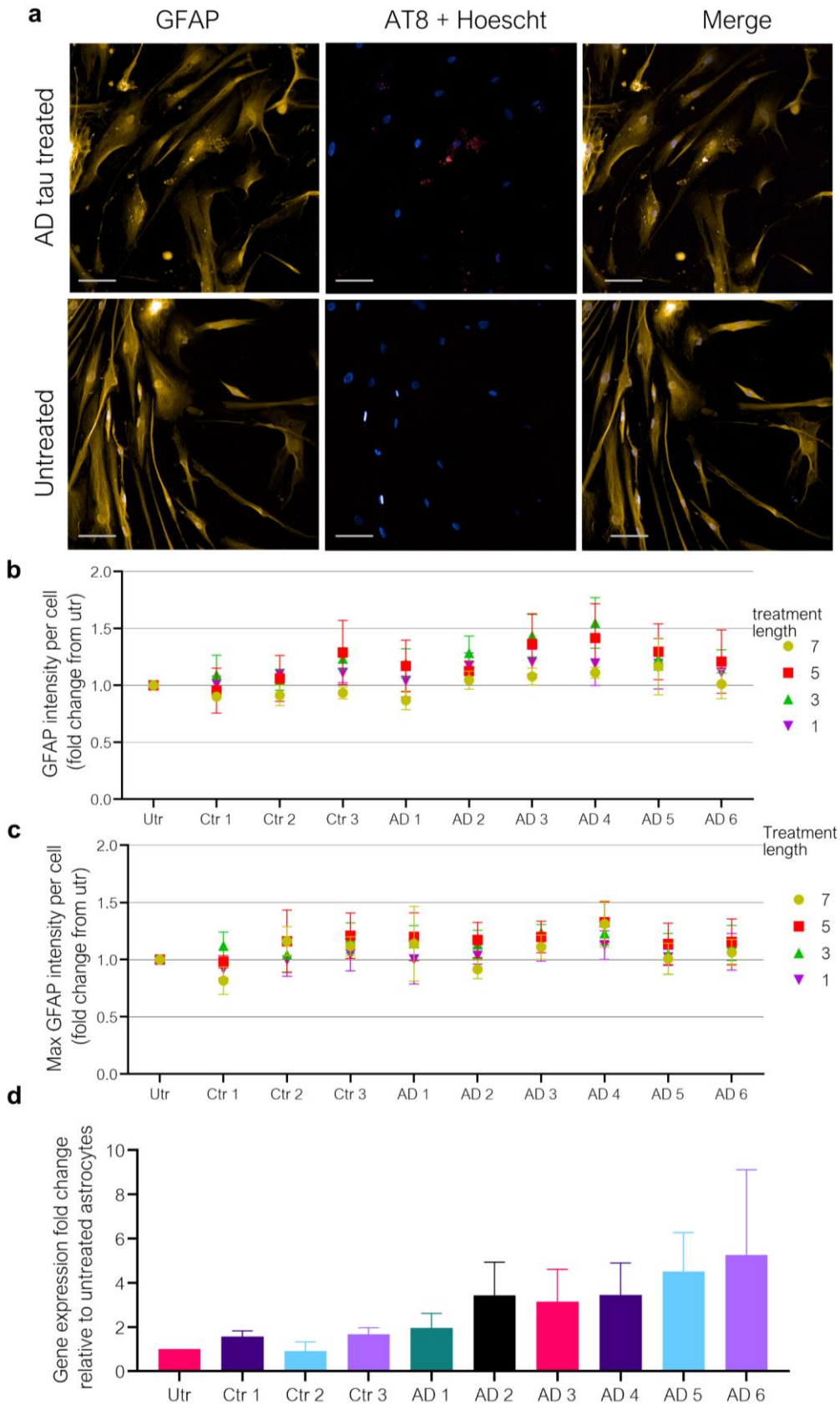
a
GFAP
AT8 + Hoescht
Merge
AD tau treated
Untreated
b
GFAP intensity per cell (fold change from utr)
2.0
1.5
1.0
0.5
0.0
Utr
Ctr 1
Ctr 2
Ctr 3
AD 1
AD 2
AD 3
AD 4
AD 5
AD 6
treatment length
7
5
3
1
c
Max GFAP intensity per cell (fold change from utr)
Treatment length
d
Gene expression fold change relative to untreated astrocytes
10
8
6
4
2
0

Figure 6.1 Global GFAP intensity does not significantly change after exposure to AD brain tau.

Representative images of day 60 iPSC-astrocytes exposed for 7 days to 0.1 ng/μL tau aggregates isolated from AD brain, control brain extracts or left untreated (a). Astrocytes were immunolabelled with antibodies against GFAP (yellow) and phospho-tau (AT8, Ser202/Thr205, red). Hoechst 33342 was used to label nuclei. Scale bar is 100uM. Images were analysed using Harmony software. Bar charts show (b) Average GFAP intensity per cell 1, 3, 5 and 7 days post-exposure. Tau exposure did not significantly alter average GFAP levels per cell. Similarly, (c) measurement of maximum GFAP intensity per cell was not significantly affected by exposure to AD brain-derived tau. (d) qPCR of day 60 astrocytes exposed to AD brain tau, control brain extracts or left untreated for 7 days showed that while global GFAP expression appeared generally increased following AD tau exposure, these changes were variable and were not significantly different from control extract-treated or untreated cells. Data shown is mean ± SEM of three-five independent astrocyte differentiation experiments each performed in duplicate (N = 3 for gene expression data, n = 5 for immunofluorescence data).

Global expression of the *GFAP* gene was also investigated in 60-day iPSC-astrocytes after 7-day exposure to 0.1 ng/uL AD derived tau aggregates or an equivalent volume of control samples, relative to untreated cells (Figure 6.1d). Expression was normalised to *GAPDH* and *βACTIN* housekeeping genes and calculated as gene expression fold change values relative to untreated astrocytes. While the mean GFAP expression for astrocytes treated with all AD tau aggregates was increased above that detected in astrocytes exposed to control brain extracts, relative to untreated, the variability of response was high, as indicated by large error bars depicting the SEM. Indeed, a one-way ANOVA of statistical analysis on the effect of AD brain tau exposure on GFAP expression revealed no significant impact ($p = 0.49$), nor were there any pairwise differences between untreated and AD tau treated or control treated samples. Moreover, the highest *GFAP* expression in AD 6 does not correlate with the highest GFAP protein expression observed in fixed astrocyte cultures, indicating that the variability of cultures as a whole do not allow any specific alterations in *GFAP* gene or protein expression to be observed when data is analysed in this way.

Next, data from the long-term tau retention assay developed in Chapter 5 was used to look at GFAP changes following removal of tau treatment. Three sets of 60-day iPSC-astrocytes were exposed to 0.1 ng/μL of human AD brain derived tau aggregates or equivalent volumes of control samples, while some astrocytes were left untreated. After 7 days, treatment was removed, and cells cultured up to either the 14-day or 21-day timepoint, after which they were fixed and immunolabelled for GFAP and AT8. Intensity values of GFAP were measured per well and graphed by case treatment (Figure 6.2). The data indicated variability in the

average GFAP intensity following exposure to AD brain tau that is not altered compared to control brain extract-exposed or untreated astrocytes. A two-way ANOVA was performed to measure the effect of timepoint and case (AD or control) on average GFAP intensity per astrocyte. The results indicated that there was not a significant interaction between the effects of timepoint case on average GFAP intensity in cells ($F(18, 90) = 0.2856$, $p = 0.998$). A simple main effects analysis showed that both case ($p = 0.976$) and treatment length ($p = 0.672$) did *not* have a significant effect on average GFAP intensity in cells. A post-hoc Holm-Šidák's test for multiple comparisons did not find any significant changes relative to day 7 timepoints.

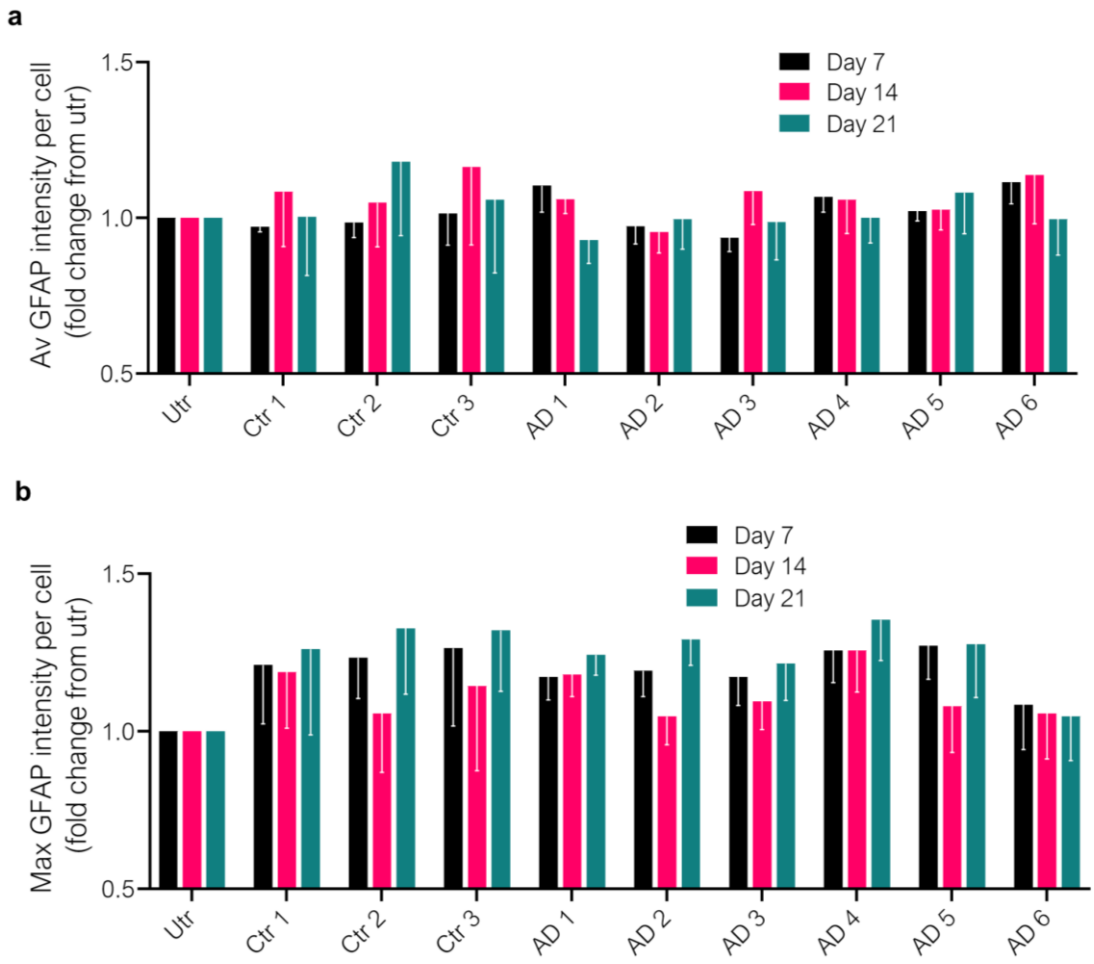

Figure 6.2 GFAP intensity in astrocytes following 7-day tau treatment.

Three sets of 60-day iPSC-astrocytes were exposed to 0.1 ng/µL of human AD brain derived tau aggregates or equivalent volumes of control samples. Some astrocytes were left untreated. After 7 days, treatment was removed, and cells cultured for further 7 or 14 days. Graph displays the (**a**) average or (**b**) the maximum intensity of GFAP labelling per cell in each well, relative to untreated cells. Results were variable and no significant changes were observed following a two-way ANOVA and post-hoc pairwise comparisons performed by Holm-Šidák's' multiple comparisons test relative to day 7 in each treatment condition. Data is mean ± SEM. N=4 (independent differentiations), each of which was performed in duplicate.

Similar findings were observed when maximum GFAP intensity was measured (Figure 6.2b), although interestingly this data suggested that GFAP might be elevated in response to both control brain extracts and AD tau, again suggesting that some factor from aged brain may induce changes in GFAP levels. Statistical analysis as above using a two-way ANOVA to measure the effect of timepoint and case (AD or control) on maximum GFAP intensity per astrocyte. The results indicated that there was not a significant interaction between the effects of timepoint case on average GFAP intensity in cells ($F(18, 90) = 0.1363$, $p>0.999$).

A simple main effects analysis showed that both case ($p = 0.4259$) and treatment length ($p = 0.1707$) did *not* have a significant effect on average GFAP intensity in cells. A post-hoc Holm-Šidák's test for multiple comparisons did not find any significant changes relative to day 7 timepoints.

Overall, these data show no global changes in GFAP intensity following tau exposure. However, these data did not take into account the presence of tau aggregates. This prompted a more specific investigation into changes in astrocytes following exposure to tau. Specifically, how differential uptake of tau may alter GFAP expression, a result that may be masked when analysing global changes in astrocyte cultures.

Observations from imaging astrocyte cultures after immunostaining with a GFAP antibody suggested that not all astrocytes internalise tau aggregates, and those that do show variation in the extent of internalisation (Figure 6.3a). Therefore, in additional analysis, astrocytes were grouped according to their relative AT8 intensity as a marker of the extent of tau internalisation. The 7-day treatment timepoint was chosen for this analysis since this was the timescale observed as allowing high levels of tau internalisation in Chapter 5. A linear classification system was used to train the imaging software to categorise each astrocyte as 'high-AT8' or 'low-AT8' based on previously calculated parameters of average/maximum AT8 intensity and detection of aggregates (spot detection based on AT8 immunostaining) (Methods 2.5.4.2). The two groups could then be compared within each treatment condition to determine whether tau uptake has a direct impact on GFAP expression.

The results indicate that both average and maximum GFAP levels are higher in high-AT8 astrocytes compared to low-AT8 astrocytes (Figure 6.3). The disparity between the two is larger for maximum AT8 intensity, indicating there are small areas of high-AT8 intensity within astrocytes that have internalised tau aggregates.

A two-way ANOVA was performed to measure the effect of AT8 level (high v low) and case (AD or control) on average GFAP intensity per astrocyte (Figure 6.3b). The results indicated that there was not a significant interaction between the effects of AT8 level and case on average GFAP intensity in cells ($F(5, 36) = 1.063$, $p = 0.3970$). A simple main effects analysis showed that AD case had a significant effect on average GFAP intensity ($p = 0.045$), showing that each AD case may differentially affect average GFAP intensity, as was previously indicated by data in Figure 6.1b. The same analysis also showed that cell AT8 level

significantly impacted average GFAP intensity in cells ($p = 0.048$). However, post-hoc Holm-Šidák's test for multiple comparisons did not find any significant pairwise differences between high and low AT8 cells for each AD case.

A further two-way ANOVA was performed on the data in (Figure 6.3b), to measure the effect of AT8 level (high v low) and case (AD or control) on maximum GFAP intensity per astrocyte (Figure 6.3c). The results indicated that there was not a significant interaction between the effects of AT8 level and case on average GFAP intensity in cells ($F(5, 48) = 0.2799$, $p = 0.922$). A simple main effects analysis showed that AD case had no significant effect on maximum GFAP intensity ($p = 0.651$), showing that it is common to exposure of astrocytes to tau extracts from all AD cases, while AT8 level did have a significant effect on maximum GFAP intensity in cells ($p < 0.0001$). A post-hoc Holm-Šidák's test for multiple comparisons found a significant pairwise differences between high and low AT8 cells for AD 6 treated cells only.

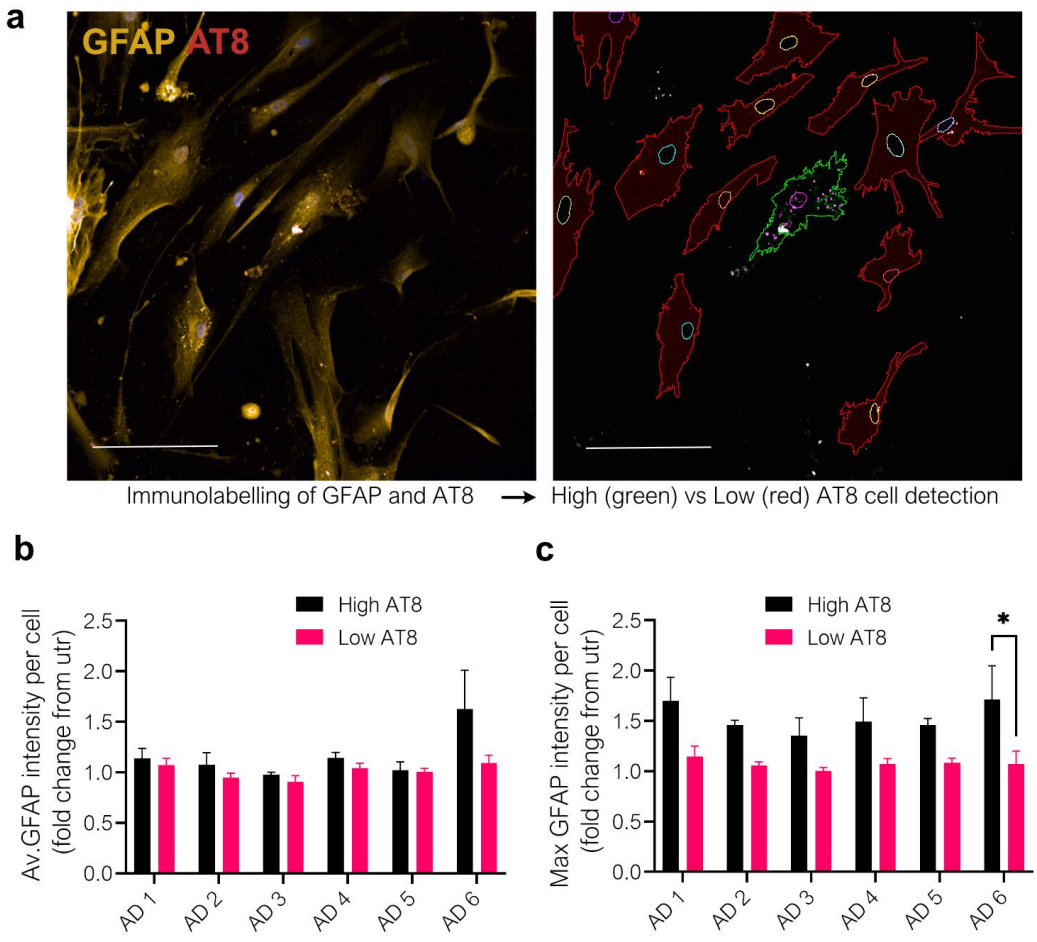

Figure 6.3 Maximum GFAP intensity is significantly increased in astrocytes with high AT8 internalisation.

Representative image of astrocytes immunolabelled (GFAP – yellow) and grouped as 'high' or 'low' AT8 depending on AT8 intensity and spot detection inside astrocytes. Red outline = low AT8, green outline = high AT8. Scale bar =100 µm. The average GFAP intensity was significantly altered by AD, but there was no difference in high vs low AT8 cells (b), however, there is a significant difference in maximum GFAP between these two groups, however there was no significant impact of AD case on maximum GFAP levels. Data is mean ± SEM. N=5 (independent differentiations), each of which was performed in duplicate.

These results suggest that the uptake of AT8 positive aggregates causes the accumulation of dense localised areas of GFAP expression that is not present in astrocytes that have not internalised similar levels of AT8 positive tau aggregates. Closer observations of immunostaining after Z-stack analysis suggest that high GFAP levels may localise in astrocytes at focal spots of tau aggregate internalisation. To quantify this, AT8 positive spots (Figure 6.4a) were analysed to detect the intensity of co-occuring GFAP and these data were compared to the average of the same measurements for all cells in that treatment condition,

relative to untreated astrocytes at each timepoint (Figure 6.4b). The results show that GFAP expression associated with AT8 spots is significantly higher than that the average GFAP value for all astrocytes exposed to AD case derived tau. In these AD treated astrocytes, GFAP intensity at points of tau aggregate internalisation was between 3.2 ± 0.71 (AD 6) and 4.19 ± 1.19 (AD 2) fold higher relative to untreated astrocytes, while the average values for all AD treated astrocytes were no higher than 1.11 ± 0.12 (AD 6) fold higher than untreated astrocytes.

A two-way ANOVA was performed to measure the effect of cell region (spot vs whole cell) and case (AD or control) on average GFAP (Figure 6.4b). The results indicated that there was not a significant interaction between the effects of AT8 level and case on average GFAP intensity in cells ($F(5, 48) = 0.1508$, $p = 0.979$). A simple main effects analysis showed that AD case had no significant effect on average GFAP intensity ($p = 0.9899$), showing that uptake of tau from each AD case has a similar effect on GFAP changes near internalised aggregates. A simple main effects analysis showed that measured cell region significantly altered average GFAP intensity ($p < 0.0001$), indicating alterations in GFAP expression are localised around internalised tau, as indicated by observations of immunolabelling. Indeed, post-hoc Holm-Šidák's test for multiple comparisons found a significant pairwise difference in GFAP intensity between these cell regions for all AD case treatments.

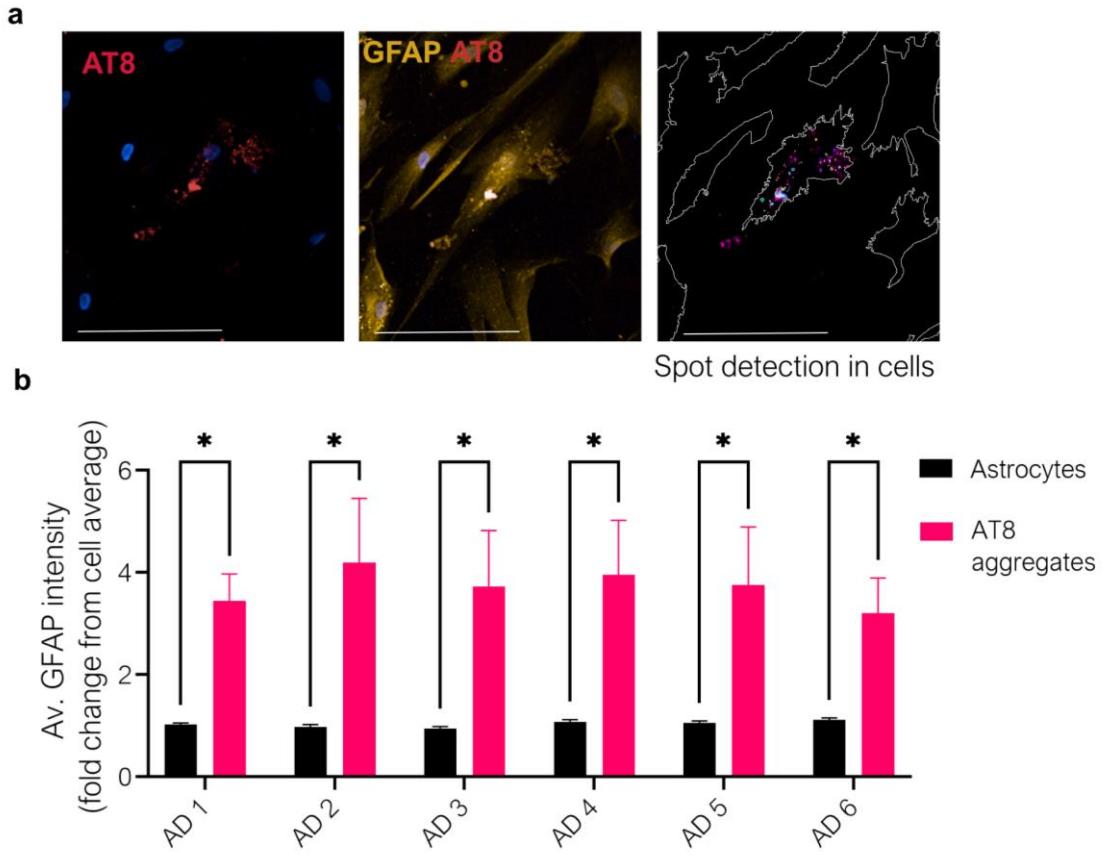

Figure 6.4 GFAP intensity is higher around internalised tau aggregates

Day-60 iPSC-Astrocytes treated for 7 days with AD-derived tau aggregates were analysed for GFAP intensity in whole cells compared to near internalised aggregates. **(a)** shows representative image of astrocytes immunolabelled (GFAP – yellow) and AT8 positive (red) spot detection inside astrocytes, white outline indicates cells and coloured outline of detected internalised AT8 spots. Scale bar =100 µm. Graph **(b)** shows the average GFAP intensity was not significantly altered by AD, but there was a difference in GFAP intensity at AT8 spots vs cells as a whole, and pairwise difference between these regions in each AD case treatment. Data is mean ± SEM. N=5 (independent differentiations), each of which was performed in duplicate.

These parameters were also investigated 7 or 14 days after the removal of a 7-day exposure to tau in day-60 astrocyte, as described previously in this chapter for Figure 6.2. The results here demonstrate that, with time, the intensity of GFAP at sites of dense tau aggregates decreases. Figure 6.5 shows that while GFAP intensity across whole astrocytes remains fairly consistent with time, GFAP intensity at the sites of AT8 aggregates is always increased relative to average GFAP intensity across the cell, peaking at the 7-day time point, and decreasing following the removal of tau for 7 (14 day time point) or 14 days (21 day

timepoint). This was a consistent finding regardless of the AD case from which the tau aggregates were obtained, although there was some variability between treatments.

A two-way ANOVA was performed on this data to measure the effect of timepoint and case on average GFAP intensity at detected AT8 positive tau aggregates within astrocytes. The results indicated that there was not a significant interaction between the effects of timepoint and AD case on average GFAP intensity at internalised tau aggregates ($F(10, 60) = 0.365$, $p = 0.957$). A simple main effects analysis showed that differing AD cases had no significant effect on average GFAP intensity at aggregates ($F(5, 60) = 0.571$, $p = 0.722$), showing tau aggregates derived from each AD case has a similar effect on localised GFAP intensity once internalised. A main effects analysis did show that timepoint had a significant impact on average GFAP intensity at internalised aggregates ($F(2, 60) = 6.622$, $p = 0.0025$), indicating that the increases in GFAP intensity at aggregates observed after tau uptake here, and described in Figure 6.4, does not remain consistent after tau treatment is removed. Indeed, a post-hoc Holm-Šidák's test for multiple comparisons found significant decreases in GFAP intensity at internalised aggregates with time after treatment for cells treated with tau from AD 2, AD 3 and AD 5. This suggests there may be some variation in how long internalised tau aggregates are able to induce GFAP changes, which may relate to features of the AD tau aggregates themselves.

These results further indicate that levels of GFAP around dense focal tau aggregates is somewhat transient. In some cases, such as when astrocytes were exposed to tau from AD cases 2 and 3, the decrease following tau removal at day 7 appeared to be dramatic and rapid. For others, a slower reduction in GFAP intensity in association with tau aggregates, was step-wise through subsequent timepoints. This indicates that astrocytes appear to respond differently to tau derived from different cases, perhaps due to some molecular characteristic of the tau aggregates. This might, for example, include differences in tau phosphorylation or seeding ability, characteristics related to AD progression (Dujardin et al., 2020).

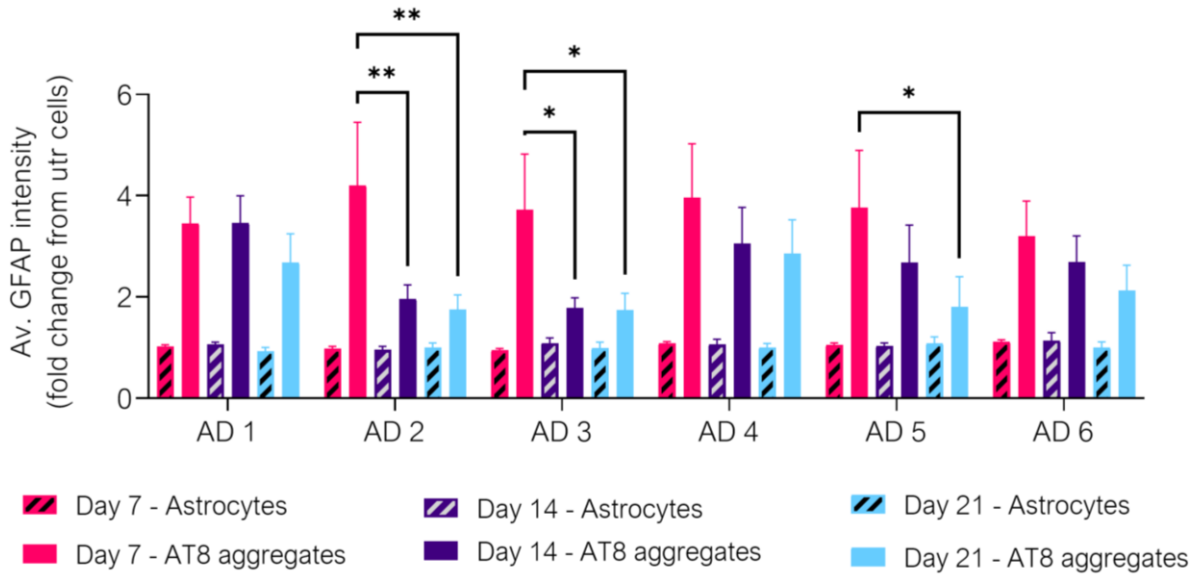

Figure 6.5 GFAP intensity around tau aggregates decreases after removal of tau from media.

Day-60 iPSC-astrocytes were treated for 7 days with AD case derived tau, equivalent control sample or left untreated. Treatment was removed and cells were fixed at day 14 or 21. Cells were detected by GFAP immunolabelling and tau aggregates by high intensity AT8 spot detection. (a) Graph shows the quantification of average GFAP intensity in AD treated astrocytes in regions of dense tau aggregates against GFAP intensity across the whole astrocyte, shown as fold change from untreated astrocytes. Average GFAP intensity at regions of dense tau aggregates is higher relative to the cell average, peaks at 7 days and decreases after tau removal for 7 days (14 day time point) and 14 days (21 day timepoint). A two-way ANOVA was performed confirming a statistical significance of timepoint on GFAP intensity, and posthoc pairwise comparison using Holm Šidák's test showed GFAP decrease at AT8 spot regions was significant in some AD cases. * $p < 0.05$. Error bars are ± SEM of n = 4 (7 day) or 3 (14,21 days) independent differentiations, performed in duplicate.

6.2.2 Changes in S100B expression after tau uptake

S100B is a calcium binding protein that is highly expressed in astrocytes (Raponi et al., 2007), although it is not exclusively astrocytic and not all astrocytes express S100B (Donato et al., 2009). S100B was recently shown to strongly localise with tau proteins in neuroblastoma cells, an interaction that was enhanced by addition of calcium, and that could protect against tau aggregation and seeding in a heparin fibrillation assay *in vitro* (Moreira et al., 2021). The iPSC-derived astrocytes used here express S100B (Figure 4.3), therefore it was of interest to examine the expression and interaction of S100B with internalised tau aggregates in iPSC-astrocytes. In addition, S100B together with GFAP were examined in paraffin-embedded sections from the postmortem AD brain tissues used to extract tau for this work.

Immunohistochemistry was performed using antibodies against AT8, GFAP and S100B on sections of temporal cortex from AD cases 1-6 (Figure 6.6) and control human tissue (Figure 6.7). In areas where AT8 immunoreactivity was apparent, there were commonly GFAP positive astrocytes that also show significant levels of S100B labelling (marked by closed arrowhead). Not all GFAP positive astrocytes near AT8 structures expressed S100B at high levels (examples marked by open arrowhead), and this did not appear related to the levels of GFAP expression in these cells. For example, in AD 3 tissue sections, only 2 of the 3 astrocytes surrounding the AT8 positive tau structures in the highlighted area of the image appear to express high levels of S100B. In AD postmortem tissue, S100B had been seen to be elevated primarily in the hippocampus and temporal lobe, and this was localised primarily in astrocytes that surround neuritic plaques (van Eldik and Griffin, 1994; Sheng et al., 1994). This upregulation suggests that S100B can be transiently upregulated in astrocytes in disease environments, but the specific mechanism and dynamics of S100B upregulation in astrocytes of AD has not been thoroughly investigated.

While the majority of S10OB positive cells observed in control brain also express GFAP, some (examples marked with pink asterisk), express little to no GFAP. This may be an astrocyte with very little detectable GFAP, but maybe other glial cells, since S100B is also expressed in myelinating oligodendrocytes in mouse brain (Du et al 2021).

Brain slices from healthy control human tissue were also examined, showing some high intensity S100B and GFAP positive astrocytes, as well as GFAP positive astrocytes with

relatively little S100B expression. This suggests that there are subsets of astrocytes with higher S100B, or that S100B expression in astrocytes is transient and reactive to the environment. No observable tau aggregates were observed in these control sections examined, and while astrocytes with differing levels of high S100B were also observed, this indicates that the variation in S100B expression in astrocytes seen in AD brain is not necessarily induced by the presence tau aggregates or other pathological features of AD.

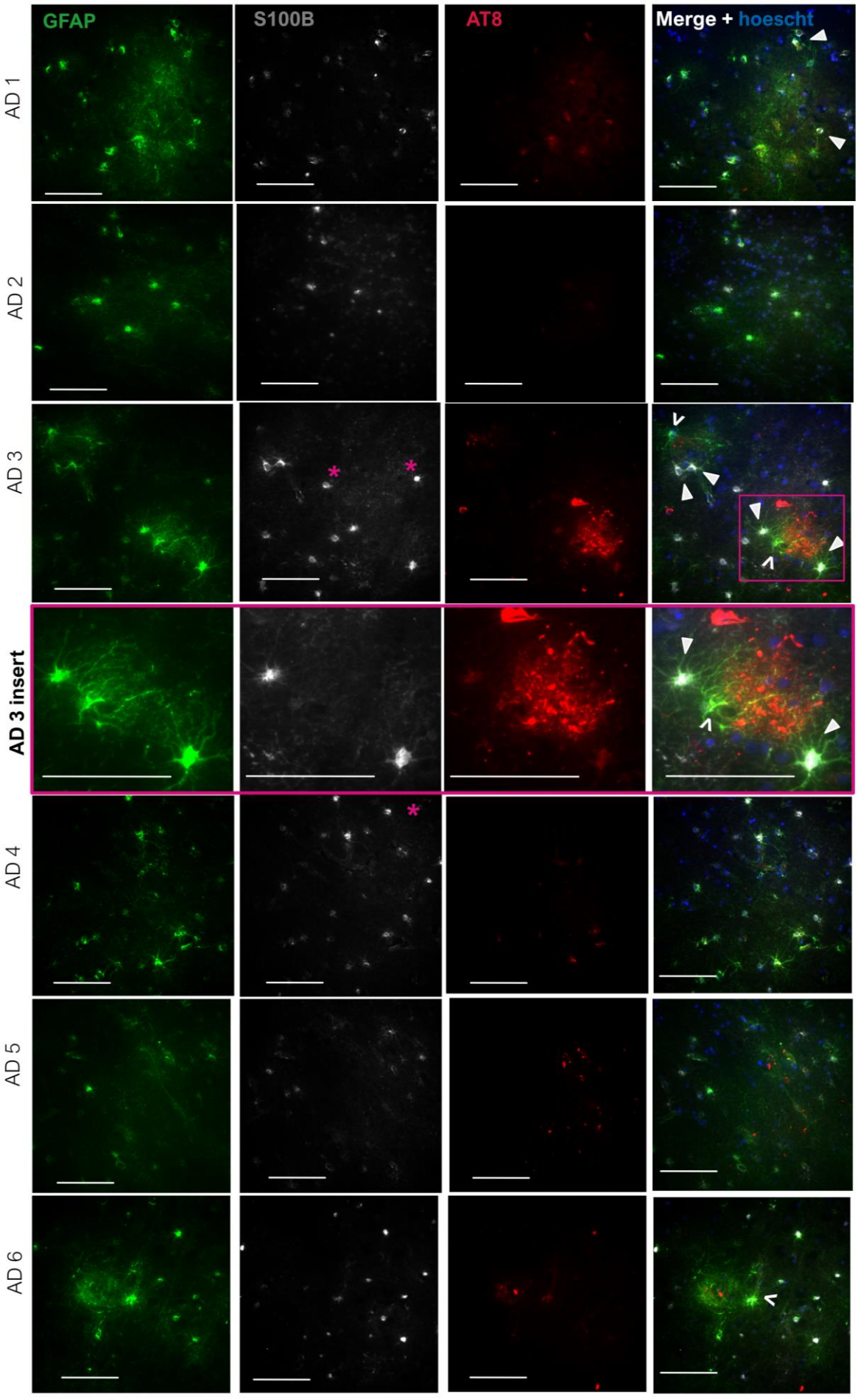
GFAP
S100B
AT8
Merge + hoescht
AD 1
AD 2
AD 3
AD 3 insert
AD 4
AD 5
AD 6

Figure 6.6 AD post-mortem tissue shows S100B and GFAP expression in astrocytes proximal to AT8 positive aggregates.

Representative brain sections from the temporal cortex of AD post-mortem tissue were immunolabelled with antibodies against GFAP (green), S100B (white) and tau phosphorylated at Ser202/Thr205 (AT8, red). Hoechst 33342 was used to stain nuclei (blue). Astrocytes in the vicinity of tau deposits were generally positive for both astrocytes markers (white filled arrowhead), though this was variable and high GFAP astrocytes with low or no S100B expression were also visible near aggregates (white open arrow heads). High intensity S100B+ve cells with no GFAP expression were also present that may be oligodendrocytes (pink asterisk). White bar scale = 100 µm.

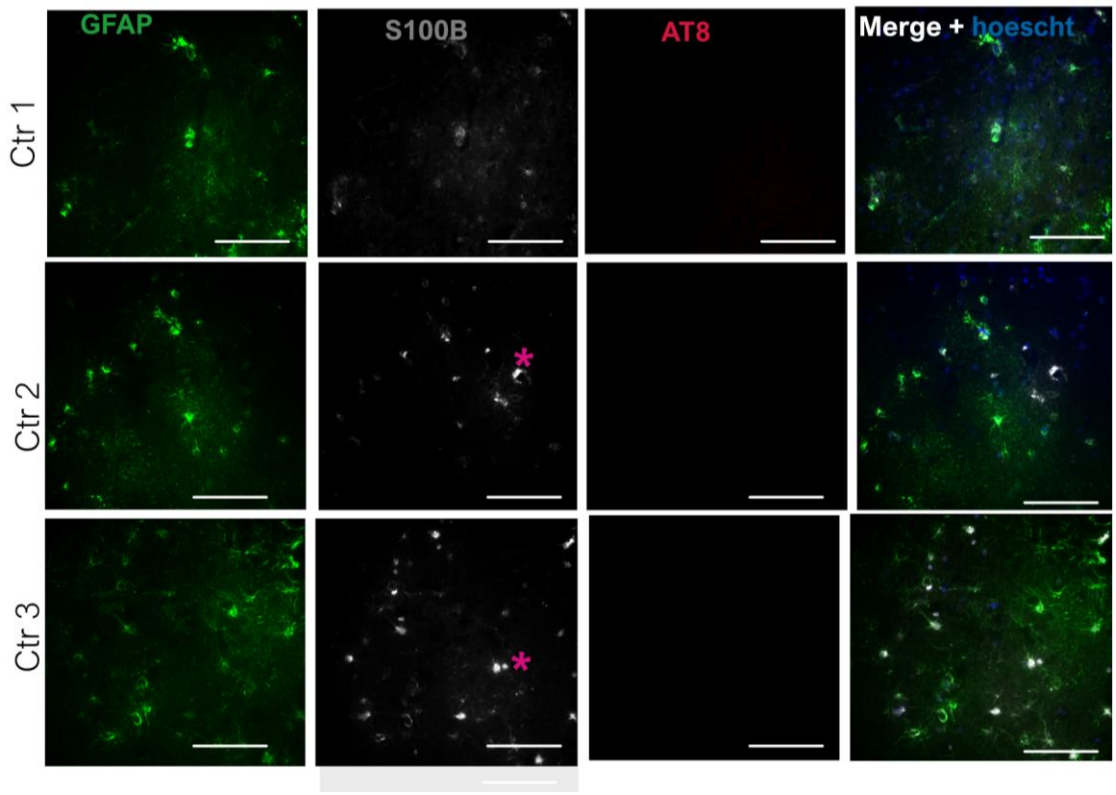

Figure 6.7 Control post-mortem tissue shows some S100B expression in GFAP+ve astrocytes.

Representative brain sections from the temporal cortex of control post-mortem tissue were immunolabelled with antibodies against GFAP (green), S100B (white) and tau phosphorylated at Ser202/Thr205 (AT8, red). Hoechst 33342 was used to stain nuclei (blue). No AT8 aggregates were detected. S100B and GFAP co-localised in several, but not all astrocytes. Some high intensity S100B+ve cells with no GFAP expression were also present that may be oligodendrocytes (pink asterisk). White bar scale = 100 µm.

Next, global changes in S100B expression in iPSC derived astrocytes was examined after 7-day exposure to 0.1 ng/µL of tau aggregates from AD cases 1-6 or control brain extracts

relative to untreated cells (Figure 6.8). The 7-day treatment was chosen for examination as it represents the timepoint at which the highest amount of tau uptake was observed in the previous chapter. Cells were immunolabelled with antibodies against GFAP, S100B and AT8, and imaged using an Opera Phenix high throughput imaging system (Perkin Elmer, MA, USA). Observations of S100B immunolabelling (Figure 6.8a) revealed that cells express S100B in a non-uniform way throughout their cell bodies as shown previously by others (Raponi et al., 2007; Hagmeyer et al., 2019). Therefore, GFAP immunoreactivity was used to select astrocytes as before, and the average S100B expression in these cells was examined. Figure 6.8b and c show that exposure of astrocytes to tau aggregates from AD cases does not increase astrocytic S100B expression, as both average and maximum S100B levels appeared unchanged relative to control brain extract-exposed and untreated cells. While cells exposed to tau from AD cases 3 and 4 have, on average, higher amounts of S100B, this was not a significant increase compared to control or untreated astrocytes when analysed by a one-way ANOVA. Indeed, the statistical analysis of this data indicated that case treatment did not to have a significant impact on average ($p = 0.788$) or maximum ($p = 0.474$) S100B intensity, with a post hoc Holm-Šidák's multiple comparison test showing no pairwise differences relative to control or untreated astrocytes.

The expression of *S100B* mRNA was also examined by qPCR (Figure 6.8c). Expression was normalised to *GAPDH* and *βACTIN* housekeeping genes and calculated as gene expression fold change values relative to untreated astrocytes. The data showed no significant changes in cells exposed to aged control human brain extracts relative to untreated cells. Cells exposed to tau aggregates extracted from four of the six AD cases (1, 3, 5 and 6) showed an increase in *S100B* gene expression, while cells exposed to tau from AD cases 2 and 4 showed a decrease in expression relative to control and untreated conditions. A one-way ANOVA performed on this gene expression data revealed there was a significant impact of treatment on S100B gene expression ($p = 0.040$), however the posthoc Holm-Šidák's test for multiple comparisons did not reveal any pairwise differences when S100B expression in AD treated astrocytes was compared to untreated or control treated astrocytes. While the gene expression changes are not reflected in S100B protein expression indicated by immunolabelling (Figure 6.8b, c), it may be that S100B can be sequestered by tau aggregates as is indicated by previous studies (Moreira et al., 2021), which would not necessarily correlate with changes in S100B mRNA levels.

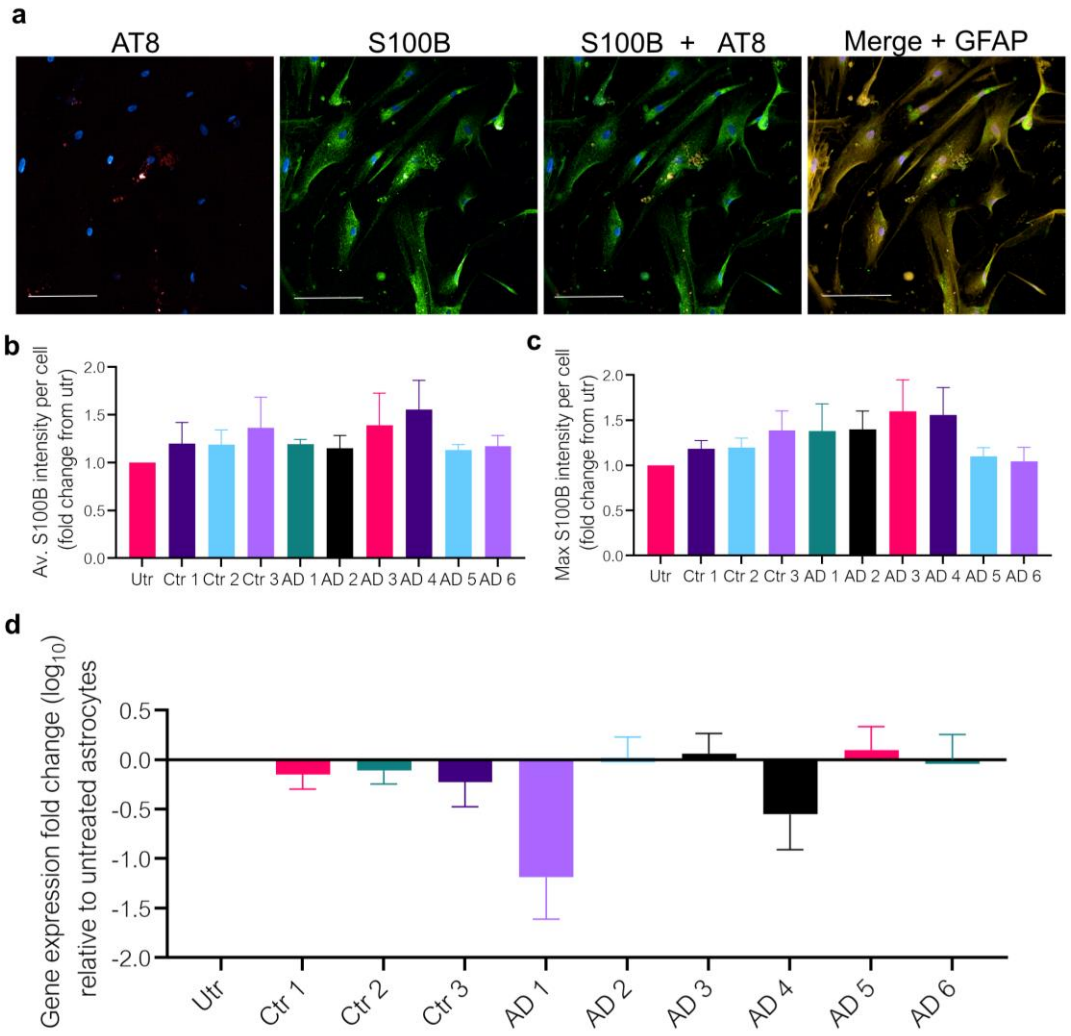

Figure 6.8 Global S100B intensity does not significantly change after exposure of iPSC-astrocytes to tau aggregates from postmortem AD brain.

Representative images of day 60 iPSC-astrocytes exposed for7 days to 0.1 ng/µL tau aggregates isolated from AD brain, control brain extracts or left untreated (**a**). Astrocytes were immunolabelled with antibodies against S100B (green), GFAP (yellow) and phospho-tau (AT8, Ser202/Thr205, red). Hoechst was used to label nuclei. Scale bar = 100 µm. Images were analysed using Harmony software. Bar charts show (**b**) average and (**c**) maximum S100B intensity is increased after treatment but not significantly altered after AD tau treatment compared to untreated or equivalent control treatment. RT-qPCR revealed global S100B gene expression is inconsistent in AD cases compared to control or untreated and S100B expression is significantly altered by case treatment (**d**). Data analysed by a one-way ANOVA with Holm-Šidák's posthoc test for multiple comparisons to control and untreated. Error bars are ± SEM of n = 3 (d) or n = 4 (b/c) independent astrocyte differentiations performed in duplicate.

Changes to S100B expression were examined 7 and 14 days after initial 7-day tau exposure at 14 and 21 day timepoints, as described above for GFAP (Section 6.2.1). At the 7-day timepoint, the data was similar to that presented in Figure 6.8 in that astrocytes exposed to

control brain or AD brain tau extracts showed some elevations in S100B relative to untreated cells. For average S100B intensity (Figure 6.9a), astrocytes treated with control brain showed a small increase in S100B expression for Ctr1 and Ctr 2 at the 14-day timepoint, while expression remained stable in Ctr 3. After a further 7 days at the 21-day timepoint, this expression appeared to decrease slightly or remain stable in control treated astrocytes.

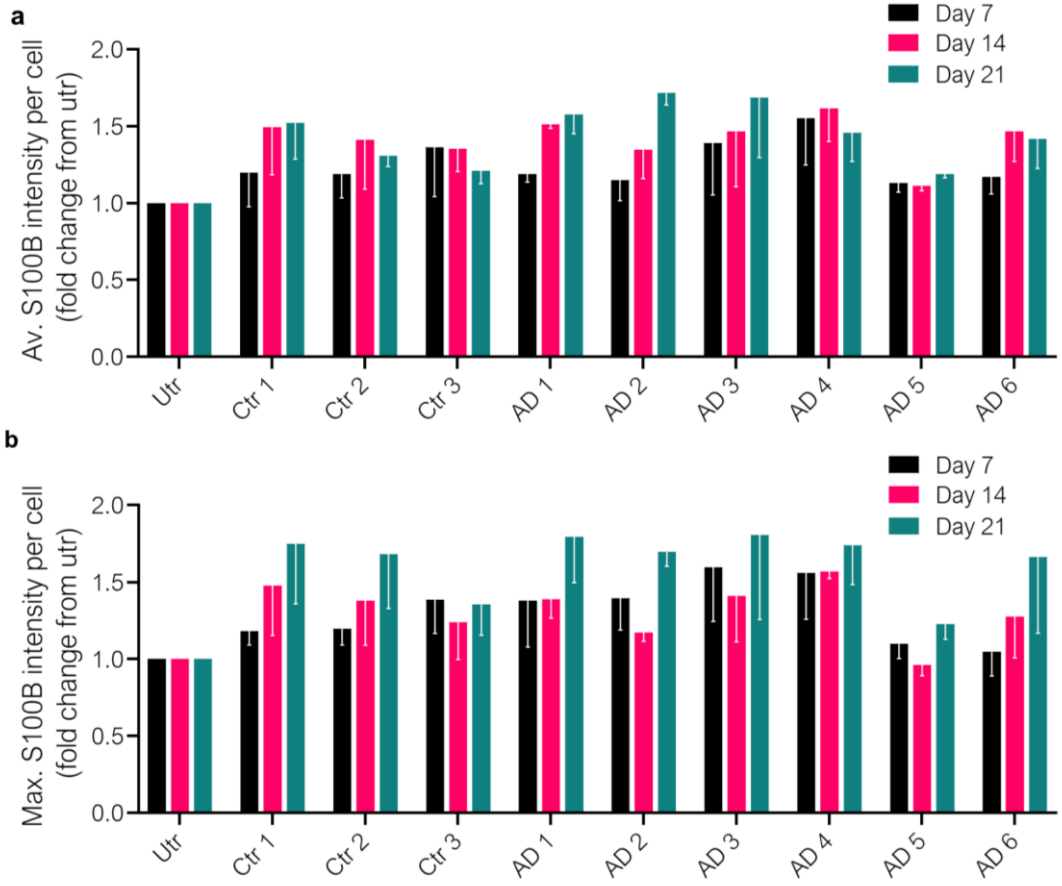

Figure 6.9 S100B expression changes with time after tau treatment.

Three sets of 60-day iPSC-astrocytes were exposed to 0.1 ng/µL of human AD brain derived tau aggregates or equivalent volumes of control samples. Some astrocytes were left untreated. After 7 days, treatment was removed, and cells cultured for further 7 or 14 days. Graph displays the average (**a**) or the maximum (**b**) intensity of S100B labelling per cell in each well, relative to untreated cells. Results indicated that time had a significant impact on maximum S100B intensities, and this appeared variable depending on case treatments. Statistical analysis performed by a two-way ANOVA and post-hoc pairwise comparisons by Holm-Šidák's' multiple comparisons test relative to day 7 in each treatment condition revealed. Data is mean ± SEM. N = 3 (independent differentiations), each of which was performed in duplicate.

For astrocytes exposed to tau from AD brain, two patterns emerged with time. A step-wise increase in average S100B expression in cells was observed in cells treated with AD 1, 2

and 3, with expression peaking at day 21, whereas in cells treated with AD 4 and 6, expression peaked at day 14 and then decreased. S100B expression in AD 5 treated cells remained fairly stable throughout timepoints analysed, showing the least increase relative to untreated or control astrocytes. To analyse significance in these changes, a two-way ANOVA was performed to measure the effect of timepoint and case (AD or control) on average S100B intensity per astrocyte. The results indicated that there was not a significant interaction between the effects of timepoint and case on average S100B intensity in cells ($F(18, 70) = 0.397$, $p = 0.984$). A simple main effects analysis showed that both case ($p = 0.1122$) and timepoint ($p = 0.064$) did not have a significant effect on average S100B intensity in cells. A post-hoc Holm-Šidák's test for multiple comparisons did not find any significant pairwise changes relative to day 7 timepoints.

For maximum S100B (Figure 6.9b), however, intensity appeared to peak at day 21 in all case treated astrocytes, with the exception of Ctr 3. In most cases, the highest level of S100B expression was found at day 21, 14 days following the removal of tau aggregates. However, for cells exposed to tau from AD cases 4 and 6, S100B expression was elevated at 14 days relative to 7 days, and then reduced slightly between 14 days and 21 days. This appeared to increase in a different pattern to average S100B intensity, where all AD treated cases except for AD 6 decreased or remained constant in their S100B expression at day 14 relative to day 7. A two-way ANOVA was performed as above to measure the effect of timepoint and case treatment on maximum S100B intensity per astrocyte. The results indicated that there was not a significant interaction between the effects of timepoint and case on average S100B intensity in cells ($F(18, 70) = 0.3062$, $p = 0.997$). A simple main effects analysis showed that timepoint did have a significant impact on maximum S100B intensity ($p = 0.018$). A simple main effects analysis to look at the effect of case treatment showed that while this did not significantly affect maximum S100B intensity, it was approaching significance ($p = 0.0521$). A post-hoc Holm-Šidák's test for multiple comparisons did not find any significant pairwise changes relative to day 7 timepoints.

Taken together, these results indicate that there are dynamic changes in S100B intensity over time. As changes were also observed in control brain treated astrocytes, it is not clear these are linked to the presence of tau aggregates. However, patterns of changes in S100B did appear to vary between control and AD treated cases, suggesting that there may be

some differences not picked up in this analysis of global S100B expression changes within cultures.

To investigate this further, astrocytes were grouped into high-AT8 and low-AT8 groups, depending on their burden of internalised tau aggregates (as described in Section 6.2.1). S100B intensity was analysed in both groups in cells that were exposed to human tau for 7 days (Figure 6.µ). The results show that average S100B intensity was higher in high-AT8 astrocytes compared to low-AT8 astrocytes, relative to untreated cells. A two-way ANOVA was performed on the data in (Figure 6.µa), to measure the effect of AT8 level (high v low) and AD case on average S100B intensity per astrocyte. The results indicated that there was not a significant interaction between the effects of AT8 level and case on average S100B intensity in cells ($F(5, 36) = 0.211$, $p = 0.956$)., A simple main effects analysis showed that AT8 level did have a significant effect on average S100B intensity in cells ($p = 0.044$). AD case had no significant effect on average S100B intensity ($p = 0.4196$), showing that it is common to exposure of astrocytes to tau extracts from all AD cases. A post-hoc Holm-Šidák's test for multiple comparisons found no significant pairwise differences between high and low AT8 cells for any AD case treatment, however.

The maximum S100B levels (Figure 6.µb) indicated a larger difference between high AT8 and low AT8 cells. In the same way a two-way ANOVA was performed on this data to measure the effect of AT8 level (high v low) and AD case on maximum S100B intensity per astrocyte. The results indicated that there was not a significant interaction between the effects of AT8 level and case on maximum S100B intensity in cells ($F(5, 36) = 0.4740$, $p = 0.793$). A simple main effects analysis showed that AT8 level did have a significant effect on average S100B intensity in cells ($p = 0.00005$) which was more significant than for average S100B, indicating there are areas of high intensity within astrocytes that have internalised AD tau. AD case had no significant effect on maximum S100B intensity ($p = 0.4196$), showing that it is common to exposure of astrocytes to tau extracts from all AD cases. A post-hoc Holm-Šidák's test for multiple comparisons found no significant pairwise differences between high and low AT8 cells for any AD case treatment, however.

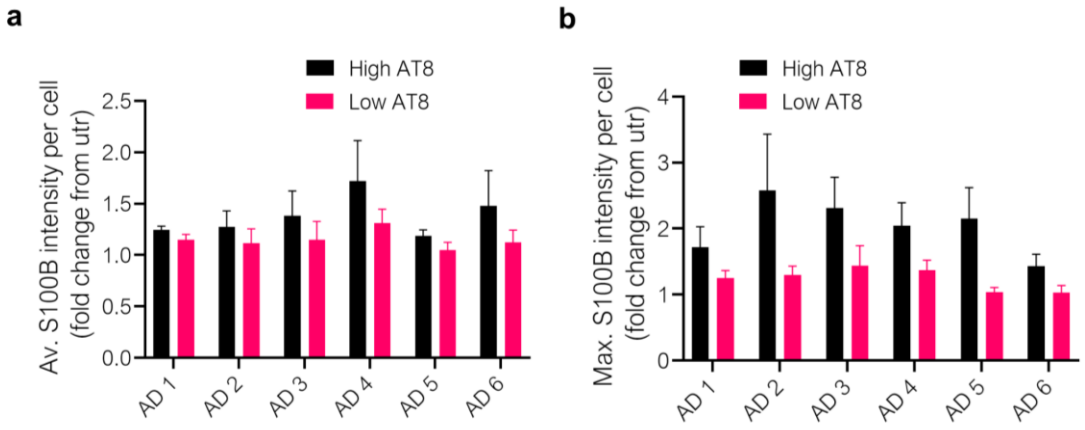

Figure 6.μ Maximum S100B intensity is significantly increased in astrocytes with high AT8 internalisation.

Following 7-day tau treatment, cells were grouped into 'low' and 'high' AT8 astrocytes depending on the amount of internalised tau, as described previously. Graphs show both the average (**a**) and maximum (**b**) S100B intensity is increased in high AT8 cells compared to low AT8 cells, relative to untreated cells. A two-way ANOVA was performed confirming significant effect of AT8 internalisation on S100B expression, although a post hoc pairwise comparison using Holm-Šidák's multiple comparisons test showed no pairwise significant differences. Error bars are mean ± SEM of n = 4 independent differentiations (performed in duplicate).

These results indicate that tau internalisation is having an impact on S100B levels specifically in cells that have internalised and accumulated AT8 positive tau, similar to previous findings with GFAP. Interestingly, immunolabelling of astrocytes treated with tau extracted from AD brain revealed high levels of S100B that localise around AT8 positive aggregates (Figure 6.10a) that was confirmed by performing a 3D Z-stack analysis of this data.

To further investigate and quantify these data, S100B fluorescence intensity was measured at sites of dense AT8 labelling, detected as described above for GFAP. S100B intensity was measured at AT8 positive spots inside astrocytes and compared to the S100B intensity of whole cells, relative to untreated astrocytes. The results demonstrate that S100B intensity is highest in association with AT8-positive aggregates when compared to average S100B levels across the whole cell (Figure 6.10b). The fold change in S100B intensity near internalise aggregates relative to untreated cells ranged from 6.81 ± 1.79 (AD case 3) to 3.45 ± 0.21 (AD 1) relative untreated cells. Whereas the average fold change in S100B intensity of whole cells after astrocytes were exposed to tau was no more than 1.45 ± 0.22 (AD 4) relative to untreated cells. This indicates that, as with GFAP, S100B can localise to internalised tau aggregates at high density. A two-way ANOVA was performed to measure

the effect of cell region (spot vs whole cells) and AD case treatment on average S100B intensity. The results indicated no interaction between these two independent variables on S100B intensity ($F(5, 36) = 1.87$, $p = 0.1244$). A simple main effects analysis indicated that cell region did have a significant effect on S100B intensity ($p<0.0001$), but that AD case did not ($p = 0.061$). Although the latter was approaching significance, and the extent of S100B did appear to vary between AD cases, it still appeared that S100B accumulates and is sequestered by AT8 positive aggregates regardless of which case the tau was derived from.

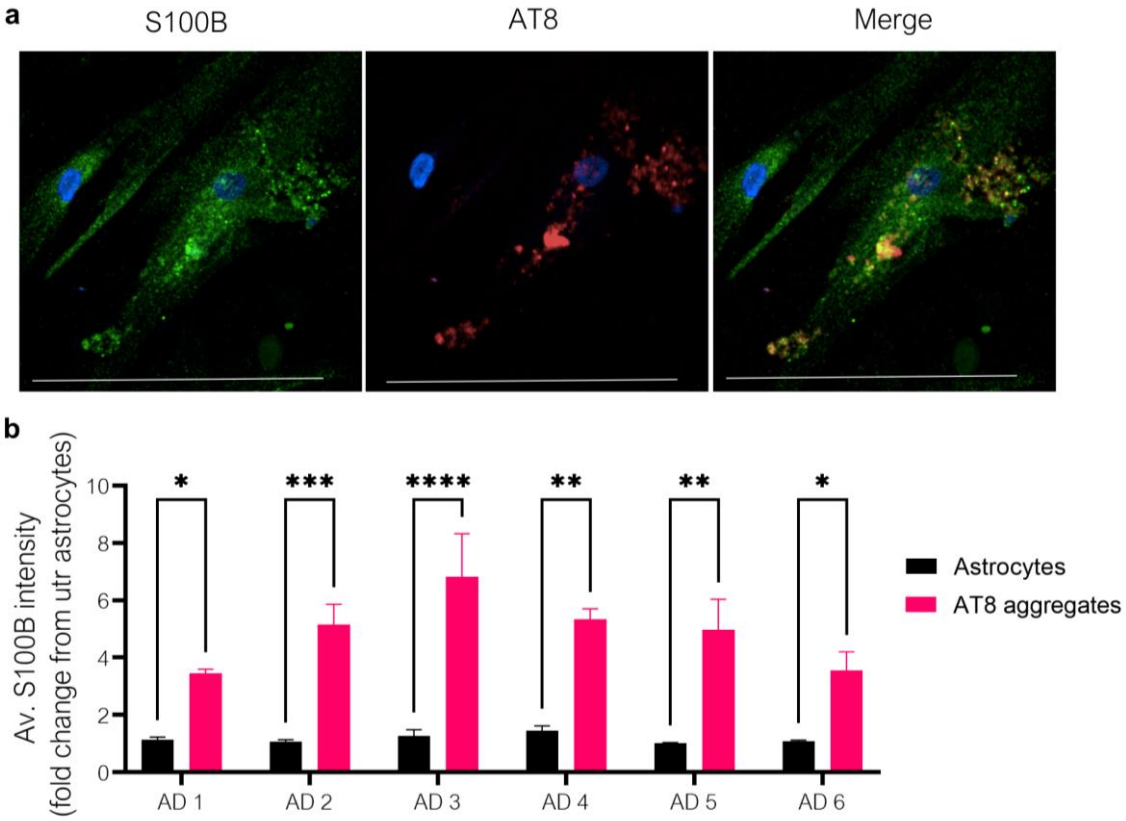

Figure 6.10 S100B intensity is elevated proximal to tau aggregates in iPSC-astrocytes exposed to AD brain derived tau.

Day-60 iPSC-Astrocytes treated for 7 days with AD-derived tau aggregates were analysed for GFAP intensity in whole cells compared to near internalised aggregates. (**a**) shows representative image of astrocytes immunolabelled (S100B – green) and high p-tau at ser202/thr205 (AT8 – red) spot regions which are detected by Harmony software and analysed for S100B intensity. Scale bar =100 µm. Graph **(b)** shows the average S100B intensity of whole cells was not significantly altered by AD, but there was a significant difference in S100B intensity at AT8 spots vs cells as a whole, and significant pairwise difference between these regions in each AD case treatment. Statistics were a two-way ANOVA and post-hoc pairwise comparisons performed by Holm-Šidák's' pairwise multiple comparisons test. Data is mean ± SEM. N=4 (independent differentiations), each of which was performed in duplicate. * $p \leq 0.05$, ** $p \leq 0.01$, *** $p \leq 0.001$, **** $p \leq 0.0001$.

As performed for GFAP, S100B levels proximal to tau aggregates were then examined after the 7-day tau treatment was removed for a further 7 days (14 day time point) or 14 days (21 day timepoint) (Figure 6.11). The results indicate that there are only subtle changes in global S100B expression in astrocytes over time, as previously determined (Figure 6.9), whereas the changes in S100B intensity in the proximity of AT8 aggregates are much more pronounced. At these regions, average S100B intensity was shown to peak at 7 days for astrocytes exposed to all sources of AD brain tau. By day 21, S100B expression near aggregates had dropped in all cases relative to day 7. For cases AD 2, 3, 4 and 5 this appeared to be a stepwise decrease, while for cells treated with AD 1 and 6 there was no decrease in S100B levels near internalised aggregates at day 14, indicating these aggregates are able to sequester S100B for longer, the reasons for this are unknown. At day 21, only S100B levels around cells with AD2 derived tau aggregates was decreased to within whole cell averages, whereas for other cases the average S100B intensity remained higher near remaining internalised aggregates compared to whole cell average, indicating that tau aggregates sequester S100B and this is relatively stable. To confirm statistical differences, a two-way ANOVA was performed to measure the effect of timepoint and AD case on S100B intensity near AT8 spots. There was no interaction between these variables ($F(10, 42) = 1.48$, $p = 0.180$). A simple main effects analysis indicated that timepoint had a significant effect on S100B intensity at AT8 aggregates ($p < 0.0001$), whereas AD case did not ($p = 0.804$), suggesting that the decrease in S100B around aggregates over time is common to all AD derived tau tested here.

Taken together, these results indicate that the increase in S100B intensity around AT8 aggregates is transient and returns to a baseline range by day 21, regardless of the disparity between AD cases at day 7. This suggests that S100B is responding to tau internalisation, rather than any seeding of further tau aggregates within astrocytes.

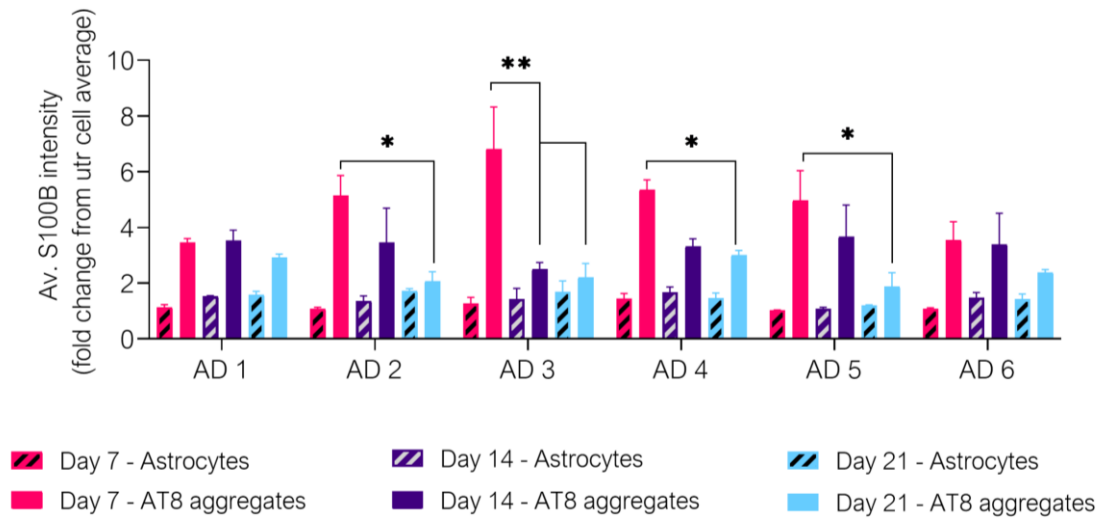

Figure 6.11 S100B intensity at tau aggregates decreases after tau removal from media

Day-60 iPSC-astrocytes were treated for 7 days with AD case derived tau, equivalent control sample or left untreated. Treatment was removed and cells were fixed at day 14 or 21. Cells were detected by GFAP immunolabelling and tau aggregates by high intensity AT8 spot detection, and levels of S100B immunofluorescence was measured. Graph shows the quantification of average S100B intensity in AD treated astrocytes in regions of dense tau aggregates against S100B intensity across the whole astrocyte, shown as fold change from untreated astrocytes. Average S100B intensity at regions of dense tau aggregates is higher relative to the cell average, peaks at 7 days and decreases after tau removal for 7 days (14 day time point) and 14 days (21 day timepoint), with variations in the relative rates of decrease between AD cases. A two-way ANOVA was performed confirming a statistical significance of timepoint on S100B intensity, and posthoc pairwise comparison using Holm Šidák's test showed S100B decrease at AT8 spot regions was significant in some AD cases. * $p < 0.05$, ** $p < 0.01$. Error bars are mean ± SEM of n = 4 (7 day) or 3 (14,21 days) independent differentiations, performed in duplicate.

6.2.3 Analysing astrocyte health and indicators of reactivity following tau uptake

Astrocytes undergo morphological changes in response to environmental changes in the brain, including in disease environments (Li et al., 2019), and in response to CNS injury (Brenner, 2014). The morphological changes are largely driven by changes in their cytoskeleton (Wilhelmsson et al., 2006). Since alterations in the cytoskeletal protein GFAP were apparent in response to AD brain tau, changes in cell morphology were examined after tau treatment. Cell roundness was determined in GFAP labelled astrocytes as an indicator of a change in morphology. A lower roundness score is indicative of astrocytes that have a large number of processes, whereas higher roundness scores indicate astrocytes which have retracted their processes in response to environmental cues or because of cell damage (Middeldorp and Hol, 2011; Schiweck et al., 2018). Astrocytes were immunolabelled with GFAP and imaged as a Z-stack to allow for 3D analysis of cells using Harmony software (Methods 2.5.4.2). Cell roundness was found not to be impacted by exposure to AD brain-derived tau aggregates when measured relative to untreated cells (Figure 6.12a) and did not show differences relative to control treated astrocytes. A one-way ANOVA confirmed that case treatment (control or AD) did not have a significant effect on cell roundness ($p = 0.694$), and no pair wise differences were observed when Holm-Šidák's test for multiple comparisons was performed relative to control or untreated. When cells treated with AD tau were grouped according to their levels of tau uptake and AT8 intensity, as in previous sections, again there appeared to be no large difference in cell roundness between astrocytes containing high or low levels of AT8 positive tau aggregates (Figure 6.12b). To analyse significance, a two-way ANOVA was performed to look at the effect of tau uptake (high v low AT8 cells) and AD case treatment on cell roundness. No significant interaction was detected between these two variables and their effect on cell roundness ($F (5, 47) = 0.4451$, $p = 0.815$). A simple main effects analysis showed no significant impact of tau uptake on cell roundness ($p = 0.079$), and no significant effect of AD case on cell roundness (0.100). A post hoc Holm-Šidák's test for multiple comparisons between high and low AT8 cells indicated no significant pairwise differences. This indicates that tau uptake is not causing morphological changes in these cells. While astrocyte morphological changes are a hallmark of PSP and common in other tauopathies (Reid et al., 2020), in vivo they form part of a wider connectome with neurons and other glial cell types in a 3D plane, and thus comparisons between morphology changes

in 2D culture are limited. It may also be that the proinflammatory environment in tauopathy brain has large impact on astrocyte morphology.

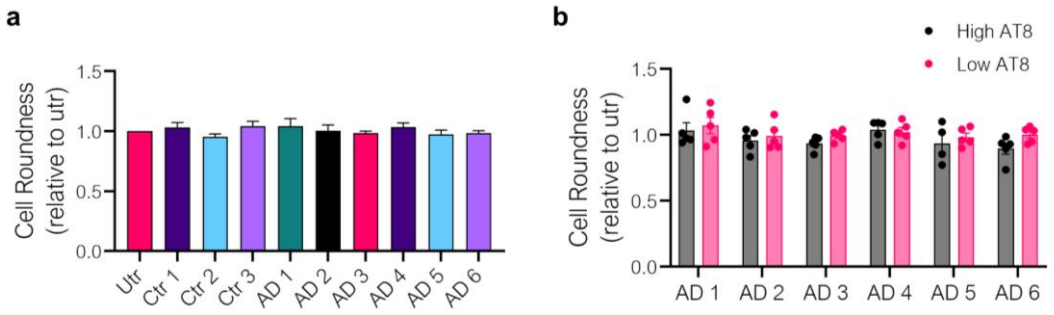

Figure 6.12 Astrocyte morphology is not significantly changed by tau uptake.

Day 60 iPSC astrocytes were treated with 0.1 ng/µL AD derived tau, control equivalent or left untreated for 7 days. Cells were fixed, immunolabelled for GFAP, imaged by Z-stack and 3D morphology of cells was measured using Harmony software. The roundness of cells was taken as an indicator of process branching and morphology change, and data is presented as fold change relative to untreated. Graphs show (**a**), cell roundness was not altered by AD tau uptake relative to untreated cells or controls. When dividing cells into low or high AT8 internalisation (**b**), cells from both groups were not significantly changes relative to untreated (and therefore controls). A one-way ANOVA was performed on (**a)** and a two-way ANOVA on (**b**) and no significant effect of case or AT8 intensity was found to alter cell roundness relative to untreated astrocytes. Error bars are ± SEM of n = 5 independent astrocyte differentiations (performed in duplicate).

Nuclei properties were utilised in the previous chapter (Section 5.3.2) to indicate cell death in response to brain derived LSS treatment, because apoptosis can be indicated by the shape and intensity of nuclei staining (Kerr, 1971; Kerr et al., 1972). Therefore, astrocyte cultures were also examined for changes in cell death after exposure to brain derived AD or control SI tau to determine if there was a negative impact of this treatment on cell health. As described previously, nuclei were determined to be healthy or dying by their shape, size and intensity of Hoescht 33342 staining (Figure 6.13a).

In astrocytes exposed to aged control brain extract or AD brain tau for 7 days, the average percentage of dying cells in culture appeared reduced compared to untreated cells (Figure 6.13b). However, this was variable, and a one-way ANOVA demonstrated that there was no overall significant impact of treatment on the % of dying cells, although the p value was approaching significance (p=0.0603). A post-hoc multiple comparison Dunnett's test

indicated that exposure to tau from AD case 1 actually decreased the proportion of dying cells in culture compared to untreated cells to 0.68 ± 0.11 fold change from untreated. However, this was not significantly lower than control treated astrocytes, indicating that there is a common factor in insoluble samples extracted from postmortem brain tissue that may reduce cell death, regardless of the presence of AD tau. This also confirms that the brain extracts from AD and control cases are not having a negative impact on the number of healthy cells in culture, and in particular do not appear to be causing apoptosis.

Interestingly, further analysis of the same cell death parameters following the removal of tau for 7 and 14 days suggested no adverse effect of brain extract exposure on the proportion of dying astrocytes in culture (Figure 6.13c). For all control brain extract treated astrocytes, the percentage of dying cells was similar to that for untreated astrocytes by day 21, suggesting that any protective effect of exposure was transient. For AD tau exposed cells, this was also the case when tau was isolated from AD cases 3 and 5. For cells treated with AD cases 1, 2, 4 and 6, the percentage of dying cells remained lower than untreated at day 21. This indicates that tau uptake from AD cases has a variable effect on cell health that can change over time. A two-way ANOVA was performed to look at the effect of case treatment (AD v Control) and timepoint on cell death. There was no reported interaction between these variables and the impact on cell death ($F(18, 100) = 1.42$, $p = 0.137$). A simple main effects analysis did find a significant effect of case treatment on % dying cells ($p = 0.0065$), but the effect of timepoint was not significant ($0 = 0.1941$), suggesting that there may be differential impacts of AD or control case treatment on % dying cells observed, but this is not likely to change over time. A post-hoc Holm-Šidák's test for multiple comparisons did not find any significant pairwise differences when AD cases were tested relative to control or untreated, nor at later timepoints relative to 7-day timepoint for each case treatment.

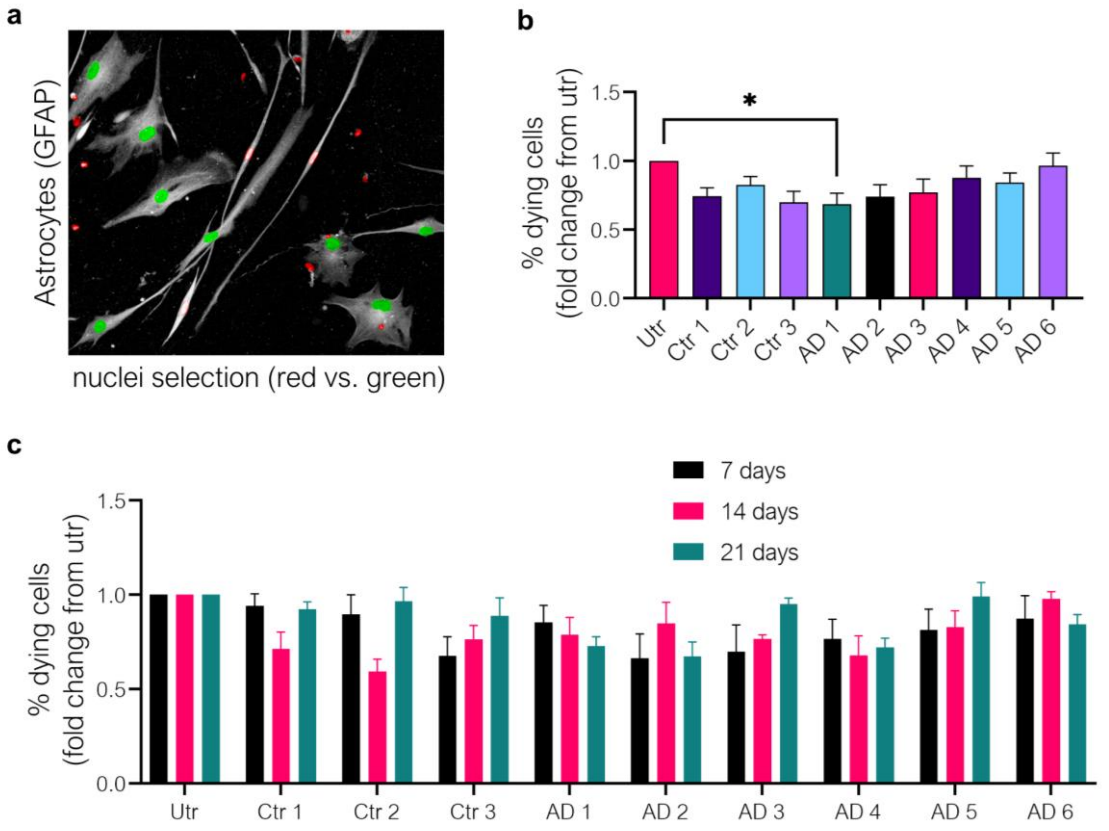

Figure 6.13 Cell death was not altered by tau uptake.

After tau treatment assays, cells were fixed and immunolabeled for GFAP and nuclei stained with Hoechst 33342. Using Harmony software, nuclei properties including intensity and morphology were used to select bright, small nuclei that were assumed to be apoptotic. (**a**). Cells were grouped as 'healthy' (green) or 'dying' (red) based on this analysis and only healthy cells have been used to detect astrocytes in previous assays This gives a measure of the number of apoptotic nuclei in culture relative to healthy nuclei, and this was calculated as the % of dying cells in culture. After 7-day tau treatment, the graph in (**b**) shows the relative proportion of dying cells was not increased by control or AD case treated cells compared to untreated, while some cases the percentage of dying cells was decreased. (**c**) Cell death was not increased after tau treatment removal in case treated cells relative to untreated, but this varied between case. A one-way ANOVA (b) and a two-way ANOVA (c) was performed on this data with Holm-Šidák's test for multiple comparisons, indicating no difference in case treatment on dying cells in (a), but that case significantly altered the % dying cells in (c), however no pairwise differences were found. Error bars are ± SEM of n=4-5 independent astrocyte differentiations (performed in duplicate).

6.2.4 Astrocyte gene expression changes after tau uptake

Specific changes in astrocyte gene expression have been associated with a reactive astrocyte state (Escartin et al., 2021). These include genes related to the innate immune response of cells such as the complement cascade, a process by which astrocytes can interact with microglia (Lian et al., 2016; Vainchtein et al., 2021), and related signalling

pathways (Ceyzériat et al., 2016). As well as secretion of other molecules such as serpina3 and lcn2 (Bi et al., 2013) that can have direct impact on other cell types. Expression of specific pathways related to tau uptake and astrocyte processing of tau may also be upregulated. Therefore, the expression levels of a targeted panel of genes previously implicated in astrocyte response in AD were investigated to give insight into astrocyte state after exposure to tau aggregates from post-mortem AD brain and controls. After treatment for 7-days RNA was extracted and RT-qPCR performed. Gene expression was normalised to *BACTIN* and *GAPDH* endogenous controls, then calculated as relative fold change from untreated by (-2^ΔΔCt).

C3 and the C3 receptor C3aR are components of the complement cascade, a system crucial for innate immunity and defence (Ricklin et al., 2016). C3 is a marker of "A1" astrocytes (Liddelow et al., 2017) and astrocytes release C3 in AD models (Lian et al., 2015). C3aR is activated in AD and tauopathy conditions (Litvinchuk et al., 2018). Therefore, the expression of these two genes was investigated by RT-qPCR (Figure 6.14a). The results showed some elevation of *C3* in astrocytes exposed to tau from only 3 of 6 AD cases (3, 4 and 5). Astrocytes exposed to tau from the other three AD cases (AD cases 1,2 AND 6) showed similar levels of *C3* as those exposed to control brain extracts and untreated cells. A one-way ANOVA showed that there are no significant differences between treated, control and untreated astrocytes ($p = 0.609$). Similarly, *C3AR* changes in astrocytes exposed to control extracts or AD brain tau relative to untreated cells were variable, with increases observed following exposure to control brain extract 3 and tau aggregates from AD case 4. There were no significant differences between groups ($p = 0.340$).

Additional markers of astrocyte reactivity were next investigated. Serpina3 is a secreted peptidase inhibitor that is induced by inflammation and nerve injury (Vicuña et al., 2015). Serpina3 was identified as a pan-reactive astrocyte marker (Swartzlander et al., 2018) and it is upregulated in prion diseases and AD (Vanni et al., 2017). LCN2 is an astrocyte secreted lipophilic protein that can induce neuronal cell death (Bi et al., 2013) and is implicated in synaptotoxicity in response to oxysterols in cell models of AD (Staurenghi et al., 2020). Both are considered markers of reactive astrocytes (Zamanian et al., 2012). Therefore, their expression was examined in astrocytes following 7-day exposure to AD brain tau or control brain extracts, by RT-qPCR (Figure 6.14b). The results were again quite variable and appeared highly dependent on the source of human brain material used. For example,

exposure of astrocytes to extracts from control brain 3, but not control brain 1 or 2, caused some increases in *SERPINA3* expression. Similarly, exposure of astrocytes to tau aggregates from AD case 1 resulted in a large increase in *SERPINA3* expression relative to untreated astrocytes (5.61 ± 1.1 fold change), but the same was not true when tau from the other AD cases was used. One-way ANOVA showed no significant effect of treatment on *SERPINA3* expression ($p = 0.0619$), however a post-hoc analysis for multiple comparisons by Dunnett's test showed a significant reduction in *SERPINA3* levels from untreated cells to those exposed to tau from AD case 1 ($p=0.0215$).

LCN2 expression was not detected in untreated cells, therefore data is presented as CT value relative to endogenous controls (Delta CT). Expression of *LCN2* was found to be low in all groups and levels were undetectable in some replicates. There was no clear effect of exposure to AD brain tau on *LCN2* levels. Together these data suggest that there may be some changes in astrocyte reactivity but only in response to specific species of tau and/or other components of postmortem brain extracts. There were certainly not clear overarching reactive changes in AD versus control groups.

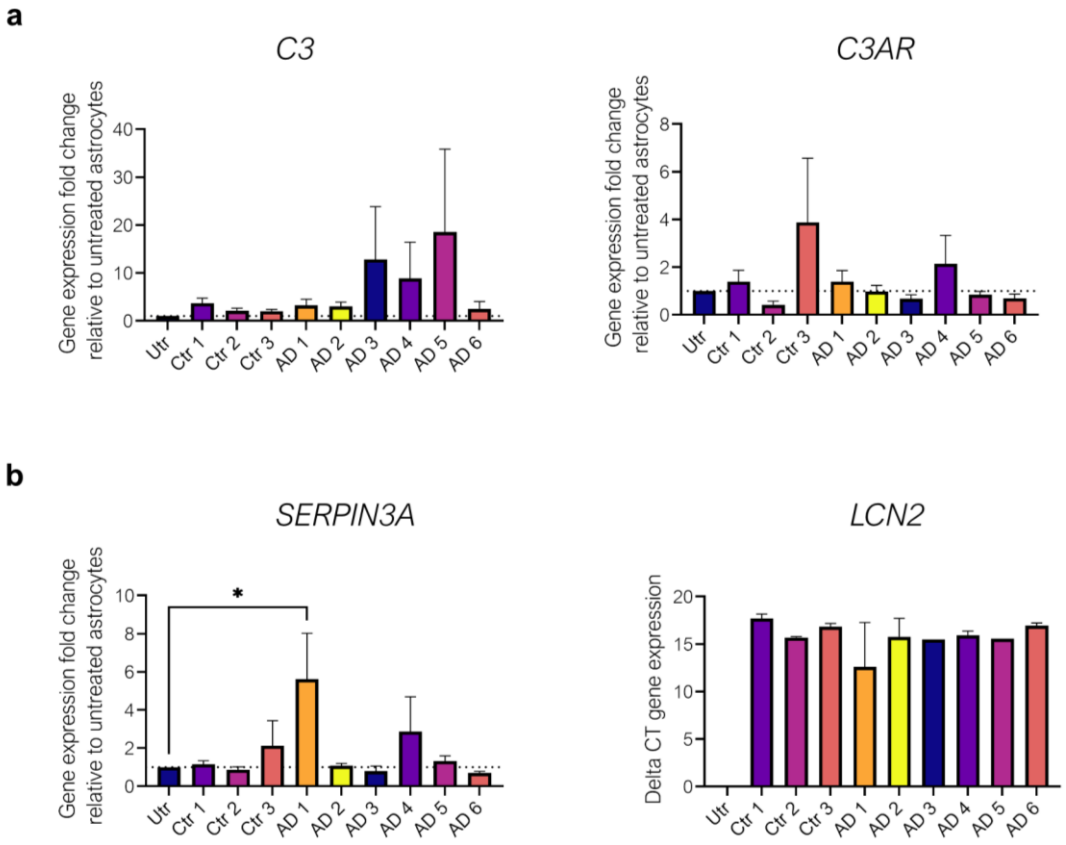

Figure 6.14 Inflammation and astrocyte reactivity related gene expression after tau treatment.

Day-60 iPSC-astrocytes were treated with 0.1 ng/ µL tau from AD brain extract as well as equivalent control brain samples and some were left untreated. After 7 days cells were lysed and extracted for RNA to perform RT-qPCR and measure gene expression of astrocyte reactivity related genes. Graphs in (**a**) show expression of *C3* and *C3aR,* genes associated with the complement cascade. Expression was highly variable and not statistically different from untreated astrocytes. **(b)** Gene expression of genes associated with reactive astrocytes, *SERPIN3A* and *LCN2*, were also examined. Only treatment with AD 1 derived tau led to a significant increase in *SERPIN3A* expression. LCN2 expression was not detected in untreated astrocytes and thus depicted as Delta CT, and expression was low or undetected for all case treated astrocytes and did not appear significantly altered by AD case relative to control. Data shown is mean ± SEM of n=3-5 from independent astrocyte differentiations. A one-way ANOVA was performed on this data with Dunnett's test for multiple comparisons. * $p < 0.05$.

Next, other processing and uptake pathways that have been implicated in astrocyte responses to tau were examined. *TFEB* is a master regulator of lysosomal biogenesis (Sardiello et al., 2009; Settembre et al., 2011), that has been shown to contribute to astrocyte uptake of extracellular tau species (Martini-Stoica et al. 2018). *LRP1* was also implicated in tau uptake in a neuroglioma cell line (Rauch et al 2020). Therefore, changes in

these genes were next investigated (Figure 6.15a). Again, the data were variable. When astrocytes were exposed to control brain extracts, for two out of three cases (1 and 2), *TFEB* expression appeared increased, while it was slightly reduced for the third (Ctrl 3). Similarly, when astrocytes were exposed to tau aggregates from five out of six AD cases (1,2,4,5,6), *TFEB* expression was reduced on average, while exposure to tau from AD case 3 led to an increase in *TFEB* expression. A one-way ANOVA confirmed no significant impact of AD tau exposure or control extract exposure on *TFEB* expression ($p = 0.784$). *LRP1* expression showed a similar variable expression pattern relative to untreated cells, and again, a one-way ANOVA showed no significant impact of treatment on LRP1 expression ($p = 0.910$).

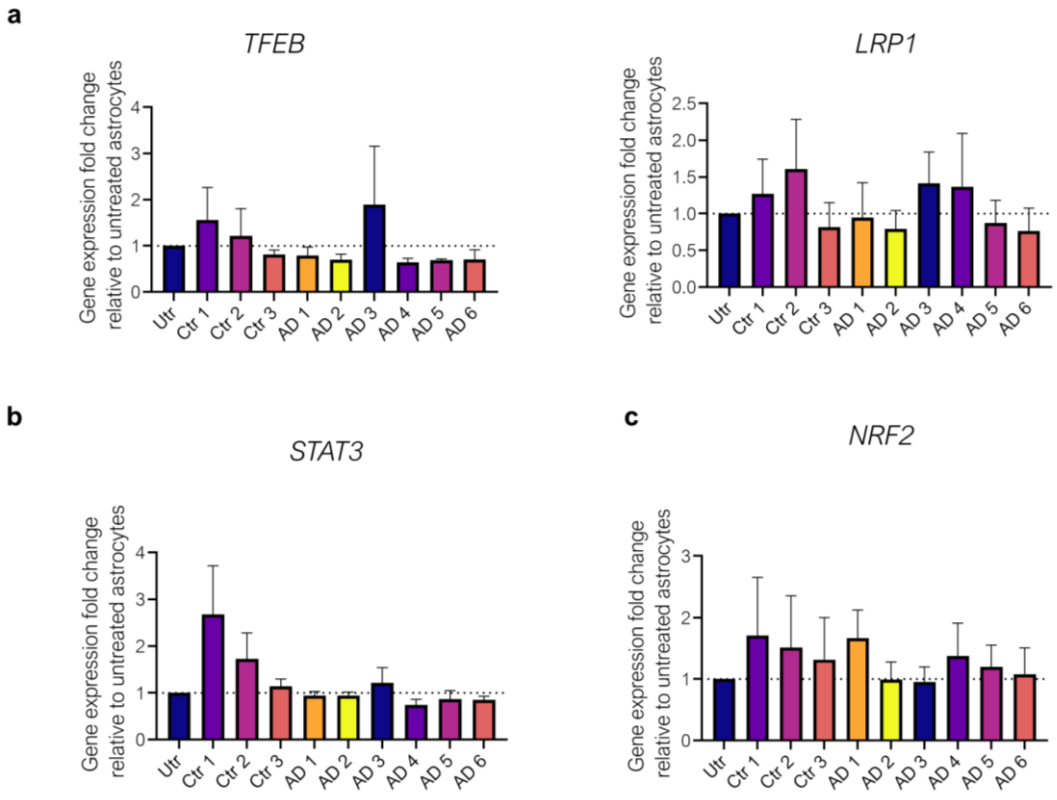

Figure 6.15 Gene expression of astrocyte genes associated with tau uptake, processing and reactivity.

Day-60 iPSC-astrocytes were treated with 0.1 ng/ µL tau from AD brain extract as well as equivalent control brain samples and some were left untreated. After 7 days cells were lysed and extracted for RNA to perform RT-qPCR and expression of genes analysed to give insight into tau uptake and processing and reactivity related signalling pathways. (**a**) Expression of lysosome and tau uptake associated genes *TFEB* and *LRP1* were examined 7-day tau treatment (**b**) STAT3, a signalling molecule associated with reactivity related call signalling pathways, was further examined and (**c**) NRF2 associated with reactivity was also examined after tau uptake. No significant changes were observed in the data analysed. Data shown as mean ± SEM of n=3-5 from independent astrocyte differentiations. A one-way ANOVA was performed on this data with Dunnett's test for multiple comparisons.

STAT3 is a transcription factor that forms part of the JAK-STAT3 signalling pathway, which is strongly implicated in astrocyte reactivity downstream of cytokine receptor activation (Levine et al., 2016) and is a direct target of C3-C3aR signalling (Litvinchuk et al., 2018). Its expression was therefore examined after tau uptake (Figure 6.15b). While astrocytes exposed to two out of three control brain extracts (1 and 2) showed higher expression of *STAT3* after treatment, this was not found after exposure to control brain extract 3. There were no obvious changes in STAT3 levels following exposure to AD brain tau. A one-way ANOVA confirmed no significant impact of treatment on *STAT3* gene expression ($p = 0.081$).

Next, quantification of levels of the transcription factor NRF2, a master regulator of detoxification, antioxidant and proteostasis genes (Pajares et al. 2017, Kobayahi et al 2016, Tebey et al 2015) were carried out. NRF2 expression is induced as a cytoprotective mechanism after exposure to Aβ or tau pathology (Jiwaji et al., 2022). NRF2 levels were somewhat increased following exposure of astrocytes to both control brain extracts and AD brain tau, but these changes were not significantly different compared to untreated (Figure 6.15c).

Taken together these data suggest that there may be subtle changes in gene expression in astrocytes that internalise tau aggregates and/or that are exposed to AD brain extracts. However, these were not as marked as was anticipated at the outset of these experiments. Had time allowed it would have been interesting to follow up on some of the changes observed to determine what factors are linked with specific gene expression changes.

6.2.5 Neuronal response to astrocyte conditioned media after astrocyte exposure to tau

Despite having not observed any marked changes in a small number of indicators of astrocyte health and reactivity, it was important to determine if changes in astrocytes upon tau uptake may change their ability to support neurons. This is important since alterations in astrocytes in AD are closely linked with synaptic degeneration and neuron death (Liddelow et al., 2017; Perez-Nievas et al., 2021; Staurenghi et al., 2021). To investigate how the uptake of tau by astrocytes may impact their support for neurons in culture, astrocyte conditioned media was collected from control brain extract or AD brain tau exposed astrocytes, and this was applied to cultured iPSC-neurons. This would allow analysis of the effects of any factors released by astrocytes following pathological tau exposure on neuronal health.

6.2.5.1 Characterisation of neurons

Neurons were derived from a common pool of neural progenitors after exposure to DAPT (Section 2.3.4, (Shi et al., 2012a, 2012b)). An overview of the protocol timeline is shown below (Figure 6.17) together with representative phase contrast images of neurons. Neurons were used at an immature state due to time restrictions caused by the COVID pandemic.

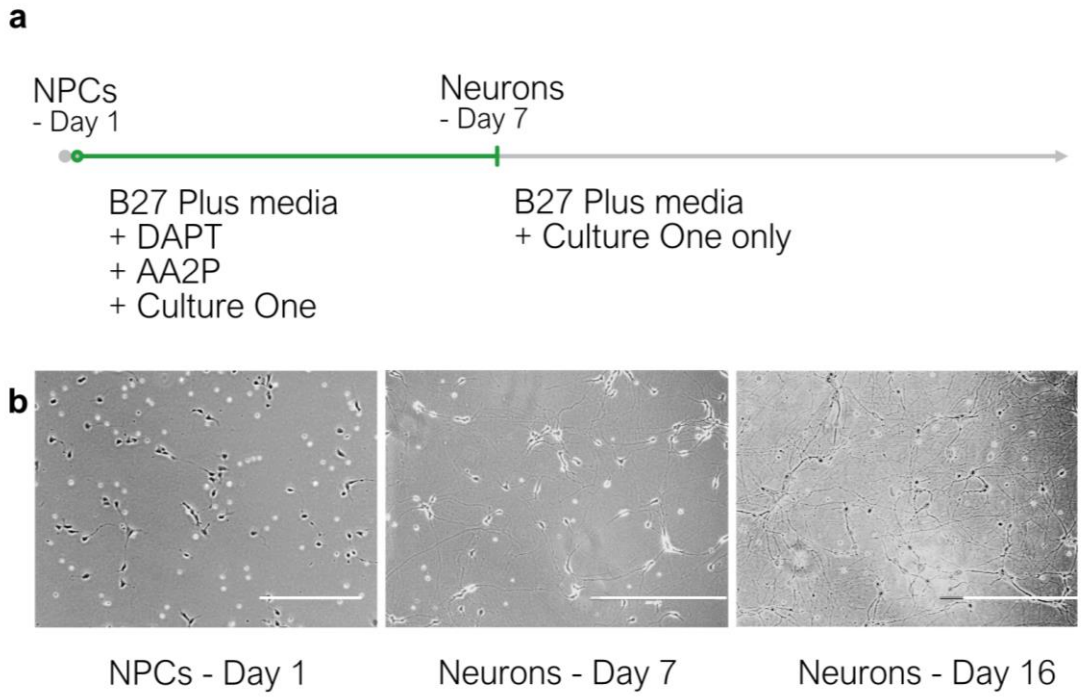

Figure 6.16 Differentiation of NPCs into neurons.

(a) Overview of the timeline of neuron differentiation from NPCs. NPCs were plated at low density for 7 days in B27 Plus media with added DAPT and AA2P to promote neuronal differentiation, and Culture One supplement to reduce unwanted glial cells, and cells were then maintained in B27 Plus media with Culture One supplement only. (b) Representative phase contrast images of NPCs and neurons at Days 1, 7 and 16 of differentiation showing increased neurite outgrowth with increasing time after differentiation. White scale bar = 400µm. n=3.

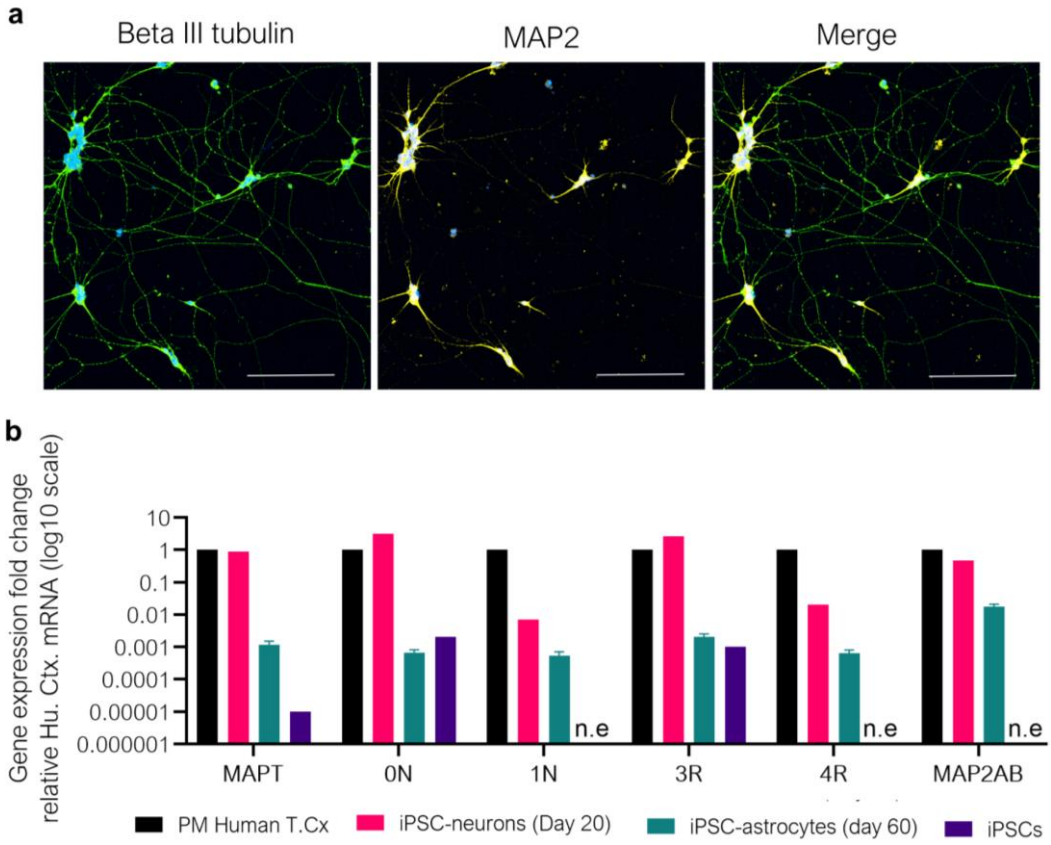

Figure 6.17 iPSC-derived neurons express neuronal markers and MAPT.

iPSC-derived neurons differentiated for 16 days from NPC were immunolabelled (**a**) with antibodies against the neuronal markers β-III-tubulin (green) and MAP2 (yellow). Hoechst 33342 was used to label nuclei. N=1. Scale bar = 100 μm **(b)** mRNA expression of total MAPT and MAPT containing domains that are alternatively spliced to generate the six main tau isoforms (0N, 1N, 2N, 3R and 4R) were measured in Day 20 iPSC-neurons, Day 60 iPSC-astrocytes and iPSCs by qPCR. mRNA was also measured in a sample of postmortem human temporal cortex (T.Cx) as a positive control. Expression is shown as fold change to human temporal cortex RNA in (b). n=1 for iPSC-neurons, iPSCs and PM human tissue and n=3 (±SEM) for iPSC astrocytes.

Neurons were first characterised for their expression of the neuronal markers βIII-tubulin and MAP2, and their gene expression of total *MAPT* and domains of tau that are alternatively spliced to give rise to the six main tau isoforms expressed in the adult CNS (0N, 1N, 2N, 3R, 4R) (Figure 6.17). The latter is important since tau splicing is developmentally regulated, with 0N3R forms of tau expressed during embryonic development, and all six isoforms, and predominantly 0N4R tau expressed in adult human brain (Guo et al., 2017). iPSC neurons typically show an immature *MAPT* expression pattern unless aged for substantial periods of time in culture (Sposito et al., 2015).

Immunocytochemistry (Figure 6.17a) of neurons at day 10 post NPC induction shows that cells express βIII-tubulin in the cell body and in projected neurites. MAP2, associated with more mature neurons, is also expressed in cell bodies as well as in proximal neurites that extend from neuronal cell bodies. This is in agreement with previous reports (Dehmelt and Halpain, 2004).

MAP2AB is an isoform of MAP2 that is particularly expressed by neurons (Przyborski and Cambray-Deakin, 1995; Dehmelt and Halpain, 2004), and this was confirmed to be expressed in 20 day iPSC-neurons by RT-qPCR. The results in Figure 6.17b are shown relative to RNA extracted from post-mortem brain tissue of a control patient, utilised as a positive control. Astrocytes and iPSCs were found to express only trace levels of all neuronal genes, as expected. In contrast, iPSC-neurons express all domains of MAPT, suggesting that all tau isoforms are expressed, at varying levels, and much more highly (479-fold higher) than was found in astrocytes. The high expression of the 0N and 3R domains indicate that the majority of tau isoform expression is the embryonic 0N3R tau isoform, as expected (Sposito et al., 2015). While 4R and 1N tau isoform expression was found to be relatively higher than that in iPSC-astrocytes, it is still dramatically lower than in adult human brain tissue, further indicating the immaturity of tau expression at this early timepoint of neuronal differentiation. Unfortunately, in these experiments the primers against 2N tau were unsuccessful and therefore the absence of 2N data is a result of a technical fault rather than an absence of 2N tau expression. As iPSC astrocytes were seen to express 2N isoforms at low levels in characterisation experiments of Chapter 4 (section 4.3.3), it would be expected that neurons may also express low levels of 2N. Whether mRNA expression of MAPT isoforms translates to protein expression in these neurons is yet to be determined.

6.2.5.2 Neurons are not adversely affected by conditioned media from astrocytes exposed to human AD brain tau aggregates

Neurons were treated as shown in protocol outline of Figure 6.18a. Briefly, astrocyte conditioned media (ACM) was derived from astrocytes that had been exposed to 0.1 ng/μL of tau aggregates from AD cases for 5 days, or to control brain extracts for the same period of time. Treatment was removed from astrocytes and replaced with neuronal media. After a further 3 days, media was taken as ACM from case treated as well as from untreated astrocytes. ACM was used to treat neurons for 3 days. Neurons treated with ACM derived

from control extract or AD tau treated astrocytes were compared to those from neurons treated with ACM from untreated astrocytes (astrocytes treated with base neuronal media only). After treatment, neurons were immunolabelled with an antibody against βIII-tubulin to detect neurites and stained with Hoechst 33342 to detect nuclei (Figure 6.18b).

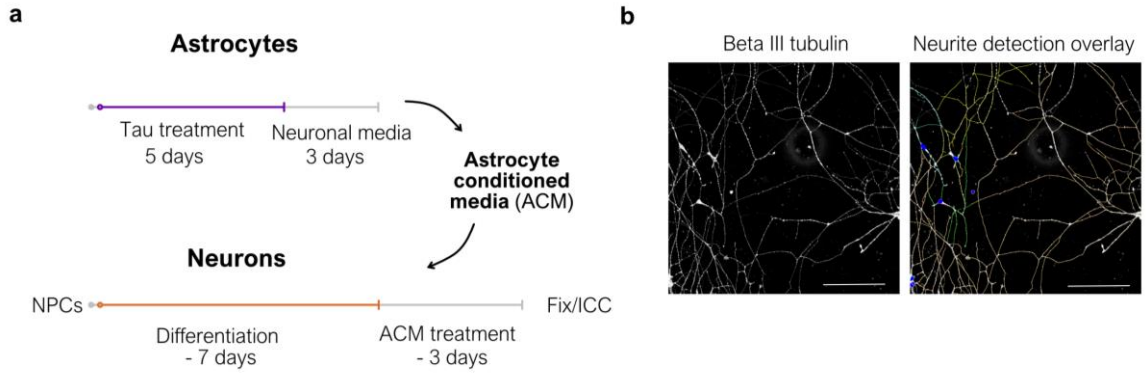

Figure 6.18 Overview of experimental design to examine the effect of astrocyte conditioned medium on neuron health.

To generate astrocyte conditioned media (ACM), day-60 iPSC-astrocytes were treated with 0.1ng/uL AD brain tau extract or control equivalent, or left untreated, for 5 days before removing and changing to neuronal media for 3 days. This ACM was then used to treat neurons for 3 days after they underwent a 7-day differentiation protocol from NPCs. (**a**) Schematic overview is shown. (**b**) Cells were immunolabelled with an antibody against beta-III-tubulin and nuclei were stained with Hoechst 33342. Imaged cells were analysed using Harmony neurite analysis software to determine measurements of neurite health. A representative image of immunostaining and Harmony software neurite detection is shown in Scale bar = 100 μm.

The morphology of neuronal nuclei were first assessed to gauge cell health in response to ACM. Additional indicators of neuron health were determined using Harmony neurite analysis software. These measurements included maximum neurite length, the number of neurite segments and the number of neurite nodes, as indicators of neuron complexity. In addition, cells were examined for the presence of AT8 in the cell body or neurites to determine if any pathogenic tau that may have been released by astrocytes, has been internalised by neurons.

When the proportion of condensed and fragmented nuclei were quantified as a proportion of total nuclei in the well, the proportion of "unhealthy" nuclei was determined to be approximately equivalent across treatment conditions, with no obvious differences between groups (Figure 6.19a). Neurons exposed to ACM from cells treated with tau from AD case 6 showed the highest proportion of unhealthy nuclei at 14.64 ± 1.12 %, compared to

untreated (11.4 ± 0.98 %) and this was not a significant difference. A one-way ANOVA showed no significant impact of ACM treatment on the percentage of dying neurons irrespective of treatment group, and similarly a post-hoc Dunnett's test showed no pairwise differences between untreated neurons and other treatment conditions.

Neurons were then analysed for changes to characteristics of their neurites after ACM treatment as indicators of neuronal complexity. Similar measurements were previously used to show that ACM collected from Aβ-stimulated astrocytes is detrimental to neuron health (Perez-Nievas et al., 2021). Relative to the untreated vehicle control, there were apparent increases in maximum neurite length following exposure to ACM from both control and more so from AD tau exposed astrocytes (Figure 6.19b). However, the results were variable, and a one-way ANOVA indicated no significant impact of ACM treatment type on maximum neurite length, A Dunnett's multiple comparisons test revealed no pairwise differences. A similar pattern was observed when the number of neurite segments and number of neurite nodes were quantified (Figure 6.19c,d). These results indicate that ACM from astrocytes stimulated with AD brain tau are not altered in a way that they fail to support neuron health. In fact, the opposite may be true, and astrocytes may release factors upon exposure to brain extracts that help promote neurite outgrowth and maturation of iPSC-neurons.

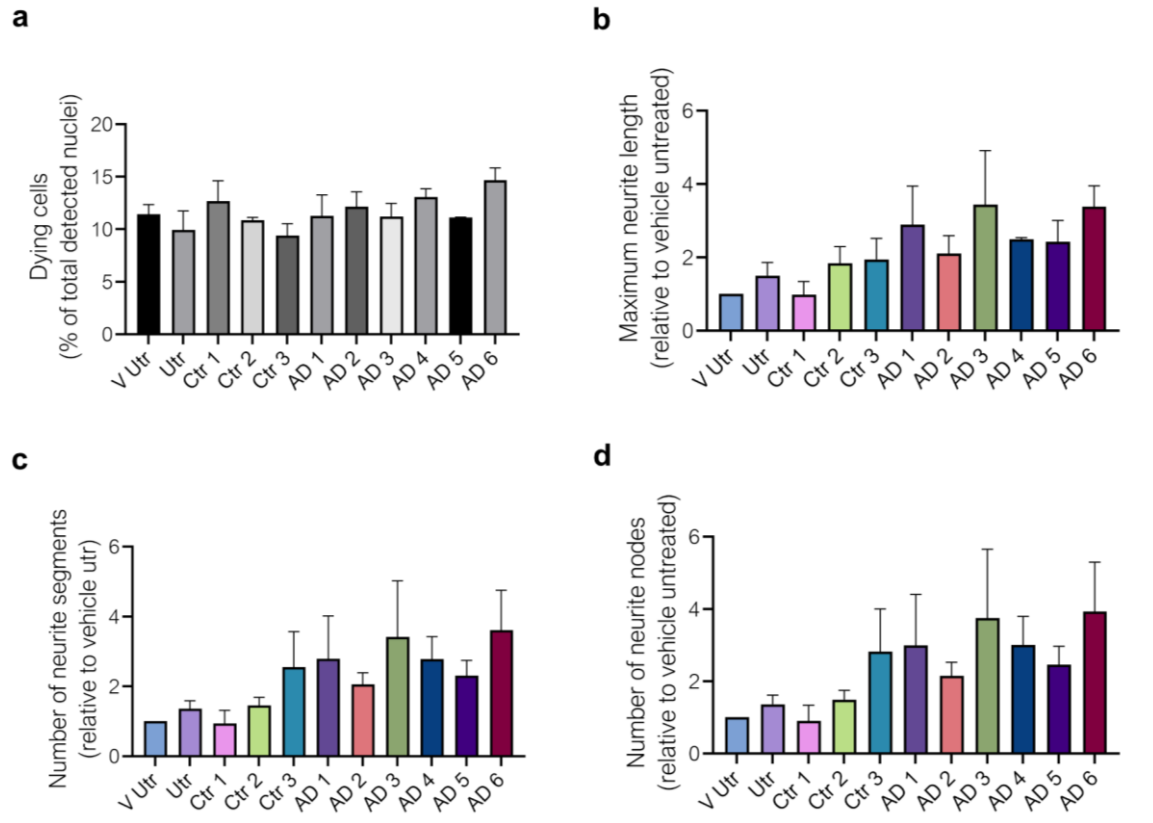

Figure 6.19 Neuron health and neurite complexity changes after ACM treatment.

7-day iPSC-neurons were treated with ACM for 3 days from astrocytes that had been treated with AD derived tau or equivalent control samples or left untreated. Cells were immunolabeled for β3tubulin, MAP2, AT8 and nuclei stained with Hoechst. Neurites were detected and analysed by Harmony software. (**a**) No increase in detected dying nuclei observed after ACM treatment, (**b**) Maximum neurite length is increased in neurons treated with ACM from AD treated astrocytes relative to vehicle untreated but is not significant and is highly variable, as are indicators of (**c**) neurite complexity such as the number of neurite segments and (**d**) the number of neurite nodes. Data shown as mean ± SEM of n=3 independent repeats. A one-way ANOVA was performed on each data set, with Dunnett's test for multiple comparisons, with no significant difference between groups.

Finally, AT8 intensity inside neurons were examined to determine if astrocytes release phosphorylated tau into media after tau treatment, that can then be internalised by neurons. Neurons were immunolabelled with the AT8 antibody and the average and maximum AT8 levels in cell bodies were determined relative to untreated cells. No significant differences in AT8 intensity were observed between groups (Figure 6.20a). A one-way ANOVA performed confirmed that ACM treatment did not significantly alter neuronal maximum or average AT8 intensity, nor were any pairwise differences revealed by post-hoc analysis. This was also the case when AT8 intensity was measured in neurites (Figure 6.20b). These results suggest

that either astrocytes do not release seed-competent tau into culture medium, or if they do that it is not internalised by neurons, at least not within the 3-day time examined here.

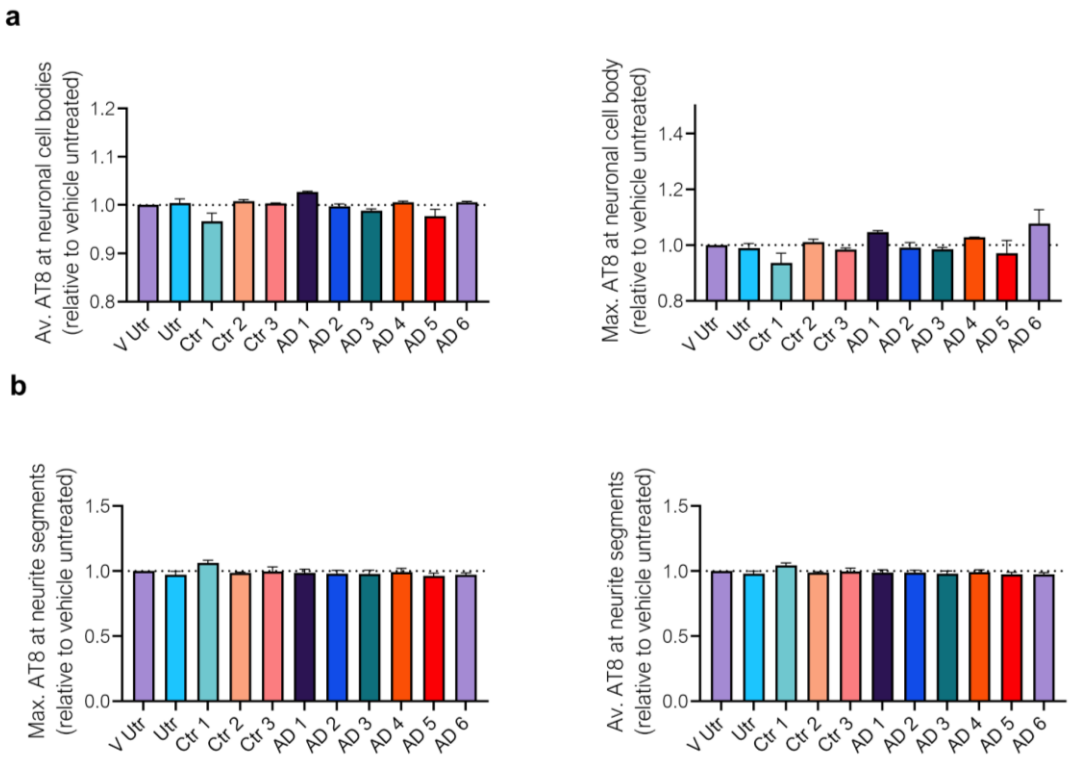

Figure 6.20 AT8 intensity in neurons after ACM treatment.

7-day iPSC-neurons were treated with ACM for 3 days from astrocytes that had been treated with AD derived tau or equivalent control samples or left untreated. No increase in detected dying nuclei after ACM treatment. Cells were immunolabeled for β3tubulin, MAP2, AT8 and nuclei stained with Hoechst. (**a**) The average and maximum AT8 intensity at neuronal cell bodies is altered by ACM treatment although this is highly variable and not significant and (**b**) there is no AT8 difference in neurites. Data shown is mean ± SEM of n=3 independent repeats, relative to vehicle untreated astrocytes. A one-way ANOVA was performed on each data set, with Dunnett's test for multiple comparisons.

6.3 Discussion

This chapter investigated the astrocytic response to the internalisation of AD derived tau aggregates. The main findings were:

- GFAP expression is not clearly altered by AD derived tau uptake but changes are localised around internalised around tau aggregates.
- S100B shows a similar pattern of associating with internalised tau aggregates.

- Astrocytes do not appear adversely affected by this tau uptake.
- Gene expression changes indicate muted and variable response in reactivity or cellular processing related genes.
- Astrocytes treated with brain extract may release factors that are beneficial to neurite outgrowth.

6.3.1 The GFAP response to internalised tau aggregates

The results presented in this chapter show that while there were few global alterations in GFAP levels following exposure of iPSC-astrocytes to AD brain-derived tau. Although intensity of GFAP immunolabelling and gene expression were generally higher for AD tau exposed astrocyte cultures, they were variable and overall were not significantly altered. There were, however, clear focal changes in GFAP at sites of AT8-positive tau accumulation. This is supported by the fact that astrocytes with high AT8 levels show higher GFAP intensity when measured by immunofluorescence. Furthermore, high levels of GFAP intensity in association with intra-astrocytic AT8 aggregates suggest that this is a cytoskeletal response to the internalisation of pathological aggregates. Whether this is a specific response to the uptake of tau aggregates or is common to the internalisation of any protein aggregate, is yet to be determined. Specific isoforms of GFAP, namely delta, have previously been shown to be particularly prone to aggregation (Nielsen and Jørgensen, 2004; Perng et al., 2008), and thus it may be that GFAP is sequestered and co-aggregates with pathological tau. Alternatively, binding between tau and GFAP may result in high local concentrations of GFAP that self-aggregate. While general increases in GFAP expression are associated with CNS injury and neurodegeneration (Brenner, 2014; Hol and Pekny, 2015; Messing and Brenner, 2020), astrocytes in these conditions are exposed to a disease or injury milieu that would comprise multiple signalling pathways and input from multiple cell types that could induce GFAP changes. The data in this chapter indicates that focal GFAP increases appear specific to a cytoskeletal response to internalised tau aggregates in the absence of a cell-wide response to pathological tau.

How astrocytic GFAP responds to the internalisation of large proteins has not been studied. It was implied in the discussion of the previous chapter that the rate of uptake of large tau aggregates may be in line with phagocytic mechanisms of internalisation. Whether phagocytosis contributes to the uptake of tau in astrocytes remains to be established, but it

is worth considering the implications for how GFAP may become involved with internalised tau aggregates. The general phagocytic process of a cell involves the remodelling of the actin cytoskeleton (Underhill and Goodridge, 2012), and so it is plausible that GFAP is altered during this process, as intermediate filaments can be connected to actin via plectins (Wiche, 1998), and can react in response to mechanical stress (Flitney et al., 2009), which may be induced by the engulfment of large tau aggregates or apoptotic cells. One study in which astrocyte primary cultures were prepared from GFAP and vimentin null mice described an increase in the motility of endosome/lysosomes (Potokar et al., 2010), and the authors postulate that upregulation of GFAP in disease states such as AD may deregulate vesicle trafficking in astrocytes. It would be interesting to explore how the association of GFAP with internalised tau aggregates might impact on cell degradation methods.

Another possibility is that any undigested tau aggregates that reside within the cytosol of astrocytes are able to attract the binding of GFAP molecules. Interestingly, the data here shows that the amount of GFAP around internalised tau aggregates reduces with time, suggesting that the focal GFAP accumulation is a transient process. *In vivo* half-life of GFAP has been observed to be approximately 28 days in mouse models (Price et al., 2010; Moody et al., 2017), so reduction in GFAP around tau aggregates within the 21 day period tested may indicate active degradation and removal of these excess proteins is occurring, and indeed mouse models have shown that GFAP is cleared by autophagy pathways (Tang et al., 2008). It is worth noting that extracellular GFAP was observed in some astrocyte cultures that had been exposed to AD tau, suggesting that there is a mechanism for GFAP excretion/GFAP/AT8 tau co-aggregates from these astrocytes. The mechanism underlying this extrusion is not understood, but could be worth investigating, considering that serum GFAP and tau are being suggested as a prognostic for neurological diseases, including AD (Heimfarth et al., 2022; Pilotto et al., 2022)

6.3.2 S100B association with internalised tau aggregates

As with GFAP, S100B was found to be upregulated in areas of the cell that harbour AT8 positive tau aggregates. This is in line with previous studies which showed that tau can interact directly with S100B *in vitro* (Baudier and Cole, 1988). While more recently, S100B has not only been demonstrated to act as a suppressor of amyloid-β aggregation (Cristóvão

et al., 2018), but it has also shown to interact with tau in a cellular model, where S100B binding to tau was found to prevent aggregation of full-length tau and pro-aggregatory tau fragments (Moreira et al., 2021). This indicates that the S100B localising near tau aggregates seen in this chapter may be a protective response of the cell, acting to protect from subsequent aggregation of the endogenous astrocytic tau. The data here shows that S100B expression around aggregates is reduced 2 weeks after tau treatment is removed, and therefore this appears to be a transient association. Because the level of S100B reduction varies between AD cases, this may indicate a differential S100B response depending on undefined molecular features of the AD patient derived tau aggregates.

6.3.3 The response of astrocytes to AD tau uptake was variable and did not indicate a strong reactive response

These data show that astrocytes undergo changes in response to their internalisation of tau. It was speculated that this may be associated with changes in astrocyte function since previous reports have shown that astrocyte reactivity is a common feature of neurodegeneration (Garwood et al., 2011, 2017; Acosta et al., 2017), even if the exact specification of a reactive astrocyte has not been well defined (Escartin et al., 2021). Therefore, changes in cell health and in the expression of astrocyte reactivity markers was investigate. The data shown here suggests that, at least at the concentration times and exposure periods studied here, tau aggregates are not sufficient to induce a robust reactive phenotype in iPSC-derived astrocytes. Cell death was also not significantly altered by tau uptake, and morphological changes to astrocytes were not observed. Indeed, in the panel of genes chosen to assay for reactivity changes, no consistent changes were observed. However, some specific changes were observed in response to the exposure of astrocytes to tau from specific AD cases or from specific controls.

This is apart from an upregulation of Serpina3 transcription factor mRNA expression in astrocytes treated with tau isolated from AD case 1. Indeed, a recent study demonstrated the striking upregulation of this transcription factor in prion disease patients and moderately in AD patients (Vanni et al., 2017), suggesting a pathway where Serpina3 is increased in neurodegeneration. The results of AD 1 treated astrocytes indicate that there may be a specific molecular phenotype of aggregated tau that can trigger this *SERPINA3* upregulation

in astrocytes. It would be interesting to explore the upstream tau related pathways that play a role in this upregulation in future experiments.

Besides Serpina3, other reactive markers were not upregulated in astrocyte cultures after AD tau uptake. Overall, uptake of tau did not appear to induce a consistent reactive response in these astrocytes, at least in the 7-day timescale tested here. This is perhaps not unexpected, as astrocytes are unlikely to instantly become 'reactive' in response to a relatively acute pathogenic tau treatment that contrasts with the long term pro-inflammatory environment that is present within AD brain. Furthermore, the absence of other cell types, particularly microglia that are intimately linked to astrocytes in their response to disease environments (Vainchtein and Molofsky, 2020), may preclude or reduce the type of response expected in astrocytes. Astrocyte response to tau is likely not a simple negative 'reactive' phenotype, as suggested by others (Chun and Lee, 2018), but may ameliorate the initial progression of tau spread by ingesting and removing pathogenic tau that would otherwise damage the neuronal circuits.

6.3.4 How does tau uptake in astrocytes affect neurons?

The astrocyte conditioned media assays on iPSC-derived neurons indicated that astrocytes do not release any factors or tau fragments after tau uptake that may have a detrimental impact on neuronal health. This is expected considering there is little evidence in this chapter that astrocytes take on a reactive phenotype, and therefore it is unlikely that cells release any commonly associated pro-inflammatory cytokines, chemokines or other factors that can affect neighbouring cells, such as IL3 (McAlpine et al., 2021) or IL6 (Zamanian et al., 2012). Indeed, mRNA expression for these cytokines was tested in astrocytes after tau treatment but was not high enough to be detected (data not shown).

Interestingly, the promotion of neurite outgrowth and complexity indicated by ACM from AD tau treated astrocytes could be linked to S100B. As S100B is secreted by astrocytes (Gerlach et al., 2006), increased levels around AT8 aggregates could lead to increased secretion in these astrocytes. It has previously been seen that low levels of S100B can actually promote neurogenesis and outgrowth (Bhattacharyya et al., 1992; Marshak et al., 1992), stimulate glial cell proliferation in rat astrocytes (Selinfreund et al., 1991), as well as being associated with pathogenic mechanisms of AD (Mrak and Griffin, 2001). It may

therefore be of interest to measure S100B excretion in these astrocytes after AD tau uptake and how this could impact other cells in culture.

6.3.5 Limitations and future directions

No AT8 was observed in neurons, suggesting that astrocytes do not release sufficient tau into the media that is detectable by AT8 antibody. It is also possible that astrocytes do not release tau within the 3 days used to condition media after tau uptake, considering that tau was still found in astrocytes 2 weeks after internalisation in the previous chapter. However, a better mode of interrogation for astrocytes spread to tau would be co-culture experiments with neurons, that might allow synaptic spread of tau to be observed.

As discussed in the previous chapter and described in method section 2.5.4, a Z-stack of images was used to determine that tau was internalised within cells, rather than membrane bound. Again, this was used to determine that high levels of GFAP and S100B were localised around these internalised tau aggregates. While the resolution appeared sufficient to determine this, higher magnification images may be useful in future work to determine at higher resolution the proximity of AT8 positive tau with the observed high abundance of S100B or GFAP molecules.

While the gene expression data was designed to give a broad indication of astrocyte changes, it was very limited in the size of the gene panel. Non-biased RNA-sequencing of astrocyte gene expression changes would allow a deeper investigation into how astrocytes respond to tau uptake, as well as allowing any astrocyte subtypes and differential responses to be measured.

While RNAseq of cell cultures may give more insight into astrocyte response, not all astrocytes internalise tau equally. Therefore, techniques such as laser capture microdissection (Civita et al., 2019) could be employed to take specific astrocytes and examine their genetic changes with single-cell RNA seq.

6.3.6 Conclusions

In summary, the results in this chapter demonstrate a focal response of GFAP and S100B to tau internalisation in astrocytes. These are two proteins that are highly expressed within astrocytes and their changes are often linked to pathological processes in AD and other

neurodegenerative diseases. Furthermore, this did not appear to correlate with reactivity related changes in astrocytes, indicating that astrocyte uptake of tau aggregates may not be detrimental to astrocytes, at least in the early stages of disease. The implications of these results and their relationship to results from previous chapters in this thesis will be explored in more detail in the following discussion chapter.

7 Discussion

While there has been a strong focus on the spread of pathogenic tau around neuronal circuits, this project sought to better understand the relationship between astrocytes and tau spread, for which less is understood. Astrocytes are an abundant cell type of the brain that are diverse in their function and contribution to brain health. With their intimate connections to neurons, they are exposed to pathogenic tau in several ways. A reactive astrocyte phenotype is a hallmark of neurodegenerative disease (Garwood et al., 2017; Escartin et al., 2021), and in some tauopathy cases astrocytes often harbour pathogenic tau inclusions (Kovacs, 2020; Reid et al., 2020). This indicates a clear role association of astrocytes with neurodegenerative processes and the potential for astrocytes to contribute to tau spread. Therefore, the ability of astrocytes to internalise pathogenic tau aggregates was a key question in this project. This then prompted further questions into how astrocytes internalise tau, and how this might induce changes in their function and ability to support neurons.

To investigate these questions, two separate models were utilised. The first results (Chapter 3) built on a previously established *in vivo* model of tau spread in mice to investigate astrocyte association with tau pathology. From these initial observations, a human *in vitro* model of astrocytes was developed in Chapter 4 to further probe the astrocyte interaction with post-mortem brain derived AD tau aggregates (Chapters 5 and 6). (Results from Chapters 5 and 6 are summarised in Figure 7.7.1 and Table 7.1).

The main findings of this thesis were:

- Astrocytes in a htau mouse model of tau spread show some association with tau deposits in the brain that arise from the peripheral injection of pathological tau from different tauopathies in different brain regions, but these showed no overt evidence of tau uptake or a reactive phenotype at the single time point examined.
- Human astrocytes generated from iPSCs increase their mature astrocyte phenotype over extended culture times and express *MAPT* isoforms. They are a suitable model to study astrocytic tau uptake *in vitro*.
- Human iPSC-derived astrocytes readily internalise tau aggregates derived from human postmortem brain and appear begin a process of degradation within 7 days of tau

internalisation. The rate of internalisation and clearance was different depending on the AD case from which tau aggregates were isolated.

- Endogenous GFAP and S100B strongly associate with internalised AD-brain derived tau aggregates in iPSC-astrocytes, however there was no clear evidence of a resulting reactive phenotype.

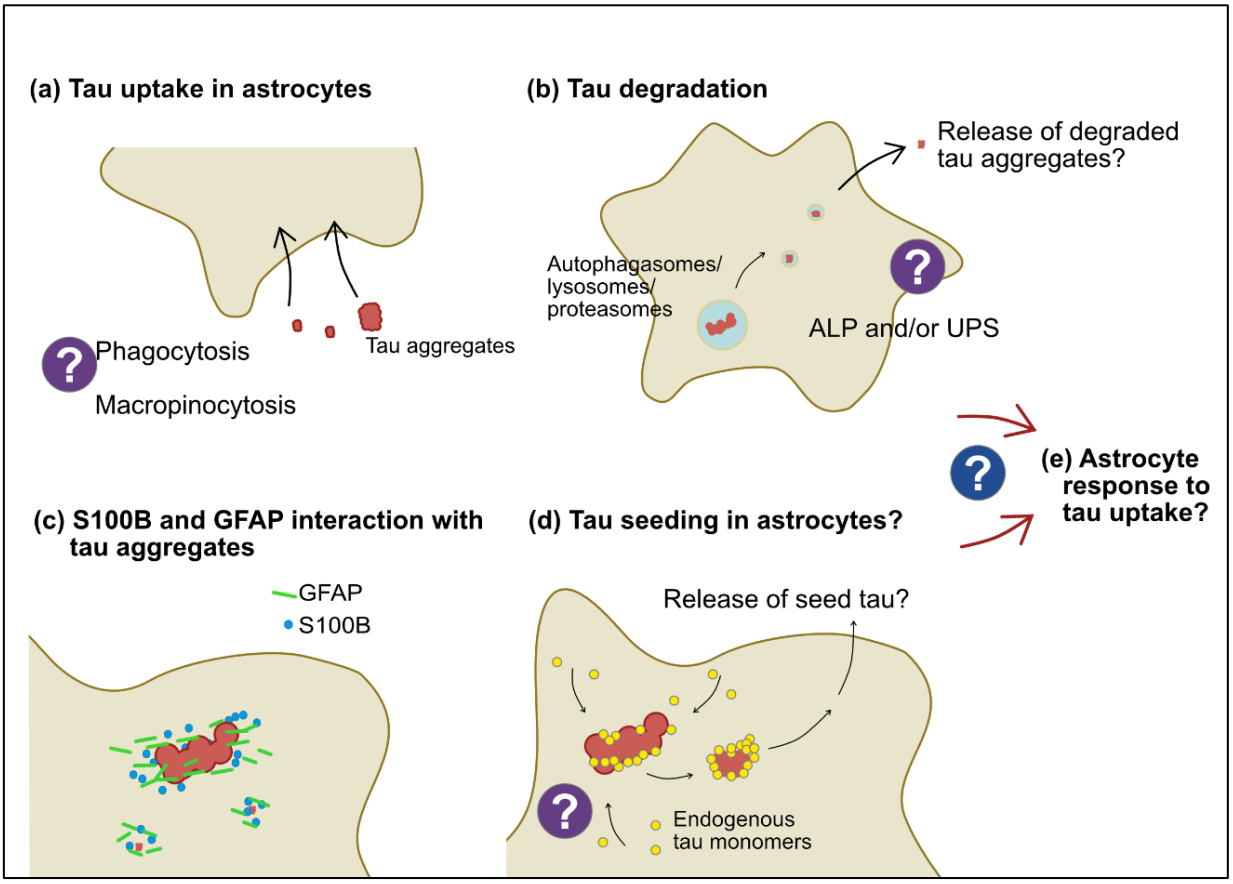

Figure legend on next page…

Figure 7.7.1 Graphical summary of iPSC-astrocyte response to tau uptake, highlighting unresolved questions.

Graphical representation of astrocyte interaction with tau as determined by results in this thesis. (**a**) After 7-day exposure to tau aggregates, day 60 iPSC-astrocytes showing a mature astrocyte phenotype (Chapter 4) were found to readily internalise AD brain derived sarkosyl-insoluble tau aggregates (Chapter 5). The exact mechanism of tau uptake remains undetermined, but a combination of phagocytosis and receptor mediated showed that astrocytes appear to degrade or otherwise clear tau since the tau aggregates progressively decreased in size and the fluorescence intensity of AT8 labelling was reduced (Chapter 5). The exact contribution of degradation pathways including the autophagy-lysosomal pathway (ALP) or the ubiquitin-proteasome system (UPS) in tau clearance remains to be established. (**c**) S100B and GFAP molecules were found to localise around internalised tau aggregates (Chapter 6), and these persisted as the size and intensity of tau aggregates decreased. How this affects the ability of astrocytes to process remaining tau aggregates or the implications for tau seeding are interesting points for future investigation. (**d**) The tau aggregates derived from some (but not all) AD cases showed a relative increase in size and immunofluorescence intensity following the removal of tau from media. This may indicate seeding of endogenous astrocytic tau since astrocytes were found to express multiple *MAPT* isoforms (Chapter 3). (**e**) Finally, no clear evidence of a reactive phenotype in AD tau treated astrocytes was found (Chapter 6), and medium from astrocytes exposed to AD tau caused no detrimental effects on neurons. Interestingly, a common theme was that astrocytes showed different responses to tau isolated from different AD cases. This may indicate consequences of molecular characteristics of tau on and retention. Longer term experiments and broader interrogation of genetic and functional changes may unearth changes to astrocytes after pathogenic tau uptake.

7.1 The role of astrocytes in tau spread

Although the majority of research has focused on tau spread via synaptically connected neurons, evidence of astrocyte uptake of tau has also emerged in published studies. Tau aggregate spread along anatomically connected circuits was beautifully demonstrated in two mouse models in which mutant human P301L tau expression was restricted to layer II neurons in the entorhinal cortex. Tau aggregates were observed to form in these neurons, and with aging tau was found to spread trans-synaptically to the dentate gyrus and seed further tau aggregation (De Calignon et al., 2012; Liu et al., 2012). Notably, De Calignon et al (2012) observed GFAP-labelled astrocytes in the dentate gyrus that contained PHF1-positive aggregates. These astrocytes express only trace levels of tau, suggesting that the astrocytes have internalised tau. Interestingly, Hillar astrocytes in the dentate gyrus were recently shown to contain tau aggregates in AD (Richetin et al., 2020), suggesting that this may be a common event in tauopathies. This is in contrast to the mouse model analysed in Chapter 3 of this thesis. While some association with tau pathology was observed, there was

no clear colocalization of pathological tau and astrocytes that might indicate astrocytic tau uptake. The differences between these models may explain these discrepancies. While there was increased tau burden in the htau model examined, the exact mechanism of this increase can only be inferred considering only one timepoint was examined in this model. Moreover, since tau was peripherally injected, the exact entry point for tau seeds from tauopathy brain extract is not clear, and if tau enters through a leaky blood brain barrier (Ryu and McLarnon, 2009), this may lead to multiple entry points. Therefore, tracking spread of tau through brain circuits becomes difficult. It is not clear if pathological tau was actively spreading through anatomically connected neuronal circuits, or if excess tau burden was triggered in specific vulnerable regions after the injection of tauopathy brain extract. Furthermore, while MC1 positive structures were observed, evidence of larger tau aggregates was sparse. It appeared likely that the MC1 labelling was localised predominantly to neuronal cell bodies. A lack of neuritic MC1 staining may indicate that tau may not be spread trans-synaptically, reducing the points at which astrocytes can uptake tau. Moreover, clear extracellular tau aggregates were not observed that might parallel the 'ghost tangles' often observed in AD cases ((Probst et al., 1982; Perez-Nievas and Serrano-Pozo, 2018), a source by which astrocytes could directly internalise exogenous tau aggregates. These factors may have worked in combination to reduce the exposure of astrocytes to aggregated tau in this mouse model. It is also important to consider that the timepoint at which mouse brains were analysed may represent a late-stage of disease, and that evidence of tau spread has been missed. Rather, the tau aggregates apparent may be as a consequence of reduced degradation capacity of specific neuronal subsets as suggested by others (Fu et al., 2018; Blaudin de Thé et al., 2021; Schaler et al., 2021). Nevertheless, this model showed that there may be selective regional vulnerability to different forms of tau, an interesting area that it was not possible to study in previously published models that relied upon regionally targeted expression or induction of pathological tau.

It seems likely that mouse astrocytes are capable of internalising tau *in vivo* and recent studies have demonstrated this more clearly. Another human tau expressing mouse model showed that astrocytes harbour tau inclusions and display relevant astrocyte tau pathology such as tufted astrocytes (PSP) and astrocytic plaques (CBD) when brains were directly injected with specific tauopathy brain derived extracts (He et al., 2020). This direct brain injection of human tau expressing mice allowed tracking of tau spread and consistent

exposure of astrocytes in injected regions to high levels of pathological tau. Another study observed some uptake of AT8 positive tau in astrocytes after initiation of mutant tau propagation from the entorhinal cortex (Asai et al., 2015). This model utilised rapid tau propagation in C57BL/6 mice induced by an adenoviral vector expressing P301L mutant tau under the control of a neuronal specific promoter. This was likely able to produce higher levels of tau pathology compared to that induced by peripheral injection of tauopathy brain extract that was indicated in the mouse model examined in Chapter 3. Others have also shown uptake of preformed tau fibrils in primary astrocytes (Martini-Stoica et al., 2018).

In a previous mouse model of tau spread, tau strains inoculated from multiple seeding sources, including AD, CBD and CTE post mortem tissue, as well as recombinant tau cell lines, were utilised to look at the ability of different tau strains to alter tau pathology *in vivo* (Kaufman et al., 2016). After injection into transgenic mice expressing the PS19 tau mutation, mice developed unique regional vulnerability dependent on tau strain, as well as cell type vulnerability that included CBD and PSP like astrocyte pathology. This indicates that it would be possible to seed this type of astrocyte pathology in mouse astrocytes. However, the expression of mutant tau in the mouse model explored in Kaufman et al. (2016) may have increased the exposure of astrocytes to tau aggregates compared to the htau model examined in Chapter 3. Furthermore, the tau strains developed that induced the astrocyte pathology described by Kaufman et al. (2016) were not those derived from CBD brain, but rather were recombinant fibrils. While this still provides evidence that astrocytes can react differently to specific tau strains in mice, it does not prove a direct link between the properties of CBD derived tau and astrocyte seeding ability, at least in this mutant mouse models used in the described study. Therefore, the human iPSC-astrocyte model developed in this project provided a model in which to further study tau uptake by human astrocytes.

The uptake of AD derived tau aggregates in astrocytes was confirmed in Chapter 5 by experiments using human iPSC-derived astrocytes that were established in Chapter 4. This is important because so far, direct evidence of tau uptake by human astrocytes is lacking *in vitro*. The AD-derived tau from all postmortem cases was readily internalised by these astrocytes, however, key questions remain as to the mechanism of this uptake (Figure 7.7.1a). While tau monomers have been observed to be taken up by specific mechanisms including those mediated by HSPGs (Perea et al., 2019), uptake of larger tau aggregates is not as well studied. In primary mouse astrocytes, Martini-Stoica et al. (2018) indicated that

uptake of preformed tau fibrils was reduced by competitive action of heparin which disrupted tau binding to HSPGs, which have previously been shown to mediate protein aggregate internalisation in neurons (Holmes et al., 2013). This implicates macropinocytosis as a route for tau aggregate internalisation by astrocytes in disease. Interestingly, Holmes et al. (2013) showed that tau enters neural precursor cells in a fluid-phase endocytosis process that does not require clathrin- or caveolin- mediated endocytosis (Holmes et al., 2013). Asai et al. (2018) showed that mouse microglia efficiently phagocytose tau aggregates *in vivo* and *in vitro*, and in these experiments, astrocytes were also observed to phagocytose tau, although significantly less than microglia, and this process that was inhibited by the introduction of cytochalasin D, which disrupts phagocytosis. The discrepancy between astrocytes and microglia in phagocytosis efficiency has been noted previously (Magnus 2002, Loov 2015, Konishi 2022). Indeed, microglia may be responsible for the majority of protein aggregate clearance in neurodegeneration since they appear better tuned for this process. Nonetheless, astrocytes are present in far larger numbers than microglia, and this does not discount the ability of a large number of astrocytes to phagocytose small amounts of aggregates each and it appears this has been overlooked in the past (Konishi et al., 2022).

The results in Chapter 5 may indicate phagocytosis as a means of uptake of large tau aggregates by astrocytes, since the uptake process continued across 7 days and was relatively slow. It would be interesting to compare this timeframe to that of human microglia. This speed of uptake, along with the size of some of the observed internalised aggregates that were beyond the 0.5 µm (some large internalised aggregates were over 10 µm length), which is indicated as a threshold for phagocytic uptake (Paul et al., 2013), further indicate that phagocytosis may be responsible for at least some of the tau uptake observed. If this is the case, specific selection of tau for uptake may not be necessary, as non-selective phagocytic uptake of latex beads in primary astrocytes has previously been observed *in vitro* (Martini-Stoica et al., 2018). However, the size of the particles may change the selectivity of tau uptake, as is evident in a study that showed that low-molecular weight tau aggregates and short fibrils are readily internalised into neurons by bulk endocytosis, whereas monomers, long fibrils and long filaments are not (Wu et al., 2013). Indeed, Martini-Stoica et al. (2018) noted that uptake of preformed tau fibrils could be reduced by competitive binding of heparin to HSPG, indicating that macropinocytosis plays a role in tau fibril uptake in astrocytes. This suggests size and conformation of tau are also important for uptake. For

astrocytes that are likely to have a better ability to phagocytose particles than neurons (Konishi et al., 2022), there may be further routes for tau uptake that are not dependent on specific HSPG or other specific mechanisms.

The uniformity in size of tau fibrils extracted from AD brain used in this study was difficult to regulate, especially with unpredictability introduced when the sarkosyl insoluble pellets were sonicated. While ICC indicated that large tau fibrils were present in the human brain samples and in iPSC-astrocytes, it is certain that smaller tau aggregates are also present in the samples used for spiking, and these different tau species may be internalised by different mechanisms. If tau aggregates were conjugated with fluorescent tags, live cell imaging could be used to determines if different size of tau aggregates are internalised at different rates. However, some fluorescent tags will significantly increase the size of the aggregates and have been shown to alter the biological properties of tau (Li et al., 2011) and so these data would have to be interpreted with caution. Further, selective inhibition of different endocytic processes, such as using cytochalasin D to inhibit phagocytosis, or treatment with heparin to block HSPG attachment and inhibit macropinocytosis, could further elucidate mechanisms of tau uptake by astrocytes. Overall, the process of uptake requires further study, but it appears likely that the different tau species (monomers, oligomers and larger aggregates) may be internalised into astrocytes by different mechanisms.

Table 7.1 Summary of changes to iPSC-astrocytes after treatment with AD derived tau or equivalent control brain extracts.

Day 60 iPSC-astrocytes were treated for 7 days with 0.1 ng / µL of sarkosyl-insoluble tau extracted from six AD cases or equivalent extracts from three control brains and compared to untreated astrocytes. In additional experiments, tau was removed from media after 7 days, and tau retention by astrocytes was measured at day 14 and 21. The table here summarises data from Chapters 5 and 6 for each case relative to untreated to compare responses to different sources of tau. Green upward and red downward arrows indicate increase and decrease from untreated, respectively. Results that were approximately in line with controls are indicated by a horizontal yellow bar. Blue bar chart symbols indicate the relative intensity of S100B and GFAP at sites of internalised tau aggregates between different AD cases. Horizontal green bars indicate the relative rate of tau internalisation between astrocytes exposed to tau aggregates from different AD cases. Yellow highlights indicate significant changes, whereas red highlights indicate data that showed significant variability. ACM = astrocyte conditioned media.

Data is summarised from the following thesis sections: 'Tau aggregate uptake (7 day treatment)' and 'Rate of uptake' data from Section 5.3.4. 'Astrocyte tau aggregates (aggs) after treatment' data at day 14 and 21 is from Section 5.3.5. 'GFAP cell average (ICC)' and 'GFAP global expression (mRNA)' and 'GFAP at tau aggregates (aggs)' is from Section 6.2.1. 'S100B cell average (ICC)' and 'S100B global expression (mRNA)' and 'S100B at tau aggregates (aggs)' data is from Section 6.2.2. '% dying cells change' and 'cell morphology change' data is from Section 6.2.3. All 'Gene expression changes after 7-day treatment' data is from Section 6.2.4. All 'ACM effect in neurons' data is from Section 6.2.5.

	Tau uptake and clearance				Changes to astrocytes after tau uptake (7 day treatment)								Gene expression changes after 7 day treatment							ACM effect on neurons	
Assay	Tau aggregate uptake (7 day treatment)	Rate of uptake	Astrocyte tau aggs after treatment - day 14	Astrocyte tau after treatment - day 21	GFAP cell average (ICC)	GFAP global expression (mRNA)	GFAP at tau aggs	S100B cell average (ICC)	S100B global expression (mRNA)	S100B at tau aggs	% dying cells change	Cell morphology change	C3	C3aR	SERPINA3	TFEB	LRP1	STAT3	NRF2	Neurite legnth/complexity after ACM	AT8 in neuronal cell body after ACM
Ctr 1	–	n/a	–	–	▼	–	n/a	–	▼	n/a	▼	–	▲	▲	–	▲	▲	▲	▲	–	–
Ctr 2	–	n/a	–	–	▼	▼	n/a	–	▼	n/a	▼	–	–	▼	–	▲	▲	▲	▲	–	▼
Ctr 3	–	n/a	–	–	▼	–	n/a	▲	▼	n/a	▼	–	–	▲	▲	▼	▼	–	▲	▲	–
AD 1	▲		▼	▲	▼	–		▲	▼		▼	–	▲	–	▲	▼	–	–	▲	▲	▲
AD 2	▲		▼	▲	–	▲		–	–		▼	–	▲	–	–	▼	▼	–	▲	▲	–
AD 3	▲		▼	▼	▲	▲		▲	▲		▼	–	▲	▼	–	▲	▲	▲	–	▲	–
AD 4	▲		▼	▲	▲	▲		▲	▼		▼	–	▲	▲	▲	▼	▲	▼	▲	▲	–
AD 5	▲		▼	▼	▲	▲		▲	▲		▼	–	▲	–	–	▼	▼	▼	▲	▲	▼
AD 6	▲		▼	▼	–	▲		▲	–		–	–	–	▼	▼	▼	▼	▼	▲	▲	▲

The next question is how astrocytes process and clear tau once internalised (Figure 7.7.1b). It is possible that the lack of tau inclusions observed in astrocytes of the htau mouse model in Chapter 3 is partly down to efficient processing of tau by these astrocytes. Martini-Stoica (2018) and colleagues showed that *TFEB*, a transcription factor considered as a master regulator of lysosome genesis, is upregulated and correlates with higher Braak staging in AD brain and was also found at higher levels in the brains of cases diagnosed with frontotemporal dementia (FTD). Furthermore, *in vitro* they showed that up-regulating TFEB expression caused enhanced uptake of preformed tau fibrils by primary mouse astrocytes. TFEB expression in iPSC-astrocytes was examined after 7-day exposure to tau aggregates from AD brain (Chapter 6), but changes were variable between repeats and no clear changes emerged. In order to further investigate astrocyte processing of tau, future experiments could interrogate multiple aspects of the autophagy lysosome pathway (ALP) and ubiquitin proteasome system (UPS). Interestingly, Asai et al. (2015) found that while there was an abundance of ubiquitinated tau in the cell lysates of primary mouse microglia that had internalised mutant tau aggregates, there was relatively little ubiquitinated tau in lysates from astrocytes, indicating that the UPS is likely not a primary mechanism for tau degradation in astrocytes. Large insoluble tau aggregates that are absorbed by iPSC-astrocytes may not be efficiently degraded by the UPS, as has been shown with large insoluble TDP-43 aggregates in human neuroblastoma and embryonic kidney cells (Scotter et al., 2014). In fact, large protein aggregates from neurodegenerative diseases can inhibit the proteasome (Thibaudeau et al., 2018). Interestingly, proteasome dysfunction in AD brain appears to directly correlate with the burden of tau PHFs that specifically co-precipitate with proteasomes (Keck et al., 2003). In the data presented in this thesis, tau aggregate size and intensity of AT8 staining decreased substantially in iPSC-astrocytes 7 days after the removal of tau from the media, indicating that astrocytes can degrade tau to some extent. Future experiments are needed confirm the contribution of specific degradation and clearance pathways, however there is substantial evidence that ALP is the primary (but not exclusive) route of degrading phosphorylated tau (Rodríguez-Martín et al., 2013), and while this may not be true for all tau species, as discussed above, ALP may be a major contributor to the astrocyte degradation of pathological tau.

For astrocytes to contribute to tau spread, they would need to be able release tau in a form that can be taken up by other cell types and seed endogenous tau in those cells. While Asai

et al. (2015) provided evidence that microglia exocytose internalised tau, no tau was detected in exosomes from astrocytes in this work. This is contrast with a recent paper which showed that primary human astrocytes release phosphorylated tau into media in association with exosomes, and that this process was enhanced upon exposure of the cells to $A\beta_{25-35}$ (Chiarini et al., 2017). Observations here in iPSC-astrocytes exposed to AD tau extracts indicated that some extracellular tau colocalises with GFAP (data not shown). This may indicate that tau aggregate fragments are exocytosed into the media, or that GFAP released by degenerating astrocytes attaches to extracellular tau that could be bound to tissue culture plates. Considering that the data in Chapter 6 shows that GFAP strongly associates with internalised tau aggregates, it appears possible that tau was co-released with GFAP, and this requires further exploration.

Once tau aggregates are internalised, further questions arise as to the potential for seeding of endogenous astrocytic tau, since it was shown in Chapter 4 that iPSC-astrocytes express all *MAPT* isoforms. In a tau aggregate clearance system developed in human embryonic kidney cells, preformed tau fibrils were shown to be internalised and efficiently cleared in the absence of soluble tau and this occurred, at least in part, by the ALP system (Guo et al., 2016). Upon inducible expression of soluble mutant tau in these cells, the authors demonstrated that the introduction of even small amounts of exogenous tau led to a rapid recovery of tau pathology within cells due to residual tau aggregates that were not cleared. This is interesting because the data in Chapter 5 of this thesis indicated potential signs of further tau aggregation, based on intensity and size measurements, two weeks after tau was removed from culture medium, for at least two of the groups exposed to AD-derived tau. Since none of the astrocytes had completely cleared the internalised tau within this two-week timeframe, this may indicate the potential for tau seeding in astrocytes. This may be reflective of disease mechanisms that were recently published, which show that tau spread occurs only in the earliest stages of disease, and that this is followed by replication of small numbers of tau seeds (Meisl et al., 2021).

Overall, this project indicates that while astrocytes may begin to clear internalised tau aggregates, seeding activity may also occur simultaneously. This is an important consideration when studying the dynamics of tau spread, where the balance between uptake, degradation and seeding are important to consider.

7.2 Molecular heterogeneity of tau

Differences observed in the rate of uptake of AD tau and its degradation over time by astrocytes may be related to molecular heterogeneity of AD tau derived from different postmortem cases. Emerging evidence has revealed patterns of tau pathology in AD, showing that this is not as consistent as once suggested by Braak staging (Braak et al., 2011), with four distinct patterns emerging in a large cohort of 1,612 cases, two of which were atypical variations of known spreading patterns and that also showed clinical heterogeneity (Vogel et al., 2021). This may be caused by variations in the post-translational modifications of tau, which also differ considerably between cases. A recent study used tau derived from post-mortem brain tissue from 32 non-familial AD cases to study molecular properties and seeding potential of tau. Interestingly, they discovered large heterogeneity among the tau samples examined, with specific phosphorylation sites that correlated with higher or lower tau seeding rates *in vitro*, and which also correlated with spreading patterns and clinical severity (Dujardin et al., 2020). This study indicated the broad variations of tau modifications that may drastically effect tau spread in AD, and it is possible that these features could impact the ability of astrocytes to uptake, process and seed pathological forms of tau. A more thorough examination of the modifications and other biophysical properties of tau species in the AD sarkosyl insoluble fractions used in this project would help to uncover any correlations between properties of tau and the parameters examined, and it would be interesting to note if specific modifications could induce astrocyte changes that might differ from other cell types of the brain.

Further analysis of the aggregation kinetics of these AD samples from the aforementioned study found that the morphology of the tau seed (the size and circularity) impacted the growth phase in a cell-based biosensor tau seeding assay (Kamath et al., 2021). For the tau extracts used in this thesis, the size of aggregates was not determined pre-treatment, and sonication may have altered some of the preformed shapes of these aggregates. Examination of the morphological properties of sarkosyl-insoluble tau species isolated from each AD case, as well any abnormal tau species isolated from control brain, would further help to correlate results in this thesis with tau properties. Table 7.1 compares the data obtained using AD brain-derived tau that is presented in Chapters 5 and 6. While some parameters, such as tau seeding and internalisation rate, were quite consistent between

cases, there was considerable variation between samples for other parameters, however there were no definitive patterns that allow further conclusions to be made.

While rates of tau internalisation and degradation from separate AD cases were explored, there may be merit in combining the data of separate AD and control cases in order to increase analysis power. Indeed, this may be more pertinent in this thesis considering the work did not take into account the molecular properties of tau derived from each AD case, which are yet to be determined. Still, the differences observed in astrocyte response may warrant the further exploration of each case individually.

7.3 Astrocyte reactivity and function in tauopathies

Because astrocyte reactivity correlates with disease progression in tauopathies and other neurodegenerative diseases including AD (Vehmas et al., 2003; Serrano-Pozo et al., 2011; Escartin et al., 2021), evidence of a 'reactive' astrocyte phenotype following the internalisation of AD tau was expected. However, the evidence in Chapter 6 indicates that the short-term internalisation of aggregated AD derived tau was not sufficient to induce a robust reactive phenotype.

The process of astrocyte transformation into a reactive state is not instantaneous and likely follows an accumulation of changes that eventually induces a reactive phenotype. Indeed, a spectrum of reactive phenotypes may exist in the brain depending on the environmental and cell signalling cues in the local environment of astrocytes (Jiwaji and Hardingham, 2022). New evidence has demonstrated the heterogeneity of astrocyte subtypes in the non-diseased brain (Miller, 2018; Batiuk et al., 2020); and how these different subtypes respond to the pathogenic environment of the neurodegenerative brain is yet to be determined, but it is logical to suggest that astrocyte subtype differences may play a role in the regional vulnerability that is observed in different tauopathies. A recent study in transgenic mouse models showed that astrocytes develop both neuroprotective responses to tau pathology in addition to deleterious responses that are characterised by neuroinflammatory pathway upregulation, amongst others. At the core of this wide ranging genetic response was *NRF2*, a master regulator of protective downstream pathways (Jiwaji et al., 2022). Experiments from Chapter 6 showed that *NRF2* was not consistently upregulated in iPSC astrocytes following their exposure to and internalisation of AD tau aggregates. Only one reactivity

related gene, *SERPINA3*, was significantly upregulated following exposure to tau from one AD case. This may indicate specific properties of abnormal tau from this AD case that are sufficient to induce a SerpinA3 response, indicating that in some instances tau uptake can induce reactive changes in astrocytes. However, with the breadth of genotypic changes associated with reactive astrocytes, unbiased RNA transcriptomics would be a crucial tool to employ in the future to more thoroughly analyse the spectrum of astrocyte responses resulting from the internalisation of AD tau aggregates by human iPSC-astrocytes.

The tau pathology observed in the htau mouse model examined in Chapter 3 also did not show robust evidence of astrocyte reactivity, over and above the astrogliosis noted in this model relative to wild-type mice (Garwood et al., 2010). This included in the regions that appeared most vulnerable to different forms of tau. This might be since the burden of tau aggregates was not significantly elevated above those already present, or because the astrocytes are already reactive and further changes were not sufficiently large to be detected. He et al. (2020) showed tau in astrocytic inclusions but no evidence of a reactive astrocytic response, as quantified by the number of GFAP positive astrocytes in the hippocampus (near the injection site) compared to controls. This means that the astrocytic plaques in astrocytes in CBD injected mice were not caused by their activation, nor did they lead to a reactive 'high GFAP' response, but simply exemplified a selective uptake and retention of CBD tau strains, as might be expected for tau isolated from brain that has common astrocyte tau inclusions (Dickson et al., 2002). Indeed, astrocytes may be resilient to the early effects of tau uptake, equivalent to early stages of disease, rather acting to clear tau and other aberrant proteins as others have suggested (Tsunemi et al., 2020; Jiwaji and Hardingham, 2022). Indeed, the HEK cells used in Guo et al. (2016) were able to hold tau fibrils over extended time periods without a large impact on the ALP or UPS system, or on astrocyte health. This may be similar to iPSC-astrocytes used here, and it would be interesting to determine if residual tau aggregates in iPSC-astrocytes cause long-term damage to astrocyte degradation processes, astrocyte function or health. In AD brain, neurons containing tau fibrils develop autophagic vacuoles (Nixon et al., 2005), indicating they are more vulnerable to this type of damage than astrocytes. However, with sufficient time, it is possible that a build-up of resistant tau fragments may disrupt the degradation machinery in astrocytes, with downstream consequences that could transform astrocytes into a reactive phenotype that could exacerbate tau pathology.

7.4 Astrocyte-neuron interactions in tauopathies

While astrocytes are crucial for normal function of neurons (Section 1.4.2), it therefore follows that their deleterious alteration in tauopathy brain could exacerbate disease pathology. In a primary mouse model of AD, it has been reported that the presence of astrocytes can exacerbate Aβ induced neurotoxicity, as well as being crucial for Aβ induced tau phosphorylation in primary neurons (Garwood et al., 2011; Perez-Nievas et al., 2021). This indicates that a neuroinflammatory environment induced by toxic Aβ oligomers are sufficient to induce astrocyte changes that are detrimental to nearby neurons. The authors of these and other studies (Ahmed et al., 2010) used oligomeric Aβ1-42, or Aβ oligomers secreted by neurons from *APP* over-expressing mice, which are widely considered to be more toxic than Aβ fibrils themselves. This may also be the case with tau, where is has also been suggested that oligomeric mutant tau is more toxic than mature tau fibrils (Ghag et al., 2018). However, this study also showed that sonication of tau fibrils created soluble toxic oligomers, and so this reiterates the need to fully characterise the properties of the AD derived tau species used to treat iPSC-astrocytes in this project. The apparent positive effect of ACM on neurite growth observed in Chapter 6 is likely further evidence that astrocytes had not entered into a reactive state that resulted in the secretion of proinflammatory cytokines or reactive oxidative species such as NO into the media, that might ameliorate neurite outgrowth (Linnerbauer et al., 2020). Furthermore, there was no clear evidence of AT8 positive tau being released into the media of astrocytes and being internalised by these neurons. Longer term experiments and direct analysis of tau in the media of pre-treated astrocyte cultures would help to elucidate how astrocytes release tau and if this is in a form that can be internalised by neurons.

Astrocytes are also critical for synapse function (Lee et al., 2020). In neurodegenerative diseases, functional changes in astrocytes contribute to synaptic dysfunction (Henstridge et al., 2019). By phagocytosing neuronal synapses that contain pathogenic tau fibrils, astrocytes may be helping to clear pathogenic tau. However, if the degradation pathways start to become disrupted by the build-up of tau that is resilient to clearance, then this process may be impaired and lead to a dysregulation of synaptic pruning, the accumulation of extracellular seed competent tau species that can be spread between neurons, and this may be one route by which astrocytes contribute to the spread of tau in disease.

7.5 Future work

In addition to the continuation of some experiments suggested in this discussion, a key progression of the assays developed in this project is needed to compare the internalisation of tau aggregates derived from different tauopathies. While the difficulties in isolating tau aggregates from PSP and PiD prevented these sources of tau being investigated in the iPSC-astrocyte model (highlighting their inherent structural differences and solubility properties), the work in this thesis has provided a strong foundation for comparing the uptake and retention of pathological tau from different tauopathies in human astrocyte cultures. Certainly, recent studies that have revealed the structural conformation of PSP tau filaments (Shi et al., 2021) and have used different protocols for tau aggregate extraction compared to the isolation of AD tau aggregates (Fitzpatrick et al., 2017). This provides a starting point for optimising the extraction of aggregates from PSP and other tauopathies tau. Furthermore, selecting brain regions that show the highest burden of tau pathology will facilitate this work. Kaufman et al. (2017) found that seed competent tau can be extracted from fixed human tissue, which gives the potential for tau pathology to be thoroughly examined by IHC prior to case selection.

Broader, unbiased approaches for analysing changes to astrocytes after tau uptake will also be beneficial. Single cell RNA sequencing (scRNAseq) provides a tool to interrogate changes in gene expression in astrocytes. Further, these changes could be mapped over long-term exposure to tau aggregates, as well as being used to compare differences in astrocyte gene expression after the uptake of different tauopathy strains. Longer term cultures may also allow any reactive phenotype of astrocytes and their impact on neurons to investigated in a co-culture environment. Furthermore, the addition of toxic Aβ oligomers along with AD tau aggregates may also help to understand the interplay between these two pathogenic proteins that drive reactivity changes in astrocytes in AD. Another approach for the mouse model would be to combine spatial transcriptomics with *in situ* sequencing, as has been elegantly used to study gene expression changes in specific cell types around plaques in a mutant human APP over-expressing mouse line (Chen et al., 2020).

The ability of internalised tau aggregates to recruit endogenous tau is certainly worth exploring, as this has large implications for how tau spreads in neurodegeneration. If the brain derived tau aggregates used here could be covalently bonded to a fluorescent tag, or

if endogenous tau expression in astrocytes could be modified to include a fluorescence reporter, then this would allow a tau seeding assay to be developing in iPSC astrocytes, similar to others have produced in HEK cells (Kamath et al., 2021)

Another key area of exploration is the ability of astrocytes to spread tau to different cell types. This would be best explored in a co-culture environment. The co-culture of untreated neurons with astrocyte pre-exposed to tau aggregates would allow the spread of pathogenic tau to neurons to be visualised, especially if they are able to form synaptic connections with sufficient time in culture, as has previously been shown in optimisation of cellular models (Aebersold et al., 2018).

7.6 Summary and conclusions

Astrocytes are a relatively overlooked cell type when studying the spread of pathological forms of tau in disease. This project has given insight into their ability to respond to pathological tau *in vivo* and internalise AD derived tau aggregates *in vitro*, which appear relatively stable within astrocytes for weeks. Moreover, this project has elucidated aspects of the GFAP and S100B response to internalised tau aggregates, the dysregulation of both being strongly associated with the progression of AD and other tauopathies. Finally, this work has shown that short-term tau internalisation by astrocytes may not be sufficient to induce a reactive response in these astrocytes. These results, along with the human iPSC-astrocyte cell model optimised in this thesis, provide a solid foundation with which to interrogate many remaining questions including specific mechanisms involved in tau uptake, processing, and release/spread to other cells, and the complex interactions between them. These questions may be crucial in fully understanding the ability of pathological tau to spread throughout tauopathy brain, and the selective vulnerability of different neural cells or brain regions to tau species.

8 Reference List

Abramov AY, Canevari L, Duchen MR (2003) Changes in intracellular calcium and glutathione in astrocytes as the primary mechanism of amyloid neurotoxicity. J Neurosci 23:5088–5095 Available at: https://pubmed.ncbi.nlm.nih.gov/12832532/ [Accessed July 17, 2022].

Acosta C, Anderson HD, Anderson CM (2017) Astrocyte dysfunction in Alzheimer disease. J Neurosci Res 95:2430–2447.

Aebersold MJ, Thompson-Steckel G, Joutang A, Schneider M, Burchert C, Forró C, Weydert S, Han H, Vörös J (2018) Simple and Inexpensive Paper-Based Astrocyte Co-culture to Improve Survival of Low-Density Neuronal Networks. Front Neurosci 12:94.

Ahmed M, Davis J, Aucoin D, Sato T, Ahuja S, Aimoto S, Elliott JI, Van Nostrand WE, Smith SO (2010) Structural conversion of neurotoxic amyloid-β1–42 oligomers to fibrils. Nat Publ Gr.

Ahmed Z, Bigio EH, Budka H, Dickson DW, Ferrer I, Ghetti B, Giaccone G, Hatanpaa KJ, Holton JL, Josephs KA, Powers J, Spina S, Takahashi H, White CL, Revesz T, Kovacs GG (2013) Globular glial tauopathies (GGT): Consensus recommendations. Acta Neuropathologica 126:537–544.

Aisen PS, Cummings J, Jack CR, Morris JC, Sperling R, Frölich L, Jones RW, Dowsett SA, Matthews BR, Raskin J, Scheltens P, Dubois B (2017) On the path to 2025: understanding the Alzheimer's disease continuum. Alzheimers Res Ther 9 Available at: https://pubmed.ncbi.nlm.nih.gov/28793924/ [Accessed July 14, 2022].

Allaman I, Bélanger M, Magistretti PJ (2011) Astrocyte-neuron metabolic relationships: for better and for worse. Trends Neurosci 34:76–87 Available at: https://pubmed.ncbi.nlm.nih.gov/21236501/ [Accessed May 3, 2022].

Allen DE, Donohue KC, Cadwell CR, Shin D, Keefe MG, Sohal VS, Nowakowski TJ (2022) Fate mapping of neural stem cell niches reveals distinct origins of human cortical astrocytes. Science 376:1441–1446 Available at: https://pubmed.ncbi.nlm.nih.gov/35587512/ [Accessed July 17, 2022].

Amiry-Moghaddam M, Frydenlund DS, Ottersen OP (2004) Anchoring of aquaporin-4 in brain: Molecular mechanisms and implications for the physiology and pathophysiology of water transport. Neuroscience 129:997–1008

Andorfer C, Acker CM, Kress Y, Hof PR, Duff K, Davies P (2005) Cell-cycle reentry and cell death in transgenic mice expressing nonmutant human tau isoforms. Journal of Neuroscience 25:5446–5454.

Andorfer C, Kress Y, Espinoza M, de Silva R, Tucker KL, Barde Y-A, Duff K, Davies P (2003) Hyperphosphorylation and aggregation of tau in mice expressing normal human tau isoforms. J Neurochem 86:582–590 Available at: http://www.ncbi.nlm.nih.gov/pubmed/12859672.

Andreadis A (2005) Tau gene alternative splicing: Expression patterns, regulation and modulation of function in normal brain and neurodegenerative diseases. Biochimica et Biophysica Acta - Molecular Basis of Disease 1739:91–103.

Anthony TE, Heintz N (2007) The folate metabolic enzyme ALDH1L1 is restricted to the midline of the early CNS, suggesting a role in human neural tube defects. Journal of Comparative Neurology 500:368–383 Available at: https://onlinelibrary.wiley.com/doi/10.1002/cne.21179.

Antosiewicz-Bourget J, Tian S, Slukvin II, Ruotti V, Smuga-Otto K, Nie J, Thomson JA, Yu J, Frane JL, Vodyanik MA, Jonsdottir GA, Stewart R (2007) Induced Pluripotent Stem Cell Lines Derived from Human Somatic Cells. Science (1979) 318:1917–1920 Available at: http://www.sciencemag.org/cgi/content/abstract/318/5858/1917%5Cnhttp://www.sciencemag.org/cgi/content/full/318/5858/1917.

Apple B (2013) Nonmammalian vertebrate glia. Neuroglia:24–31.

Arai T, Ikeda K, Akiyama H, Tsuchiya K, Yagishita S, Takamatsu J (2001) Intracellular processing of aggregated tau differs between corticobasal degeneration and progressive supranuclear palsy. NeuroReport 12:935–938.

Arakhamia T, Lee CE, Carlomagno Y, Duong DM, Kundinger SR, Wang K, Williams D, DeTure M, Dickson DW, Cook CN, Seyfried NT, Petrucelli L, Fitzpatrick AWP (2020) Posttranslational Modifications Mediate the Structural Diversity of Tauopathy Strains. Cell 180:633-644.e12 Available at: https://doi.org/10.1016/j.cell.2020.01.027.

Arcuri C, Giambanco I, Bianchi R, Donato R (2002) Annexin V, annexin VI, S100A1 and S100B in developing and adult avian skeletal muscles. Neuroscience 109:371–388 Available at: https://pubmed.ncbi.nlm.nih.gov/11801372/ [Accessed July 18, 2022].

Armstrong MJ et al. (2013) Criteria for the diagnosis of corticobasal degeneration. Neurology 80:496–503 Available at: https://n.neurology.org/content/80/5/496 [Accessed July 12, 2022].

Aronov S, Aranda G, Behar L, Ginzburg I (2001) Axonal Tau mRNA Localization Coincides with Tau Protein in Living Neuronal Cells and Depends on Axonal Targeting Signal. Journal of Neuroscience 21:6577–6587 Available at: https://www.jneurosci.org/content/21/17/6577 [Accessed April 27, 2022].

Asai H, Ikezu S, Tsunoda S, Medalla M, Luebke J, Haydar T, Wolozin B, Butovsky O, Kügler S, Ikezu T (2015) Depletion of microglia and inhibition of exosome synthesis halt tau propagation. Nat Neurosci 18:1584–1593.

Asai H, Ikezu S, Tsunoda S, Medalla M, Luebke J, Haydar T, Wolozin B, Butovsky O, Kügler S, Ikezu T (2015) Depletion of microglia and inhibition of exosome synthesis halt tau propagation. Nature Neuroscience 18:1584–1593.

Attwell D, Buchan AM, Charpak S, Lauritzen M, MacVicar BA, Newman EA (2010) Glial and neuronal control of brain blood flow. Nature 468:232–243.

Baker M, Litvan I, Houlden H, Adamson J, Dickson D, Perez-Tur J, Hardy J, Lynch T, Bigio E, Hutton M (1999) Association of an extended haplotype in the tau gene with progressive supranuclear palsy.

Barbar L, Jain T, Zimmer M, Kruglikov I, Sadick JS, Wang M, Kalpana K, Rose IVL, Burstein SR, Rusielewicz T, Nijsure M, Guttenplan KA, di Domenico A, Croft G, Zhang B, Nobuta H, Hébert JM, Liddelow SA, Fossati V (2020) CD49f Is a Novel Marker of Functional and Reactive Human iPSC-Derived Astrocytes. Neuron 107:436-453.e12 Available at: https://doi.org/10.1016/j.neuron.2020.05.014 [Accessed April 21, 2022].

Barghorn S, Zheng-Fischhofer Q, Ackmann M, Biernat J, Von Bergen M, Mandelkow EM, Mandelkow E (2000) Structure, microtubule interactions, and paired helical filament aggregation by tau mutants of frontotemporal dementias. Biochemistry 39:11714–11721.

Barmada SJ, Serio A, Arjun A, Bilican B, Daub A, Ando DM, Tsvetkov A, Pleiss M, Li X, Peisach D, Shaw C, Chandran S, Finkbeiner S (2014) Autophagy induction enhances TDP43 turnover and survival in neuronal ALS models. Nat Chem Biol 10:677–685 Available at: https://pubmed.ncbi.nlm.nih.gov/24974230/ [Accessed July 20, 2022].

Barooji YF, Hvid KG, Istúriz Petitjean I, Brickman JM, Oddershede LB, Bendix PM (2021) Changes in cell morphology and actin organization in embryonic stem cells cultured under different conditions. Cells 10 Available at: /pmc/articles/PMC8616278/ [Accessed July 18, 2022].

Basak JM, Verghese PB, Yoon H, Kim J, Holtzman DM (2012) Low-density lipoprotein receptor represents an apolipoprotein E-independent pathway of Aβ uptake and degradation by astrocytes. J Biol Chem 287:13959–13971 Available at: http://www.jbc.org/article/S0021925820529682/fulltext [Accessed July 22, 2022].

Batiuk MY, Martirosyan A, Wahis J, de Vin F, Marneffe C, Kusserow C, Koeppen J, Viana JF, Oliveira JF, Voet T, Ponting CP, Belgard TG, Holt MG (2020) Identification of region-specific astrocyte subtypes at single cell resolution. Nat Commun 11:1–15.

Batiuk MY, Martirosyan A, Wahis J, de Vin F, Marneffe C, Kusserow C, Koeppen J, Viana JF, Oliveira JF, Voet T, Ponting CP, Belgard TG, Holt MG (2020) Identification of region-specific astrocyte subtypes at single cell resolution. Nature Communications 11:1–15.

Bayraktar OA et al. (2020) Astrocyte layers in the mammalian cerebral cortex revealed by a single-cell in situ transcriptomic map. Nat Neurosci 23:500–509 Available at: https://pubmed.ncbi.nlm.nih.gov/32203496/ [Accessed July 16, 2022].

Beers J, Linask KL, Chen JA, Siniscalchi LI, Lin Y, Zheng W, Rao M, Chen G (2015) A cost-effective and efficient reprogramming platform for large-scale production of integration-free human induced pluripotent stem cells in chemically defined culture. Sci Reports 2015 51 5:1–9 Available at: https://www.nature.com/articles/srep11319 [Accessed July 19, 2022].

Bell RD, Winkler EA, Singh I, Sagare AP, Deane R, Wu Z, Holtzman DM, Betsholtz C, Armulik A, Sallstrom J, Berk BC, Zlokovic B v. (2012) Apolipoprotein e controls cerebrovascular integrity via cyclophilin A. Nature 485:512–516 Available at: http://dx.doi.org/10.1038/nature11087.

Bellenguez C et al. (2017) Contribution to Alzheimer's disease risk of rare variants in TREM2, SORL1, and ABCA7 in 1779 cases and 1273 controls. Neurobiology of Aging 59:220.e1-220.e9 Available at: http://dx.doi.org/10.1016/j.neurobiolaging.2017.07.001 [Accessed April 26, 2022].

Benarroch EE (2007) Aquaporin-4, homeostasis, and neurologic disease. Neurology 69:2266 LP – 2268 Available at: http://n.neurology.org/content/69/24/2266.abstract.

Bennett RE, Robbins AB, Hu M, Cao X, Betensky RA, Clark T, Das S, Hyman BT (2018) Tau induces blood vessel abnormalities and angiogenesis-related gene expression in P301L transgenic mice and human Alzheimer's disease. Proc Natl Acad Sci U S A 115:E1289–E1298.

Bergmans BA, de Strooper B (2010) Γ-Secretases: From Cell Biology To Therapeutic Strategies. The Lancet Neurology 9:215–226 Available at: http://dx.doi.org/10.1016/S1474-4422(09)70332-1.

Bhattacharyya A, Oppenheim RW, Prevette D, Moore BW, Brackenbury R, Ratner N (1992) S100 is present in developing chicken neurons and Schwann cells and promotes motor neuron survival in vivo. J Neurobiol 23:451–466 Available at: https://pubmed.ncbi.nlm.nih.gov/1634890/ [Accessed July 25, 2022].

Bi F, Huang C, Tong J, Qiu G, Huang B, Wu Q, Li F, Xu Z, Bowser R, Xia XG, Zhou H (2013) Reactive astrocytes secrete lcn2 to promote neuron death. Proc Natl Acad Sci U S A 110:4069–4074 Available at: www.pnas.org/cgi/doi/10.1073/pnas.1218497110 [Accessed July 1, 2022].

Biernat J, Mandelkow E-M (1999) The Development of Cell Processes Induced by tau Protein Requires Phosphorylation of Serine 262 and 356 in the Repeat Domain and Is Inhibited by Phosphorylation in the Proline-rich Domains.

Binder LI (1985) The distribution of tau in the mammalian central nervous system. The Journal of Cell Biology 101:1371–1378 Available at: http://www.jcb.org/cgi/doi/10.1083/jcb.101.4.1371.

Bindocci E, Savtchouk I, Liaudet N, Becker D, Carriero G, Volterra A (2017) Three-dimensional Ca2+ imaging advances understanding of astrocyte biology. Science (1979) 356.

Blair LJ, Frauen HD, Zhang B, Nordhues BA, Bijan S, Lin YC, Zamudio F, Hernandez LD, Sabbagh JJ, Selenica MLB, Dickey CA (2015) Tau depletion prevents progressive blood-brain barrier damage in a mouse model of tauopathy. Acta Neuropathol Commun 3:8.

Blaudin de Thé FX, Lassus B, Schaler AW, Fowler SL, Goulbourne CN, Jeggo R, Mannoury la Cour C, Millan MJ, Duff KE (2021) P62 accumulates through neuroanatomical circuits in response to tauopathy propagation. Acta Neuropathol Commun 9 Available at: https://doi.org/10.1186/s40478-021-01280-w.

Blaudin de Thé FX, Lassus B, Schaler AW, Fowler SL, Goulbourne CN, Jeggo R, Mannoury la Cour C, Millan MJ, Duff KE (2021) P62 accumulates through neuroanatomical circuits in response to tauopathy propagation. Acta Neuropathologica Communications 9 Available at: https://doi.org/10.1186/s40478-021-01280-w.

Bohlen CJ, Bennett FC, Tucker AF, Collins HY, Mulinyawe SB, Barres BA (2017) Diverse Requirements for Microglial Survival, Specification, and Function Revealed by Defined-Medium Cultures. Neuron 94:759-773.e8 Available at: http://dx.doi.org/10.1016/j.neuron.2017.04.043 [Accessed May 3, 2022].

Botez G, Probst A, Ipsen S, Tolnay M (1999) Astrocytes expressing hyperphosphorylated tau protein without glial fibrillary tangles in argyrophilic grain disease. Acta Neuropathologica 98:251–256.

Boyko S, Qi1 X, Chen TH, Surewicz K, Surewicz WK (2019) Liquid-liquid phase separation of tau protein: The crucial role of electrostatic interactions. J Biol Chem 294:11054–11059 Available at: https://pubmed.ncbi.nlm.nih.gov/31097543/ [Accessed April 30, 2022].

Boyles JK, Pitas RE, Wilson E, Mahley RW, Taylor JM (1985) Apolipoprotein E associated with astrocytic glia of the central nervous system and with nonmyelinating glia of the peripheral nervous system.

Braak H, Alafuzov I, Arzberger T, Kretzschmar H, Kelly ·, Tredici D (2006) Staging of Alzheimer disease-associated neuroWbrillary pathology using paraYn sections and immunocytochemistry. Acta Neuropathol 112:389–404.

Braak H, Braak E (1991) Neuropathological stageing of Alzheimer-related changes. Acta Neuropathol 82:239–259 Available at: http://www.ncbi.nlm.nih.gov/pubmed/1759558.

Braak H, Braak E (1997) Frequency of stages of Alzheimer-related lesions in different age categories. Neurobiol Aging 18:351–357 Available at: https://pubmed.ncbi.nlm.nih.gov/9330961/ [Accessed July 14, 2022].

Braak H, Thal DR, Ghebremedhin E, del Tredici K (2011) Stages of the Pathologic Process in Alzheimer Disease: Age Categories From 1 to 100 Years. Journal of Neuropathology & Experimental Neurology 70:960–969 Available at: https://academic.oup.com/jnen/article-lookup/doi/10.1097/NEN.0b013e318232a379.

Brenner M (2014) Role of GFAP in CNS injuries. Neurosci Lett 565:7–13 Available at: http://dx.doi.org/10.1016/j.neulet.2014.01.055.

Brenner M (2014) Role of GFAP in CNS injuries. Neuroscience Letters 565:7–13 Available at: http://dx.doi.org/10.1016/j.neulet.2014.01.055.

Brier MR, Gordon B, Friedrichsen K, McCarthy J, Stern A, Christensen J, Owen C, Aldea P, Su Y, Hassenstab J, Cairns NJ, Holtzman DM, Fagan AM, Morris JC, Benzinger TLS, Ances BM (2016) Tau and Ab imaging, CSF measures, and cognition in Alzheimer's disease. Science Translational Medicine 8:1–10.

Bright J, Hussain S, Dang V, Wright S, Cooper B, Byun T, Ramos C, Singh A, Parry G, Stagliano N, Griswold-Prenner I (2015) Human secreted tau increases amyloid-beta production. Neurobiology of Aging 36:693–709 Available at: http://dx.doi.org/10.1016/j.neurobiolaging.2014.09.007.

Brodaty H, Breteler MMB, Dekosky ST, Dorenlot P, Fratiglioni L, Hock C, Kenigsberg PA, Scheltens P, de Strooper B (2011) The World of Dementia Beyond 2020. J Am Geriatr Soc 59:923–927 Available at: https://onlinelibrary.wiley.com/doi/full/10.1111/j.1532-5415.2011.03365.x [Accessed July 13, 2022].

Bushong EA, Martone ME, Ellisman MH (2004) Maturation of astrocyte morphology and the establishment of astrocyte domains during postnatal hippocampal development. International Journal of Developmental Neuroscience 22:73–86.

Caffrey TM, Joachim C, Wade-Martins R (2008) Haplotype-specific expression of the N-terminal exons 2 and 3 at the human MAPT locus. Neurobiology of Aging 29:1923–1929.

Cahoy JD, Emery B, Kaushal A, Foo LC, Zamanian JL, Christopherson KS, Xing Y, Lubischer JL, Krieg PA, Krupenko SA, Thompson WJ, Barres BA (2008) A transcriptome database for astrocytes, neurons, and oligodendrocytes: A new resource for understanding brain development and function. Journal of Neuroscience 28:264–278.

Caiazzo M, Giannelli S, Valente P, Lignani G, Carissimo A, Sessa A, Colasante G, Bartolomeo R, Massimino L, Ferroni S, Settembre C, Benfenati F, Broccoli V (2015) Direct conversion of fibroblasts into functional astrocytes by defined transcription factors. Stem Cell Reports 4:25–36 Available at: http://dx.doi.org/10.1016/j.stemcr.2014.12.002.

Cairns NJ et al. (2007) Neuropathologic diagnostic and nosologic criteria for frontotemporal lobar degeneration: Consensus of the Consortium for Frontotemporal Lobar Degeneration. Acta Neuropathologica 114:5–22.

Ceyzériat K, Abjean L, Carrillo-de Sauvage MA, Ben Haim L, Escartin C (2016) The complex STATes of astrocyte reactivity: How are they controlled by the JAK-STAT3 pathway? Neuroscience 330:205–218.

Chai X, Dage JL, Citron M (2012) Constitutive secretion of tau protein by an unconventional mechanism. Neurobiology of Disease 48:356–366 Available at: http://dx.doi.org/10.1016/j.nbd.2012.05.021.

Chambers SM, Fasano CA, Papapetrou EP, Tomishima M, Sadelain M, Studer L (2009a) Highly efficient neural conversion of human ES and iPS cells by dual inhibition of SMAD signaling. Nat Biotechnol 27:275–280 Available at: http://www.ncbi.nlm.nih.gov/pubmed/19252484%0Ahttp://www.pubmedcentral.nih.gov/articlerender.fcgi?artid=PMC2756723.

Chambers SM, Fasano CA, Papapetrou EP, Tomishima M, Sadelain M, Studer L (2009b) Highly efficient neural conversion of human ES and iPS cells by dual inhibition of SMAD signaling. Nature Biotechnology 27:275–280.

Chen D, Drombosky KW, Hou Z, Sari L, Kashmer OM, Ryder BD, Perez VA, Woodard DNR, Lin MM, Diamond MI, Joachimiak LA (2019) Tau local structure shields an amyloid-forming motif and controls aggregation propensity. Nature Communications 10 Available at: https://doi.org/10.1038/s41467-019-10355-1.

Chen J, Kanai Y, Cowan NJ, Hirokawa N (1992) Projection domains of MAP2 and tau determine spacings between microtubules in dendrites and axons. Nature 360:674–677 Available at: https://www.nature.com/articles/360674a0 [Accessed April 28, 2022].

Chen MM, Hu ZL, Ding JH, Du RH, Hu G (2021) Astrocytic Kir6.1 deletion aggravates neurodegeneration in the lipopolysaccharide-induced mouse model of Parkinson's disease via astrocyte-neuron cross talk through complement C3-C3R signaling. Brain Behav Immun 95:310–320 Available at: https://pubmed.ncbi.nlm.nih.gov/33838249/ [Accessed July 16, 2022].

Chen WT et al. (2020) Spatial Transcriptomics and In Situ Sequencing to Study Alzheimer's Disease. Cell 182:976-991.e19 Available at: https://pubmed.ncbi.nlm.nih.gov/32702314/ [Accessed July 29, 2022].

Chiarini A, Armato U, Gardenal E, Gui L, Dal Prà I (2017) Amyloid β-exposed human astrocytes overproduce phospho-tau and overrelease it within exosomes, effects suppressed by calcilytic NPS 2143-Further implications for Alzheimer's therapy. Front Neurosci 11:1–9.

Choi SS, Lee HJ, Lim I, Satoh JI, Kim SU (2014) Human astrocytes: Secretome profiles of cytokines and chemokines. PLoS ONE 9.

Chun H, Lee CJ (2018) Reactive astrocytes in Alzheimer's disease: A double-edged sword. Neurosci Res 126:44–52 Available at: http://dx.doi.org/10.1016/j.neures.2017.11.012.

Chung WS, Verghese PB, Chakraborty C, Joung J, Hyman BT, Ulrich JD, Holtzman DM, Barres BA (2016) Novel allele-dependent role for APOE in controlling the rate of synapse pruning by astrocytes. Proc Natl Acad Sci U S A 113:10186–10191 Available at: www.pnas.org/cgi/doi/10.1073/pnas.1609896113 [Accessed July 5, 2022].

Civita P, Franceschi S, Aretini P, Ortenzi V, Menicagli M, Lessi F, Pasqualetti F, Giuseppe Naccarato A, Maria Mazzanti C (2019) Laser capture microdissection and RNA-seq analysis: High sensitivity approaches to explain histopathological heterogeneity in human glioblastoma FFPE archived tissues. Front Oncol 9:482.

Clarke LE, Barres BA (2013) Emerging roles of astrocytes in neural circuit development. Nature Reviews Neuroscience 14:311–321.

Clavaguera F, Akatsu H, Fraser G, Crowther RA, Frank S, Hench J, Probst A, Winkler DT, Reichwald J, Staufenbiel M, Ghetti B, Goedert M, Tolnay M (2013) Brain homogenates from human tauopathies

induce tau inclusions in mouse brain. Proceedings of the National Academy of Sciences 110:9535–9540.

Cocks G, Curran S, Gami P, Uwanogho D, Jeffries AR, Kathuria A, Lucchesi W, Wood V, Dixon R, Ogilvie C, Steckler T, Price J (2014) The utility of patient specific induced pluripotent stem cells for the modelling of Autistic Spectrum Disorders. Psychopharmacology (Berl) 231:1079 Available at: /pmc/articles/PMC3932164/ [Accessed July 29, 2022].

Connell JW, Gibb GM, Betts JC, Blackstock WP, Gallo JM, Lovestone S, Hutton M, Anderton BH (2001) Effects of FTDP-17 mutations on the in vitro phosphorylation of tau by glycogen synthase kinase 3β identified by mass spectrometry demonstrate certain mutations exert long-range conformational changes.

Cooper GM (2000) Endocytosis. In: The Cell: A Molecular Approach. 2nd edition Available at: https://www.ncbi.nlm.nih.gov/books/NBK9831/.

Crary JF et al. (2014) Primary age-related tauopathy (PART): a common pathology associated with human aging. Acta Neuropathologica 128:755–766.

Cripps D, Thomas SN, Jeng Y, Yang F, Davies P, Yang AJ (2006) Alzheimer disease-specific conformation of hyperphosphorylated paired helical filament-Tau is polyubiquitinated through Lys-48, Lys-11, and Lys-6 ubiquitin conjugation. J Biol Chem 281:10825–10838 Available at: https://pubmed.ncbi.nlm.nih.gov/16443603/ [Accessed July 16, 2022].

Cristóvão JS, Morris VK, Cardoso I, Leal SS, Martínez J, Botelho HM, Göbl C, David R, Kierdorf K, Alemi M, Madl T, Fritz G, Reif B, Gomes CM (2018) The neuronal S100B protein is a calcium-tuned suppressor of amyloid- aggregation. Sci Adv 4:1–14.

Croft CL, Wade MA, Kurbatskaya K, Mastrandreas P, Hughes MM, Phillips EC, Pooler AM, Perkinton MS, Hanger DP, Noble W (2017) Membrane association and release of wild-type and pathological tau from organotypic brain slice cultures. Cell Death Dis 2017 83 8:e2671–e2671 Available at: https://www.nature.com/articles/cddis201797 [Accessed July 15, 2022].

Crowther RA (1991a) Straight and paired helical filaments in Alzheimer disease have a common structural unit. Available at: https://www.pnas.org.

Crowther RA (1991b) Straight and paired helical filaments in Alzheimer disease have a common structural unit (neurofllriary tangles/neuropathdology/antibody labeling/electron microscopy/image processing).

Crowther RA, Goedert M (2000) Abnormal tau-containing filaments in neurodegenerative diseases. Journal of Structural Biology 130:271–279.

Cruz JC, Tseng HC, Goldman JA, Shih H, Tsai LH (2003) Aberrant Cdk5 activation by p25 triggers pathological events leading to neurodegeneration and neurofibrillary tangles. Neuron 40:471–483 Available at: http://www.neuron.org/cgi/ [Accessed April 29, 2022].

Cvekl A, Callaerts P (2017) PAX6: 25th anniversary and more to learn. Exp Eye Res 156:10–21 Available at: http://dx.doi.org/10.1016/j.exer.2016.04.017.

Danbolt NC (2001) Glutamate uptake. Progress in Neurobiology 65:1–105.

Darmanis S, Sloan SA, Zhang Y, Enge M, Caneda C, Shuer LM, Gephart MGH, Barres BA, Quake SR (2015) A survey of human brain transcriptome diversity at the single cell level. Proc Natl Acad Sci U S A 112:7285–7290.

de Calignon A, Polydoro M, Suárez-Calvet M, William C, Adamowicz DH, Kopeikina KJ, Pitstick R, Sahara N, Ashe KH, Carlson GA, Spires-Jones TL, Hyman BT (2012) Propagation of Tau Pathology in a Model of Early Alzheimer's Disease. Neuron 73:685–697.

Decker JM, Krüger L, Sydow A, Zhao S, Frotscher M, Mandelkow E, Mandelkow EM (2015) Pro-aggregant Tau impairs mossy fiber plasticity due to structural changes and Ca(++) dysregulation. Acta Neuropathol Commun 3:23 Available at: https://pubmed.ncbi.nlm.nih.gov/25853683/ [Accessed July 16, 2022].

Dehmelt L, Halpain S (2004) Protein family review The MAP2 / Tau family of microtubule-associated proteins. Genome Biol 6:1–10 Available at: http://genomebiology.com/2004/6/1/204.

Delekate A, Füchtemeier M, Schumacher T, Ulbrich C, Foddis M, Petzold GC (2014) Metabotropic P2Y1 receptor signalling mediates astrocytic hyperactivity in vivo in an Alzheimer's disease mouse model. Nature Communications 5:5422 Available at: www.nature.com/naturecommunications.

Deture MA, Dickson DW (2019) The neuropathological diagnosis of Alzheimer's disease. Mol Neurodegener 14:1–18.

Deture MA, Dickson DW (2019) The neuropathological diagnosis of Alzheimer's disease. Molecular Neurodegeneration 14:1–18.

DeVos SL, Goncharoff DK, Chen G, Kebodeaux CS, Yamada K, Stewart FR, Schuler DR, Maloney SE, Wozniak DF, Rigo F, Bennett CF, Cirrito JR, Holtzman DM, Miller TM (2013) Antisense reduction of tau in adult mice protects against seizures. J Neurosci 33:12887–12897 Available at: https://pubmed.ncbi.nlm.nih.gov/23904623/ [Accessed July 15, 2022].

Di Maria E, Tabaton M, Vigo T, Abbruzzese G, Bellone E, Donati C, Frasson E, Marchese R, Montagna P, Munoz DG, Pramstaller PP, Zanusso G, Ajmar F, Mandich P (2000) Corticobasal degeneration shares a common genetic background with progressive supranuclear palsy. Annals of Neurology 47:374–377.

Dickey CA, Kamal A, Lundgren K, Klosak N, Bailey RM, Dunmore J, Ash P, Shoraka S, Zlatkovic J, Eckman CB, Patterson C, Dickson DW, Nahman NS, Hutton M, Burrows F, Petrucelli L (2007) The high-affinity HSP90-CHIP complex recognizes and selectively degrades phosphorylated tau client proteins. J Clin Invest 117:648–658 Available at: https://pubmed.ncbi.nlm.nih.gov/17304350/ [Accessed July 16, 2022].

Dickson DW (2001) Neuropathology of Pick's disease. Neurology 56:S16–S20 Available at: http://www.neurology.org/cgi/doi/10.1212/WNL.56.suppl_4.S16.

Dickson DW, Bergeron C, Chin SS, Duyckaerts C, Horoupian D, Ikeda K, Jellinger K, Lantos PL, Lippa CF, Mirra SS, Tabaton M, Vonsattel JP, Wakabayashi K, Litvan I (2002) Office of rare diseases neuropathologic criteria for corticobasal degeneration. J Neuropathol Exp Neurol 61:935–946.

Dickson DW, Bergeron C, Chin SS, Duyckaerts C, Horoupian D, Ikeda K, Jellinger K, Lantos PL, Lippa CF, Mirra SS, Tabaton M, Vonsattel JP, Wakabayashi K, Litvan I (2002) Office of rare diseases neuropathologic criteria for corticobasal degeneration. Journal of Neuropathology and Experimental Neurology 61:935–946.

Dickson DW, Kouri N, Murray ME, Josephs KA (2011) Neuropathology of frontotemporal lobar degeneration-Tau (FTLD-Tau). Journal of Molecular Neuroscience 45:384–389.

Dickson DW, Rademakers R, Hutton ML (2007) Progressive supranuclear palsy: Pathology and genetics. Brain Pathology 17:74–82.

Dixit R, Ross JL, Goldman YE, Holzbaur ELF (2008) Differential regulation of dynein and kinesin motor proteins by tau. Science 319:1086–1089 Available at: https://pubmed.ncbi.nlm.nih.gov/18202255/ [Accessed July 15, 2022].

Donato R, Sorci G, Riuzzi F, Arcuri C, Bianchi R, Brozzi F, Tubaro C, Giambanco I (2009) S100B's double life: Intracellular regulator and extracellular signal. Biochim Biophys Acta - Mol Cell Res 1793:1008–1022 Available at: http://dx.doi.org/10.1016/j.bbamcr.2008.11.009.

Donato R, Sorci G, Riuzzi F, Arcuri C, Bianchi R, Brozzi F, Tubaro C, Giambanco I (2009) S100B's double life: Intracellular regulator and extracellular signal. Biochimica et Biophysica Acta - Molecular Cell Research 1793:1008–1022 Available at: http://dx.doi.org/10.1016/j.bbamcr.2008.11.009.

Drewes G, Trinczek B, Illenberger S, Biernat J, Schmitt-Ulms G, Meyer HE, Mandelkow EM, Mandelkow E (1995) Microtubule-associated protein/microtubule affinity-regulating kinase (p110mark). A novel protein kinase that regulates tau-microtubule interactions and dynamic instability by phosphorylation at the Alzheimer-specific site serine 262. J Biol Chem 270:7679–7688 Available at: https://pubmed.ncbi.nlm.nih.gov/7706316/ [Accessed July 15, 2022].

Dujardin S et al. (2020) Tau molecular diversity contributes to clinical heterogeneity in Alzheimer's disease. Nat Med Available at: http://dx.doi.org/10.1038/s41591-020-0938-9.

Dujardin S et al. (2020) Tau molecular diversity contributes to clinical heterogeneity in Alzheimer's disease. Nature Medicine Available at: http://dx.doi.org/10.1038/s41591-020-0938-9.

Dujardin S, Bégard S, Caillierez R, Lachaud C, Carrier S, Lieger S, Gonzalez JA, Deramecourt V, Déglon N, Maurage CA, Frosch MP, Hyman BT, Colin M, Buée L (2018) Different tau species lead to heterogeneous tau pathology propagation and misfolding. Acta Neuropathol Commun 6:132.

Eftekharzadeh B et al. (2018) Tau Protein Disrupts Nucleocytoplasmic Transport in Alzheimer's Disease. Neuron 99:925-940.e7 Available at: https://doi.org/10.1016/j.neuron.2018.07.039.

Eisele YS, Obermüller U, Heilbronner G, Baumann F, Kaeser SA, Wolburg H, Walker LC, Staufenbiel M, Heikenwalder M, Jucker M (2010) Peripherally Applied Aβ-Containing Inoculates Induce Cerebral β-Amyloidosis. Science (1979) 330:980–982 Available at: https://www.science.org/doi/10.1126/science.1194516.

Elie A, Prezel E, Guérin C, Denarier E, Ramirez-Rios S, Serre L, Andrieux A, Fourest-Lieuvin A, Blanchoin L, Arnal I (2015) Tau co-organizes dynamic microtubule and actin networks. Scientific Reports 5:1–10.

Ellis EF, Willoughby KA, Sparks SA, Chen T (2007) S100B protein is released from rat neonatal neurons, astrocytes, and microglia by in vitro trauma and anti-S100 increases trauma-induced delayed neuronal injury and negates the protective effect of exogenous S100B on neurons. J Neurochem 101:1463–1470 Available at: https://pubmed.ncbi.nlm.nih.gov/17403138/ [Accessed May 31, 2022].

Ericson J, Rashbass P, Schedl A, Brenner-Morton S, Kawakami A, van Heyningen V, Jessell TM, Briscoe J (1997) Pax6 controls progenitor cell identity and neuronal fate in response to graded Shh signaling. Cell 90:169–180.

Escartin C et al. (2021) Reactive astrocyte nomenclature, definitions, and future directions. Nat Neurosci 24:312–325 Available at: https://www.nature.com/articles/s41593-020-00783-4.

Escartin C et al. (2021) Reactive astrocyte nomenclature, definitions, and future directions. Nature Neuroscience 24:312–325 Available at: https://www.nature.com/articles/s41593-020-00783-4.

Escott-Price V, Hardy J (2022) Genome-wide association studies for Alzheimer's disease: bigger is not always better. Brain Commun 4 Available at: https://pubmed.ncbi.nlm.nih.gov/35663382/ [Accessed July 28, 2022].

Estivill-Torrus G, Pearson H, van Heyningen V, Price DJ, Rashbass P (2002) Pax6 is required to regulate the cell cycle and the rate of progression from symmetrical to asymmetrical division in mammalian cortical progenitors. Development 129:455–466.

Eulenburg V, Gomeza J (2010) Neurotransmitter transporters expressed in glial cells as regulators of synapse function. Brain Research Reviews 63:103–112 Available at: http://dx.doi.org/10.1016/j.brainresrev.2010.01.003.

Fá M et al. (2016) Extracellular Tau Oligomers Produce An Immediate Impairment of LTP and Memory. Scientific Reports 6:1–15.

Falcon B, Cavallini A, Angers R, Glover S, Murray TK, Barnham L, Jackson S, O'Neill MJ, Isaacs AM, Hutton ML, Szekeres PG, Goedert M, Bose S (2015) Conformation determines the seeding potencies of native and recombinant Tau aggregates. Journal of Biological Chemistry 290:1049–1065.

Falcon B, Zhang W, Murzin AG, Murshudov G, Garringer HJ, Vidal R, Crowther RA, Ghetti B, Scheres SHW, Goedert M (2018) Structures of filaments from Pick's disease reveal a novel tau protein fold. Nature 561:137–140 Available at: http://dx.doi.org/10.1038/s41586-018-0454-y.

Feinstein SC, Wilson L (2005) Inability of tau to properly regulate neuronal microtubule dynamics: a loss-of-function mechanism by which tau might mediate neuronal cell death. Biochimica et Biophysica Acta (BBA) - Molecular Basis of Disease 1739:268–279.

Ferrer I, López-González I, Carmona M, Arregui L, Dalfó E, Torrejón-Escribano B, Diehl R, Kovacs GG (2014) Glial and neuronal tau pathology in tauopathies: Characterization of disease-specific phenotypes and tau pathology progression. Journal of Neuropathology and Experimental Neurology 73:81–97.

Finkbeiner S (2020) The Autophagy Lysosomal Pathway and Neurodegeneration. Cold Spring Harb Perspect Biol 12 Available at: https://pubmed.ncbi.nlm.nih.gov/30936119/ [Accessed July 16, 2022].

Fitzpatrick AWP, Falcon B, He S, Murzin AG, Murshudov G, Garringer HJ, Crowther RA, Ghetti B, Goedert M, Scheres SHW (2017) Cryo-EM structures of tau filaments from Alzheimer's disease. Nature 547:185–190 Available at: http://dx.doi.org/10.1038/nature23002.

Flitney EW, Kuczmarski ER, Adam SA, Goldman RD (2009) Insights into the mechanical properties of epithelial cells: the effects of shear stress on the assembly and remodeling of keratin intermediate filaments. The FASEB Journal 23:2110–2119.

Fontaine SN, Zheng D, Sabbagh JJ, Martin MD, Chaput D, Darling A, Trotter JH, Stothert AR, Nordhues BA, Lussier A, Baker J, Shelton L, Kahn M, Blair LJ, Stevens SM, Dickey CA (2016) DnaJ/Hsc70 chaperone complexes control the extracellular release of neurodegenerative-associated proteins. EMBO J 35:1537–1549 Available at: https://pubmed.ncbi.nlm.nih.gov/27261198/ [Accessed July 15, 2022].

Foo LC, Dougherty JD (2013) Aldh1L1 is expressed by postnatal neural stem cells in vivo. Glia 61:1533 Available at: /pmc/articles/PMC3777382/ [Accessed July 18, 2022].

Forner S, Baglietto-Vargas D, Martini AC, Trujillo-Estrada L, LaFerla FM (2017) Synaptic Impairment in Alzheimer's Disease: A Dysregulated Symphony. Trends in Neurosciences 40:347–357 Available at: http://dx.doi.org/10.1016/j.tins.2017.04.002.

Forrest SL, Kril JJ, Halliday GM (2019) Cellular and regional vulnerability in frontotemporal tauopathies. Acta Neuropathologica 138:705–727 Available at: https://doi.org/10.1007/s00401-019-02035-7.

Forrest SL, Kril JJ, Stevens CH, Kwok JB, Hallupp M, Kim WS, Huang Y, McGinley C V., Werka H, Kiernan MC, Götz J, Spillantini MG, Hodges JR, Ittner LM, Halliday GM (2018) Retiring the term FTDP-17 as MAPT mutations are genetic forms of sporadic frontotemporal tauopathies. Brain 141:521–534.

Frandemiche ML, de Seranno S, Rush T, Borel E, Elie A, Arnal I, Lanté F, Buisson A (2014) Neurobiology of Disease Activity-Dependent Tau Protein Translocation to Excitatory Synapse Is Disrupted by Exposure to Amyloid-Beta Oligomers.

Freeman MR (2010) Specification and morphogenesis of astrocytes. Science (1979) 330:774–778 Available at: https://www.science.org/doi/full/10.1126/science.1190928 [Accessed April 19, 2022].

Frisoni GB, Altomare D, Thal DR, Ribaldi F, van der Kant R, Ossenkoppele R, Blennow K, Cummings J, van Duijn C, Nilsson PM, Dietrich PY, Scheltens P, Dubois B (2022) The probabilistic model of Alzheimer disease: the amyloid hypothesis revised. Nature Reviews Neuroscience 23:53–66.

Fu H, Hardy J, Duff KE (2018) Selective vulnerability in neurodegenerative diseases. Nat Neurosci 21:1350–1358 Available at: http://dx.doi.org/10.1038/s41593-018-0221-2.

Fujioka S, van Gerpen JA, Uitti RJ, Dickson DW, Wszolek ZK (2014) Familial Progressive Supranuclear Palsy: A Literature Review. Neurodegenerative Diseases 13:180–182 Available at: https://www.karger.com/Article/FullText/354975 [Accessed July 17, 2022].

Furness JB (2012) The enteric nervous system and. 9.

Furuta A, Rothstein JD, Martin JL (1997) Glutamate transporter protein subtypes are expressed differentially during rat cns development. Journal of Neuroscience 17:8363–8375.

Gandhi NS, Landrieu I, Byrne C, Kukic P, Amniai L, Cantrelle FX, Wieruszeski JM, Mancera RL, Jacquot Y, Lippens G (2015) A phosphorylation-induced turn defines the Alzheimer's disease AT8 antibody epitope on the tau protein. Angewandte Chemie - International Edition 54:6819–6823.

Garcia ADR, Doan NB, Imura T, Bush TG, Sofroniew M v. (2004) GFAP-expressing progenitors are the principal source of constitutive neurogenesis in adult mouse forebrain. Nature Neuroscience 2004 7:11 7:1233–1241 Available at: https://www.nature.com/articles/nn1340 [Accessed July 18, 2022].

Garwood CJ, Pooler AM, Atherton J, Hanger DP, Noble W (2011) Astrocytes are important mediators of Aβ-induced neurotoxicity and tau phosphorylation in primary culture. Cell Death and Disease 2 Available at: www.nature.com/cddis.

Garwood CJ, Pooler AM, Atherton J, Hanger DP, Noble W (2011) Astrocytes are important mediators of Aβ-induced neurotoxicity and tau phosphorylation in primary culture. Cell Death Dis 2:e167-9 Available at: http://dx.doi.org/10.1038/cddis.2011.50.

Garwood CJ, Ratcliffe LE, Simpson JE, Heath PR, Ince PG, Wharton SB (2017) Review: Astrocytes in Alzheimer's disease and other age-associated dementias: a supporting player with a central role. Neuropathol Appl Neurobiol 43:281–298.

Garwood CJ, Ratcliffe LE, Simpson JE, Heath PR, Ince PG, Wharton SB (2017) Review: Astrocytes in Alzheimer's disease and other age-associated dementias: a supporting player with a central role. Neuropathology and Applied Neurobiology 43:281–298.

Gatto N, dos Santos Souza C, Shaw AC, Bell SM, Myszczynska MA, Powers S, Meyer K, Castelli LM, Karyka E, Mortiboys H, Azzouz M, Hautbergue GM, Márkus NM, Shaw PJ, Ferraiuolo L (2020) Directly converted astrocytes retain the ageing features of the donor fibroblasts and elucidate the astrocytic contribution to human CNS health and disease. Aging Cell:1–22.

Geiszler PC, Barron MR, Pardon MC (2016) Impaired burrowing is the most prominent behavioral deficit of aging htau mice. Neuroscience 329:98–111 Available at: http://dx.doi.org/10.1016/j.neuroscience.2016.05.004.

Gerlach R, Demel G, König HG, Gross U, Prehn JHM, Raabe A, Seifert V, Kögel D (2006) Active secretion of S100B from astrocytes during metabolic stress. Neuroscience 141:1697–1701 Available at: https://pubmed.ncbi.nlm.nih.gov/16782283/ [Accessed July 25, 2022].

Ghag G, Bhatt N, Cantu D V., Guerrero-Munoz MJ, Ellsworth A, Sengupta U, Kayed R (2018) Soluble tau aggregates, not large fibrils, are the toxic species that display seeding and cross-seeding behavior. Protein Sci 27:1901–1909.

Ghag G, Bhatt N, Cantu D v., Guerrero-Munoz MJ, Ellsworth A, Sengupta U, Kayed R (2018) Soluble tau aggregates, not large fibrils, are the toxic species that display seeding and cross-seeding behavior. Protein Science 27:1901–1909.

Giannakopoulos P, Herrmann FR, Bussière T, Bouras C, Kövari E, Perl DP, Morrison JH, Gold G, Hof PR (2003) Tangle and neuron numbers, but not amyloid load, predict cognitive status in Alzheimer's disease. Neurology 60:1495–1500 Available at: https://pubmed.ncbi.nlm.nih.gov/12743238/ [Accessed July 14, 2022].

Glennon EB, Lau DHW, Gabriele RMC, Taylor MF, Troakes C, Opie-Martin S, Elliott C, Killick R, Hanger DP, Perez-Nievas BG, Noble W (2020) Bridging integrator 1 protein loss in Alzheimer's disease promotes synaptic tau accumulation and disrupts tau release. Brain Communications 2 Available at: https://academic.oup.com/braincomms/article/2/1/fcaa011/5736128.

Goedert M, Eisenberg DS, Crowther RA (2017) Propagation of Tau Aggregates and Neurodegeneration. Annu Rev Neurosci 40:189–210.

Goedert M, Jakes R (1990) Expression of separate isoforms of human tau protein: correlation with the tau pattern in brain and effects on tubulin polymerization. The EMBO Journal 9:4225–4230.

Goedert M, Spillantini MG, Falcon B, Zhang W, Newell KL, Hasegawa M, Scheres SHW, Ghetti B (2021) Tau Protein and Frontotemporal Dementias. Advances in Experimental Medicine and Biology 1281:177–199.

Goedert M, Spillantini MG, Jakes R, Rutherford D, Crowther RA (1989a) Multiple isoforms of human microtubule-associated protein tau: sequences and localization in neurofibrillary tangles of Alzheimer's disease. Neuron 3:519–526.

Goedert M, Spillantini MG, Potier MC, Ulrich J, Crowther RA (1989) Cloning and sequencing of the cDNA encoding an isoform of microtubule-associated protein tau containing four tandem repeats: differential expression of tau protein mRNAs in human brain. EMBO J 8:393–399.

Goedert M, Spillantini MG, Potier MC, Ulrich J, Crowther RA (1989b) Cloning and sequencing of the cDNA encoding an isoform of microtubule-associated protein tau containing four tandem repeats: differential expression of tau protein mRNAs in human brain. EMBO Journal 8:393–399.

Gómez-Isla T, Hollister R, West H, Mui S, Growdon JH, Petersen RC, Parisi JE, Hyman BT (1997) Neuronal loss correlates with but exceeds neurofibrillary tangles in Alzheimer's disease. Annals of Neurology 41:17–24 Available at: https://onlinelibrary.wiley.com/doi/10.1002/ana.410410106.

Gorno-Tempini ML et al. (2011) Classification of primary progressive aphasia and its variants. Neurology 76:1006–1014 Available at: https://pubmed.ncbi.nlm.nih.gov/21325651/ [Accessed July 13, 2022].

Greenberg SG, Davies P (1990) A preparation of Alzheimer paired helical filaments that displays distinct tau proteins by polyacrylamide gel electrophoresis. Proc Natl Acad Sci 87:5827–5831 Available at: http://www.pnas.org/cgi/doi/10.1073/pnas.87.15.5827.

Greenberg SG, Davies P (1990) A preparation of Alzheimer paired helical filaments that displays distinct tau proteins by polyacrylamide gel electrophoresis. Proceedings of the National Academy of Sciences 87:5827–5831 Available at: http://www.pnas.org/cgi/doi/10.1073/pnas.87.15.5827.

Guerreiro RJ, Gustafson DR, Hardy J (2012) The genetic architecture of Alzheimer's disease: Beyond APP, PSENS and APOE. Neurobiology of Aging 33:437–456 Available at: http://dx.doi.org/10.1016/j.neurobiolaging.2010.03.025.

Guix FX, Corbett GT, Cha DJ, Mustapic M, Liu W, Mengel D, Chen Z, Aikawa E, Young-Pearse T, Kapogiannis D, Selkoe DJ, Walsh DM (2018) Detection of Aggregation-Competent Tau in Neuron-Derived Extracellular Vesicles. Int J Mol Sci 19 Available at: https://pubmed.ncbi.nlm.nih.gov/29495441/ [Accessed July 15, 2022].

Guo JL, Buist A, Soares A, Callaerts K, Calafate S, Stevenaert F, Daniels JP, Zoll BE, Crowe A, Brunden KR, Moechars D, Lee VMY (2016) The dynamics and turnover of tau aggregates in cultured cells: INSIGHTS INTO THERAPIES FOR TAUOPATHIES. J Biol Chem 291:13175–13193 Available at: http://www.jbc.org/article/S0021925820394606/fulltext [Accessed July 26, 2022].

Guo JL, Narasimhan S, Changolkar L, He Z, Stieber A, Zhang B, Gathagan RJ, Iba M, McBride JD, Trojanowski JQ, Lee VMY (2016) Unique pathological tau conformers from Alzheimer's brains transmit tau pathology in nontransgenic mice. The Journal of Experimental Medicine 213:2635–2654.

Guo T, Noble W, Hanger DP (2017) Roles of tau protein in health and disease. Acta Neuropathologica 133:665–704.

Habib N, McCabe C, Medina S, Varshavsky M, Kitsberg D, Dvir-Szternfeld R, Green G, Dionne D, Nguyen L, Marshall JL, Chen F, Zhang F, Kaplan T, Regev A, Schwartz M (2020) Disease-associated astrocytes in Alzheimer's disease and aging. Nature Neuroscience Available at: http://dx.doi.org/10.1038/s41593-020-0624-8.

Hachem S, Aguirre A, Vives V, Marks A, Gallo V, Legraverend C (2005) Spatial and temporal expression of S100B in cells of oligodendrocyte lineage. Glia 51:81–97 Available at: https://pubmed.ncbi.nlm.nih.gov/15782413/ [Accessed July 18, 2022].

Hagmeyer S, Romão MA, Cristóvão JS, Vilella A, Zoli M, Gomes CM, Grabrucker AM (2019) Distribution and relative abundance of S100 proteins in the brain of the APP23 Alzheimer's disease model mice. Front Neurosci 13:1–10.

Haj-Yahya M, Lashuel HA (2018) Protein Semisynthesis Provides Access to Tau Disease-Associated Post-translational Modifications (PTMs) and Paves the Way to Deciphering the Tau PTM Code in Health and Diseased States. J Am Chem Soc 140:6611–6621.

Hamano T, Gendron TF, Causevic E, Yen SH, Lin WL, Isidoro C, Deture M, Ko LW (2008) Autophagic-lysosomal perturbation enhances tau aggregation in transfectants with induced wild-type tau

expression. Eur J Neurosci 27:1119–1130 Available at: https://pubmed.ncbi.nlm.nih.gov/18294209/ [Accessed July 16, 2022].

Han X, Chen M, Wang F, Windrem M, Wang S, Shanz S, Xu Q, Oberheim NA, Bekar L, Betstadt S, Silva AJ, Takano T, Goldman SA, Nedergaard M (2013) Forebrain engraftment by human glial progenitor cells enhances synaptic plasticity and learning in adult mice. Cell Stem Cell 12:342–353 Available at: http://dx.doi.org/10.1016/j.stem.2012.12.015.

Hanger DP, Anderton BH, Noble W (2009) Tau phosphorylation: the therapeutic challenge for neurodegenerative disease. Trends in Molecular Medicine 15:112–119.

Hanger DP, Brion JP, Gallo JM, Cairns NJ, Luthert PJ, Anderton BH (1991) Tau in Alzheimer's disease and Down's syndrome is insoluble and abnormally phosphorylated. Biochem J 275:99–104.

Hanger DP, Byers HL, Wray S, Leung KY, Saxton MJ, Seereeram A, Reynolds CH, Ward MA, Anderton BH (2007) Novel phosphorylation sites in Tau from Alzheimer brain support a role for casein kinase 1 in disease pathogenesis. J Biol Chem 282:23645–23654 Available at: http://www.jbc.org/article/S0021925820545791/fulltext [Accessed July 15, 2022].

Hanseeuw BJ et al. (2019) Association of Amyloid and Tau With Cognition in Preclinical Alzheimer Disease: A Longitudinal Study. JAMA Neurol 76:915 Available at: /pmc/articles/PMC6547132/ [Accessed July 28, 2022].

Harada A, Oguchi K, Okabe S, Kuno J, Terada S, Ohshima T, Sato-Yoshitake R, Takei Y, Noda T, Hirokawa N (1994) Altered microtubule organization in small-calibre axons of mice lacking tau protein. Nature 369:488–491 Available at: https://pubmed.ncbi.nlm.nih.gov/8202139/ [Accessed July 15, 2022].

Hardy JA, Higgins GA (1992) Alzheimer's disease: the amyloid cascade hypothesis. Science 256:184–185 Available at: https://pubmed.ncbi.nlm.nih.gov/1566067/ [Accessed July 28, 2022].

Harrison IF, Ismail O, Machhada A, Colgan N, Ohene Y, Nahavandi P, Ahmed Z, Fisher A, Meftah S, Murray TK, Ottersen OP, Nagelhus EA, O'Neill MJ, Wells JA, Lythgoe MF (2020) Impaired glymphatic function and clearance of tau in an Alzheimer's disease model. Brain 143:2576–2593.

He Z, McBride JD, Xu H, Changolkar L, Kim S jung, Zhang B, Narasimhan S, Gibbons GS, Guo JL, Kozak M, Schellenberg GD, Trojanowski JQ, Lee VMY (2020) Transmission of tauopathy strains is independent of their isoform composition. Nature Communications 11 Available at: http://dx.doi.org/10.1038/s41467-019-13787-x.

Hefendehl JK, LeDue J, Ko RWY, Mahler J, Murphy TH, MacVicar BA (2016) Mapping synaptic glutamate transporter dysfunction in vivo to regions surrounding Aβ plaques by iGluSnFR two-photon imaging. Nature Communications 2016 7:1 7:1–13 Available at: https://www.nature.com/articles/ncomms13441 [Accessed July 17, 2022].

Hefti MM, Farrell K, Kim SH, Bowles KR, Fowkes ME, Raj T, Crary JF (2018) High-resolution temporal and regional mapping of MAPT expression and splicing in human brain development. PLoS One 13:1–14.

Hefti MM, Kim SH, Bell AJ, Betters RK, Fiock KL, Iida MA, Smalley ME, Farrell K, Fowkes ME, Crary JF (2019) Tau phosphorylation and aggregation in the developing human brain. Journal of Neuropathology and Experimental Neurology 78:930–938 Available at: https://academic.oup.com/jnen/article/78/10/930/5554202.

Heimfarth L, Passos FRS, Monteiro BS, Araújo AA de S, Quintans Júnior LJ, Quintans J de SS (2022) Serum glial fibrillary acidic protein is a body fluid biomarker: A valuable prognostic for neurological disease – A systematic review. International Immunopharmacology 107.

Heneka MT et al. (2015) Neuroinflammation in Alzheimer's disease. The Lancet Neurology 14:388–405.

Henstridge CM, Tzioras M, Paolicelli RC (2019) Glial contribution to excitatory and inhibitory synapse loss in neurodegeneration. Front Cell Neurosci 13:1–26.

Herrmann JE, Imura T, Song B, Qi J, Ao Y, Nguyen TK, Korsak RA, Takeda K, Akira S, Sofroniew M V. (2008) STAT3 is a critical regulator of astrogliosis and scar formation after spinal cord injury. J Neurosci 28:7231–7243 Available at: https://pubmed.ncbi.nlm.nih.gov/18614693/ [Accessed July 22, 2022].

Hoffmann NA, Dorostkar MM, Blumenstock S, Goedert M, Herms J (2014) Impaired plasticity of cortical dendritic spines in P301S tau transgenic mice. Acta Neuropathologica Communications 2:1–11.

Hogg M et al. (2003) The L266V tau mutation is associated with frontotemporal dementia and Pick-like 3R and 4R tauopathy. Acta Neuropathologica 106:323–336.

Höglinger GU et al. (2011) Identification of common variants influencing risk of the tauopathy progressive supranuclear palsy. Nature Genetics 43:699–705.

Hol EM, Pekny M (2015) Glial fibrillary acidic protein (GFAP) and the astrocyte intermediate filament system in diseases of the central nervous system. Curr Opin Cell Biol 32:121–130 Available at: http://dx.doi.org/10.1016/j.ceb.2015.02.004.

Hol EM, Pekny M (2015) Glial fibrillary acidic protein (GFAP) and the astrocyte intermediate filament system in diseases of the central nervous system. Current Opinion in Cell Biology 32:121–130 Available at: http://dx.doi.org/10.1016/j.ceb.2015.02.004.

Holmes BB, DeVos SL, Kfoury N, Li M, Jacks R, Yanamandra K, Ouidja MO, Brodsky FM, Marasa J, Bagchi DP, Kotzbauer PT, Miller TM, Papy-Garcia D, Diamond MI (2013) Heparan sulfate proteoglycans mediate internalization and propagation of specific proteopathic seeds. Proceedings of the National Academy of Sciences 110:E3138–E3147.

Holmes BB, DeVos SL, Kfoury N, Li M, Jacks R, Yanamandra K, Ouidja MO, Brodsky FM, Marasa J, Bagchi DP, Kotzbauer PT, Miller TM, Papy-Garcia D, Diamond MI (2013) Heparan sulfate proteoglycans mediate internalization and propagation of specific proteopathic seeds. Proc Natl Acad Sci 110:E3138–E3147.

Holmes BB, Diamond MI (2014) Prion-like Properties of Tau Protein : The Importance of Extracellular Tau as a Therapeutic Target *. 289:19855–19861.

Hoover BR, Reed MN, Su J, Penrod RD, Kotilinek LA, Grant MK, Pitstick R, Carlson GA, Lanier LM, Yuan LL, Ashe KH, Liao D (2010) Tau Mislocalization to Dendritic Spines Mediates Synaptic Dysfunction Independently of Neurodegeneration. Neuron 68:1067–1081 Available at: http://dx.doi.org/10.1016/j.neuron.2010.11.030.

Horonchik L, Tzaban S, Ben-Zaken O, Yedidia Y, Rouvinski A, Papy-Garcia D, Barritault D, Vlodavsky I, Taraboulos A (2005) Heparan sulfate is a cellular receptor for purified infectious prions. Journal of Biological Chemistry 280:17062–17067.

Hu K (2014) Vectorology and factor delivery in induced pluripotent stem cell reprogramming. Stem Cells Dev 23:1301–1315 Available at: https://pubmed.ncbi.nlm.nih.gov/24625220/ [Accessed May 31, 2022].

Hubbard JA, Hsu MS, Seldin MM, Binder DK (2015) Expression of the astrocyte water channel aquaporin-4 in the mouse brain. ASN Neuro 7.

Hutton M et al. (1998) Association of missense and 5-splice-site mutations in tau with the inherited dementia FTDP-17.

Hynd MR, Scott HL, Dodd PR (2004) Glutamate-mediated excitotoxicity and neurodegeneration in Alzheimer's disease. Neurochem Int 45:583–595 Available at: https://pubmed.ncbi.nlm.nih.gov/15234100/ [Accessed July 17, 2022].

Iadecola C, Nedergaard M (2007) Glial regulation of the cerebral microvasculature. Nature Neuroscience 10:1369–1376.

Ihara Y, Morishima-Kawashima M, Nixon R (2012) The Ubiquitin-Proteasome System and the Autophagic-Lysosomal System in Alzheimer Disease. Cold Spring Harbor Perspectives in Medicine

2:a006361–a006361 Available at: http://perspectivesinmedicine.cshlp.org/lookup/doi/10.1101/cshperspect.a006361.

Ikeda K, Akiyama H, Arai T, Kondo H, Haga C, Iritani S, Tsuchiya K (1998) Alz-50/Gallyas-positive lysosome-like intraneuronal granules in Alzheimer's disease and control brains. Neurosci Lett 258:113–116 Available at: https://pubmed.ncbi.nlm.nih.gov/9875540/ [Accessed July 16, 2022].

Ikeda K, Haga C, Akiyama H, Kase K, Iritani S (1992) Coexistence of paired helical filaments and glial filaments in astrocytic processes within ghost tangles. Neurosci Lett 148:126–128 Available at: https://pubmed.ncbi.nlm.nih.gov/1338646/ [Accessed July 17, 2022].

Iliff JJ, Chen MJ, Plog BA, Zeppenfeld DM, Soltero M, Yang L, Singh I, Deane R, Nedergaard M (2014) Impairment of glymphatic pathway function promotes tau pathology after traumatic brain injury. Journal of Neuroscience 34:16180–16193.

Iliff JJ, Wang M, Liao Y, Plogg BA, Peng W, Gundersen GA, Benveniste H, Vates GE, Deane R, Goldman SA, Nagelhus EA, Nedergaard M (2012) A paravascular pathway facilitates CSF flow through the brain parenchyma and the clearance of interstitial solutes, including amyloid β. Science Translational Medicine 4.

Irwin DJ, Brettschneider J, McMillan CT, Cooper F, Olm C, Arnold SE, van Deerlin VM, Seeley WW, Miller BL, Lee EB, Lee VMY, Grossman M, Trojanowski JQ (2016a) Deep clinical and neuropathological phenotyping of Pick disease. Annals of Neurology 79:272–287.

Ismael S, Sindi G, Colvin RA, Lee D (2021) Activity-dependent release of phosphorylated human tau from Drosophila neurons in primary culture. J Biol Chem 297 Available at: https://pubmed.ncbi.nlm.nih.gov/34473990/ [Accessed July 15, 2022].

Itagaki S, McGeer PL, Akiyama H, Zhu S, Selkoe D (1989) Relationship of microglia and astrocytes to amyloid deposits of Alzheimer disease. J Neuroimmunol 24:173–182 Available at: https://pubmed.ncbi.nlm.nih.gov/2808689/ [Accessed July 14, 2022].

Ittner LM, Ke YD, Delerue F, Bi M, Gladbach A, van Eersel J, Wölfing H, Chieng BC, Christie MJ, Napier IA, Eckert A, Staufenbiel M, Hardeman E, Götz J (2010) Dendritic function of tau mediates amyloid-β toxicity in alzheimer's disease mouse models. Cell 142:387–397.

Jariel-Encontre I, Bossis G, Piechaczyk M (2008) Ubiquitin-independent degradation of proteins by the proteasome. Biochim Biophys Acta 1786:153–177 Available at: https://pubmed.ncbi.nlm.nih.gov/18558098/ [Accessed July 16, 2022].

Jeganathan S, von Bergen M, Brutlach H, Steinhoff HJ, Mandelkow E (2006) Global hairpin folding of tau in solution. Biochemistry 45:2283–2293 Available at: https://pubs.acs.org/sharingguidelines [Accessed April 28, 2022].

Jellinger KA et al. (2015) PART, a distinct tauopathy, different from classical sporadic Alzheimer disease. Acta Neuropathologica 129:757–762.

Jessen NA, Munk ASF, Lundgaard I, Nedergaard M (2015) The Glymphatic System: A Beginner's Guide. Neurochemical Research 40:2583–2599.

Jiang S, Bhaskar K (2020) Degradation and Transmission of Tau by Autophagic-Endolysosomal Networks and Potential Therapeutic Targets for Tauopathy. Frontiers in Molecular Neuroscience 13 Available at: www.frontiersin.org.

Jicha GA, Bowser R, Kazam IG, Davies P (1997) Alz-50 and MC-1, a new monoclonal antibody raised to paired helical filaments, recognize conformational epitopes on recombinant tau. Journal of Neuroscience Research 48:128–132.

Jiwaji Z et al. (2022) Reactive astrocytes acquire neuroprotective as well as deleterious signatures in response to Tau and Aß pathology. Nat Commun 13:135 Available at: http://www.ncbi.nlm.nih.gov/pubmed/35013236.

Jiwaji Z, Hardingham GE (2022) Good, bad, and neglectful: Astrocyte changes in neurodegenerative disease. Free Radic Biol Med 182:93–99 Available at: https://doi.org/10.1016/j.freeradbiomed.2022.02.020.

Jo A, Denduluri S, Zhang B, Wang Z, Yin L, Yan Z, Kang R, Shi LL, Mok J, Lee MJ, Haydon RC (2014a) The versatile functions of Sox9 in development, stem cells, and human diseases. Available at: http://dx.doi.org/10.1016/j.gendis.2014.09.004www.sciencedirect.com [Accessed July 18, 2022].

Jo S et al. (2014b) GABA from reactive astrocytes impairs memory in mouse models of Alzheimer's disease. Nature Medicine 2014 20:8 20:886–896 Available at: https://www.nature.com/articles/nm.3639 [Accessed July 17, 2022].

John H, Gerald H (1992) Alzheimer' s Disease : The Amyloid Cascade Hypothesis. Science (1979) 256:184–185.

Jonsson T et al. (2013) Variant of TREM2 Associated with the Risk of Alzheimer's Disease. New England Journal of Medicine 368:107–116 Available at: http://www.nejm.org/doi/10.1056/NEJMoa1211103.

Josephs KA, Hodges JR, Snowden JS, MacKenzie IR, Neumann M, Mann DM, Dickson DW (2011) Neuropathological background of phenotypical variability in frontotemporal dementia. Acta Neuropathologica 122:137–153.

Jucker M, Walker LC (2018) Propagation and spread of pathogenic protein assemblies in neurodegenerative diseases. Nature Neuroscience 21:1341–1349 Available at: http://dx.doi.org/10.1038/s41593-018-0238-6.

Kahlson MA, Colodner KJ (2015) Glial tau pathology in tauopathies: Functional consequences. Journal of Experimental Neuroscience 9s2:43–50.

Kamath T V, Klickstein N, Commins C, Fernandes AR, Oakley DH, Frosch MP, Hyman BT, Dujardin S (2021) Kinetics of tau aggregation reveals patient specific tau characteristics among Alzheimer's cases. Brain Commun Available at: https://academic.oup.com/braincomms/advance-article/doi/10.1093/braincomms/fcab096/6263855.

Kamath T v, Klickstein N, Commins C, Fernandes AR, Oakley DH, Frosch MP, Hyman BT, Dujardin S (2021) Kinetics of tau aggregation reveals patient specific tau characteristics among Alzheimer's cases. Brain Communications Available at: https://academic.oup.com/braincomms/advance-article/doi/10.1093/braincomms/fcab096/6263855.

Kanekiyo T, Bu G (2014) The low-density lipoprotein receptor-related protein 1 and amyloid-β clearance in Alzheimer's disease. Frontiers in Aging Neuroscience 6:1–12.

Kang P, Lee HK, Glasgow SM, Finley M, Donti T, Gaber ZB, Graham BH, Foster AE, Novitch BG, Gronostajski RM, Deneen B (2012) Sox9 and NFIA Coordinate a Transcriptional Regulatory Cascade during the Initiation of Gliogenesis. Neuron 74:79–94 Available at: http://dx.doi.org/10.1016/j.neuron.2012.01.024.

Kanmert D, Cantlon A, Muratore CR, Jin M, O'malley XT, Lee G, Tracy X, Young-Pearse L, Selkoe DJ, Walsh DM (2015) C-Terminally Truncated Forms of Tau, But Not Full-Length Tau or Its C-Terminal Fragments, Are Released from Neurons Independently of Cell Death.

Karch CM, Jeng AT, Goate AM (2013) Calcium phosphatase calcineurin influences tau metabolism. Neurobiol Aging 34:374–386 Available at: https://pubmed.ncbi.nlm.nih.gov/22676853/ [Accessed July 15, 2022].

Karlsson M et al. (2021a) A single–cell type transcriptomics map of human tissues. Sci Adv 7:1–10 Available at: www.proteinatlas.org.

Kaufman SK, Sanders DW, Thomas TL, Ruchinskas AJ, Vaquer-Alicea J, Sharma AM, Miller TM, Diamond MI (2016) Tau Prion Strains Dictate Patterns of Cell Pathology, Progression Rate, and Regional Vulnerability In Vivo. Neuron 92:796–812 Available at: http://dx.doi.org/10.1016/j.neuron.2016.09.055.

Kaufman SK, Thomas TL, Del Tredici K, Braak H, Diamond MI (2017) Characterization of tau prion seeding activity and strains from formaldehyde-fixed tissue. Acta Neuropathol Commun 5:41.

Kaur J, Fahmy LM, Davoodi-Bojd E, Zhang L, Ding G, Hu J, Zhang Z, Chopp M, Jiang Q (2021) Waste Clearance in the Brain. Front Neuroanat 15:1–18.

Keck S, Nitsch R, Grune T, Ullrich O (2003) Proteasome inhibition by paired helical filament-tau in brains of patients with Alzheimer's disease. J Neurochem 85:115–122 Available at: https://onlinelibrary.wiley.com/doi/full/10.1046/j.1471-4159.2003.01642.x [Accessed July 26, 2022].

Kehler J, Tolkunova E, Koschorz B, Pesce M, Gentile L, Boiani M, Lomelí H, Nagy A, McLaughlin KJ, Schöler HR, Tomilin A (2004) Oct4 is required for primordial germ cell survival. EMBO Rep 5:1078–1083.

Kelleher I, Garwood C, Hanger DP, Anderton BH, Noble W (2007) Kinase activities increase during the development of tauopathy in htau mice. Journal of Neurochemistry 103:2256–2267.

Keller D, Erö C, Markram H (2018) Cell densities in the mouse brain: A systematic review. Frontiers in Neuroanatomy 12.

Kent W, Sugnet C, Furey T, Roskin K, Pringle T, Zahler A, Haussler D (2002) The human genome browser at UCSC. Genome Res 12:996–1006.

Kerr JFR (1971) Shrinkage necrosis: A distinct mode of cellular death. The Journal of Pathology 105:13–20 Available at: https://onlinelibrary.wiley.com/doi/10.1002/path.1711050103.

Kerr JFR, Wyllie AH, Currie AR (1972) Apoptosis: A basic biological phenomenon with wide-ranging implications in tissue kinetics. British Journal of Cancer 26:239–257.

Khakh BS, Deneen B (2019) The Emerging Nature of Astrocyte Diversity. Annual Review of Neuroscience 42:187–207 Available at: https://doi.org/10.1146/annurev-neuro-070918-.

Khani M, Gibbons E, Bras J, Guerreiro R (2022) Challenge accepted: uncovering the role of rare genetic variants in Alzheimer's disease. Mol Neurodegener 17 Available at: https://pubmed.ncbi.nlm.nih.gov/35000612/ [Accessed July 28, 2022].

Kim KS, Miller DL, Sapienza VJ, Chen C-MJ, Bai C, Grundke-Iqbal I, Currie JR, Wisniewski HM (1988) Production and characterization of monoclonal antibodies reactive to synthetic cerebrovascular amyloid peptide. Neurosci Res Commun 2:121–130.

Kimura T, Whitcomb DJ, Jo J, Regan P, Piers T, Heo S, Brown C, Hashikawa T, Murayama M, Seok H, Sotiropoulos I, Kim E, Collingridge GL, Takashima A, Cho K (2013) Microtubule-associated protein tau is essential for long-term depression in the hippocampus. Philos Trans R Soc Lond B Biol Sci 369 Available at: https://pubmed.ncbi.nlm.nih.gov/24298146/ [Accessed July 16, 2022].

Kishore U, Grinstein S, Sørensen Dalgaard T, Rosales carosal C, Uribe-Querol E, Rosales C (2020) Phagocytosis: Our Current Understanding of a Universal Biological Process. Front Immunol | www.frontiersin.org 1:1066 Available at: www.frontiersin.org.

Knopman DS, Amieva H, Petersen RC, Chételat G, Holtzman DM, Hyman BT, Nixon RA, Jones DT (2021) Alzheimer disease. Nature Reviews Disease Primers 7:33 Available at: http://www.ncbi.nlm.nih.gov/pubmed/33986301.

Knops J, Kosik KS, Lee G, Pardee JD, Cohen-Gould L, McConlogue L (1991) Overexpression of tau in a nonneuronal cell induces long cellular processes. J Cell Biol 114:725–733 Available at: https://pubmed.ncbi.nlm.nih.gov/1678391/ [Accessed July 15, 2022].

Komori T, Arai N, Oda M, Nakayama H, Mori H, Yagishita S, Takahashi T, Amano N, Murayama S, Murakami S, Shibata N, Kobayashi M, Sasaki S, Iwata M (1998) Astrocytic plaques and tufts of abnormal fibers do not coexist in corticobasal degeneration and progressive supranuclear palsy. Acta Neuropathologica 96:401–408.

Kondo K, Hashimoto H, Kitanaka J ichi, Sawada M, Suzumura A, Marunouchi T, Baba A (1995) Expression of glutamate transporters in cultured glial cells. Neuroscience Letters 188:140–142.

Konishi H, Koizumi S, Kiyama H (2022) Phagocytic astrocytes: Emerging from the shadows of microglia. Glia 70:1009–1026.

Konzack S, Thies E, Marx A, Mandelkow EM, Mandelkow E (2007) Swimming against the tide: mobility of the microtubule-associated protein tau in neurons. J Neurosci 27:9916–9927 Available at: https://pubmed.ncbi.nlm.nih.gov/17855606/ [Accessed July 15, 2022].

Kosik KS, Orecchio LD, Bakalis S, Neve RL (1989) Developmentally regulated expression of specific tau sequences. Neuron 2:1389–1397 Available at: http://www.cell.com/article/0896627389900779/fulltext [Accessed April 12, 2022].

Kouri N et al. (2015) Genome-wide association study of corticobasal degeneration identifies risk variants shared with progressive supranuclear palsy. Nature Communications 6:1–7.

Kouri N, Whitwell JL, Josephs KA, Rademakers R, Dickson DW (2011) Corticobasal degeneration: A pathologically distinct 4R tauopathy. Nature Reviews Neurology 7:263–272.

Kovacs G (2018) Understanding the Relevance of Aging-Related Tau Astrogliopathy (ARTAG). Neuroglia 1:339–350.

Kovacs GG (2015) Invited review: Neuropathology of tauopathies: Principles and practice. Neuropathology and Applied Neurobiology 41:3–23.

Kovacs GG (2020) Astroglia and Tau: New Perspectives. Front Aging Neurosci 12:1–14 Available at: https://www.frontiersin.org/article/10.3389/fnagi.2020.00096/full.

Kovacs GG (2020) Astroglia and Tau: New Perspectives. Frontiers in Aging Neuroscience 12:1–14 Available at: https://www.frontiersin.org/article/10.3389/fnagi.2020.00096/full.

Kovacs GG et al. (2016) Aging-related tau astrogliopathy (ARTAG): harmonized evaluation strategy. Acta Neuropathologica 131:87–102.

Kovacs GG et al. (2020) Distribution patterns of tau pathology in progressive supranuclear palsy. Acta Neuropathologica 140:99–119 Available at: https://doi.org/10.1007/s00401-020-02158-2.

Kovacs GG, Budka H (2010) Current concepts of neuropathological diagnostics in practice: Neurodegenerative diseases. Clinical Neuropathology 29:271–288.

Kovacs GG, Robinson JL, Xie SX, Lee EB, Grossman M, Wolk DA, Irwin DJ, Weintraub D, Kim CF, Schuck T, Yousef A, Wagner ST, Suh E, van Deerlin VM, Lee VMY, Trojanowski JQ (2017) Evaluating the patterns of aging-related tau astrogliopathy unravels novel insights into brain aging and neurodegenerative diseases. Journal of Neuropathology and Experimental Neurology 76:270–288.

Krencik R, Weick JP, Liu Y, Zhang ZJ, Zhang SC (2011) Specification of transplantable astroglial subtypes from human pluripotent stem cells. Nature Biotechnology 29:528–534 Available at: http://dx.doi.org/10.1038/nbt.1877.

Krüger U, Wang Y, Kumar S, Mandelkow EM (2012) Autophagic degradation of tau in primary neurons and its enhancement by trehalose. Neurobiol Aging 33:2291–2305 Available at: https://pubmed.ncbi.nlm.nih.gov/22169203/ [Accessed July 16, 2022].

Krupenko SA (2009) FDH: An aldehyde dehydrogenase fusion enzyme in folate metabolism. Chemico-Biological Interactions 178:84–93.

Krupenko SA, Oleinik N v (2002) 10-formyltetrahydrofolate dehydrogenase, one of the major folate enzymes, is down-regulated in tumor tissues and possesses suppressor effects on cancer cells. Cell growth & differentiation : the molecular biology journal of the American Association for Cancer Research 13:227–236.

Kuchibhotla K v., Lattarulo CR, Hyman BT, Bacskai BJ (2009) Synchronous hyperactivity and intercellular calcium waves in astrocytes in Alzheimer mice. Science 323:1211–1215 Available at: https://pubmed.ncbi.nlm.nih.gov/19251629/ [Accessed July 17, 2022].

Kurbatskaya K, Phillips EC, Croft CL, Dentoni G, Hughes MM, Wade MA, Al-Sarraj S, Troakes C, O'Neill MJ, Perez-Nievas BG, Hanger DP, Noble W (2016) Upregulation of calpain activity precedes tau phosphorylation and loss of synaptic proteins in Alzheimer's disease brain. Acta Neuropathol Commun 4:34 Available at: http://dx.doi.org/10.1186/s40478-016-0299-2.

Lancaster CE, Fountain A, Dayam RM, Somerville E, Sheth J, Jacobelli V, Somerville A, Terebiznik MR, Botelho RJ (2021) Phagosome resolution regenerates lysosomes and maintains the degradative capacity in phagocytes. The Journal of Cell Biology 220 Available at: /pmc/articles/PMC8241537/ [Accessed July 5, 2022].

Largo-Barrientos P, Apóstolo N, Creemers E, Callaerts-Vegh Z, Swerts J, Davies C, McInnes J, Wierda K, de Strooper B, Spires-Jones T, de Wit J, Uytterhoeven V, Verstreken P (2021) Lowering Synaptogyrin-3 expression rescues Tau-induced memory defects and synaptic loss in the presence of microglial activation. Neuron 109:767-777.e5.

Lasagna-Reeves CA, Castillo-Carranza DL, Sengupta U, Sarmiento J, Troncoso J, Jackson GR, Kayed R (2012) Identification of oligomers at early stages of tau aggregation in Alzheimer's disease. FASEB J 26:1946–1959 Available at: www.fasebj.org.

Lécuyer MA, Kebir H, Prat A (2016) Glial influences on BBB functions and molecular players in immune cell trafficking. Biochimica et Biophysica Acta - Molecular Basis of Disease 1862:472–482.

Lee CYD, Landreth GE (2010) The role of microglia in amyloid clearance from the AD brain. Journal of Neural Transmission 117:949–960.

Lee G, Neve RL, Kosik KS (1989) The microtubule binding domain of tau protein. Neuron 2:1615–1624 Available at: http://www.cell.com/article/0896627389900500/fulltext [Accessed April 28, 2022].

Lee HG, Wheeler MA, Quintana FJ (2022) Function and therapeutic value of astrocytes in neurological diseases. Nature Reviews Drug Discovery 2022 21:5 21:339–358 Available at: https://www.nature.com/articles/s41573-022-00390-x [Accessed July 16, 2022].

Lee JH, Kim J young, Noh S, Lee H, Lee SY, Mun JY, Park H, Chung WS (2020) Astrocytes phagocytose adult hippocampal synapses for circuit homeostasis. Nat 2020 5907847 590:612–617 Available at: https://www.nature.com/articles/s41586-020-03060-3 [Accessed July 22, 2022].

Lee L, Kosuri P, Arancio O (2014) Picomolar Amyloid-β Peptides Enhance Spontaneous Astrocyte Calcium Transients. J Alzheimers Dis 38:49 Available at: /pmc/articles/PMC4116306/ [Accessed July 17, 2022].

Lehre KP, Danbolt NC (1998) The number of glutamate transport subtype molecules at glutamatergic synapses: Chemical and stereological quantification in young adult rat brain. Journal of Neuroscience 18:8751–8757.

Lei P, Ayton S, Finkelstein DI, Spoerri L, Ciccotosto GD, Wright DK, Wong BXW, Adlard PA, Cherny RA, Lam LQ, Roberts BR, Volitakis I, Egan GF, McLean CA, Cappai R, Duce JA, Bush AI (2012) Tau deficiency induces parkinsonism with dementia by impairing APP-mediated iron export. Nat Med 18:291–295 Available at: https://pubmed.ncbi.nlm.nih.gov/22286308/ [Accessed July 16, 2022].

Levin R, Grinstein S, Canton J (2016) The life cycle of phagosomes: formation, maturation, and resolution. Immunological Reviews 273:156–179.

Levine J, Kwon E, Paez P, Yan W, Czerwieniec G, Loo JA, Sofroniew M V., Wanner IB (2016) Traumatically injured astrocytes release a proteomic signature modulated by STAT3-dependent cell survival. Glia 64:668–694 Available at: https://onlinelibrary.wiley.com/doi/full/10.1002/glia.22953 [Accessed July 22, 2022].

Levitt P, Rakic P (1980) Immunoperoxidase localization of glial fibrillary acidic protein in radial glial cells and astrocytes of the developing rhesus monkey brain. Journal of Comparative Neurology 193:815–840.

Li D, Cho YK (2020) High specificity of widely used phospho-tau antibodies validated using a quantitative whole-cell based assay. Journal of Neurochemistry 152:122–135 Available at: https://onlinelibrary.wiley.com/doi/10.1111/jnc.14830.

Li K, Li J, Zheng J, Qin S (2019) Reactive Astrocytes in Neurodegenerative Diseases. Aging Dis 10:664 Available at: http://www.aginganddisease.org/EN/10.14336/AD.2018.0720.

Li X, Kumar Y, Zempel H, Mandelkow EM, Biernat J, Mandelkow E (2011) Novel diffusion barrier for axonal retention of Tau in neurons and its failure in neurodegeneration. EMBO J 30:4825 Available at: /pmc/articles/PMC3243615/ [Accessed July 29, 2022].

Li Y, Cheng D, Cheng R, Zhu X, Wan T, Liu J, Zhang R (2014) Mechanisms of U87 Astrocytoma Cell Uptake and Trafficking of Monomeric versus Protofibril Alzheimer's Disease Amyloid-β Proteins. PLoS

One 9:e99939 Available at: https://journals.plos.org/plosone/article?id=10.1371/journal.pone.0099939 [Accessed July 22, 2022].

Lian H, Litvinchuk A, Chiang ACA, Aithmitti N, Jankowsky JL, Zheng H (2016) Astrocyte-microglia cross talk through complement activation modulates amyloid pathology in mouse models of alzheimer's disease. Journal of Neuroscience 36:577–589.

Lian H, Yang L, Cole A, Sun L, Chiang ACA, Fowler SW, Shim DJ, Rodriguez-Rivera J, Taglialatela G, Jankowsky JL, Lu HC, Zheng H (2015) NFκB-Activated Astroglial Release of Complement C3 Compromises Neuronal Morphology and Function Associated with Alzheimer's Disease. Neuron 85:101–115 Available at: http://dx.doi.org/10.1016/j.neuron.2014.11.018.

Liang X, Yin N, Liang S, Yang R, Liu S, Lu Y, Jiang L, Zhou Q, Jiang G, Faiola F (2020) Bisphenol A and several derivatives exert neural toxicity in human neuron-like cells by decreasing neurite length. Food and Chemical Toxicology 135:111015 Available at: https://doi.org/10.1016/j.fct.2019.111015.

Liang Z, Valla J, Sefidvash-Hockley S, Rogers J, Li R (2002) Effects of estrogen treatment on glutamate uptake in cultured human astrocytes derived from cortex of Alzheimer's disease patients. J Neurochem 80:807–814 Available at: https://pubmed.ncbi.nlm.nih.gov/11948244/ [Accessed July 17, 2022].

Liddelow SA et al. (2017) Neurotoxic reactive astrocytes are induced by activated microglia. Nature 541:481–487 Available at: http://dx.doi.org/10.1038/nature21029.

Liddelow SA, Marsh SE, Stevens B (2020) Microglia and Astrocytes in Disease: Dynamic Duo or Partners in Crime? Trends in Immunology 41:820–835 Available at: https://doi.org/10.1016/j.it.2020.07.006.

Limanaqi F, Biagioni F, Gambardella S, Familiari P, Frati A, Fornai F (2020) Promiscuous Roles of Autophagy and Proteasome in Neurodegenerative Proteinopathies. Int J Mol Sci 21 Available at: https://pubmed.ncbi.nlm.nih.gov/32344772/ [Accessed July 16, 2022].

Lin Y, Fichou Y, Zeng Z, Hu NY, Han S (2020) Electrostatically Driven Complex Coacervation and Amyloid Aggregation of Tau Are Independent Processes with Overlapping Conditions. ACS Chemical Neuroscience 11:615–627 Available at: https://dx.doi.org/10.1021/acschemneuro.9b00627 [Accessed April 30, 2022].

Ling H et al. (2020) Fulminant corticobasal degeneration: a distinct variant with predominant neuronal tau aggregates. Acta Neuropathologica 139:717–734 Available at: https://doi.org/10.1007/s00401-019-02119-4.

Ling H, Kovacs GG, Vonsattel JPG, Davey K, Mok KY, Hardy J, Morris HR, Warner TT, Holton JL, Revesz T (2016) Astrogliopathy predominates the earliest stage of corticobasal degeneration pathology. Brain 139:3237–3252.

Linnerbauer M, Wheeler MA, Quintana FJ (2020) Astrocyte Crosstalk in CNS Inflammation. Neuron 108:608–622.

Lionnet A, Wade MA, Corbillé A-G, Prigent A, Paillusson S, Tasselli M, Gonzales J, Durieu E, Rolli-Derkinderen M, Coron E, Duchalais E, Neunlist M, Perkinton MS, Hanger DP, Noble W, Derkinderen P (2018) Characterisation of tau in the human and rodent enteric nervous system under physiological conditions and in tauopathy. Acta Neuropathologica Communications 6:65 Available at: http://creativecommons.org/publicdomain/zero/1.0/.

Litvinchuk A, Wan YW, Swartzlander DB, Chen F, Cole A, Propson NE, Wang Q, Zhang B, Liu Z, Zheng H (2018) Complement C3aR Inactivation Attenuates Tau Pathology and Reverses an Immune Network Deregulated in Tauopathy Models and Alzheimer's Disease. Neuron 100:1337-1353.e5 Available at: https://doi.org/10.1016/j.neuron.2018.10.031.

Liu C, Götz J (2013) Profiling murine tau with 0N, 1N and 2N isoform-specific antibodies in brain and peripheral organs reveals distinct subcellular localization, with the 1N isoform being enriched in the nucleus. PLoS One 8:1–18.

Liu C, Hu J, Zhao N, Wang J, Wang N, Cirrito JR, Kanekiyo T, Holtzman DM, Bu G (2017) Astrocytic LRP1 Mediates Brain Aβ Clearance and Impacts Amyloid Deposition. J Neurosci 37:4023–4031 Available at: http://www.ncbi.nlm.nih.gov/pubmed/28275161.

Liu L, Drouet V, Wu JW, Witter MP, Small SA, Clelland C, Duff K (2012) Trans-synaptic spread of tau pathology in vivo. PLoS ONE 7:1–9.

Liu Y, Zhang S, Li X, Liu E, Wang X, Zhou Q, Ye J, Wang JZ (2020) Peripheral inflammation promotes brain tau transmission via disrupting blood-brain barrier. Biosci Rep 40:1–15

Llorens-Martin M, Teixeira CM, Fuster-Matanzo A, Jurado-Arjona J, Borrell V, Soriano E, Avila J, Hernández F (2012) Tau Isoform with Three Microtubule Binding Domains is a Marker of New Axons Generated from the Subgranular Zone in the Hippocampal Dentate Gyrus: Implications for Alzheimer's Disease. Journal of Alzheimer's Disease 29:921–930.

Loh YH et al. (2006) The Oct4 and Nanog transcription network regulates pluripotency in mouse embryonic stem cells. Nature Genetics 38:431–440.

Loomis PA, Howardt TH, Castleberryt RP, Binder L 1 (1990) Identification of nuclear X isoforms in human neuroblastoma cells (nucleolus/microtubule-associated proteins/Alzheimer disease/Down syndrome). Available at: https://www.pnas.org.

Lööv C, Hillered L, Ebendal T, Erlandsson A (2012) Engulfing astrocytes protect neurons from contact-induced apoptosis following injury. PLoS ONE 7.

Lööv C, Mitchell CH, Simonsson M, Erlandsson A (2015) Slow degradation in phagocytic astrocytes can be enhanced by lysosomal acidification. Glia 63:1997–2009.

Lowe VJ et al. (2018) Widespread brain tau and its association with ageing, Braak stage and Alzheimer's dementia. Brain 141:271–287 Available at: www.nitrc.org/projects/bnv/.

Lowery J, Kuczmarski ER, Herrmann H, Goldma RD (2015) Intermediate Filaments Play a Pivotal Role in Regulating Cell Architecture and Function. J Biol Chem 290:17145–17153 Available at: https://pubmed.ncbi.nlm.nih.gov/25957409/ [Accessed July 18, 2022].

Ludwin SK, Kosek JC, Eng LF (1976) The topographical distribution of S-100 and GFA proteins in the adult rat brain: an immunohistochemical study using horseradish peroxidase-labelled antibodies. J Comp Neurol 165:197–207 Available at: https://pubmed.ncbi.nlm.nih.gov/1107363/ [Accessed July 17, 2022].

Lundgaard I, Osório MJ, Kress BT, Sanggaard S, Nedergaard M (2014) White matter astrocytes in health and disease. Neuroscience 276:161–173.

Luo Q, Wu J, Erö C, Gewaltig M-O, Keller D, Markram H (2018) A Cell Atlas for the Mouse Brain. Frontiers in Neuroinformatics | www.frontiersin.org 12:84 Available at: www.frontiersin.org.

Ma FC, Wang HF, Cao XP, Tan CC, Tan L, Yu JT (2018) Meta-Analysis of the Association between Variants in ABCA7 and Alzheimer's Disease. Journal of Alzheimer's Disease 63:1261–1267.

Mächler P, Wyss MT, Elsayed M, Stobart J, Gutierrez R, von Faber-Castell A, Kaelin V, Zuend M, San Martín A, Romero-Gómez I, Baeza-Lehnert F, Lengacher S, Schneider BL, Aebischer P, Magistretti PJ, Barros LF, Weber B (2016) In Vivo Evidence for a Lactate Gradient from Astrocytes to Neurons. Cell Metabolism 23:94–102.

Maekawa M, Takashima N, Arai Y, Nomura T, Inokuchi K, Yuasi S, Osumi N (2005) Pax6 is required for production and maintenance of progenitor cells in postnatal hippocampal neurogenesis. Genes to Cells 10:1001–1014 Available at: https://onlinelibrary.wiley.com/doi/full/10.1111/j.1365-2443.2005.00893.x [Accessed July 19, 2022].

Magistretti PJ, Allaman I (2018) Lactate in the brain: from metabolic end-product to signalling molecule. Nature Reviews Neuroscience 2018 19:4 19:235–249 Available at: https://www.nature.com/articles/nrn.2018.19 [Accessed July 16, 2022].

Magnus T, Chan A, Linker RA, Toyka K v., Gold R (2002) Astrocytes are less efficient in the removal of apoptotic lymphocytes than microglia cells: Implications for the role of glial cells in the inflamed central nervous system. Journal of Neuropathology and Experimental Neurology 61:760–766.

Mahmoud S, Gharagozloo M, Simard C, Gris D (2019) Astrocytes Maintain Glutamate Homeostasis in the CNS by Controlling the Balance between Glutamate Uptake and Release. Cells 8:184 Available at: www.mdpi.com/journal/cells.

Mamber C, Kamphuis W, Haring NL, Peprah N, Middeldorp J (2012) GFAPd Expression in Glia of the Developmental and Adolescent Mouse Brain. PLoS One 7:52659 Available at: www.plosone.org.

Mann CN, Devi SS, Kersting CT, Bleem A v, Karch CM, Holtzman DM, Gallardo G (2022) Astrocytic α2-Na+/K+ ATPase inhibition suppresses astrocyte reactivity and reduces neurodegeneration in a tauopathy mouse model. Science Translational Medicine 14:1–12.

Marlatt MW, Bauer J, Aronica E, van Haastert ES, Hoozemans JJM, Joels M, Lucassen PJ (2014) Proliferation in the alzheimer hippocampus is due to microglia, not astroglia, and occurs at sites of amyloid deposition. Neural Plasticity 2014.

Marshak DR, Pesce SA, Stanley LC, Griffin WST (1992) Increased S100 beta neurotrophic activity in Alzheimer's disease temporal lobe. Neurobiol Aging 13:1–7 Available at: https://pubmed.ncbi.nlm.nih.gov/1371849/ [Accessed July 25, 2022].

Martini S, Bernoth K, Main H, Ortega GDC, Lendahl U, Just U, Schwanbeck R (2013) A critical role for Sox9 in Notch-induced astrogliogenesis and stem cell maintenance. Stem Cells 31:741–751.

Martini-Stoica H, Cole AL, Swartzlander DB, Chen F, Wan YW, Bajaj L, Bader DA, Lee VMY, Trojanowski JQ, Liu Z, Sardiello M, Zheng H (2018) TFEB enhances astroglial uptake of extracellular tau species and reduces tau spreading. J Exp Med 215:2355–2377.

tau species and reduces tau spreading. Journal of Experimental Medicine 215:2355–2377.

Martín-Maestro P, Sproul A, Martinez H, Paquet D, Gerges M, Noggle S, Starkov AA (2019) Autophagy Induction by Bexarotene Promotes Mitophagy in Presenilin 1 Familial Alzheimer's Disease iPSC-Derived Neural Stem Cells. Molecular Neurobiology 56:8220–8236.

Masliah E, Alford M, DeTeresa R, Mallory M, Hansen L (1996) Deficient glutamate transport is associated with neurodegeneration in Alzheimer's disease. Ann Neurol 40:759–766 Available at: https://pubmed.ncbi.nlm.nih.gov/8957017/ [Accessed July 17, 2022].

McAlpine CS et al. (2021) Astrocytic interleukin-3 programs microglia and limits Alzheimer's disease. Nature 595 Available at: https://doi.org/10.1038/s41586-021-03734-6.

McCarron M, McCallion P, Reilly E, Dunne P, Carroll R, Mulryan N (2017) A prospective 20-year longitudinal follow-up of dementia in persons with Down syndrome. J Intellect Disabil Res 61:843–852 Available at: https://pubmed.ncbi.nlm.nih.gov/28664561/ [Accessed July 13, 2022].

McInnes J, Wierda K, Snellinx A, Bounti L, Wang YC, Stancu IC, Apóstolo N, Gevaert K, Dewachter I, Spires-Jones TL, de Strooper B, de Wit J, Zhou L, Verstreken P (2018) Synaptogyrin-3 Mediates Presynaptic Dysfunction Induced by Tau. Neuron 97:823-835.e8.

McKee AC, Cairns NJ, Dickson DW, Folkerth RD, Dirk Keene C, Litvan I, Perl DP, Stein TD, Vonsattel JP, Stewart W, Tripodis Y, Crary JF, Bieniek KF, Dams-O'Connor K, Alvarez VE, Gordon WA (2016) The first NINDS/NIBIB consensus meeting to define neuropathological criteria for the diagnosis of chronic traumatic encephalopathy. Acta Neuropathologica 131:75–86.

McKee AC, Stein TD, Kiernan PT, Alvarez VE (2015) The neuropathology of chronic traumatic encephalopathy. Brain Pathology 25:350–364.

McKenzie AT, Wang M, Hauberg ME, Fullard JF, Kozlenkov A, Keenan A, Hurd YL, Dracheva S, Casaccia P, Roussos P, Zhang B (2018) Brain Cell Type Specific Gene Expression and Co-expression Network Architectures. Scientific Reports 8:1–19 Available at: http://dx.doi.org/10.1038/s41598-018-27293-5.

McMillan P, Korvatska E, Poorkaj P, Evstafjeva Z, Robinson L, Greenup L, Leverenz J, Schellenberg GD, D'Souza I (2008) Tau isoform regulation is region- and cell-specific in mouse brain. Journal of Comparative Neurology 511:788–803.

Meisl G, Hidari E, Allinson K, Rittman T, DeVos SL, Sanchez JS, Xu CK, Duff KE, Johnson KA, Rowe JB, Hyman BT, Knowles TPJ, Klenerman D (2021) In vivo rate-determining steps of tau seed

accumulation in Alzheimer's disease. Sci Adv 7 Available at: https://www.science.org/doi/10.1126/sciadv.abh1448 [Accessed July 29, 2022].

Merezhko M, Brunello CA, Yan X, Vihinen H, Jokitalo E, Uronen RL, Huttunen HJ (2018) Secretion of Tau via an Unconventional Non-vesicular Mechanism. Cell Reports 25:2027-2035.e4 Available at: https://doi.org/10.1016/j.celrep.2018.10.078.

Messing A, Brenner M (2020) GFAP at 50. ASN Neuro 12 Available at: https://us.sagepub.com/en- [Accessed January 28, 2022].

Meyer K, Ferraiuolo L, Miranda CJ, Likhite S, McElroy S, Renusch S, Ditsworth D, Lagier-Tourenne C, Smith RA, Ravits J, Burghes AH, Shaw PJ, Cleveland DW, Kolb SJ, Kaspar BK (2014) Direct conversion of patient fibroblasts demonstrates non-cell autonomous toxicity of astrocytes to motor neurons in familial and sporadic ALS. Proceedings of the National Academy of Sciences 111:829–832 Available at: http://www.pnas.org/cgi/doi/10.1073/pnas.1314085111.

Middeldorp J, Hol EM (2011) GFAP in health and disease. Prog Neurobiol 93:421–443 Available at: http://dx.doi.org/10.1016/j.pneurobio.2011.01.005.

Miller JD, Ganat YM, Kishinevsky S, Bowman RL, Liu B, Tu EY, Mandal PK, Vera E, Shim JW, Kriks S, Taldone T, Fusaki N, Tomishima MJ, Krainc D, Milner TA, Rossi DJ, Studer L (2013) Human iPSC-based modeling of late-onset disease via progerin-induced aging. Cell Stem Cell 13:691–705 Available at: http://www.cell.com/article/S1934590913004979/fulltext [Accessed May 31, 2022].

Miller SJ (2018) Astrocyte heterogeneity in the adult central nervous system. Front Cell Neurosci 12:15 Available at: www.frontiersin.org.

Min SW, Cho SH, Zhou Y, Schroeder S, Haroutunian V, Seeley WW, Huang EJ, Shen Y, Masliah E, Mukherjee C, Meyers D, Cole PA, Ott M, Gan L (2010) Acetylation of tau inhibits its degradation and contributes to tauopathy. Neuron 67:953–966 Available at: http://dx.doi.org/10.1016/j.neuron.2010.08.044.

Mirbaha H, Chen D, Morazova OA, Ruff KM, Sharma AM, Liu X, Goodarzi M, Pappu R v., Colby DW, Mirzaei H, Joachimiak LA, Diamond MI (2018) Inert and seed-competent tau monomers suggest structural origins of aggregation. Elife 7 Available at: https://doi.org/10.7554/eLife.36584.001.

Molofsky A v., Glasgow SM, Chaboub LS, Tsai HH, Murnen AT, Kelley KW, Fancy SPJ, Yuen TJ, Madireddy L, Baranzini S, Deneen B, Rowitch DH, Oldham MC (2013) Expression Profiling of Aldh1l1-Precursors in the Developing Spinal Cord Reveals Glial Lineage-Specific Genes and Direct Sox9-Nfe2l1 Interactions. Glia 61:1518 Available at: /pmc/articles/PMC3909648/ [Accessed July 18, 2022].

Molofsky AV, Deneen B (2015) Astrocyte development: A Guide for the Perplexed. GLIA 63:1320–1329.

Moody LR, Barrett-Wilt GA, Sussman MR, Messing A (2017) Glial fibrillary acidic protein exhibits altered turnover kinetics in a mouse model of Alexander disease. J Biol Chem 292:5814–5824 Available at: https://pubmed.ncbi.nlm.nih.gov/28223355/ [Accessed July 25, 2022].

Mookherjee P, Green PS, Watson GS, Marques MA, Tanaka K, Meeker KD, Meabon JS, Li N, Zhu P, Olson VG, Cook DG (2011) GLT-1 loss accelerates cognitive deficit onset in an Alzheimer's disease animal model. J Alzheimers Dis 26:447–455 Available at: https://pubmed.ncbi.nlm.nih.gov/21677376/ [Accessed July 17, 2022].

Moreira GG, Cantrelle F, Quezada A, Carvalho FS, Cristóvão JS, Sengupta U, Puangmalai N, Carapeto AP, Rodrigues MS, Cardoso I, Fritz G, Herrera F, Kayed R, Landrieu I, Gomes CM (2021) Dynamic interactions and Ca2+-binding modulate the holdase-type chaperone activity of S100B preventing tau aggregation and seeding. Nature Communications 12:6292 Available at: https://www.nature.com/articles/s41467-021-26584-2.

Moreira GG, Cantrelle F, Quezada A, Carvalho FS, Cristóvão JS, Sengupta U, Puangmalai N, Carapeto AP, Rodrigues MS, Cardoso I, Fritz G, Herrera F, Kayed R, Landrieu I, Gomes CM (2021) Dynamic interactions and Ca2+-binding modulate the holdase-type chaperone activity of S100B

preventing tau aggregation and seeding. Nat Commun 12:6292 Available at: https://www.nature.com/articles/s41467-021-26584-2.

Morishima-Kawashima M, Hasegawa M, Takio K, Suzuki M, Titani K, Ihara Y (1993) Ubiquitin is conjugated with amino-terminally processed tau in paired helical filaments. Neuron 10:1151–1160 Available at: https://pubmed.ncbi.nlm.nih.gov/8391280/ [Accessed July 16, 2022].

Morris HR, Baker M, Yasojima K, Houlden H, Khan MN, Wood NW, Hardy J, Grossman M, Trojanowski J, Revesz T, Bigio EH, Bergeron C, Janssen JC, McGeer PL, Rossor MN, Lees AJ, Lantos PL, Hutton M (2002) Analysis of tau haplotypes in Pick's disease. Neurology 59:443–445.

Mrak RE, Griffin WST (2001) The role of activated astrocytes and of the neurotrophic cytokine S100B in the pathogenesis of Alzheimer's disease. Neurobiol Aging 22:915–922.

Mukrasch MD, Markwick P, Biernat J, von Bergen M, Bernadó P, Griesinger C, Mandelkow E, Zweckstetter M, Blackledge M (2007a) Highly populated turn conformations in natively unfolded tau protein identified from residual dipolar couplings and molecular simulation. J Am Chem Soc 129:5235–5243.

Mukrasch MD, von Bergen M, Biernat J, Fischer D, Griesinger C, Mandelkow E, Zweckstetter M (2007b) The "jaws" of the tau-microtubule interaction. Journal of Biological Chemistry 282:12230–12239 Available at: http://dx.doi.org/10.1074/jbc.M607159200.

Mullan M, Crawford F, Axelman K, Houlden H, Lilius L, Winblad B, Lannfelt L (1992) A pathogenic mutation for probable Alzheimer's disease in the APP gene at the N-terminus of beta-amyloid. Nat Genet 1:345–347 Available at: https://pubmed.ncbi.nlm.nih.gov/1302033/ [Accessed July 13, 2022].

Müller MS, Fouyssac M, Taylor CW (2018) Effective Glucose Uptake by Human Astrocytes Requires Its Sequestration in the Endoplasmic Reticulum by Glucose-6-Phosphatase-β. Current Biology 28:3481 Available at: /pmc/articles/PMC6224479/ [Accessed July 16, 2022].

Nacher J, Varea E, Blasco-Ibañez JM, Castillo-Gomez E, Crespo C, Martinez-Guijarro FJ, McEwen BS (2005) Expression of the transcription factor Pax6 in the adult rat dentate gyrus. J Neurosci Res 81:753–761.

Narasimhan S, Changolkar L, Riddle DM, Kats A, Stieber A, Weitzman SA, Zhang B, Li Z, Roberson ED, Trojanowski JQ, Lee VMY (2020) Human tau pathology transmits glial tau aggregates in the absence of neuronal tau. The Journal of Experimental Medicine 217 Available at: https://rupress.org/jem/article/doi/10.1084/jem.20190783/132744/Human-tau-pathology-transmits-glial-tau-aggregates.

Narasimhan S, Guo JL, Changolkar L, Stieber A, McBride JD, Silva L v., He Z, Zhang B, Gathagan RJ, Trojanowski JQ, Lee VMY (2017) Pathological Tau Strains from Human Brains Recapitulate the Diversity of Tauopathies in Nontransgenic Mouse Brain. The Journal of Neuroscience 37:11406–11423 Available at: http://www.jneurosci.org/lookup/doi/10.1523/JNEUROSCI.1230-17.2017.

Nawashiro H, Messing A, Azzam N, Brenner M (1998) Mice lacking GFAP are hypersensitive to traumatic cerebrospinal injury. Neuroreport 9:1691–1696 Available at: https://pubmed.ncbi.nlm.nih.gov/9665584/ [Accessed July 18, 2022].

Neary D, Snowden JS, Gustafson L, Passant U, Stuss D, Black S, Freedman M, Kertesz A, Robert PH, Albert M, Boone K, Miller BL, Cummings J, Benson DF (1998) Frontotemporal lobar degeneration. Neurology 51:1546–1554 Available at: https://n.neurology.org/content/51/6/1546 [Accessed July 13, 2022].

Newington JT, Harris RA, Cumming RC (2013) Reevaluating Metabolism in Alzheimer's Disease from the Perspective of the Astrocyte-Neuron Lactate Shuttle Model. Journal of Neurodegenerative Diseases 2013:13 Available at: http://dx.

Neyrinck K et al. (2021) SOX9-induced Generation of Functional Astrocytes Supporting Neuronal Maturation in an All-human System. Stem Cell Reviews and Reports 17:1855–1873.

Nichols E et al. (2022) Estimation of the global prevalence of dementia in 2019 and forecasted prevalence in 2050: an analysis for the Global Burden of Disease Study 2019. Lancet Public Heal 7:e105–e125 Available at: www.thelancet.com/ [Accessed July 28, 2022].

Nichols J, Zevnik B, Anastassiadis K, Niwa H, Klewe-Nebenius D, Chambers I, Schöler H, Smith A (1998) Formation of pluripotent stem cells in the mammalian embryo depends on the POU transcription factor Oct4. Cell 95:379–391.

Nielsen AL, Jørgensen AL (2004) Self-assembly of the cytoskeletal glial fibrillary acidic protein is inhibited by an isoform-specific C terminus. J Biol Chem 279:41537–41545 Available at: https://pubmed.ncbi.nlm.nih.gov/15284230/ [Accessed July 25, 2022].

Nishimura M, Namba Y, Ikeda K, Oda M (1992) Glial fibrillary tangles with straight tubules in the brains of patients with progressive supranuclear palsy. Neuroscience Letters 143:35–38.

Nixdorf-Bergweiler BE, Albrecht D (1994) Developmental Changes in the Number, Size, and Orientation of GFAP-Positive Cells in the CA1 Region of Rat Hippocampus.

Nixon RA, Wegiel J, Kumar A, Yu WH, Peterhoff C, Cataldo A, Cuervo AM (2005) Extensive Involvement of Autophagy in Alzheimer Disease: An Immuno-Electron Microscopy Study. J Neuropathol Exp Neurol 64:113–122 Available at: https://academic.oup.com/jnen/article/64/2/113/2916595 [Accessed July 27, 2022].

Nixon RA, Yang DS (2011) Autophagy failure in Alzheimer's disease-locating the primary defect. Neurobiology of Disease 43:38–45 Available at: www.sciencedirect.com [Accessed April 26, 2022].

Noble W, Olm V, Takata K, Casey E, Meyerson J, Gaynor K, LaFrancois J, Wang L, Kondo T, Davies P, Burns M, Nixon R, Dickson D, Matsuoka Y, Ahlijanian M (2003) Cdk5 Is a Key Factor in Tau Aggregation and Tangle Formation In Vivo as candidates in pathogenic tau phosphorylation. The activity of cdk5 is regulated by its binding with neuron- specific activator proteins p35, p25, and p39. Cleavage. Neuron 38:555–565.

O'Brien RJ, Wong PC (2011) Amyloid Precursor Protein Processing and Alzheimer's Disease. http://dx.doi.org/101146/annurev-neuro-061010-113613 34:185–204 Available at: https://www.annualreviews.org/doi/abs/10.1146/annurev-neuro-061010-113613 [Accessed July 14, 2022].

Oberheim NA, Wang X, Goldman S, Nedergaard M (2006) Astrocytic complexity distinguishes the human brain. Trends in Neurosciences 29:547–553.

Oide T, Ohara S, Yazawa M, Itoh N, Tokuda T, Ikeda SI (2002) Progressive supranuclear palsy with asymmetric tau pathology presenting with unilateral limb dystonia. Acta Neuropathol 104:209–214 Available at: https://pubmed.ncbi.nlm.nih.gov/12111365/ [Accessed July 13, 2022].

Olabarria M, Goldman JE (2017) Disorders of Astrocytes: Alexander Disease as a Model. Annual Review of Pathology: Mechanisms of Disease 12:131–152 Available at: https://www.annualreviews.org/doi/abs/10.1146/annurev-pathol-052016-100218 [Accessed May 29, 2022].

O'Leary LA, Davoli MA, Belliveau C, Tanti A, Ma JC, Farmer WT, Turecki G, Murai KK, Mechawar N (2020) Characterization of Vimentin-Immunoreactive Astrocytes in the Human Brain. Front Neuroanat 14.

Oliet SHR, Piet R, Poulain DA (2001) Control of glutamate clearance and synaptic efficacy by glial coverage of neurons. Science (1979) 292:923–926 Available at: https://pubmed.ncbi.nlm.nih.gov/11340204/ [Accessed July 16, 2022].

Orr AG, Hsiao EC, Wang MM, Ho K, Kim DH, Wang X, Guo W, Kang J, Yu GQ, Adame A, Devidze N, Dubal DB, Masliah E, Conklin BR, Mucke L (2015) Astrocytic adenosine receptor A2A and Gs-coupled signaling regulate memory. Nature Neuroscience 18:423–439.

Osborn LM, Kamphuis W, Wadman WJ, Hol EM (2016) Astrogliosis: An integral player in the pathogenesis of Alzheimer's disease. Progress in Neurobiology 144:121–141 Available at: http://dx.doi.org/10.1016/j.pneurobio.2016.01.001.

Osumi N, Shinohara H, Numayama-Tsuruta K, Maekawa M (2008) Concise Review: Pax6 Transcription Factor Contributes to both Embryonic and Adult Neurogenesis as a Multifunctional Regulator. Stem Cells 26:1663–1672 Available at: www.StemCells.com [Accessed July 19, 2022].

Ott A, Breteler monique MB, van Harskamp F, Claus jules J, van der Cammen TJM, Grobbee DE, Hofman A (1995) Prevalence of Alzheimer's disease and vascular dementia: association with education. The Rotterdam study. BMJ 310:970–973 Available at: https://www.bmj.com/content/310/6985/970 [Accessed July 14, 2022].

Otvos L, Feiner L, Lang E, Szendrei GI, Goedert M, Lee VM (1994) Monoclonal antibody PHF-1 recognizes tau protein phosphorylated at serine residues 396 and 404. Journal of Neuroscience Research 39:669–673.

Paholikova K, Salingova B, Opattova A, Skrabana R, Majerova P, Zilka N, Kovacech B, Zilkova M, Barath P, Novaka M (2015) N-terminal truncation of microtubule associated protein tau dysregulates its cellular localization. J Alzheimers Dis 43:915–926 Available at: https://pubmed.ncbi.nlm.nih.gov/25147106/ [Accessed July 15, 2022].

Parpura V, Basarsky TA, Liu F, Jeftinijatt K (1994) Glutamate-mediated astrocyte-neuron signalling. Nature 369:744–747.

Patterson M, Chan DN, Ha I, Case D, Cui Y, Handel B van, Mikkola HK, Lowry WE (2011) Defining the nature of human pluripotent stem cell progeny. Cell Research 2011 22:1 22:178–193 Available at: https://www.nature.com/articles/cr2011133 [Accessed May 31, 2022].

Paul D, Achouri S, Yoon YZ, Herre J, Bryant CE, Cicuta P (2013) Phagocytosis Dynamics Depends on Target Shape. Biophys J 105:1143 Available at: /pmc/articles/PMC3762343/ [Accessed July 29, 2022].

Pei JJ, Tanaka T, Tung YC, Braak E, Iqbal K, Grundke-Iqbal I (1997) Distribution, levels, and activity of glycogen synthase kinase-3 in the Alzheimer disease brain. J Neuropathol Exp Neurol 56:70–78 Available at: https://pubmed.ncbi.nlm.nih.gov/8990130/ [Accessed April 29, 2022].

Pelvig DP, Pakkenberg H, Regeur L, Oster S, Pakkenberg B (2003) Neocortical Glial Cell Numbers in Alzheimer's Disease. Dementia and Geriatric Cognitive Disorders 16:212–219 Available at: https://www.karger.com/Article/FullText/72805 [Accessed May 19, 2022].

Perea G, Navarrete M, Araque A (2009) Tripartite synapses: astrocytes process and control synaptic information. Trends in Neurosciences 32:421–431 Available at: http://www.cell.com/article/S0166223609001015/fulltext [Accessed May 3, 2022].

Perea JR, López E, Díez-Ballesteros JC, Ávila J, Hernández F, Bolós M (2019) Extracellular Monomeric Tau Is Internalized by Astrocytes. Front Neurosci 13:1–7 Available at: https://www.frontiersin.org/article/10.3389/fnins.2019.00442/full.

Perez-Nievas BG et al. (2013) Dissecting phenotypic traits linked to human resilience to Alzheimer's pathology. Brain 136:2510–2526 Available at: https://academic.oup.com/brain/article/136/8/2510/429567.

Perez-Nievas BG, Johnson L, Beltran-Lobo P, Hughes MM, Gammallieri L, Tarsitano F, Myszczynska MA, Vazquez-Villasenor I, Jimenez-Sanchez M, Troakes C, Wharton SB, Ferraiuolo L, Noble W (2021) Astrocytic C–X–C motif chemokine ligand-1 mediates β-amyloid-induced synaptotoxicity. J Neuroinflammation 18:1–17 Available at: https://jneuroinflammation.biomedcentral.com/articles/10.1186/s12974-021-02371-0 [Accessed July 29, 2022].

Perez-Nievas BG, Serrano-Pozo A (2018) Deciphering the astrocyte reaction in Alzheimer's disease. Front Aging Neurosci 10:114.

Perl DP (2010) Neuropathology of Alzheimer's disease. Mount Sinai Journal of Medicine 77:32–42 Available at: www.interscience.wiley.com.

Perng M Der, Wen SF, Gibbon T, Middeldorp J, Sluijs J, Hol EM, Quinlan RA (2008) Glial Fibrillary Acidic Protein Filaments Can Tolerate the Incorporation of Assembly-compromised GFAP-δ, but with Consequences for Filament Organization and αB-Crystallin Association. Mol Biol Cell 19:4521 Available at: /pmc/articles/PMC2555932/ [Accessed July 25, 2022].

Petry FR, Pelletier J, Bretteville A, Morin F, Calon F, Hébert SS, Whittington RA, Planel E (2014) Specificity of anti-Tau antibodies when analyzing mice models of Alzheimer's disease: Problems and solutions. PLoS ONE 9.

Pfrieger FW, Ungerer N (2011) Cholesterol metabolism in neurons and astrocytes. Prog Lipid Res 50:357–371 Available at: https://pubmed.ncbi.nlm.nih.gov/21741992/ [Accessed May 3, 2022].

Pick A (1892) Uber die Beziehungen der senilen Hirnatrophie zur Aphasie. Prag Med Wochenschr 17:165–167.

Pickart CM (2001) Ubiquitin enters the new millennium. Mol Cell 8:499–504 Available at: https://pubmed.ncbi.nlm.nih.gov/11583613/ [Accessed July 16, 2022].

Pilotto A, Parigi M, Bonzi G, Battaglio B, Ferrari E, Mensi L, Benussi A, Caratozzolo S, Cosseddu M, Turrone R, Archetti S, Ashton NJ, Zetterberg H, Giliani S, Padovani A, Pado A (2022) Differences Between Plasma and Cerebrospinal Fluid p-tau181 and p-tau231 in Early Alzheimer's Disease. J Alzheimer's Dis 87:991–997.

Piras A, Collin L, Grüninger F, Graff C, Rönnbäck A (2016) Autophagic and lysosomal defects in human tauopathies: analysis of post-mortem brain from patients with familial Alzheimer disease, corticobasal degeneration and progressive supranuclear palsy. Acta Neuropathol Commun 4:22.

Polanco JC, Scicluna BJ, Hill AF, Götz J (2016) Extracellular vesicles isolated from the brains of rTg4510 mice seed tau protein aggregation in a threshold-dependent manner. Journal of Biological Chemistry 291:12445–12466.

Polydoro M, Acker CM, Duff K, Castillo PE, Davies P (2009) Age-Dependent Impairment of Cognitive and Synaptic Function in the htau Mouse Model of Tau Pathology. Journal of Neuroscience 29:10741–10749.

Pooler AM, Phillips EC, Lau DHW, Noble W, Hanger DP (2013) Physiological release of endogenous tau is stimulated by neuronal activity. EMBO Reports 14:389–394 Available at: http://dx.doi.org/10.1038/embor.2013.15.

Pooler AM, Usardi A, Evans CJ, Philpott KL, Noble W, Hanger DP (2012) Dynamic association of tau with neuronal membranes is regulated by phosphorylation. Neurobiology of Aging 33:431.e27-431.e38 Available at: http://dx.doi.org/10.1016/j.neurobiolaging.2011.01.005.

Potokar M, Stenovec M, Gabrijel M, Li L, Kreft M, Grilc S, Pekny M, Zorec R (2010) Intermediate filaments attenuate stimulation-dependent mobility of endosomes/lysosomes in astrocytes. Glia 58:1208–1219.

Praschberger R, Kuenen S, Schoovaerts N, Kaempf N, Janssens J, Swerts J, Nachman E, Calatayud C, Aerts S, Poovathingal S, Verstreken P (2022) Neuronal identity defines a-synuclein and tau toxicity. bioRxiv Available at: https://doi.org/10.1101/2022.06.24.496376.

Price JC, Guan S, Burlingame A, Prusiner SB, Ghaemmaghami S (2010) Analysis of proteome dynamics in the mouse brain. Proc Natl Acad Sci U S A 107:14508–14513 Available at: /pmc/articles/PMC2922600/ [Accessed July 25, 2022].

Prigent A, Chapelet | Guillaume, de Guilhem De Lataillade A, Oullier T, Durieu E, Arnaud Bourreille |, Duchalais E, Hardonnière K, Neunlist | Michel, Noble W, Saadia Kerdine-Römer |, Derkinderen | Pascal, Rolli-Derkinderen M (2020) Tau accumulates in Crohn's disease gut. The FASEB Journal 34:9285–9296.

Prince M, Ali GC, Guerchet M, Prina AM, Albanese E, Wu YT (2016) Recent global trends in the prevalence and incidence of dementia, and survival with dementia. Alzheimer's Research and Therapy 8 Available at: http://dx.doi.org/10.1186/s13195-016-0188-8.

Probst A, Ulrich J, Heitz PU (1982) Senile dementia of Alzheimer type: Astroglial reaction to extracellular neurofibrillary tangles in the hippocampus. Acta Neuropathol 1982 571 57:75–79 Available at: https://link.springer.com/article/10.1007/BF00688880 [Accessed July 26, 2022].

Przyborski SA, Cambray-Deakin MA (1995) Developmental regulation of MAP2 variants during neuronal differentiation in vitro. Brain Res Dev Brain Res 89:187–201 Available at: https://pubmed.ncbi.nlm.nih.gov/8612323/ [Accessed July 25, 2022].

Rambotti MG, Giambanco I, Spreca A, Donato R (1999) S100B and S100A1 proteins in bovine retina:their calcium-dependent stimulation of a membrane-bound guanylate cyclase activity as investigated by ultracytochemistry. Neuroscience 92:1089–1101 Available at: https://pubmed.ncbi.nlm.nih.gov/10426548/ [Accessed July 18, 2022].

Ramsden M, Kotilinek L, Forster C, Paulson J, McGowan E, SantaCruz K, Guimaraes A, Yue M, Lewis J, Carlson G, Hutton M, Ashe KH (2005) Age-dependent neurofibrillary tangle formation, neuron loss, and memory impairment in a mouse model of human tauopathy (P301L). Journal of Neuroscience 25:10637–10647.

Raponi E, Agenes F, Delphin C, Assard N, Baudier J, Legraverend C, Deloulme J-C (2007) S100B expression defines a state in which GFAP-expressing cells lose their neural stem cell potential and acquire a more mature developmental stage. Glia 55:165–177 Available at: https://onlinelibrary.wiley.com/doi/full/10.1002/glia.20445 [Accessed May 16, 2021].

Rascovsky K et al. (2011) Sensitivity of revised diagnostic criteria for the behavioural variant of frontotemporal dementia. Brain 134:2456–2477 Available at: https://pubmed.ncbi.nlm.nih.gov/21810890/ [Accessed July 13, 2022].

Rauch JN, Chen JJ, Sorum AW, Miller GM, Sharf T, See SK, Hsieh-Wilson LC, Kampmann M, Kosik KS (2018) Tau Internalization is Regulated by 6-O Sulfation on Heparan Sulfate Proteoglycans (HSPGs). Sci Rep 8:1–10.

Rauch JN, Luna G, Guzman E, Audouard M, Challis C, Sibih YE, Leshuk C, Hernandez I, Wegmann S, Hyman BT, Gradinaru V, Kampmann M, Kosik KS (2020) LRP1 is a master regulator of tau uptake and spread. Nature 1:1–5 Available at: http://www.nature.com/articles/s41586-020-2156-5.

Raux G, Guyant-Maréchal L, Martin C, Bou J, Penet C, Brice A, Hannequin D (2005) Molecular diagnosis of autosomal dominant early onset Alzheimer's disease: an update. J Med Genet 42:793–795 Available at: www.jmedgenet.com.

Re DB, le Verche V, Yu C, Amoroso MW, Politi KA, Phani S, Ikiz B, Hoffmann L, Koolen M, Nagata T, Papadimitriou D, Nagy P, Mitsumoto H, Kariya S, Wichterle H, Henderson CE, Przedborski S (2014) Necroptosis drives motor neuron death in models of both sporadic and familial ALS. Neuron 81:1001–1008.

Rebeiz JJ, Kolodny EH, Richardson EP (1968) Corticodentatonigral Degeneration With Neuronal Achromasia. Archives of Neurology 18:20–33 Available at: https://jamanetwork.com/journals/jamaneurology/fullarticle/567770 [Accessed July 13, 2022].

Reid MJ, Beltran-Lobo P, Johnson L, Perez-Nievas BG, Noble W (2020) Astrocytes in Tauopathies. Front Neurol 11:1–9.

Richetin K, Steullet P, Pachoud M, Perbet R, Parietti E, Maheswaran M, Eddarkaoui S, Bégard S, Pythoud C, Rey M, Caillierez R, Q Do K, Halliez S, Bezzi P, Buée L, Leuba G, Colin M, Toni N, Déglon N (2020) Tau accumulation in astrocytes of the dentate gyrus induces neuronal dysfunction and memory deficits in Alzheimer's disease. Nature Neuroscience 23:1567–1579 Available at: https://doi.org/10.1038/s41593-020-00728-x.

Ricklin D, Reis ES, Mastellos DC, Gros P, Lambris JD (2016) Complement component C3 – The "Swiss Army Knife" of innate immunity and host defense. Immunol Rev 274:33–58.

Ries M, Sastre M (2016) Mechanisms of Aβ clearance and degradation by glial cells. Front Aging Neurosci 8:160.

Robbins JP, Perfect L, Ribe EM, Maresca M, Dangla-Valls A, Foster EM, Killick R, Nowosiad P, Reid MJ, Polit LD, Nevado AJ, Ebner D, Bohlooly-Y M, Buckley N, Pangalos MN, Price J, Lovestone S (2018) Clusterin Is Required for β-Amyloid Toxicity in Human iPSC-Derived Neurons. Frontiers in Neuroscience 12:1–13 Available at: https://www.frontiersin.org/article/10.3389/fnins.2018.00504/full.

Robbins JP, Perfect L, Ribe EM, Maresca M, Dangla-Valls A, Foster EM, Killick R, Nowosiad P, Reid MJ, Polit LD, Nevado AJ, Ebner D, Bohlooly-Y M, Buckley N, Pangalos MN, Price J, Lovestone S (2018) Clusterin Is Required for β-Amyloid Toxicity in Human iPSC-Derived Neurons. Front Neurosci 12:1–13 Available at: https://www.frontiersin.org/article/10.3389/fnins.2018.00504/full.

Robbins M, Clayton E, Kaminski Schierle GS (2021) Synaptic tau: A pathological or physiological phenomenon? Acta Neuropathol Commun 9:1–30 Available at: https://doi.org/10.1186/s40478-021-01246-y.

Rodríguez-Martín T, Cuchillo-Ibáñez I, Noble W, Nyenya F, Anderton BH, Hanger DP (2013) Tau phosphorylation affects its axonal transport and degradation. Neurobiol Aging 34:2146–2157.

Rose CR, Ziemens D, Untiet V, Fahlke C (2018) Molecular and cellular physiology of sodium-dependent glutamate transporters. Brain Research Bulletin 136:3–16 Available at: https://doi.org/10.1016/j.brainresbull.2016.12.013.

Rothstein JD, Martin L, Levey AI, Dykes-Hoberg M, Jin L, Wu D, Nash N, Kuncl RW (1994) Localization of neuronal and glial glutamate transporters. Neuron 13:713–725.

Rothstein JD, Patel S, Regan MR, Haenggeli C, Huang YH, Bergles DE, Jin L, Hoberg MD, Vidensky S, Chung DS, Shuy VT, Bruijn LI, Su ZZ, Gupta P, Fisher PB (2005) Beta-lactam antibiotics offer neuroprotection by increasing glutamate transporter expression. Nature 433:73–77 Available at: https://pubmed.ncbi.nlm.nih.gov/15635412/ [Accessed July 17, 2022].

Ryu JK, McLarnon JG (2009) A leaky blood-brain barrier, fibrinogen infiltration and microglial reactivity in inflamed Alzheimer's disease brain. J Cell Mol Med 13:2911–2925 Available at: https://pubmed.ncbi.nlm.nih.gov/18657226/ [Accessed July 28, 2022].

Saito Y, Ruberu NN, Sawabe M, Arai T, Tanaka N, Kakuta Y, Yamanouchi H, Murayama S (2004) Staging of argyrophilic grains: An age-associated tauopathy. Journal of Neuropathology and Experimental Neurology 63:911–918.

Saman S, Kim WH, Raya M, Visnick Y, Miro S, Saman S, Jackson B, McKee AC, Alvarez VE, Lee NCY, Hall GF (2012) Exosome-associated tau is secreted in tauopathy models and is selectively phosphorylated in cerebrospinal fluid in early Alzheimer disease. Journal of Biological Chemistry 287:3842–3849 Available at: http://dx.doi.org/10.1074/jbc.M111.277061.

Sanmarco LM, Wheeler MA, Gutiérrez-Vázquez C, Polonio CM, Linnerbauer M, Pinho-Ribeiro FA, Li Z, Giovannoni F, Batterman K v, Scalisi G, Zandee SEJ, Heck ES, Alsuwailm M, Rosene DL, Becher B, Chiu IM, Prat A, Quintana FJ (2021) Gut-licensed IFNγ + NK cells drive LAMP1 + TRAIL + anti-inflammatory astrocytes Identification of LAMP1 + astrocytes. Nature 590:473 Available at: https://doi.org/10.1038/s41586-020-03116-4 [Accessed January 27, 2022].

Santello M, Toni N, Volterra A (2019) Astrocyte function from information processing to cognition and cognitive impairment. Nature Neuroscience 22:154–166 Available at: http://dx.doi.org/10.1038/s41593-018-0325-8.

Sarrazin S, Lamanna WC, Esko JD (2011) Heparan Sulfate Proteoglycans. Cold Spring Harbor Perspectives in Biology 3:a004952–a004952 Available at: http://cshperspectives.cshlp.org/lookup/doi/10.1101/cshperspect.a004952.

Schaler AW, Runyan AM, Clelland CL, Sydney EJ, Fowler SL, Figueroa HY, Shioda S, Santa-Maria I, Duff KE, Myeku N (2021) PAC1 receptor-mediated clearance of tau in postsynaptic compartments attenuates tau pathology in mouse brain. Sci Transl Med 13 Available at: https://pubmed.ncbi.nlm.nih.gov/34039738/ [Accessed July 29, 2022].

Scheff SW, Price DA, Schmitt FA, Mufson EJ (2006) Hippocampal synaptic loss in early Alzheimer's disease and mild cognitive impairment. Neurobiology of Aging 27:1372–1384.

Schindelin J, Arganda-Carreras I, Frise E, Kaynig V, Longair M, Pietzsch T, Preibisch S, Rueden C, Saalfeld S, Schmid B, Tinevez JY, White DJ, Hartenstein V, Eliceiri K, Tomancak P, Cardona A (2012) Fiji: An open-source platform for biological-image analysis. Nature Methods 9:676–682.

Schindowski K, Bretteville A, Leroy K, Bégard S, Brion JP, Hamdane M, Buée L (2006) Alzheimer's disease-like tau neuropathology leads to memory deficits and loss of functional synapses in a novel

mutated tau transgenic mouse without any motor deficits. American Journal of Pathology 169:599–616.

Schiweck J, Eickholt BJ, Murk K (2018) Important shapeshifter: Mechanisms allowing astrocytes to respond to the changing nervous system during development, injury and disease. Front Cell Neurosci 12:261.

Schiweck J, Eickholt BJ, Murk K (2018) Important shapeshifter: Mechanisms allowing astrocytes to respond to the changing nervous system during development, injury and disease. Frontiers in Cellular Neuroscience 12:261.

Schmitt A, Asan E, Püschel B, Kugler P (1997) Cellular and regional distribution of the glutamate transporter GLAST in the CNS of rats: Nonradioactive in situ hybridization and comparative immunocytochemistry. J Neurosci 17:1–10.

Schmitt A, Asan E, Püschel B, Kugler P (1997) Cellular and regional distribution of the glutamate transporter GLAST in the CNS of rats: Nonradioactive in situ hybridization and comparative immunocytochemistry. Journal of Neuroscience 17:1–10.

Schnitzer J, Franke WW, Schachner M (1981) Immunocytochemical demonstration of vimentin in astrocytes and ependymal cells of developing and adult mouse nervous system. The Journal of Cell Biology 90:435 Available at: /pmc/articles/PMC2111851/?report=abstract [Accessed July 17, 2022].

Schonberger O, Horonchik L, Gabizon R, Papy-Garcia D, Barritault D, Taraboulos A (2003) Novel heparan mimetics potently inhibit the scrapie prion protein and its endocytosis. Biochemical and Biophysical Research Communications 312:473–479.

Schreiner AE, Durry S, Aida T, Stock MC, Rüther U, Tanaka K, Rose CR, Kafitz KW (2014) Laminar and subcellular heterogeneity of GLAST and GLT-1 immunoreactivity in the developing postnatal mouse hippocampus. J Comp Neurol 522:204–224.

Schreiner AE, Durry S, Aida T, Stock MC, Rüther U, Tanaka K, Rose CR, Kafitz KW (2014) Laminar and subcellular heterogeneity of GLAST and GLT-1 immunoreactivity in the developing postnatal mouse hippocampus. Journal of Comparative Neurology 522:204–224.

Scott CE, Wynn SL, Sesay A, Cruz C, Cheung M, Gaviro MVG, Booth S, Gao B, Cheah KSE, Lovell-Badge R, Briscoe J (2010) SOX9 induces and maintains neural stem cells. Nat Neurosci 13:1181–1189.

Scott CE, Wynn SL, Sesay A, Cruz C, Cheung M, Gaviro MVG, Booth S, Gao B, Cheah KSE, Lovell-Badge R, Briscoe J (2010) SOX9 induces and maintains neural stem cells. Nature Neuroscience 13:1181–1189.

Scotter EL, Vance C, Nishimura AL, Lee YB, Chen HJ, Urwin H, Sardone V, Mitchell JC, Rogelj B, Rubinsztein DC, Shaw CE (2014) Differential roles of the ubiquitin proteasome system and autophagy in the clearance of soluble and aggregated TDP-43 species. J Cell Sci 127:1263–1278 Available at: https://journals.biologists.com/jcs/article/127/6/1263/54855/Differential-roles-of-the-ubiquitin-proteasome [Accessed July 26, 2022].

Seiberlich V, Bauer NG, Schwarz L, Ffrench-Constant C, Goldbaum O, Richter-Landsberg C (2015) Downregulation of the microtubule associated protein Tau impairs process outgrowth and myelin basic protein mRNA transport in oligodendrocytes. Glia 63:1621–1635.

Selinfreund RH, Barger SW, Pledger WJ, Van Eldik LJ (1991) Neurotrophic protein S100 beta stimulates glial cell proliferation. Proc Natl Acad Sci U S A 88:3554 Available at: /pmc/articles/PMC51490/?report=abstract [Accessed July 25, 2022].

Selkoe DJ, Hardy J (2016) The amyloid hypothesis of Alzheimer's disease at 25 years. EMBO Mol Med 8:595–608 Available at: https://pubmed.ncbi.nlm.nih.gov/27025652/ [Accessed July 28, 2022].

Semyanov A, Henneberger C, Agarwal A (2020) Making sense of astrocytic calcium signals — from acquisition to interpretation. Nature Reviews Neuroscience 21:551–564 Available at: www.nature.com/nrn.

Sergeant N, Delacourte A, Buée L (2005) Tau protein as a differential biomarker of tauopathies. Biochimica et Biophysica Acta - Molecular Basis of Disease 1739:179–197.

Serrano-Pozo A, Das S, Hyman BT (2021) APOE and Alzheimer's disease: advances in genetics, pathophysiology, and therapeutic approaches. The Lancet Neurology 20:68–80 Available at: http://dx.doi.org/10.1016/S1474-4422(20)30412-9.

Serrano-Pozo A, Frosch MP, Masliah E, Hyman BT (2011a) Neuropathological alterations in Alzheimer disease. Cold Spring Harbor Perspectives in Medicine 1:1–23.

Serrano-Pozo A, Mielke ML, Gómez-Isla T, Betensky RA, Growdon JH, Frosch MP, Hyman BT (2011) Reactive glia not only associates with plaques but also parallels tangles in Alzheimer's disease. Am J Pathol 179:1373–1384 Available at: http://dx.doi.org/10.1016/j.ajpath.2011.05.047.

Serrano-Pozo A, Mielke ML, Gómez-Isla T, Betensky RA, Growdon JH, Frosch MP, Hyman BT (2011b) Reactive glia not only associates with plaques but also parallels tangles in Alzheimer's disease. American Journal of Pathology 179:1373–1384 Available at: http://dx.doi.org/10.1016/j.ajpath.2011.05.047.

Setó-Salvia N, Esteras N, de Silva R, de Pablo-Fernandez E, Arber C, Toomey CE, Polke JM, Morris HR, Rohrer JD, Abramov AY, Patani R, Wray S, Warner TT (2022) Elevated 4R-tau in astrocytes from asymptomatic carriers of the MAPT 10+16 intronic mutation. Journal of Cellular and Molecular Medicine 26:1327–1331.

Shaltouki A, Peng J, Liu Q, Rao MS, Zeng X (2013) Efficient generation of astrocytes from human pluripotent stem cells in defined conditions. Stem Cells 31:941–952.

Shang F, Taylor A (2011) Ubiquitin-proteasome pathway and cellular responses to oxidative stress. Free Radic Biol Med 51:5–16 Available at: https://pubmed.ncbi.nlm.nih.gov/21530648/ [Accessed July 16, 2022].

Sheng JG, ak RE, Griffin WST (1994) S100 beta protein expression in Alzheimer disease: potential role in the pathogenesis of neuritic plaques. J Neurosci Res 39:398–404 Available at: https://pubmed.ncbi.nlm.nih.gov/7884819/ [Accessed July 24, 2022].

Shi Y et al. (2021) Structure-based classification of tauopathies. Nature 598:359–363 Available at: http://dx.doi.org/10.1038/s41586-021-03911-7.

Shi Y, Kirwan P, Livesey FJ (2012a) Directed differentiation of human pluripotent stem cells to cerebral cortex neurons and neural networks. Nature Protocols 7:1836–1846.

Shi Y, Kirwan P, Smith J, Robinson HPC, Livesey FJ (2012b) Human cerebral cortex development from pluripotent stem cells to functional excitatory synapses. Nat Neurosci 15:477–486.

Shibata T, Yamada K, Watanabe M, Ikenaka K, Wada K, Tanaka K, Inoue Y (1997) Glutamate transporter GLAST is expressed in the radial glia-astrocyte lineage of developing mouse spinal cord. J Neurosci 17:9212–9219.

Shibuki K, Gomi H, Chen L, Bao S, Kim JJ, Wakatsuki H, Fujisaki T, Fujimoto K, Katoh A, Ikeda T, Chen C, Thompson RF, Itohara S (1996) Deficient cerebellar long-term depression, impaired eyeblink conditioning, and normal motor coordination in GFAP mutant mice. Neuron 16:587–599 Available at: https://pubmed.ncbi.nlm.nih.gov/8785056/ [Accessed July 18, 2022].

Shiga A, Takahashi H, Tada M, Nishizawa M, Yokoyama Y, Onodera O, Kitamura H, Kakita A, Hasegawa K, Ikeuchi T, Someya T, Toyoshima Y (2015) Pathological and Clinical Spectrum of Progressive Supranuclear Palsy: With Special Reference to Astrocytic Tau Pathology. Brain Pathology 26:155–166.

Sidoryk-Węgrzynowicz M, Struzyńska L (2019) Astroglial contribution to tau-dependent neurodegeneration. Biochemical Journal 476:3493–3504.

Sillen A, Barbier P, Landrieu I, Lefebvre S, Wieruszeski JM, Leroy A, Peyrot V, Lippens G (2007) NMR investigation of the interaction between the neuronal protein Tau and the microtubules. Biochemistry 46:3055–3064 Available at: https://pubs.acs.org/sharingguidelines [Accessed July 15, 2022].

Simonovitch S, Schmukler E, Bespalko A, Iram T, Frenkel D, Holtzman DM, Masliah E, Michaelson DM, Pinkas-Kramarski R (2016) Impaired Autophagy in APOE4 Astrocytes. J Alzheimers Dis 51:915–927 Available at: https://pubmed.ncbi.nlm.nih.gov/26923027/ [Accessed July 20, 2022].

Singleton E et al. (2021) Heterogeneous distribution of tau pathology in the behavioural variant of Alzheimer's disease. J Neurol Neurosurg Psychiatry 0:1–9 Available at: https://www.

Skripuletz T, Hackstette D, Bauer K, Gudi V, Pul R, Voss E, Berger K, Kipp M, Baumgärtner W, Stangel M (2013) Astrocytes regulate myelin clearance through recruitment of microglia during cuprizone-induced demyelination. Brain 136:147–167 Available at: https://academic.oup.com/brain/article/136/1/147/430328 [Accessed June 1, 2022].

Slooter AJC, Cruts M, Kalmijn S, Hofman A, Breteler MMB, Van Broeckhoven C, Van Duijn CM (1998) Risk estimates of dementia by apolipoprotein E genotypes from a population-based incidence study: The Rotterdam study. Archives of Neurology 55:964–968.

Small SA, Simoes-Spassov S, Mayeux R, Petsko GA (2017) Endosomal Traffic Jams Represent a Pathogenic Hub and Therapeutic Target in Alzheimer's Disease. Trends in Neurosciences 40:592–602 Available at: http://dx.doi.org/10.1016/j.tins.2017.08.003 [Accessed April 26, 2022].

Sofroniew M v, Vinters H v (2010) Astrocytes: biology and pathology. Acta Neuropathol 119:7–35 Available at: http://www.ncbi.nlm.nih.gov/pubmed/20012068%0Ahttp://www.pubmedcentral.nih.gov/articlerender.fcgi?artid=PMC2799634.

Söllvander S, Nikitidou E, Brolin R, Söderberg L, Sehlin D, Lannfelt L, Erlandsson A (2016) Accumulation of amyloid-β by astrocytes result in enlarged endosomes and microvesicle-induced apoptosis of neurons. Molecular Neurodegeneration 11:1–19 Available at: http://dx.doi.org/10.1186/s13024-016-0098-z.

Solomon DA, Smikle R, Reid MJ, Mizielinska S (2021) Altered Phase Separation and Cellular Impact in C9orf72-Linked ALS/FTD. Frontiers in Cellular Neuroscience 15:1–24 Available at: https://www.frontiersin.org/articles/10.3389/fncel.2021.664151/full.

Spaethling JM et al. (2017) Primary cell culture of live neurosurgically-resected aged adult human brain cells and single cell transcriptomics. Cell Rep 18:791 Available at: /pmc/articles/PMC5316103/ [Accessed May 30, 2022].

Spanos F, Liddelow SA (2020) An Overview of Astrocyte Responses in Genetically Induced Alzheimer's Disease Mouse Models. Cells 9:1–33.

Spicakova T, O'Brien MM, Duran GE, Sweet-Cordero A, Sikic BI (2010) Expression and silencing of the microtubule-associated protein Tau in breast cancer cells. Molecular Cancer Therapeutics 9:2970–2981.

Spires-Jones TL, Hyman BT (2014) The Intersection of Amyloid Beta and Tau at Synapses in Alzheimer's Disease. Neuron 82:756–771 Available at: http://dx.doi.org/10.1016/j.neuron.2014.05.004 [Accessed April 26, 2022].

Sposito T, Preza E, Mahoney CJ, Setó-Salvia N, Ryan NS, Morris HR, Arber C, Devine MJ, Houlden H, Warner TT, Bushell TJ, Zagnoni M, Kunath T, Livesey FJ, Fox NC, Rossor MN, Hardy J, Wray S (2015) Developmental regulation of tau splicing is disrupted in stem cell-derived neurons from frontotemporal dementia patients with the 10 + 16 splice-site mutation in MAPT. Hum Mol Genet 24:5260–5269.

Stamer K, Vogel R, Thies E, Mandelkow E, Mandelkow EM (2002) Tau blocks traffic of organelles, neurofilaments, and APP vesicles in neurons and enhances oxidative stress. J Cell Biol 156:1051–1063 Available at: https://pubmed.ncbi.nlm.nih.gov/11901170/ [Accessed July 15, 2022].

Staurenghi E, Cerrato V, Gamba P, Testa G, Giannelli S, Leoni V, Caccia C, Buffo A, Noble W, Perez-Nievas BG, Leonarduzzi G (2021) Oxysterols present in Alzheimer's disease brain induce synaptotoxicity by activating astrocytes: A major role for lipocalin-2. Redox Biol 39 Available at: https://pubmed.ncbi.nlm.nih.gov/33360775/ [Accessed July 29, 2022].

Steele JC, Richardson JC, Olszewski J (1964) PROGRESSIVE SUPRANUCLEAR PALSY. A HETEROGENEOUS DEGENERATION INVOLVING THE BRAIN STEM, BASAL GANGLIA AND CEREBELLUM WITH VERTICAL GAZE AND PSEUDOBULBAR PALSY, NUCHAL DYSTONIA AND DEMENTIA. Arch Neurol 10:333–359 Available at: https://pubmed.ncbi.nlm.nih.gov/14107684/ [Accessed July 13, 2022].

Stefansson H et al. (2005) A common inversion under selection in Europeans. Nature Genetics 37:129–137.

Stein TD, Alvarez VE, McKee AC (2014) Chronic traumatic encephalopathy: a spectrum of neuropathological changes following repetitive brain trauma in athletes and military personnel. Alzheimer's Research & Therapy 6:4.

Stelzmann RA, Norman Schnitzlein H, Reed Murtagh F (1995) An English translation of Alzheimer's 1907 paper, "Uber eine eigenartige Erkankung der Hirnrinde." Clin Anat 8:429–431 Available at: https://pubmed.ncbi.nlm.nih.gov/8713166/ [Accessed July 14, 2022].

Stobart JL, Ferrari KD, Barrett MJP, Glück C, Stobart MJ, Zuend M, Weber B (2018) Cortical Circuit Activity Evokes Rapid Astrocyte Calcium Signals on a Similar Timescale to Neurons. Neuron 98:726-735.e4 Available at: https://doi.org/10.1016/j.neuron.2018.03.050 [Accessed April 20, 2022].

Stopschinski BE, Holmes BB, Miller GM, Manon VA, Vaquer-Alicea J, Prueitt WL, Hsieh-Wilson LC, Diamond MI (2018) Specific glycosaminoglycan chain length and sulfation patterns are required for cell uptake of tau versus -synuclein and -amyloid aggregates. Journal of Biological Chemistry 293:10826–10840.

Su B, Wang X, Drew KL, Perry G, Smith MA, Zhu X (2008) Physiological regulation of tau phosphorylation during hibernation. Journal of Neurochemistry 105:2098–2108.

Sultan A, Nesslany F, Violet M, Bégard S, Loyens A, Talahari S, Mansuroglu Z, Marzin D, Sergeant N, Humez S, Colin M, Bonnefoy E, Buée L, Galas MC (2011) Nuclear Tau, a key player in neuronal DNA protection. Journal of Biological Chemistry 286:4566–4575.

Swanson RA, Liu J, Miller JW, Rothstein JD, Farrell K, Stein BA, Longuemare MC (1997) Neuronal Regulation of Glutamate Transporter Subtype Expression in Astrocytes. Journal of Neuroscience 17:932–940 Available at: https://www.jneurosci.org/content/17/3/932 [Accessed May 31, 2022].

Swartzlander DB, Propson NE, Roy ER, Saito T, Saido T, Wang B, Zheng H (2018) Concurrent cell type–specific isolation and profiling of mouse brains in inflammation and Alzheimer's disease. JCI Insight 3 Available at: https://insight.jci.org/articles/view/121109.

Szabo A, Akkouh IA, Vandenberghe M, Osete JR, Hughes T, Heine V, Smeland OB, Glover JC, Andreassen OA, Djurovic S (n.d.) ARTICLE OPEN A human iPSC-astroglia neurodevelopmental model reveals divergent transcriptomic patterns in schizophrenia. Available at: https://doi.org/10.1038/s41398-021-01681-4 [Accessed July 18, 2022].

Tai HC, Wang BY, Serrano-Pozo A, Frosch MP, Spires-Jones TL, Hyman BT (2014) Frequent and symmetric deposition of misfolded tau oligomers within presynaptic and postsynaptic terminals in Alzheimer's disease. Available at: http://www.actaneurocomms.org/content/2/1/146.

Tarasoff-Conway JM, Carare RO, Osorio RS, Glodzik L, Butler T, Fieremans E, Axel L, Rusinek H, Nicholson C, Zlokovic B v., Frangione B, Blennow K, Ménard J, Zetterberg H, Wisniewski T, de Leon MJ (2015) Clearance systems in the brain - Implications for Alzheimer disease. Nat Rev Neurol 11:457–470.

Takahashi K, Kong Q, Lin Y, Stouffer N, Schulte DA, Lai L, Liu Q, Chang LC, Dominguez S, Xing X, Cuny GD, Hodgetts KJ, Glicksman MA, Lin CLG (2015) Restored glial glutamate transporter EAAT2 function as a potential therapeutic approach for Alzheimer's disease. The Journal of Experimental Medicine 212:319 Available at: /pmc/articles/PMC4354363/ [Accessed July 17, 2022].

Takahashi K, Yamanaka S (2006) Induction of pluripotent stem cells from mouse embryonic and adult fibroblast cultures by defined factors. Cell 126:663–676 Available at: http://www.ncbi.nlm.nih.gov/pubmed/16904174.

Tang G, Yue Z, Talloczy Z, Hagemann T, Cho W, Messing A, Sulzer DI, Goldman JE (2008) Autophagy induced by Alexander disease-mutant GFAP accumulation is regulated by p38/MAPK and mTOR signaling pathways. Hum Mol Genet 17:1540–1555 Available at: https://pubmed.ncbi.nlm.nih.gov/18276609/ [Accessed July 20, 2022].

Tardivel M, Bégard S, Bousset L, Dujardin S, Coens A, Melki R, Buée L, Colin M (2016) Tunneling nanotube (TNT)-mediated neuron-to neuron transfer of pathological Tau protein assemblies. Acta Neuropathol Commun 4:117 Available at: http://dx.doi.org/10.1186/s40478-016-0386-4.

TCW J, Wang M, Pimenova AA, Bowles KR, Hartley BJ, Lacin E, Machlovi SI, Abdelaal R, Karch CM, Phatnani H, Slesinger PA, Zhang B, Goate AM, Brennand KJ (2017) An Efficient Platform for Astrocyte Differentiation from Human Induced Pluripotent Stem Cells. Stem Cell Reports 9:600–614 Available at: http://dx.doi.org/10.1016/j.stemcr.2017.06.018.

Terry RD (1963) The Fine Structure of Neurofibrillary Tangles in Alzheimer's Disease. Journal of Neuropathology & Experimental Neurology 22:629–642.

Thal DR, Rüb U, Orantes M, Braak H (2002) Phases of A beta-deposition in the human brain and its relevance for the development of AD. Neurology 58:1791–1800 Available at: https://pubmed.ncbi.nlm.nih.gov/12084879/ [Accessed July 14, 2022].

Thambisetty M, An Y, Tanaka T (2013) Alzheimer's disease risk genes and the age-at-onset phenotype. Neurobiology of Aging 34:2696.e1-2696.e5.

Thibaudeau TA, Anderson RT, Smith DM (2018) A common mechanism of proteasome impairment by neurodegenerative disease-associated oligomers. Nat Commun 9.

Thies E, Mandelkow EM (2007) Missorting of tau in neurons causes degeneration of synapses that can be rescued by the kinase MARK2/Par-1. Journal of Neuroscience 27:2896–2907.

Thinakaran G, Koo EH (2008) Amyloid precursor protein trafficking, processing, and function. Journal of Biological Chemistry 283:29615–29619.

Thrower JS, Hoffman L, Rechsteiner M, Pickart CM (2000) Recognition of the polyubiquitin proteolytic signal. EMBO J 19:94–102 Available at: https://pubmed.ncbi.nlm.nih.gov/10619848/ [Accessed July 16, 2022].

Tong X, Ao Y, Faas GC, Nwaobi SE, Xu J, Haustein MD, Anderson MA, Mody I, Olsen ML, Sofroniew M v., Khakh BS (2014) Astrocyte Kir4.1 ion channel deficits contribute to neuronal dysfunction in Huntington's disease model mice. Nat Neurosci 17:694–703 Available at: https://pubmed.ncbi.nlm.nih.gov/24686787/ [Accessed July 16, 2022].

Torres AK, Jara C, Olesen MA, Tapia-Rojas C (2021) Pathologically phosphorylated tau at S396/404 (PHF-1) is accumulated inside of hippocampal synaptic mitochondria of aged Wild-type mice. Scientific Reports 11:1–17 Available at: https://doi.org/10.1038/s41598-021-83910-w.

Trabzuni D, Wray S, Vandrovcova J, Ramasamy A, Walker R, Smith C, Luk C, Gibbs JR, Dillman A, Hernandez DG, Arepalli S, Singleton AB, Cookson MR, Pittman AM, de silva R, Weale ME, Hardy J, Ryten M (2012) MAPT expression and splicing is differentially regulated by brain region: Relation to genotype and implication for tauopathies. Human Molecular Genetics 21:4094–4103.

Tselnicker IF, Boisvert MM, Allen NJ (2014) The role of neuronal versus astrocyte-derived heparan sulfate proteoglycans in brain development and injury. Biochemical Society Transactions 42:1263–1269.

Tsuboi Y, Josephs KA, Boeve BF, Litvan I, Caselli RJ, Caviness JN, Uitti RJ, Bott AD, Dickson DW (2005) Increased tau burden in the cortices of progressive supranuclear palsy presenting with corticobasal syndrome. Mov Disord 20:982–988 Available at: https://pubmed.ncbi.nlm.nih.gov/15834857/ [Accessed July 13, 2022].

Tsunemi T, Ishiguro Y, Yoroisaka A, Valdez C, Miyamoto K, Ishikawa K, Saiki S, Akamatsu W, Hattori N, Krainc D (2020) Astrocytes protect human dopaminergic neurons from α-synuclein accumulation and propagation. J Neurosci 40:8618–8628.

Turnbull J, Powell A, Guimond S (2001) Heparan sulfate: Decoding a dynamic multifunctional cell regulator. Trends in Cell Biology 11:75–82.

Uhlén M et al. (2015) Tissue-based map of the human proteome. Science (1979) 347.

Ukmar-Godec T, Fang P, Ibáñez de Opakua A, Henneberg F, Godec A, Pan KT, Cima-Omori MS, Chari A, Mandelkow E, Urlaub H, Zweckstetter M (2020) Proteasomal degradation of the intrinsically disordered protein tau at single-residue resolution. Science Advances 6:1–13.

Ullensvang K, Lehre KP, Storm-Mathisen J, Danbolt NC (1997) Differential developmental expression of the two rat brain glutamate transporter proteins GLAST and GLT. European Journal of Neuroscience 9:1646–1655.

Underhill DM, Goodridge HS (2012) Information processing during phagocytosis. Nature Reviews Immunology 12:492–502.

Usardi A, Pooler AM, Seereeram A, Reynolds CH, Derkinderen P, Anderton B, Hanger DP, Noble W, Williamson R (2011) Tyrosine phosphorylation of tau regulates its interactions with Fyn SH2 domains, but not SH3 domains, altering the cellular localization of tau. FEBS Journal 278:2927–2937.

Vainchtein ID, Molofsky A v. (2020) Astrocytes and Microglia: In Sickness and in Health. Trends in Neurosciences 43:144–154 Available at: https://doi.org/10.1016/j.tins.2020.01.003.

Vainchtein ID, Molofsky A V. (2020) Astrocytes and Microglia: In Sickness and in Health. Trends Neurosci 43:144–154 Available at: https://doi.org/10.1016/j.tins.2020.01.003.

van Eldik LJ, Griffin WST (1994) S100 beta expression in Alzheimer's disease: relation to neuropathology in brain regions. Biochim Biophys Acta 1223:398–403 Available at: https://pubmed.ncbi.nlm.nih.gov/7918676/ [Accessed July 24, 2022].

Vanni S, Moda F, Zattoni M, Bistaffa E, De Cecco E, Rossi M, Giaccone G, Tagliavini F, Haïk S, Deslys JP, Zanusso G, Ironside JW, Ferrer I, Kovacs GG, Legname G (2017) Differential overexpression of SERPINA3 in human prion diseases. Sci Rep 7 Available at: www.nature.com/scientificreports/.

Vasile F, Dossi E, Rouach N (2017) Human astrocytes: structure and functions in the healthy brain. Brain Struct Funct 222:2017–2029.

Vasile F, Dossi E, Rouach N (2017) Human astrocytes: structure and functions in the healthy brain. Brain Structure and Function 222:2017–2029.

Vehmas AK, Kawas CH, Stewart WF, Troncoso JC (2003) Immune reactive cells in senile plaques and cognitive decline in Alzheimer's disease. Neurobiol Aging 24:321–331.

Vehmas AK, Kawas CH, Stewart WF, Troncoso JC (2003) Immune reactive cells in senile plaques and cognitive decline in Alzheimer's disease. Neurobiology of Aging 24:321–331.

Velebit J, Horvat A, Smolič T, Prpar Mihevc S, Rogelj B, Zorec R, Vardjan N (2020) Astrocytes with TDP-43 inclusions exhibit reduced noradrenergic cAMP and Ca2+ signaling and dysregulated cell metabolism. Sci Reports 2020 101 10:1–18 Available at: https://www.nature.com/articles/s41598-020-62864-5 [Accessed July 22, 2022].

Vicuña L, Strochlic DE, Latremoliere A, Bali KK, Simonetti M, Husainie D, Prokosch S, Riva P, Griffin RS, Njoo C, Gehrig S, Mall MA, Arnold B, Devor M, Woolf CJ, Liberles SD, Costigan M, Kuner R (2015) The serine protease inhibitor SerpinA3N attenuates neuropathic pain by inhibiting T cell-derived leukocyte elastase. Nat Med 21:518 Available at: /pmc/articles/PMC4450999/ [Accessed July 29, 2022].

Vijayan VK, Gedes JW, Anderson KJ, Chang-Chui H, Ellis WG, Cotman CW (1991) Astrocyte hypertrophy in the Alzheimer's disease hippocampal formation. Exp Neurol 112:72–78 Available at: https://pubmed.ncbi.nlm.nih.gov/2013308/ [Accessed July 17, 2022].

Violet M, Delattre L, Tardivel M, Sultan A, Chauderlier A, Caillierez R, Talahari S, Nesslany F, Lefebvre B, Bonnefoy E, Buée L, Galas MC (2014) A major role for Tau in neuronal DNA and RNA protection in vivo under physiological and hyperthermic conditions. Front Cell Neurosci 8 Available at: https://pubmed.ncbi.nlm.nih.gov/24672431/ [Accessed July 15, 2022].

Vogel JW et al. (2021) Four distinct trajectories of tau deposition identified in Alzheimer's disease. Nat Med 27:871–881 Available at: https://doi.org/10.1038/s41591-021-01309-6.

Vogel JW et al. (2021) Four distinct trajectories of tau deposition identified in Alzheimer's disease. Nature Medicine 27:871–881 Available at: https://doi.org/10.1038/s41591-021-01309-6.

Vogels T, Leuzy A, Cicognola C, Ashton NJ, Smolek T, Novak M, Blennow K, Zetterberg H, Hromadka T, Zilka N, Schöll M (2019) Propagation of Tau Pathology: Integrating Insights From Postmortem and In Vivo Studies. Biological Psychiatry:1–11 Available at: https://doi.org/10.1016/j.biopsych.2019.09.019.

Volterra A, Liaudet N, Savtchouk I (2014) Astrocyte Ca2+ signalling: an unexpected complexity. Nat Rev Neurosci 15:327–335 Available at: https://pubmed.ncbi.nlm.nih.gov/24739787/ [Accessed July 17, 2022].

von Bergen M, Friedhoff P, Biernat J, Heberle J, Mandelkow EM, Mandelkow E (2000) Assembly of τ protein into Alzheimer paired helical filaments depends on a local sequence motif (306VQIVYK311) forming β structure. Proc Natl Acad Sci U S A 97:5129–5134 Available at: www.pnas.org [Accessed April 14, 2022].

Wakida NM, Cruz GMS, Ro CC, Moncada EG, Khatibzadeh N, Flanagan LA, Berns MW (2018) Phagocytic response of astrocytes to damaged neighboring cells. PLoS ONE 13.

Wang JZ, Grundke-Iqbal I, Iqbal K (1996) Glycosylation of microtubule-associated protein tau: An abnormal posttranslational modification in Alzheimer's disease. Nature Medicine 2:871–875.

Wang P, Ye Y (2021) Filamentous recombinant human Tau activates primary astrocytes via an integrin receptor complex. Nat Commun 12 Available at: https://doi.org/10.1038/s41467-020-20322-w.

Wang Y, Balaji V, Kaniyappan S, Krüger L, Irsen S, Tepper K, Chandupatla R, Maetzler W, Schneider A, Mandelkow E, Mandelkow EM (2017) The release and trans-synaptic transmission of Tau via exosomes. Molecular Neurodegeneration 12:1–25 Available at: http://dx.doi.org/10.1186/s13024-016-0143-y.

Wang Y, Mandelkow E (2012) Degradation of tau protein by autophagy and proteasomal pathways. In: Biochemical Society Transactions, pp 644–652. Portland Press. Available at: /biochemsoctrans/article/40/4/644/85586/Degradation-of-tau-protein-by-autophagy-and [Accessed May 1, 2022].

Wang Y, Mandelkow E (2016) Tau in physiology and pathology. Nature Reviews Neuroscience 17:5–21.

Wanner IB, Anderson MA, Song B, Levine J, Fernandez A, Gray-Thompson Z, Ao Y, Sofroniew M V. (2013) Glial scar borders are formed by newly proliferated, elongated astrocytes that interact to corral inflammatory and fibrotic cells via STAT3-dependent mechanisms after spinal cord injury. J Neurosci 33:12870–12886 Available at: https://pubmed.ncbi.nlm.nih.gov/23904622/ [Accessed July 22, 2022].

Warren NM, Piggott MA, Perry EK, Burn DJ (2005) Cholinergic systems in progressive supranuclear palsy. Brain 128:239–249 Available at: https://academic.oup.com/brain/article/128/2/239/402606 [Accessed July 13, 2022].

Weaver CL, Espinoza M, Kress Y, Davies P (2000) Conformational change as one of the earliest alterations of tau in Alzheimer's disease. Neurobiology of Aging 21:719–727.

Wei ML, Andreadis A (1998) Splicing of a regulated exon reveals additional complexity in the axonal microtubule-associated protein tau. J Neurochem 70:1346–1356 Available at: https://pubmed.ncbi.nlm.nih.gov/9523550/ [Accessed July 15, 2022].

Weingarten MD, Lockwood AH, Hwo SY, Kirschner MW (1975) A protein factor essential for microtubule assembly. Proceedings of the National Academy of Sciences 72:1858–1862.

Wesseling H et al. (2020) Tau PTM Profiles Identify Patient Heterogeneity and Stages of Alzheimer's Disease. Cell 183:1699-1713.e13 Available at: https://doi.org/10.1016/j.cell.2020.10.029.

Wharton SB, Minett T, Drew D, Forster G, Matthews F, Brayne C, Ince PG (2016) Epidemiological pathology of Tau in the ageing brain: application of staging for neuropil threads (BrainNet Europe protocol) to the MRC cognitive function and ageing brain study. Acta Neuropathol Commun 4:11 Available at: http://dx.doi.org/10.1186/s40478-016-0275-x.

Wheeler MA et al. (2020) MAFG-driven astrocytes promote CNS inflammation. Nature 578:593–599 Available at: https://pubmed.ncbi.nlm.nih.gov/32051591/ [Accessed July 16, 2022].

Wiche G (1998) Role of plectin in cytoskeleton organization and dynamics. Journal of Cell Science 111:2477–2486.

Wilhelmsson U, Bushong EA, Price DL, Smarr BL, Phung V, Terada M, Ellisman MH, Pekny M (2006) Redefining the concept of reactive astrocytes as cells that remain within their unique domains upon reaction to injury. Proc Natl Acad Sci U S A 103:17513–17518 Available at: www.pnas.orgcgidoi10.1073pnas.0602841103 [Accessed July 1, 2022].

Williams DR, de Silva R, Paviour DC, Pittman A, Watt HC, Kilford L, Holton JL, Revesz T, Lees AJ, Lila R (2005) Characteristics of two distinct clinical phenotypes in pathologically proven progressive supranuclear palsy: Richardson's syndrome and PSP-parkinsonism. Brain 128:1247–1258.

Williams DR, Lees AJ, Wherrett JR, Steele JC (2008) J. Clifford Richardson and 50 years of progressive supranuclear palsy. Neurology 70:566–573 Available at: https://pubmed.ncbi.nlm.nih.gov/18268249/ [Accessed July 13, 2022].

Wong E, Cuervo AM (2010) Integration of Clearance Mechanisms: The Proteasome and Autophagy. Cold Spring Harbor Perspectives in Biology 2 Available at: /pmc/articles/PMC2982176/ [Accessed July 16, 2022].

Wray S, Saxton M, Anderton BH, Hanger DP (2008) Direct analysis of tau from PSP brain identifies new phosphorylation sites and a major fragment of N-terminally cleaved tau containing four microtubule-binding repeats. Journal of Neurochemistry 105:2343–2352.

Wu G, Schöler HR (2014) Role of Oct4 in the early embryo development. Cell Regen 3:3:7 Available at: https://cellregeneration.springeropen.com/articles/10.1186/2045-9769-3-7 [Accessed July 19, 2022].

Wu JW, Herman M, Liu L, Simoes S, Acker CM, Figueroa H, Steinberg JI, Margittai M, Kayed R, Zurzolo C, Di Paolo G, Duff KE (2013) Small misfolded tau species are internalized via bulk endocytosis and anterogradely and retrogradely transported in neurons. J Biol Chem 288:1856–1870.

Wu JW, Hussaini SA, Bastille IM, Rodriguez GA, Mrejeru A, Rilett K, Sanders DW, Cook C, Fu H, Boonen RACM, Herman M, Nahmani E, Emrani S, Figueroa YH, Diamond MI, Clelland CL, Wray S, Duff KE (2016) Neuronal activity enhances tau propagation and tau pathology in vivo. Nature Neuroscience 19:1085–1092.

Wu M, Zhang M, Yin X, Chen K, Hu Z, Zhou Q, Cao X, Chen Z, Liu D (2021) The role of pathological tau in synaptic dysfunction in Alzheimer's diseases. Transl Neurodegener 10 Available at: https://pubmed.ncbi.nlm.nih.gov/34753506/ [Accessed July 16, 2022].

Wu T, Dejanovic B, Gandham VD, Carano RAD, Sheng M, Hanson JE, Wu T, Dejanovic B, Gandham VD, Gogineni A, Edmonds R, Schauer S (2019) Complement C3 Is Activated in Human AD Brain and Is Required for Neurodegeneration in Mouse Models of Amyloidosis and Tauopathy Article Complement C3 Is Activated in Human AD Brain and Is Required for Neurodegeneration in Mouse Models of Amyloidosis and T. CellReports 28:2111-2123.e6 Available at: https://doi.org/10.1016/j.celrep.2019.07.060.

Wyss-Coray T, Loike JD, Brionne TC, Lu E, Anankov R, Yan F, Silverstein SC, Husemann J (2003) Adult mouse astrocytes degrade amyloid-β in vitro and in situ. Nat Med 9:453–457.

Xia Y et al. (2020) Tau Ser208 phosphorylation promotes aggregation and reveals neuropathologic diversity in Alzheimer's disease and other tauopathies. Acta Neuropathologica Communications 8:1–17.

Xia Y, Prokop S, Giasson BI (2021) “Don’t Phos Over Tau”: recent developments in clinical biomarkers and therapies targeting tau phosphorylation in Alzheimer’s disease and other tauopathies. Molecular Neurodegeneration 16:1–19.

Xu Z, Xiao N, Chen Y, Huang H, Marshall C, Gao J, Cai Z, Wu T, Hu G, Xiao M (2015) Deletion of aquaporin-4 in APP/PS1 mice exacerbates brain Aβ accumulation and memory deficits. Mol Neurodegener 10:1–16 Available at: http://dx.doi.org/10.1186/s13024-015-0056-1.

Yagishita S, Itoh Y, Nan W, Amano N (1981) Reappraisal of the fine structure of Alzheimer’s neurofibrillary tangles. Acta Neuropathologica 54:239–246.

Yagishita S, Murayama M, Ebihara T, Maruyama K, Takashima A (2015) Glycogen Synthase Kinase 3β-mediated Phosphorylation in the Most C-terminal Region of Protein Interacting with C Kinase 1 (PICK1) Regulates the Binding of PICK1 to Glutamate Receptor Subunit GluA2. The Journal of Biological Chemistry 290:29438 Available at: /pmc/articles/PMC4705946/ [Accessed July 16, 2022].

Yamada K, Cirrito JR, Stewart FR, Jiang H, Finn MB, Holmes BB, Binder LI, Mandelkow EM, Diamond MI, Lee VMY, Holtzman DM (2011) In vivo microdialysis reveals age-dependent decrease of brain interstitial fluid tau levels in P301S human tau transgenic mice. J Neurosci 31:13110–13117 Available at: https://pubmed.ncbi.nlm.nih.gov/21917794/ [Accessed July 15, 2022].

Yamada K, Holth JK, Liao F, Stewart FR, Mahan TE, Jiang H, Cirrito JR, Patel TK, Hochgräfe K, Mandelkow EM, Holtzman DM (2014) Neuronal activity regulates extracellular tau in vivo. J Exp Med 211:387–393 Available at: https://pubmed.ncbi.nlm.nih.gov/24534188/ [Accessed July 17, 2022].

Yamada M, Hamaguchi T (2018) The sulfation code for propagation of neurodegeneration. J Biol Chem 293:10841–10842.

Yamamoto N, Ishikuro R, Tanida M, Suzuki K, Ikeda-Matsuo Y, Sobue K (2018) Insulin-signaling Pathway Regulates the Degradation of Amyloid β-protein via Astrocytes. Neuroscience 385:227–236.

Yan Y, Shin S, Jha BS, Liu Q, Sheng J, Li F, Zhan M, Davis J, Bharti K, Zeng X, Rao M, Malik N, Vemuri MC (2013) Efficient and Rapid Derivation of Primitive Neural Stem Cells and Generation of Brain Subtype Neurons From Human Pluripotent Stem Cells. Stem Cells Translational Medicine 2:862–870 Available at: http://www.sigmaaldrich.com.

Yang Y, Vidensky S, Jin L, Jie C, Lorenzini I, Frankl M, Rothstein JD (2011) Molecular comparison of GLT1+ and ALDH1L1+ astrocytes in vivo in astroglial reporter mice. Glia 59:200–207.

Yong VW, Moumdjian R, Yong FP, Ruijs TCG, Freedman MS, Cashman N, Antel JP (1991) γ-Interferon promotes proliferation of adult human astrocytes in vitro and reactive gliosis in the adult mouse brain in vivo. Proc Natl Acad Sci U S A 88:7016–7020.

Yu Y, Run X, Liang Z, Li Y, Liu F, Liu Y, Iqbal K, Grundke-Iqbal I, Gong CX (2009) Developmental regulation of tau phosphorylation, tau kinases, and tau phosphatases. Journal of Neurochemistry 108:1480–1494 Available at: https://onlinelibrary.wiley.com/doi/full/10.1111/j.1471-4159.2009.05882.x [Accessed July 15, 2022].

Yuan A, Kumar A, Peterhoff C, Duff K, Nixon RA (2008) Axonal transport rates in vivo are unaffected by tau deletion or overexpression in mice. J Neurosci 28:1682–1687 Available at: https://pubmed.ncbi.nlm.nih.gov/18272688/ [Accessed July 15, 2022].

Zamanian JL, Xu L, Foo LC, Nouri N, Zhou L, Giffard RG, Barres BA (2012) Genomic analysis of reactive astrogliosis. J Neurosci 32:6391–6410.

Zamanian JL, Xu L, Foo LC, Nouri N, Zhou L, Giffard RG, Barres BA (2012) Genomic analysis of reactive astrogliosis. Journal of Neuroscience 32:6391–6410.

Zappia M, Annesi G, Nicoletti G, Serra P, Arabia G, Pugliese P, Messina D, Caracciolo M, Romero N, Annesi F, Pasqua AA, Spadafora P, Civitelli D, Romeo N, Epifanio A, Morgante L, Quattrone A (2003) Association of tau gene polymorphism with Parkinson’s disease. Neurological Sciences 24:223–224.

Zeng Y, Yang J, Zhang B, Gao M, Su Z, Huang Y (2021) The structure and phase of tau: from monomer to amyloid filament. Cellular and Molecular Life Sciences 78:1873–1886 Available at: https://doi.org/10.1007/s00018-020-03681-x.

Zhang W, Falcon B, Murzin AG, Fan J, Crowther RA, Goedert M, Scheres SHW (2019) Heparin-induced tau filaments are polymorphic and differ from those in alzheimer's and pick's diseases. Elife 8.

Zhang W, Tarutani A, Newell KL, Murzin AG, Matsubara T, Falcon B, Vidal R, Garringer HJ, Shi Y, Ikeuchi T, Murayama S, Ghetti B, Hasegawa M, Goedert M, Scheres SHW (2020) Novel tau filament fold in corticobasal degeneration. Nature 580 Available at: http://dx.doi.org/10.1038/s41586-020-2043-0.

Zhang Y, Chen K, Sloan SA, Bennett ML, Scholze AR, O'Keeffe S, Phatnani HP, Guarnieri P, Caneda C, Ruderisch N, Deng S, Liddelow SA, Zhang C, Daneman R, Maniatis T, Barres BA, Wu JQ (2014) An RNA-sequencing transcriptome and splicing database of glia, neurons, and vascular cells of the cerebral cortex. Journal of Neuroscience 34:11929–11947.

Zhang Y, Chen K, Sloan SA, Bennett ML, Scholze AR, O'Keeffe S, Phatnani HP, Guarnieri P, Caneda C, Ruderisch N, Deng S, Liddelow SA, Zhang C, Daneman R, Maniatis T, Barres BA, Wu JQ (2014) An RNA-sequencing transcriptome and splicing database of glia, neurons, and vascular cells of the cerebral cortex. J Neurosci 34:11929–11947.

Zhang Y, Wu KM, Yang L, Dong Q, Yu JT (2022) Tauopathies : new perspectives and challenges. Molecular Neurodegeneration:1–29 Available at: https://doi.org/10.1186/s13024-022-00533-z.

Zhao Y, Jaber V, Lukiw WJ (2017) Secretory products of the human GI tract microbiome and their potential impact on Alzheimer's disease (AD): Detection of lipopolysaccharide (LPS) in AD hippocampus. Front Cell Infect Microbiol 7:318.

Zhong Q, Congdon EE, Nagaraja HN, Kuret J (2012) Tau isoform composition influences rate and extent of filament formation. Journal of Biological Chemistry 287:20711–20719 Available at: http://www.jbc.org/article/S0021925820499405/fulltext [Accessed April 14, 2022].

Zhukareva V, Mann D, Pickering-Brown S, Uryu K, Shuck T, Shah K, Grossman M, Miller BL, Hulette CM, Feinstein SC, Trojanowski JQ, M-Y Lee V (2002) Sporadic Pick's Disease: A Tauopathy Characterized by a Spectrum of Pathological Isoforms in Gray and White Matter. Available at: www.interscience.wiley.com.

Zimmer ER, Parent MJ, Souza DG, Leuzy A, Lecrux C, Kim HI, Gauthier S, Pellerin L, Hamel E, Rosa-Neto P (2017) [18F]FDG PET signal is driven by astroglial glutamate transport. Nature Neuroscience 2017 20:3 20:393–395 Available at: https://www.nature.com/articles/nn.4492 [Accessed July 16, 2022].